



A University of Sussex PhD thesis

Available online via Sussex Research Online:

<http://sro.sussex.ac.uk/>

This thesis is protected by copyright which belongs to the author.

This thesis cannot be reproduced or quoted extensively from without first obtaining permission in writing from the Author

The content must not be changed in any way or sold commercially in any format or medium without the formal permission of the Author

When referring to this work, full bibliographic details including the author, title, awarding institution and date of the thesis must be given

Please visit Sussex Research Online for more information and further details



Mechanochemistry and the Zincke Reaction

Mary Wong

Thesis submitted in partial fulfilment for the degree of
Doctor of Philosophy

Completed with supervision by
Dr Barny Greenland and Professor Mark Bagley

Acknowledgements

My thanks to Ian Edmond for whom no number of superlatives will suffice. My children, Isla and Milo. All my extended family members, but for help with the thesis, my nephew Dr Henry Wong. David Roberts, Jean Seyed-Safi, Janet Cottingham, and Emma Foster for career-defining moments. Annabelle, Camy, and DebbieDebbie for believing.

At Sussex: Dr Barny Greenland, Prof Mark Bagley, Dr John Turner, Prof John Spencer, Prof Ali Nokhodchi, Dr Ramón González-Méndez, Dr Alaa Abdul-Sada, Dr Chris Dadswell, Dr Iain Day, Dr Mark Roe, Dr Ian Crossley, Dr Steven Pearce, Verity Holmes, Dr Aiden Fisher, Dr Dan Guest, Paul Andrews, Dr Andy McGown, Sergi Ortoll, Dr Arathy Jose, Dr Raysa T Khan, Lydia Panther, Hugo Emerit, Alex Burns, Alan Mayers, Yasmin Kapadia, Zephyr Leader. The helpful assistance of Karen Scruby, Trudy Myers, Dr Sarah Lilley, Dr Kath Adley, Dr Roy Fox, Shamim Choudhary, Dr Jed McDonald, Dr Luke Young, Pablo Murray, Dan Bartlett, Ieuan Williams, Barry Thorogood, Alethia Wimble, and Hannah Boniface.

Chemistry, as an academic pursuit, has been in my life since 1981, when I had the great fortune of being taught by Dr Christopher Botton and Roy Hedley, who sadly died in 1986. Without their inspirational teaching, my life would have been very different growing up in Birkenhead. I was suitably equipped by them to study Chemistry with Mathematics and Physics in what was then MOLS at the University of Sussex in 1985, attending lectures given by Profs Sir Harry Kroto, John Nixon, John Murrell, Dr David Walton to name but a few, and laboratory sessions led by Prof Norman Billingham and Dr Jim Hanson. My third year project was with Prof Michael Lappert in his lab with Dr Gerry Lawless in Chichester I, which was very handy for the tearoom.

Finally, thank you to the National Health Service and, especially my parents.

We acknowledge financial support from the ERDF: Labfact InterReg V project 121.

Declaration

I hereby declare that this thesis has not been and will not be submitted in whole or in part to another University for the award of any other degree.

Signature:

Abbreviations

°C	degrees centigrade
3D	three dimensional
a	annum
Å	ångström
Ac	acetate
adi	adipic acid
A _N RORC	nucleophilic addition, ring-opening and ring-closing
API	active pharmaceutical ingredient
atm	atmosphere
AU	arbitrary units
BC	Before Christ
BOC	<i>tert</i> -Butyloxycarbonyl
BPin	boronic acid pinacol ester
Bz	benzoyl
c-	c plane
<i>ca.</i>	circa
Cat.	catalyst
CBZ	carbamazepine <chem>SMILES NC(N1C2=C(C=CC=N2)C=CC3=C1N=CC=C3)=O</chem>
CED	cumulative energy demand (of solvents)
cf	confer
COF	covalent organic framework
conv.	conversion
CSD	Cambridge Structure Database
Cy5	Cyanine 5
Cy7	Cy7
<i>d</i> -	deuterium
DABCO	1,4-Diazabicyclo[2.2.2]octane
Da	Dalton
DCM	dichloromethane

dhta	2,5-dihydroxyterephthalic acid
DMA	dimethylacetamide
DMSO	dimethyl sulfoxide
EA	elemental analysis
EDG	electron donating group
EHS	environmental health and safety score
eq.	equivalent
Et	ethyl
<i>et al.</i>	et alia
EWG	electron withdrawing group
ϵ	molar extinction coefficient
FAM	Fluorescein amidites
FDA	Federal Drug Agency (U.S.)
<i>FLARE™ systems</i>	Fluorescence-Assisted Resection and Exploration
g	gram
Gly	glycine
h	hour
<i>h</i>	Planck's Constant
Hb	haemoglobin
HDPE	high density polyethylene
HITC	1,1',3,3',3',3'-Hexamethylindotricarbocyanine
HME	hot melt extrusion
HR	high resolution
HS	hardened steel
Hz	Hertz
ICG	Indocyanine green
ICP MS	Inductively coupled plasma mass spectrometry
I_{\max}	or λ_{\max} wavelength absorption maxima
<i>in situ</i>	in the reaction mixture
<i>in vivo</i>	within the living
IR	infrared

IUPAC	International Union of Pure and Applied Chemistry
J	joule
k	kilo
k_R	bimolecular rate constant
LAG	liquid assisted grinding
litre	L
m	metre
M	molar
MAC	matrix-assisted co-crystallisation
MAS NMR	Magic angle spinning nuclear magnetic resonance
MB	methylene blue
Me	methyl
min	minute
M_n	The molecular mass M of n polymer molecules
MOF	metal-organic framework
mol	mole
mp	melting point
MS	mass spectrometry
MSR	mechanically induced self-propagating reaction
MW	microwave activation
N	Newton
NCT	nicotinamide
NDI	naphthalene diimide
NIR	near infrared
NMR	nuclear magnetic resonance
\emptyset	diameter
OLED	organic light emitting diode
OPV	organic photovoltaic
P	pressure
PBM	planetary ball mill
PDI	perylene diimide

Pd-PEPPSI-iPent	Dichloro[1,3-bis(2,6-Di-3-pentylphenyl)imidazol-2-ylidene](3-chloropyridyl)palladium(II), [1,3-Bis(2,6-Di-3-pentylphenyl)imidazol-2-ylidene](3-chloropyridyl)dichloropalladium(II), [1,3-Bis(2,6-Di-3-pentylphenyl)imidazol-2-ylidene](3-chloropyridyl)palladium(II) dichloride
pK _a	the negative base-10 logarithm of the acid dissociation constant (K _a) of a solution
PLA	polylactic acid
ppm	parts per million
R	organic group
rpm	revolutions per minute
RT	room temperature
s	second
S	energy state
SET	single electron transfer
SHS	Self-Propagating High-Temperature Synthesis
SI	Supplementary Information
S _N Ar	Aromatic nucleophilic substitution
SS	stainless steel
SSE	single screw extruder
STY	space time yield
T	temperature
t	time
TaqMAN	hydrolysis probe, TaqMan is a portmanteau of Taq Polymerase with the video game PacMan
TBAB	Tetrabutylammonium bromide
TBS	<i>tert</i> -butyldimethylsilyl
<i>t</i> -Bu	<i>tertiary</i> -Butyl
THF	tetrahydrofuran
TLC	thin layer chromatography
T _m	milling time
TMS	tetramethylsilane
Tp-Pa1 Keto	1,3,5-Benzenetricarboxaldehyde, 2,4,6-trihydroxy-, polymer with 1,4-benzenediamine. Ketone formation.

t_R	retention time
t_r	residency time <i>in biotechnology</i>
Trp	tryptophan
TSE	twin-screw extruder
UV-vis	Ultraviolet-visible spectroscopy
v/v	volume per volume
VBM	vibratory ball mill
VOC	volatile organic chemicals
vs	versus
w/w	weight by weight
Δ	heating
δ	chemical shift
$\Delta\lambda$	wavelength difference
λ	wavelength
$\nu, (\nu_{ex} \nu_{em})$	frequency (of excitation, emission)
Φ	Quantum Yield

List of Figures

Figure 1-1 (a) Ball symbol for ball milling taken from Hanusa ² <i>et al.</i> (b) and (c) screws in place of reaction arrows for extrusion reactions used by Browne ³ <i>et al.</i> (d) and (e) in this thesis, the screws icon are used with reaction arrows.....	2
Figure 1-2 Examples of the Types of Mechanical Activation of Materials (I) non-reactive milling to smaller particles (II) sheet-forming of malleable metals (III) formation of polymorphic materials (IV) Cocrystallisation (V) Reactive Ball-milling.....	4
Figure 1-3 The 12 Principles of Green Chemistry by Anastas and Warner ³³	6
Figure 1-4 (L) A cobble used as an abrading tool from the Tabun Cave in Israel taken from ³⁵ and (R) a contemporary pestle and mortar.....	6
Figure 1-5 The Zincke Chloride salt, 1-1 and the di-Zincke salt, 1-2	8
Figure 1-6 Environmental, Health and Safety Score vs Cumulative Energy Demand (MJ/kg) taken from ⁴⁴	10
Figure 1-7 (L) Retsch MM400 (VBM) and (R) Retsch PM100 (PBM) pictures taken from ⁴⁸	11
Figure 1-8 The modes of action for (L) VBM and (R) PBM.....	12
Figure 1-9 (a) Thermal Image of two balls colliding and (b) Orange sparks of molten iron from striking thermite balls.....	14
Figure 1-10 Greenland group's three Palladium coupling reactions in VBM, picture adapted from ⁵⁷	17
Figure 1-11 'Temperature development in ball mills during synthesis', pictures taken from ⁸⁵	22
Figure 1-12 (L) 3D printed mini-milling jar fitted inside the NMR coil with eccentric wheel attachment and (R) the dimensions in mm of the milling jar, taken from ⁸⁶	23
Figure 1-13 Product evolution as a function of time and vibrational frequency the number of balls was kept constant at 50. All curves were recorded through repeated single pulse acquisition measurements with a time resolution of 16 s. The rate constants of the exponential fits amount to 393 s ⁻¹ and 143 s ⁻¹ for 25, and 35 Hz, respectively, taken from ⁸⁶	23
Figure 1-14 (L) ThermoFisher Process 11 Twin Screw Extruder, taken from ⁹⁰ (R) Schematic for a twin screw types of extruder, picture from ⁹¹	24
Figure 1-15 Thermo-Scientific™ Pharma twin-screw extruders for HME showing different screw sizes in mm, picture taken from ¹¹⁶	32
Figure 1-16 Parallel Lima TSE Photos from ¹¹⁷	32
Figure 1-17 Monomers for a selection of fully conjugated polymer systems.....	34
Figure 1-18 A unimer 1-38 , dimer 1-39 , and a hexacationic trimer 1-40	35
Figure 2-1 ¹ H NMR spectrum for 1-2 with H _{3'} , d, 9.31 ppm, H _{5'} , dd 8.83 ppm and H _{6'} d 8.20 ppm.....	44
Figure 2-2 Time delay from 1 to 25 seconds gives correct integrated values for ¹ H NMR spectrum of the di-Zincke salt, 1-2	44
Figure 2-3 ¹ H NMR Spectra for reaction between di Zincke salt 1-2 and 2-ethylaniline 2-2a (A) di Zincke salt, 1-2 in d ₆ -DMSO (B) Crude reaction	

	mixture from ZrO ₂ jar (C) Crude reaction mixture from SS jar (D) Crude reaction mixture from HS jar.	46
Figure 2-4	¹ H NMR stack of (A) di-Zincke salt 1-2 (B) crude product mixture and (C) 4-phenoxyaniline 2-1b	48
Figure 2-5	¹ H NMR spectra for reaction monitoring of the substitution of the di-Zincke salt 1-2 (A) di Zincke salt 1-2 (B) after 5 min (C) after 10 min (D) after 15 min (E) isolated product p-tolyl viologen 2-2c (F) leaving group, dinitroaniline 2-3	49
Figure 2-6	Formation of major side product (i) diarylamine 2-4 which may also result from	53
Figure 2-7	The ¹ H NMR spectrum for 2-2j in Table 2-1	54
Figure 2-8	Stack of ¹ H NMR of final product of (A) viologen 2-5c , the crude reaction mixture sampled at (B) 20 °C (C) 85 °C and (D) 115 °C (E) the leaving group dinitroaniline 2-3	59
Figure 2-9	Carousel reactor with 12 stations, picture taken from ¹³⁵	60
Figure 2-10	Diamine with electron donating methoxy groups, 1-42	65
Figure 2-11	Four methods of synthesis 1-44 . ¹ H NMR Spectra of (A) 1-chloro-2,4-dinitrobenzene 1-35 (B) Crude product mixture from heat and stir at 80 °C with minimal solvent to reflux (C) Crude product mixture of solution synthesis heated to reflux, at 80 °C (D) Crude product mix from ZrO ₂ VBM(E) Crude product mix from WC VBM (F) Isolated product 1-44	67
Figure 2-12	¹ H NMR spectra of purified asymmetric Zincke salt 1-47 , in D ₂ O	68
Figure 2-13	¹ H NMR for the diamine 1-43	70
Figure 2-14	¹ H NMR stacked spectra for (A) asymmetric Zincke salt 1-47 (B) the diamine 1-43 and (C) the crude product after attempt from 30 min of VBM with WC, to make the hexacation 1-48	73
Figure 3-1	Reactivity study on aniline derivatives. Conditions: conventional heating (80 °C), 96 h, Zincke salt 1-1 (0.2 mmol), RC ₆ H ₄ NH ₂ (2 equiv), EtOH/H ₂ O : 60/40 (1 mL). (a) Yields were measured by ¹ H NMR spectroscopy in DMSO-d ₆ in the presence of diethyl fumarate as external standard. (b) For pK _a values, see references. ¹³⁷⁻¹⁴⁰ Figure with legends (sic) taken from ¹³⁰	76
Figure 3-2	Assignment of the ¹ H NMR for Mono-Zincke chloride 1-1 with (A) 1 sec and (B) 10 sec relaxation delay	78
Figure 3-3	(L) VBM of the crude product mixture (Centre) Structure of p-tolyl Cy5, 3-8a and (R) after recrystallisation	79
Figure 3-4	¹ H NMR stack of reaction between equimolar mono-Zincke salt 1-1 and p-toluidine, (A) isolated product 3-8a (B) crude reaction mixture from ball mill (C) 3-1a (D) 2-3 and (E) 1-1	80
Figure 3-5	¹ H NMR spectra stack showing conversion as a function of time oscillated where spectrum (A) is isolated product 3-8a (B) after 15 min (C) after 10 min (D) after 5 min of oscillation time and (E) starting material p-toluidine 3-1a	81
Figure 3-6	Shi <i>et al.</i> Structure of {12}Annulene gemini surfactants, 3-11	83
Figure 3-7	¹ H NMR spectra stack of the products of the mono-Zincke salt 1-1 and aniline 3-1b reaction in VBM where spectrum (A) Cy5 3-8b (B) the crude product mixture and (C) the leaving group 2-3	85

Figure 3-8	(Left flask) Crude product dissolved in methanol, (Right flask) precipitation into warm diethyl ether	85
Figure 3-9	Photograph of the Cy5 3-8a-g products showing the range of vivid red powders produced.....	86
Figure 3-10	(L) The result of filtering the crude through celite after activation in WC vessels, and (R) the magnetic property of the filtered solid with a magnet retriever	87
Figure 3-11	(a) damaged WC 15 mm diameter balls compared with the unused ball at the top of the picture. (b) enlarged picture of damaged WC ball (c) a chip of zirconium oxide that had come away from a stained ZrO ₂ milling ball	88
Figure 3-12	X-ray crystallography of compounds with counter-ions removed for clarity, 3-8a-g showing solid state structures for methoxy substrate 3-8c , p-tolyl substrate 3-8a and phenyl substrate 3-8d which were determined Z=2.	89
Figure 3-13	Photophysical data of cyanine 5 compounds as observed using UV/vis absorption spectroscopy (4.5 μM, methanol) for 3-8 a-g	90
Figure 3-14	Possible structures from the substitution of the Zincke Salt	92
Figure 3-15	Stacked ¹ H NMR spectra (B) Zincke salt 3-14a , and (A) 1-38 and (C) 1-37	93
Figure 3-16	Evolution of substituted pyridinium salt 3-16a over 180 minutes milling time using ¹ H NMR stacked spectra to analyse for conversion (A) crude product mixture at after 30 min milling time (B) 90 min (C) 180 min and (D) the isolated product 3-14a	94
Figure 3-17	A series of long polymethine molecular wires	97
Figure 3-18	A symmetry breaking Peierls transition	98
Figure 3-19	Bond lengths in the Cy5 methine chain	98
Figure 4-1	Molecules that have NIR properties and delocalisation in the heptamethine chain for 4-1 and 4-2	104
Figure 4-2	A Jablonski diagram showing all the possible radiative and non-radiative transition, diagram adapted from ¹⁹¹	105
Figure 4-3	Cyanine Homologous Series 4-12 and target Cyanine 4-13	108
Figure 4-4	¹ H NMR spectrum for Cy7, 4-14	113
Figure 4-5	Comparison of J _{HH} of the methine protons in Cy5 3-8b and Cy7 4-14	114
Figure 4-6	Stacked ¹ H NMR spectra (aliphatic region) showing (A) indole 4-15 starting material, (B) the crude product mixture and (C) the target Cy7 molecule 4-14 using Bromo cy5 3-8g	115
Figure 4-7	Cy5 3-8b reaction with Indole 4-15 after 60 minutes oscillation in the MM400 forms a sticky coating on the ZrO ₂ balls.....	118
Figure 4-8	¹ H NMR of the isolated 4-bromophenyl pyridinium salt, 3-2	118
Figure 4-9	Assignment of the ring-closed product, the pyridinium salt 3-2g , from a ¹ H NMR spectroscopy analysis where (A) 4-bromopyridinium salt 3-2g (B) Crude product mixture for Entry 4-4 c and (C) bromoaniline 3-1g	119
Figure 4-10	VBM of indole and Zincke Salt 1-1 with Bromoaniline 3-1g as catalyst, Stacked ¹ H NMR spectra (aliphatic region) showing (A) indolium salt 4-15 starting material, (B) the crude product mixture and (C) the target Cy7 molecule 4-14	122
Figure 4-11	Assignment of methyl groups Me ₁ from the starting material Indole 4-15 and Me ₄ from the target compound Cy7 4-14 in experiments using a	

	range of substituted anilines 3-1a-g . ¹ H NMR Spectra for (A) indole 4-15 then crude reaction mixtures (B) aniline 3-1b (C) 4-fluoroaniline 3-1e (D) p-tolyl aniline 3-1a (E) 4-phenoxyaniline 3-1d (F) p-aniso aniline 3-1c (G) 4-chloroaniline 3-1f and (H) 4-bromoaniline 3-1g (I) Cy7, 4-14	124
Figure 4-12	Plot of Aniline pK _a vs percentage conversion.....	125
Figure 4-13	Top: the starting reagents Bromoaniline 3-1g , sodium acetate, Zincke salt 1-1 – the indole is in the jar at the rear – it is a pale pink crystalline solid. Bottom: (L) The 125 mL Stainless Steel PBM and milling balls and (R) the crude reaction mixture after 60 minutes in the PBM	128
Figure 4-14	Stacked ¹ H NMR spectra for sampled crude from PM100 to make Cy7 where (A) indole starting material, 4-15 (B) Crude product mixture at T = 20 min (C) Crude product mixture at T = 40 min (D) Crude product mixture at = 60 min (E) Isolated Cy7, 4-14	129
Figure 4-15	Stacked ¹ H NMR spectra for (A) crude product of Zincke salt 1-1 with indolium salt 4-15 after 60 min in the PM100 (B) the closed ring bromopyridinium salt 3-2g	130
Figure 4-16	Filtration of the opaque green mixture gave a red glitter 4-14.2-3	131
Figure 4-17	The ¹ H NMR of the red cocrystal and the assignments of the two molecules present.....	131
Figure 4-18	Stacked ¹ H NMR spectra (A) of Cy7 4-14 (B) cocrystal Cy7 4-14 and dinitroaniline 2-3 (C) dinitroaniline 2-3	132
Figure 4-19	X-Ray Crystal Structure of the Cocrystal Cy7:Dinitroaniline	133
Figure 4-20	Crystal packing of the cocrystal seen in planes (a), and (b)	133
Figure 4-22	Percentage conversion using signals Me ₄ and Me ₁ for Twin Screw Extrusion Experiments using ¹ H NMR spectroscopy where spectra (A) indolium salt 4-15 and the Twin Screw extruded crude products for Entries 1-7 (B)-(H), (I) the isolated target molecule Cy7 4-14	135
Figure 4-23	(Top) UV-Vis absorption spectra for 4-14 and (bottom) measurement of the Stokes shift fuorimetry for Cy7 4-14	137
Figure 4-24	UV-Vis Investigation by Štacková <i>et al.</i> ‘Deciphering the Structure–Property Relations in Substituted Heptamethine Cyanines,’ figure from ²⁰⁷	138
Figure 5-1	The structures of ICG 4-1 and MB 5-1	140
Figure 5-2	The absorption and emission profiles of indocyanine green 4-1 and methylene blue 5-1 , taken from ²¹³	142
Figure 5-3	6-carboxyfluorescein (FAM), 5-2	143
Figure 5-4	The ‘Optical Window’ – wavelengths where absorbance is lowest making imaging possible © [2007] IEEE, picture taken from ²¹⁷	143
Figure 5-5	Energy diagrams for the different excited states of oxygen	144
Figure 5-6	Patent search by the University of Sussex IP Department: Application and Issued Trend.....	146
Figure 5-7	¹ H NMR spectroscopy spectra for (A) the crude product mixture with methine protons highlighted (B) the mono-Zincke salt 1-1 , with a methine proton highlighted (C) bromoaniline 3-1g catalyst and, (D) 4-19 with a methyl proton highlighted	152
Figure 5-8	¹ H NMR spectrum of (A) sodium acetate, 5-5 and (B) four times recrystallised ICG 4-1 from water and acetone	154

Figure 5-9	Sodium acetate optimisation for ICG Synthesis by VBM – stacked ¹ H spectra of (A) isolated ICG 4-1 (B) VBM using 2.5 eq. NaOAc 5-5 (C) VBM using 5.0 eq. NaOAc 5-5 (D) VBM using 7.5 eq. NaOAc 5-5 (E) starting material 4-19	156
Figure 5-10	Suggested formation of sodium indolene 5-6 by deprotonation with sodium acetate 5-5	157
Figure 5-11	Crude ¹ H NMR spectrum from heat and stir synthesis of ICG 4-1	158
Figure 5-12	Heat and stir ICG 4-1 , purified by flash chromatography, yield 72%.....	159
Figure 5-13	Intermediates 5-7 and 5-8 from ring-opening of the Zincke salt 1-1	163
Figure 5-14	Cascade reactions follow from the nucleophilicity and pK _{aH} values ¹³³ of competing species	163
Figure 5-15	The general set-up for continuous solid reactor, picture taken from ⁹⁸	165
Figure 5-16	The FilaFab 350 Pro EX, designed to extrude filament ready for 3D printing ²³²	166
Figure 5-17	Unsuccessful synthesis of 3-8g by stirring using 1 eq. 1-1 and 2 eq. 3-1g ..	167
Figure 5-18	Extrusion of bromoaniline 3-1g with mono-Zincke salt 1-1 where the stack shows ¹ H NMR spectra for (A) Crude extruded product (B) bromopyridinium salt 3-2 (C) pre-mix of 'E' used for extrusion experiment one week later (D) bromoaniline 3-1g premixed with mono-Zincke salt 1-1 in the Kenwood Mini-Chopper (E) bromoaniline 3-1g (F) mono-Zincke salt 1-1	168
Figure 5-19	Pre-mixing the four reagents for SSE	169
Figure 5-20	The first ICG 4-1 extrudate from the SSE, and dissolving a sample in methanol showing the distinctive green colour of this dye	170
Figure 5-21	Quality control: collecting separate fractions for analysis.....	171
Figure 5-22	A typical stack of ¹ H NMR spectra for ICG extrusion experiments to quantify conversion where (A) bromoaniline, 3-1g (B) the leaving group dinitroaniline 2-3 (C) The crude extrudate (D) isolated ICG 4-1 (E) starting material 4-19	172
Figure 5-23	Stack of ¹ H NMR spectra for starting materials 1-1 (B), 4-19 (C) and the crude product mixture containing target compound ICG 4-1 (A)	175
Figure 5-24	Scheme for extrusion of ICG 4-1 using 5-10 sodium acetate trihydrate, conversion by ¹ H NMR 74%	176
Figure 5-25	¹ H NMR stack (contracted) of purified ICG 4-1 using different techniques with impurities highlighted (A) crude extrudate ICG 4-1 (B) MeOH/Et ₂ O recrystallisation (C) EtOAc wash (D) H ₂ O/(CH ₃) ₂ CO recrystallisation (E) MeCN recrystallisation followed by H ₂ O/(CH ₃) ₂ CO recrystallisation (F) EtOAc/H ₂ O bisolvent wash – colloidal (G) Column chromatography (H) CH ₃ Cl/EtOAc bisolvent wash	178
Figure 5-26	¹ H NMR spectrum of ICG 4-1 , 0.5 g (72%) by column chromatography	180
Figure 5-27	ICG 4-1 obtained using column chromatography, methanol chloroform gradient 2:8, purity 97 % (HPLC UV)	181
Figure 5-28	A cross-section of the extrusion screws for the manufacture of perylene dyes, picture taken from ⁹²	182
Figure 5-29	The Filafab Pro 350 Ex – (A) outer casing removed (B) The barrel with heating elements (C) The nozzle adapter and die components of the Filafab extruder.....	183

Figure 5-30	^1H NMR of samples taken from (A) outside the die (B) inside the nozzle (C) End of the screw (D) Column product 4-1 (E), (F) and (G) screw positions marked 5,7 and 9.....	183
Figure 5-31	General form of an asymmetric heptamethine dye 5-11	186
Figure 6-1	Viologens synthesis in VBM 2-1 a-o , and heat and stir 2-6 a-j in Chapter 2.	187
Figure 6-2	(L) 5-anilino-N-p-aniso-2,4-pentadienylideniminium chloride 3-8c	188

List of Schemes

Scheme 1-1	Imine Formation taken from ³	3
Scheme 1-2	An S _N 1 reaction mechanism using the protic solvent methanol	8
Scheme 1-3	An S _N 2 reaction mechanism featuring the polar aprotic solvent, acetone	9
Scheme 1-4	Suzuki-Miyaura cross-coupling reaction in a VBM	15
Scheme 1-5	Sonogashira coupling in a VBM	15
Scheme 1-6	The Sonogashira reaction. I General representation of Pd/Cu catalysed and Cu-free Sonogashira reaction. II Textbook mechanism for the Pd/Cu catalysed Sonogashira cross-coupling reaction that is synergistically catalysed by Pd and Cu. III Mechanistic proposal for Cu-free Sonogashira reaction. OA oxidative addition, TM transmetallation, RE reductive elimination (cis–trans isomerization steps are omitted for clarity) taken from ⁵⁴	16
Scheme 1-7	Greenland group's Buchwald-Hartwig amination of NDI, 1-15	17
Scheme 1-8	Negishi Cross-Coupling in 2 steps using VBM.....	18
Scheme 1-9	Acylation and Borylation in VBM, scheme adapted from ⁶⁴	19
Scheme 1-10	Synthetic Route to the functional MOF-74 as a catalyst for a selective CO ₂ reduction reaction to methanol, taken from ⁷³	20
Scheme 1-11	A mechanochemical synthesis of Tp-Pa1 – Keto Form, 1-20	20
Scheme 1-12	Matrix-assisted cocrystallisation (MAC) in the simultaneous production and formulation of pharmaceutical cocrystals using HME. Hydrogen bonding (dashed lines) synthons for (L) the CBZ-Nic cocrystal and (R) CBZ, polymorphic form III	25
Scheme 1-13	Twin screw extrusion TSE fluorination with Selectfluor.....	26
Scheme 1-14	Twin screw extrusion for a peptide coupling reaction	26
Scheme 1-15	Twin screw extrusion for the multi-component Ugi Reaction adapted from ⁹⁷	27
Scheme 1-16	The Ugi Reaction Mechanism	28
Scheme 1-17	SSE experiments for small organic molecule targets 1-28, 1-29, 1-30	29
Scheme 1-18	General Scheme for the Twin Screw Extrusion of Perylene Dyes and the structures of Pigment Black 31, 1-31 and Pigment Black 32, 1-32	30
Scheme 1-19	The 'Beat and Heat' method from ball milling compared with Extrusion... ..	30
Scheme 1-20	Model reactions: TSE synthesised hydantoin-based APIs 1-33 and 1-34	31
Scheme 1-21	Gilch polymerisation by VBM ¹²⁰	34
Scheme 1-22	Solution syntheses of poly(pyridinium phenylenes) – a fully conjugated π system.....	35
Scheme 1-23	Colour-coded Mechanistic Scheme for the Zincke Reaction.....	36
Scheme 1-24	Synthesis of the di-Zincke salt, 1-2	37
Scheme 1-25	Reaction of the di-Zincke salt, 1-2 with the di-aniline 1-43	37
Scheme 1-26	Multi-step Zincke Reaction to give an asymmetric Zincke salt, 1-48	38
Scheme 1-27	Formation of hexacationic species 1-49	39
Scheme 1-28	The molecules with the Zincke and di-Zincke salts as precursors for functional molecules in this work.....	42
Scheme 2-1	The solution synthesis of the di-Zincke salt 1-2	43
Scheme 2-2	Reaction between the di-Zincke salt 1-2 and 2-ethylaniline 2-1a	45

Scheme 2-3	VBM of di-Zincke salt 1-2 with 4-phenoxyaniline 2-1b using 1 x 12 mm ball	47
Scheme 2-4	Reaction of the di-Zincke salt 1-2 and p-tolyl aniline 2-1c	49
Scheme 2-5	Reaction of the di-Zincke salt 1-2 and aniline 2-1a-o	51
Scheme 2-6	Scheme for the reaction between anilines 2-4a-p and the di-Zincke salt 1-2 using ball-milling and classical solution methods.....	55
Scheme 2-7	Heat and stir reaction of di-Zincke chloride 1-2 and 4-aminobenzoate 2-4c	58
Scheme 2-8	Heat and stir experiment for the di-Zincke salt 1-2 with low melting point anilines	61
Scheme 2-9	Comparison of Heat and Stir vs VBM for low-converting anilines 2-15c, i and j	63
Scheme 2-10	Three-step procedure of asymmetric Zincke salt 1-47 synthesis.....	66
Scheme 2-11	Synthesis of 1-46 from 1-44 by heat and stir and VBM	67
Scheme 2-12	Synthesis of 1-47 from 1-46 using 4 different condition.....	68
Scheme 2-13	Three scenarios for S _N Ar reaction mechanism	69
Scheme 2-14	The substitution of the di-Zincke salt 1-2 to form the diamine 1-43	71
Scheme 2-15	Reaction to form the hexacation 1-48 (a trimer) via VBM.....	72
Scheme 3-1	Zeghib's microwave activation of the Zincke salt with anilines ¹³⁰	75
Scheme 3-2	Microwave activation conditions for substitution of the mono-Zincke salt 1-1	76
Scheme 3-3	Solvent-free synthesis of the Zincke salt 1-1 , 87% isolated yield.....	77
Scheme 3-4	A solvent-free route to substituted pyridinium salts, 3-2	78
Scheme 3-5	Ratios of reagents to achieve Cy5 products from the mono-Zincke salt, 1-1	80
Scheme 3-6	Structures of the intermediates of the Zincke Reaction	82
Scheme 3-7	Reaction between mono-Zincke chloride 1-1 and p-toluidine 3-1a via VBM	82
Scheme 3-8	Yamaguchi <i>et al.</i> and their postulated reaction of the Zincke salt 1-1 with Anilines to give 3-10	83
Scheme 3-9	VBM of mono-Zincke salt 1-1 with anilines 3-1a-g using ZrO ₂ and WC ball milling jars	84
Scheme 3-10	(A) Cy5 from reaction between mono-Zincke Salt 1-1 and anilines 3-1 and (B) di-Zincke salt 1-2 and anilines, the leaving group dinitroaniline 2-3 is not included for clarity	91
Scheme 3-11	Reactions for substituted pyridyl Zincke salts, 3-16a-c	92
Scheme 3-12	Reaction of 4-phenyl Zincke salt 1-1 with aniline 3-1b	94
Scheme 3-13	Cis and trans forms of the open ring Zincke intermediate, 3-8	95
Scheme 3-14	Katoh's synthesis of pentamethine dimers, 3-17	95
Scheme 3-15	Štacková ¹⁶⁴ <i>et al.</i> - Approach to a substituted heptamethine cyanine chain by the ring opening of Zincke salts.....	96
Scheme 3-16	The Formation of the Pyridinium Salt 3-2 requiring the neutral cis conformation of the Cy5 intermediate, 3-26	100
Scheme 3-17	Marvell's scheme accounting for the pH-independent behaviour in the basic region and for the reduction in rate of cyclisation with increasing acidity in solution.....	101
Scheme 3-18	Suggested ring closure to 3-25 by nucleophilic addition	101
Scheme 3-19	Suggested electrocyclisation of the non-polar transition state 3-26 cis ...	102

Scheme 4-1	Synthetic routes for the Cy5 to Cy7 transformation	106
Scheme 4-2	Synthetic route using aldehyde 4-9 to form Cy11-X 4-10	107
Scheme 4-3	Conjugate Addition of Cy5 3-8 to form Cy7 4-16	108
Scheme 4-4	Kodak's synthesis of ICG 4-1	110
Scheme 4-5	A one-step condensation reaction to ICG 4-1	111
Scheme 4-6	VBM of bromo Cy5 3-1g , 44% isolated yield Cy7 4-14	112
Scheme 4-7	Reactions of Cy5 3-8a-g with the Indolinium salt 4-15 in the VBM.....	116
Scheme 4-8	VBM of the Zincke Salt 1-1 with Indole 4-15 using Bromoaniline 3-1g as a catalyst	121
Scheme 4-9	VBM of the Zincke Salt 1-1 and indolium salt 4-15 with a selection of Anilines 3-1a-g	123
Scheme 4-10	Reaction scheme for the PBM of heptamethine Cy7 4-14 from Zincke salt 1-1 and Indolium salt 4-15	127
Scheme 4-11	Twin screw extrusion of the Zincke salt with indole	134
Scheme 5-1	Dishman scheme for their ICG 4-1 patent ²²⁶	147
Scheme 5-2	Biophore India patent ²²⁷ for making ICG 4-1 with the mono-Zincke salt 1-1 as a precursor	148
Scheme 5-3	Solvent-free synthesis of the mono-Zincke salt 1-1 and the naphthyl sulfonate 4-19	150
Scheme 5-4	Synthesis of ICG 4-1 in the VBM	151
Scheme 5-5	VBM of mono-Zincke salt 1-1 with naphthyl indole sulfonate 4-19	155
Scheme 5-6	Heat and stir reagents for synthesis of ICG 4-1 on a hotplate	157
Scheme 5-7	Heat and stir reagents for synthesis of ICG 4-1 in a carousel.....	160
Scheme 5-8	The ring-opening steps in the Zincke reaction mechanism with aniline	162
Scheme 5-9	A mechanism for the one-pot synthesis of ICG 4-1 from proposed.....	164
Scheme 5-10	Extrusion of mono-Zincke salt 1-1 and bromoaniline 3-1g	166
Scheme 5-11	SSE of Indocyanine Green 4-1	169
Scheme 5-12	Heat and stir of ICG 4-1 using sodium acetate trihydrate 5-10	174
Scheme 6-1	Solvent-free reactive extrusion of the NIR imaging dye indocyanine green 4-1	189
Scheme 6-2	Generic SSE of compounds	191
Scheme 6-3	SSE of new compound	191

List of Tables

Table 2-1	The substitution of the di-Zincke salt, 1-2 with a selection of anilines 2-1a-o in the VBM to give bipyridinium salt 2-2a-o	52
Table 2-2	Comparison of 4 different ways to make the precursors for hexacation 1-48	71
Table 3-1	VBM of Mono-Zincke salt with anilines, *damaged balls	86
Table 4-1	Percentage conversions for substituted Cy5 3-8a-g to Cy7 4-14 using VBM .	117
Table 4-2	(top)% Conversion by ¹ H NMR spectroscopy from the Zincke salt 1-1 to Cy7 4-14 with aniline substituted aniline catalyst 3-1a-g.....	125
Table 4-3	Extruder conditions and the percentage conversions to 4-14 for each.....	136
Table 5-1	Photophysical properties ²¹³ for ICG 4-1 and MB 5-1.....	141
Table 5-2	Conversion to ICG 4-1 – the effect of changing variables of sodium acetate 5-5 and the catalyst, bromoaniline 3-1g	160
Table 5-3	Optimisation of the synthesis of ICG 4-1 by extrusion and Heat and Stir.....	173
Table 5-4	Conversion data, by ¹ H NMR spectroscopy, to ICG 4-1 , using sodium acetate trihydrate 5-10 , in heat and stir and extrusion experiments	177

List of Charts

Chart 2-1	The % conversion of di-Zincke salt 1-2 vs the pK _a value of aniline 2-4a-p using VBM	56
Chart 2-2	Solvent free synthesis of substituted viologen 2-7a-j by heating and stirring of anilines 2-6a-j with the di-Zincke salt 1-2	62
Chart 2-3	Comparison of conversion by ¹ H NMR spectroscopy for select anilines 2-15c, I and j	63

Chapters

1. Introduction.....	1
1.1 Greener synthesis through mechanochemistry	5
1.2 Solvent use in synthetic chemistry	7
1.3 Vibratory (VBM) and planetary ball mills (PBM).....	11
1.4 Ball charge and reagent requirements for reactive VBM.....	12
1.5 State-of-the-art mechanochemistry in organic synthesis	14
1.6 Functional materials in mechanochemistry	19
1.7 Monitoring reaction progress	21
1.8 Continuous reactive extrusion - twin screw (TSE) and single screw (SSE)	24
1.9 New chemical targets - electro active materials by mechanochemistry	33
1.10 Overview of the aims and scope of thesis	40
2. Towards the synthesis of viologen containing oligomers	43
2.1 Synthesis of viologen containing molecules with varying end groups.....	43
2.2 Mechanochemistry of viologens.....	45
2.3 Conclusion from VBM of the di-Zincke salt 1-2 with nucleophilic anilines...	55
2.4 Finding substrate scope using optimised conditions	56
2.5 Effect of the melting point of anilines in 'heat and stir' experiments	57
2.6 Conclusion from the solvent- free substitution reactions of the di-Zincke salt	64
2.7 Multi-step reactions of oligomers towards a hexameric viologen oligomers.	65
2.8 Conclusion	74
2.9 Further investigation of the Zincke reaction	74
3. Mono Zincke salt and cyanine 5 dyes	75
3.1 Nucleophilic substitutions of the mono-Zincke salt	75
3.2 Solvent-free synthesis of the mono-Zincke salt	77
3.3 Ball-milling the mono-Zincke salt with nucleophilic anilines	78
3.4 General synthesis of cyanine 5 dyes in VBM	84

3.5	X-ray crystallography of compounds 3.3 a-g	88
3.6	UV/ Vis absorption properties of cyanine 5 dyes	90
3.7	Synthesis of <i>p</i> -substituted pyridinium Zincke salts.....	90
3.8	Electronic symmetry in Cy5 salts	97
3.9	Understanding the Zincke reaction mechanism.....	99
4.	Heptamethine or Cy7 dyes	103
4.1	Introduction.....	103
4.2	Processes leading to fluorescence in NIR dyes.....	104
4.3	Heptamethine dyes – from Cy5 to Cy7.....	106
4.4	First patented route to Indocyanine Green 4-1	109
4.5	Route to Cy7 using substituted Cy5 3-8a-g	112
4.6	Cy5 transformation to Cy7 in the VBM.....	116
4.7	From Zincke salts to Cy7	120
4.8	Scale-Up of the Zincke to Cy7 in the Planetary Ball Mill.....	127
4.9	Electronic symmetry in Cy7	Error! Bookmark not defined.
4.10	Twin screw extrusion of Cy7 4-14	133
4.11	UV-Vis and fluorescence studies of Cy7	136
4.12	Conclusion	139
5.	Indocyanine Green: a new process for synthesis by SSE.....	140
5.1	Background of Indocyanine Green (ICG) 4-1	140
5.2	Photophysical properties of fluorophores ICG 4.1 and MB 5.1	141
5.3	Patented synthetic routes to ICG 4-1	145
5.4	Solvent-free synthesis of mono-Zincke salt 1-1 and the indolium salt 4-19 149	
5.5	VBM synthesis of ICG, 4-1	151
5.6	Understanding the role of sodium acetate 5-5 in the synthesis of ICG 4-1	155
5.7	ICG 4-1 optimisation carousel - heating and stirring.....	159
5.8	Single screw extrusion.....	165
5.9	Reactive extrusion of Indocyanine Green 4-1	168
5.10	Effect of melting temperature of sodium acetate in the SSE of ICG 4-1	174
5.11	Purification of ICG extrudate	178
5.12	Best purification for ICG 4-1	179

5.13	Reactivity in the SSE	181
5.14	Conclusion for the reactive extrusion of ICG.....	185
6.	Conclusion	187
7.	Experimental	193
	Bibliography.....	216
	Appendices	230
	Appendix 1: Ball milling	230
	Appendix 2: X-Ray Crystallography Data.....	233

Abstract

Mechanochemistry in this thesis is taken to mean the formation of new covalent chemical bonds using any form of mechanical activation, and usually in a solvent free environment. This is in contrast to typical chemical reactions which take place in solvents and are often promoted by thermal energy. The opening chapter begins by giving an overview to the history and development of mechanochemistry to the present day. It then discusses the position of mechanochemical synthesis in the burgeoning field of 'Green' chemistry, specifically by looking at the solvent free aspects of synthesis using this technique via reaction monitoring through to continuous synthetic methods. This is achieved by making a selection of small molecules and organic materials – those containing the atoms C, H, N, O and S only. This thesis gives an overview of the specific chemistry relevant to the syntheses undertaken: the Zincke reaction, its pyridinium and anilino products and their use as precursors for the synthesis of useful functional polymeric conductors, and polymethine dyes.

1. Introduction

Mechanochemistry is scientific discipline that has been identified and developed in the last 150 years. It has its roots in mechanical activation which is concerned with structural changes to materials that have been brought about by mechanical energy. Mechanochemistry, in the form of ball milling, uses energy generated by an oscillating or rotating ball mill at high frequencies which gives the milling medium (balls) the kinetic energy to collide with the reagents, walls of the vessel and each other to facilitate chemical transformation. The methodology is solvent-free although solvent can be added, if it promotes reactivity. At the gram scale of synthesis, volumes of liquid added are in the microlitres and is given the term LAG, or Liquid Assisted Grinding.

The influence of mechanochemistry in research and development terms has grown far wider than just to synthetic bench chemists.¹ This brings with it a new lexicon, as experts in different fields such as materials, pharmaceuticals, polymer and crystal engineering may use the same or similar terms to describe a process and in different contexts. Mechanical activation are two such words where better definition would bring clarity. The field is so new that the symbol for ball milling, a form of mechanical activation, was first suggested in 2016 by Hanusa.² The three-ball symbol is used in conjunction with the reaction arrow in mechanochemistry schemes.

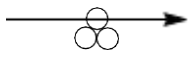
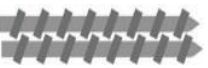
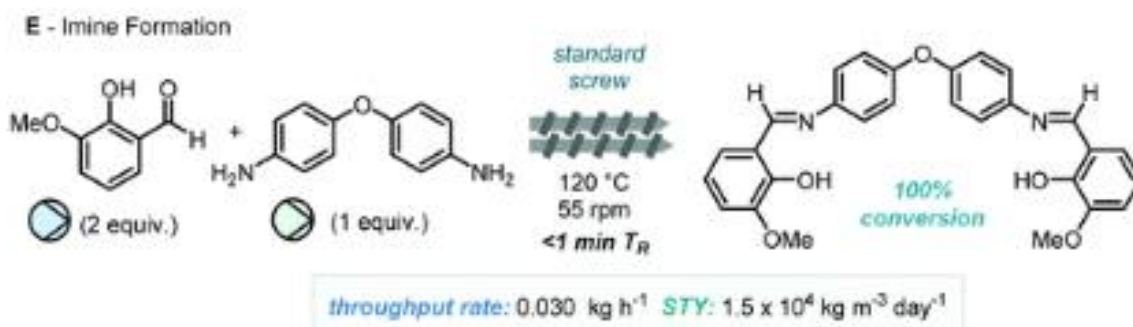
Symbol	Type of mechanical activation	Variables
a	 Vibratory Ball Mill (VBM) Planetary Ball Mill (PBM)	time, t frequency of oscillation, Hz number and size of balls
b	 Twin screw extrusion	time, t screw speed, rpm torque, Nm temperature, T (max. 450°C)
c	 Single screw extrusion	time, t screw speed, rpm temperature, T (max. 250°C)
d	 Twin screw extrusion	time, t screw speed, rpm torque, Nm temperature, T (max. 450°C)
e	 Single screw extrusion	time, t screw speed, rpm temperature, T (max. 250°C)

Figure 1-1 (a) Ball symbol for ball milling taken from Hanusa² *et al.* (b) and (c) screws in place of reaction arrows for extrusion reactions used by Browne³ *et al.* (d) and (e) in this thesis, the screws icon are used with reaction arrows

There is yet to be a formalised symbol for extrusion but it is noted that in the review paper by Browne *et al.* concerning reactive extrusion³, they use twin and single screws shown in **Figure 1-1 (b)** and **(c)** to represent the reaction arrows in between the chemical structures or reagents and products in place of the commonly used black arrow, as shown in **Scheme 1-1**.



Scheme 1-1 Imine Formation taken from³

In this thesis a symbol with screws will be used *in addition* to the reaction arrow, **(d)** and **(e)**, to signify reactive extrusion.

Other terms that have been applied to mechanical activation include grinding,⁴⁻⁸ tribochemistry,^{1,9} Hot Melt Extrusion (HME),¹⁰⁻¹² and mechanical alloying.¹³⁻¹⁶ This is an illustrative but not exhaustive list of the many ways that change can be induced in materials using mechanical force as the primary agent.

Mechanical activation encompasses different processes of which mechanochemistry is a sub-set. **Figure** 1-2 sets out the types of changes that can be achieved using mechanical activation. Where new intermolecular bonds between atoms are formed, this constitutes a chemical transformation and so the term '*mechanochemistry*' is applicable and is used to make the distinction from other forms of mechanical activation. Categories I – V in the table show examples of mechanical activation but only Category V is considered as mechanochemistry.

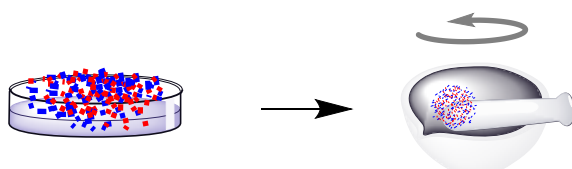
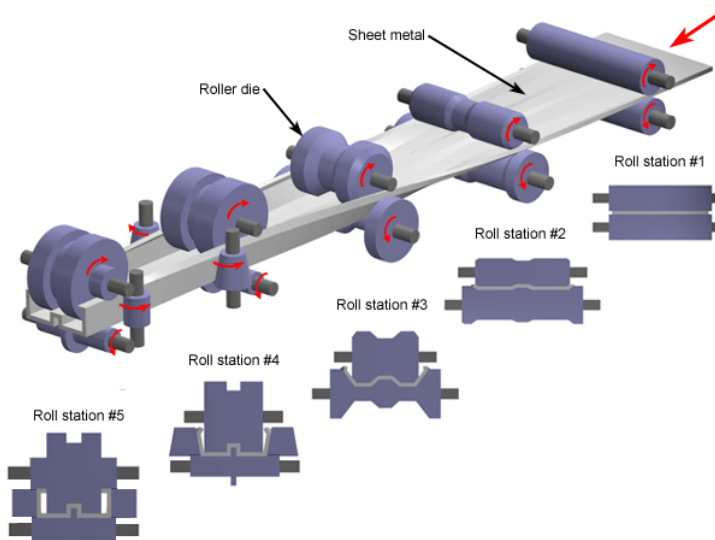
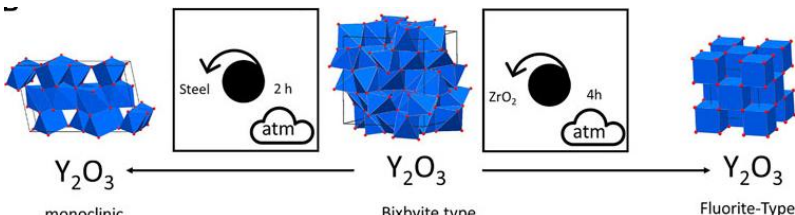
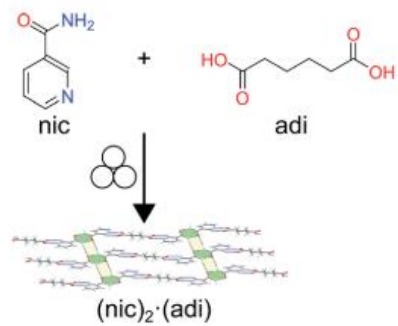
<p>I</p> <p>Milling particles to a small size</p>	
<p>II</p> <p>Generating new or larger surfaces, taken from¹⁷</p>	 <p>Copyright © 2009 CustomPartNet</p>
<p>III</p> <p>Transformations in polymorphic materials, taken from⁴</p>	 <p>Y₂O₃ (monoclinic) ← [Steel, 2 h, atm] Y₂O₃ (Bixbyite type) → [ZrO₂, 4 h, atm] Y₂O₃ (Fluorite-Type)</p>
<p>IV</p> <p>Cocrystallisation Scheme taken from¹⁸</p>	 <p>nic + adi → (nic)₂·(adi)</p>
<p>V Mechanochemistry</p> <p>Reactions via mechanical activation including ball-milling and extrusion</p>	<p>COFs / MOFs / Organometallic complex formation / Small organic molecules / Redox reactions / Ion exchange / Polymerisation / Telescoped reactions / Cascade reactions – all the wide-ranging classes of reaction conducted in solvent-free conditions</p>

Figure 1-2 Examples of the Types of Mechanical Activation of Materials (I) non-reactive milling to smaller particles (II) sheet-forming of malleable metals (III) formation of polymorphic materials (IV) Cocrystallisation (V) Reactive Ball-milling

1.1 Greener synthesis through mechanochemistry

Mechanochemistry is fast emerging as an efficient and cost-effective method for synthesis of novel compounds. Its 'green' credentials are further endorsed by the fact that the process does not require any solvent. Chemical transformations that can be conducted using this solvent-free methodology has been increasingly investigated in recent times^{19–26} and is the primary methodology used in this thesis. Discoveries utilising solvent-free methods include results that are not achievable via solution chemistry, new reactivities, selectivity, and even the trimerisation of fullerenes.²⁷ Mechanochemistry is thus a valuable addition to the methodologies available to the modern synthetic chemist, alongside the more established routes such as solution, thermal, photochemical, flow, microwave, sonochemistry and electrochemical activation.

Organised labour using machine manufacturing and the advent of steam engines in the mid-1800s which shaped the Industrial Revolution meant that technological advances spread widely and quickly between trading partners. For the chemical industries, new innovations also created unexpected problems e.g. early refrigerants and the discovery of a hole in the ozone layer,²⁸ poisonous lead in pipes, paints and petrol, acid rain²⁹ resulting from nitrous oxides and sulfides from the combustion of fossil fuels, pesticides used in agriculture that persist in the food chain and is also a disruptor of biodiversity.³⁰ Air pollution in densely populated areas and plastic pollution in our oceans³¹ are an ongoing topic of public discourse and are highlighted by international climate change conferences organised by the United Nations Committee and are an emotive cause for environmental activism.

There are also 'endangered' elements³² that are used and not recycled in mobile phones leading to sustainability issues. In the 1990s a set of 12 Principles of Green Chemistry,³³ created by Anastas and Warner and published by the American Chemical Society to help address growing problems. Green chemistry, then, is an ongoing attempt to address the problems that chemicals and chemical processes can sometimes cause.

The 12 Green Principles

1. Prevent waste
2. Atom economy
3. Less hazardous synthesis
4. Design benign chemicals
5. Benign solvents and auxiliaries
6. Design for energy efficiency
7. Use of renewable feedstocks
8. Reduce derivatives
9. Catalysis vs stoichiometric
10. Design for degradation
11. Real time analysis of pollution prevention
12. Inherently benign chemistry for accident prevention

Figure 1-3 The 12 Principles of Green Chemistry by Anastas and Warner³³

Mechanical activation through human activity, is as ‘old as the hills,’ evidence of the use of mechanical activation - as a means of grinding husks off grain, for example, by our ancestors has been dated to the Holocene and Pleistocene Epochs³⁴ some 1.6 million years ago. A recent archaeological find by Schimelmitz³⁵ and co-workers has shown human-induced wear on a dolomite cobble when compared to wear due to natural processes of weathering, from the Tabun Cave in Israel. They have dated this as between 300 – 400 ka. With further refinement, the technology took the form of what we recognise today as a pestle and mortar.



Figure 1-4 (L) A cobble used as an abrading tool from the Tabun Cave in Israel taken from³⁵ and (R) a contemporary pestle and mortar

The earliest documented chemical transformation utilising mechanical activation is considered to be the extraction of mercury from its ore cinnabar³⁶ (mercury sulfide). A description of the procedure was written in Theophrastus’ book *On Stones* in the fourth

century B.C. The clearest translation was provided by Eichholz³⁷ - quicksilver (mercury) “is made by pounding cinnabar with vinegar in a copper mortar with a copper pestle.”

1.2 Solvent use in synthetic chemistry

In 2000, Tanaka and Toda³⁸ in their paper, Solvent-Free Organic Synthesis which has been cited over 2,000 times on Clarivate™ made the following observation concerning solvents and the liquid state,

*Crushed grapes give wine by fermentation, but dried grapes do not result in wine. Although milk turns sour and shaking of milk gives cheese, dried milk can be kept unaltered. Similarly dried meat can be stored for a long time, whereas meat soup rapidly putrefies on standing. By observation of these phenomena, one can see that conversion of one material into another one occurs in the liquid state. One of the most famous ancient philosophers in Greece, Aristotle, summarised these observations by concluding, “No Coopora nisi Fluida”, which means “No reaction occurs in the absence of solvent”. Such philosophies had a big influence of the evolution of the modern sciences in Europe, and this provides one historical reason most organic reactions have been studied in solution. **Nevertheless, it is remarkable that chemists still carry out their reactions in solution, even when a special reason for the use of solvent cannot be found [my emphasis].***

The opening paragraphs from a publication by Tanaka *et al.* goes on to detail a plethora of organic transformations in the solid state. Published 22 years ago, and despite the growth in solvent-free methodologies, chemical transformation using solution chemistry continues to be the preferred route as evidenced by searching for solvent-free preparations using ReAxys.

For example, a search on the synthesis of the Zincke Chloride salt **1-1**, discovered in 1904, returned 37 published preparations where only four examples are solvent-free.³⁹ For the di-Zincke salt, **1-2**, ReAxys returned 44 preparations, all of them used solvent with 29 dissolving their starting materials in acetonitrile before heating under reflux.

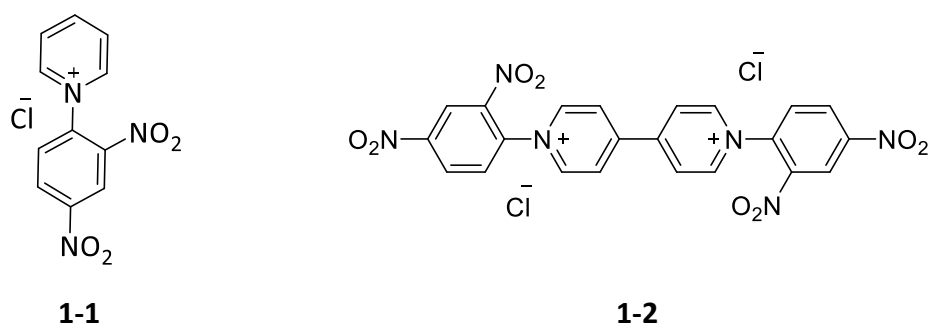
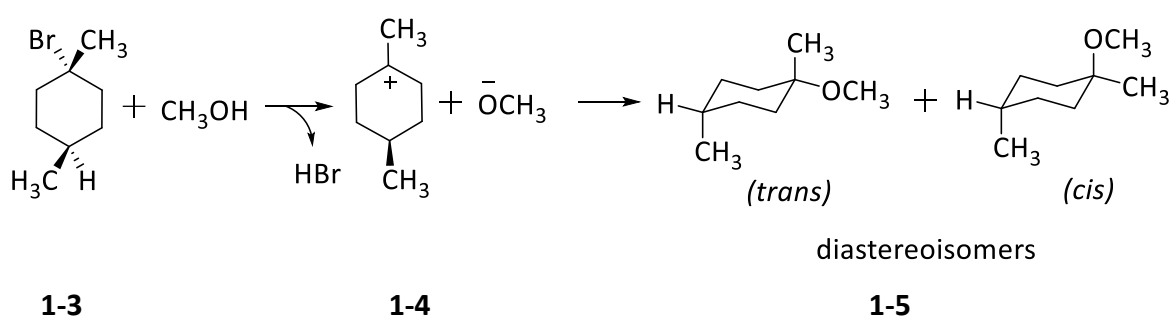


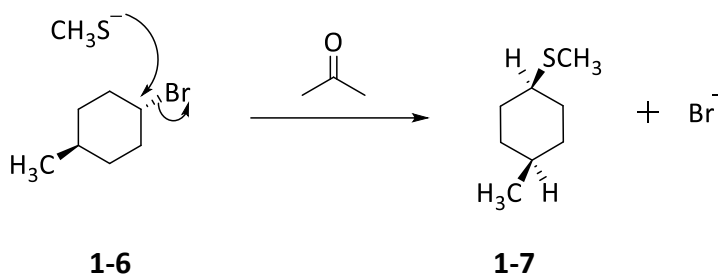
Figure 1-5 The Zincke Chloride salt, 1-1 and the di-Zincke salt, 1-2

There are circumstances, however, such as when solvated ions can affect the stereochemistry of products. For example, reactions can be either S_N1 or S_N2 depending on whether the nucleophile is in a protic or aprotic solvent. In **Scheme 1-1**, a textbook example,⁴⁰ where methanol is the polar protic solvent and the weak nucleophile in this reaction. The electrophile is the tertiary alkyl bromide **1-3** and as the substitution happens at a chiral carbon, the process proceeds with partially racemised products via an S_N1 mechanism to give **1-5**. The substitution can occur from both sides of the carbocation intermediate. Experimentally, however, the conformer with methyl groups in axial (↑↓) positions is energetically the least stable of the possible conformers and so the product has predominantly the methyl in the equatorial conformation, **1-5 (Z)**.



Scheme 1-2 An S_N1 reaction mechanism using the protic solvent methanol

When the nucleophile is the thiolate anion in the reaction as shown in **Scheme 1-3**. The electrophile is the secondary alkyl bromide **1-6**, and both S_N1 and S_N2 mechanisms are possible. However, S_N2 is the favoured pathway because the solvent is acetone which is aprotic and so the reaction prefers to proceed with an inversion of configuration.



Scheme 1-3 An S_N2 reaction mechanism featuring the polar aprotic solvent, acetone

Selectivity through the use of solvent is a useful tool and can give an advantage in designing synthetic pathways. Effects such as these have particular relevance in pharmaceutical and medicinal chemistry.⁴¹

For reactions that do not need a determined chirality in their products, the use of solvent by default in synthesis should be questioned. The belief that solvents are an essential medium for chemical reactions may have developed from Aristotle's false statement, "No Coopora nisi Fluida". This could be a consequence of our collective approach to problem-solving. When we are presented with a difficulty, we often think that the addition of something to a problem will help solve it. There is new research to support the idea that 'People Systematically Overlook Subtractive Changes'.⁴² The notion is also embedded in the language that describes our world. 'Solve' is from the Latin root *solvere* which means "dissolve, loosen or solve" and refers to a changing the physical or figurative state. Together, these are powerful and suggestible ideas with an enduring legacy.

With the exception of solvent-free purification using sublimation, the predominant methods for the removal of unwanted side-products formed during the reaction involve solvent. Purification methodologies such as recrystallisation, precipitation and trituration use far greater quantities of solvent than when used for the initial synthesis. We can reduce the use of the more harmful solvents if we were to move to greener alternatives such as water and acetone. For example, biofuels that are obtained from the shorter lifecycles (tens of years) of available biomass materials compared with fossil fuels, which are formed from very slow geological processes (millions of years). can be assessed to give measurable improvements for waste and sustainability.⁴³

The use of petrochemicals from fossil fuels are already problematic because they are hazardous materials in themselves. After fractionally distilled solvents have been used for the relatively short few hours during a reaction, for example, they then become a waste product which are bound for incineration and ultimately the release of greenhouse gases into the atmosphere. Studies into the least harmful volatile organic chemicals (VOCs) can help us create greener practices for industry.⁴⁴ Qualitative data as shown in illustrate the extent to which creating these solvents through distillation as well as getting rid of them after they have served their purpose consume large amounts of energy. A solvent's Cumulative Energy Demand (CED) can be quantified and when plotted against Environmental Health and Safety (EHS) score. This helpfully shows that solvents such as tetrahydrofuran, formaldehyde and dioxane are particularly high tariff in terms of harmfulness when compared with ethanol and methyl acetate.

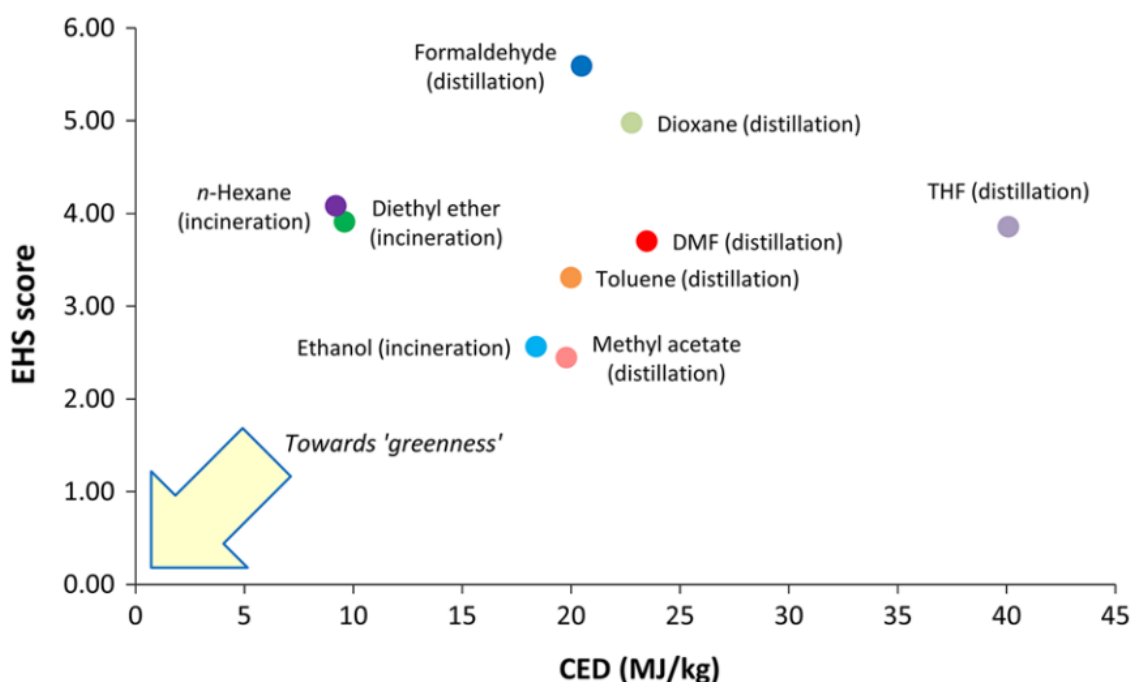


Figure 1-6 Environmental, Health and Safety Score vs Cumulative Energy Demand (MJ/kg) taken from⁴⁴

Biomass derived solvents that are widely available include water, methanol and acetone and the metrics for sustainability⁴⁵ continue to be developed in novel ways including investigating useful solvents derived from natural products.⁴⁶ In combination with solvent-free synthesis, working with greener solvents would bring dual benefits towards the goal

of developing novel functional materials at scale. Global concern about climate change and food security make any enterprise, large or small, that seeks to address these issues an ongoing imperative. We can improve upon efforts to reduce waste and be more judicious with the use of finite resources. Valuable savings in time and energy can result, both should be considered as ‘consumables’, and are not endlessly expendable even within our lifetimes. Doing nothing or simply continuing the planet’s current trajectory is creating unsurmountable problems for climate and food for future generations.⁴⁷

A search on the term ‘Mechanochemical’ in Clarivate’s Web of Science™ database shows 12,400 academic publications (31 October 2021). In the first week as a PhD student (September 2018) a search on the same term garnered *ca.* 9,400 individual items. It is no surprise that the literature on the subject has grown by 30% during this studentship and is a welcome indication of a movement towards improved sustainability and reducing harm to our planet. Using a solvent-free technique such as the ball mill for chemical synthesis is a constructive step towards addressing these issues. Furthermore, by developing this further and using other solvent-free, mechanochemical methods such as reactive extrusion to show that useful products can be produced at scale. This would be desirable outcome and could have an impact on the current drivers of climate change and global warming.

1.3 Vibratory (VBM) and planetary ball mills (PBM)

The ball-mill has given the bench chemist a greater energetic advantage over the pestle and mortar.²⁰ There are a number of types of ball-mill: oscillating (vibratory/shaker/mixer), planetary, magnetic, gravity, and roller mills.



Figure 1-7 (L) Retsch MM400 (VBM) and (R) Retsch PM100 (PBM) pictures taken from⁴⁸

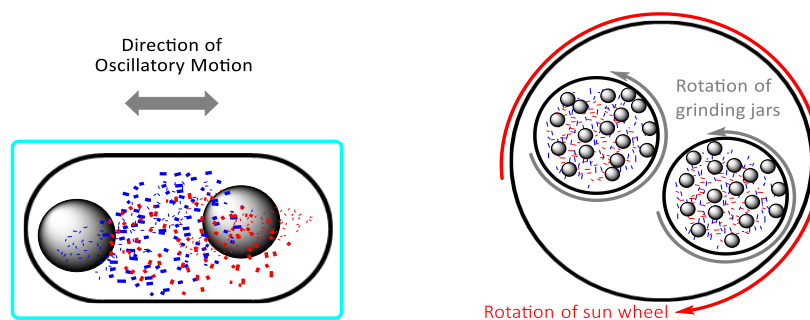


Figure 1-8 The modes of action for (L) VBM and (R) PBM

Because of their differing modes of action, they may produce different forms or proportions of products from identical starting materials. Instruments for ball-milling include the oscillating Retsch MM400 and the planetary Retsch PM100. These are shown in **Figure 1-7**, the simple harmonic motion made by the machine makes the balls inside the jars move horizontally, left to right and back again, up to 30 times per second. The planetary ball mill shown on the right involves rotation of the reactor vessels containing the milling balls contrary to the rotation of the base sun-wheel. They are easy to operate: the vessel(s) are loaded with stoichiometrically-accurate, weighed reagents and milling media in the form of a milling ball and any other auxiliary items, the apparatus are then secured, and the machine is set to oscillate or rotate at the desired frequency and for any set time.

1.4 Ball charge and reagent requirements for reactive VBM

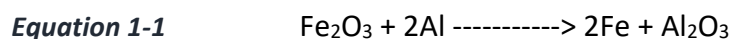
There are a number of machines available for ball milling, the model used in the majority of this work is the Retsch Mixer Mill 400 or MM400. They recommend milling loads according to their Ball Charge table (see Appendix 1). Milling conditions as outlined by the table allow for the optimisation of the environment for reactions to occur. The 'loading' of the jars will therefore affect the experiment's outcome. The recommended loading is approximately 1/3 sample or reagents and 1/3 ball charge. This means that the remaining third should be space to allow movement/collisions of the contents. The milling machines were originally designed to grind down larger particles into finer powders and the Ball Charge table reflects this; they do not provide instructions for use as a method for reactive synthetic chemistry. The more recent and increasing use of the ball mill for

mechanochemistry has brought attention to unintended (and unwanted) effects from ball milling. For example Chua⁴⁹ *et al.* reported that their ball milling experiments using sulfur-doped graphene resulted in impurities from the ball-milling apparatus. This results in particles of the grinding media being present in the reaction mixture. There are pros and cons to this scenario – experiments requiring the catalytic effects, for example, of copper or palladium would have auxiliary reagents present in the mixture. Using copper⁵⁰ or palladium⁵¹ balls however, has been shown to be effective in mechanochemical reactions and has been given the name mechanocatalysis.

Each reaction will have unique energetics giving rise to exotherms (or endotherms) which will have an effect on overall reactivity in the vessel as well as the heat energy generated by the collisions themselves. Studies concerning temperatures achieved in the ball mill by Takacs⁵² undertook to look deeply into this question in all its complexity, using a variety of materials including investigating highly exothermic reactions and ignition within the ball mill where they are described as ‘miniforging’ events.

In mechanochemistry, it is instructive to think about the action of the milling media and their impact on reagents inside the reaction vessel and to consider the energy transfers that are occurring in the system. It can be shown that with each impact of the milling balls, thermal energy is derived from the kinetic energy of bringing the balls together using a thermal imaging camera.

Using 2 x 50 mm chrome steel ball bearings and knocking them together with a sheet of paper in between, shows that heat is generated with each impact. In **Figure 1-9 (a)** warm spots are shown in yellow and the cooler surfaces are purple. This can be repeated to show a chemical transformation when using a rusty ball and a ball covered in aluminium foil, **Figure 1-9 (b)**. When these are forcefully struck together – there is a highly exothermic metal displacement reaction:



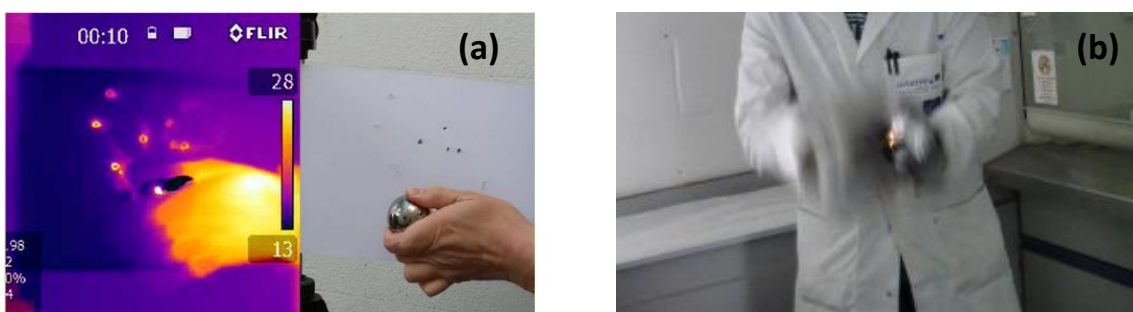


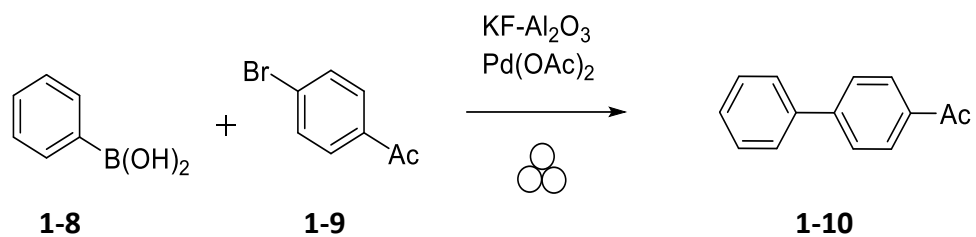
Figure 1-9 (a) Thermal Image of two balls colliding and (b) Orange sparks of molten iron from striking thermite balls

Orange-yellow sparks of molten iron can be seen when the balls are struck. In bulk, this reaction is known as the thermite reaction,⁵³ temperatures required for its initiation are over 600 °C and once above its activation energy, the reaction can reach temperatures of 3000 °C. Thus giving an insight into the high amounts of thermal energy that can be achieved by the action of colliding spheres, and gives an appreciation of the heat transferred during collisions when agents are vigorously shaken in a VBM.

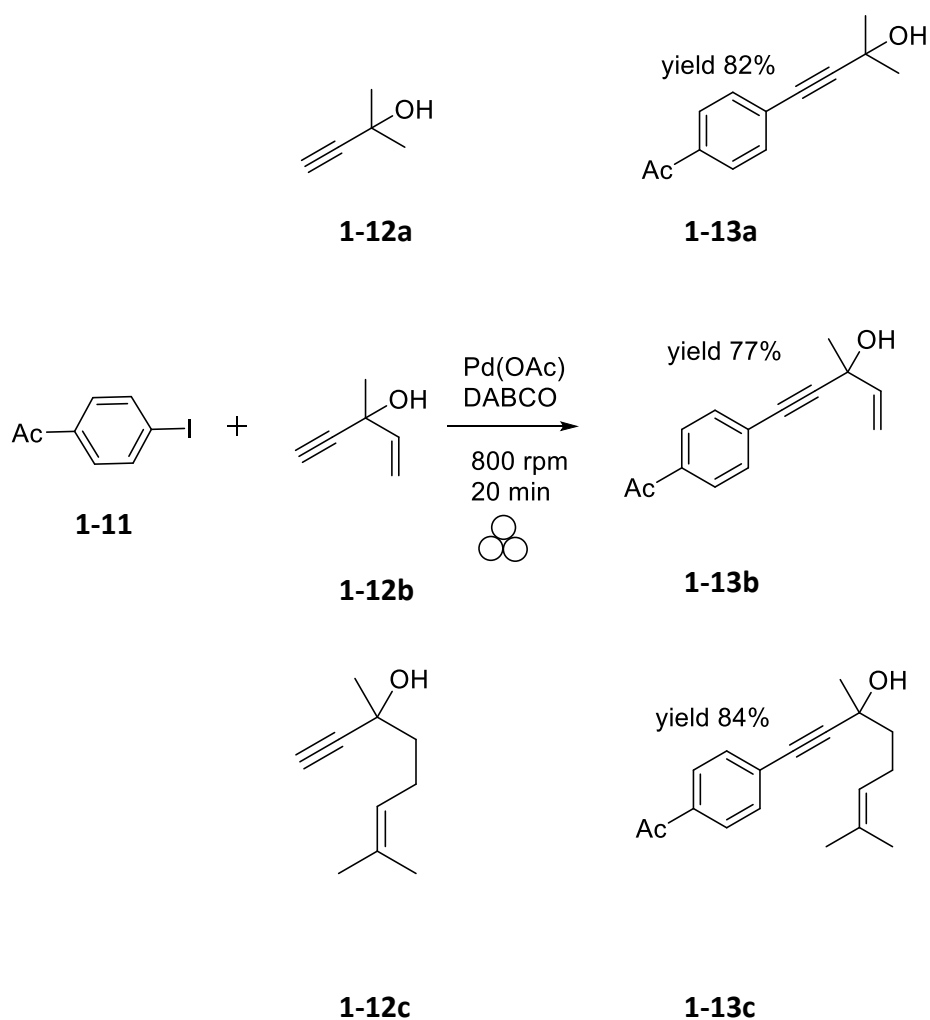
Understanding the practicalities of using a VBM in organic chemistry synthesis also includes understanding its limitations and how these drawbacks may be addressed. We investigate reaction-monitoring and production at scale for the reactions involving the Zincke salt. A literature survey for the possibilities for using VBM in organic synthesis gives plenty of examples of different types of transformation that is possible. A selection of small organic molecule synthesis in VBM establishes its versatility. An illustration of the breadth is discussed in the following section.

1.5 State-of-the-art mechanochemistry in organic synthesis

VBM investigations for Named Reactions have been reported including the Suzuki-Miyaura cross-couplings **Scheme 1-3**, and the Sonogishira,⁵ shown in **Scheme 1-4**, showing the reaction of *p*-iodoacetophenone **1-11**, and 3 different hydroxy-acetylenes **1-12a-c**. These gave good to excellent isolated yields of **1-13a-c**, (77 – 84%) with short milling times (20 min) using a Pd catalyst.



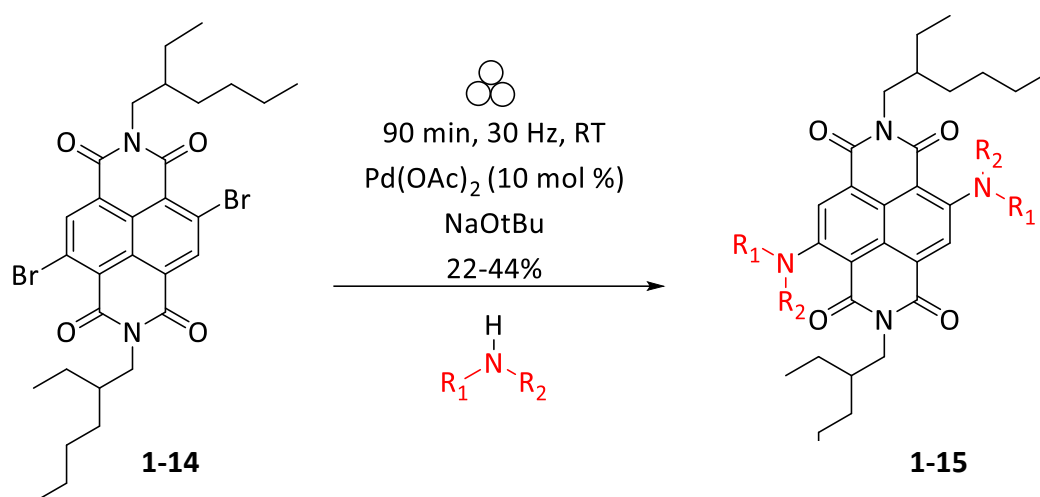
Scheme 1-4 Suzuki-Miyaura cross-coupling reaction in a VBM



Scheme 1-5 Sonogishira

coupling in a VBM

The mechanistic, Palladium-catalysed route is described by Gazvoda *et al.*⁵⁴ **Scheme 1-6.**



Scheme 1-7 Greenland group's Buchwald-Hartwig amination of NDI, **1-15**

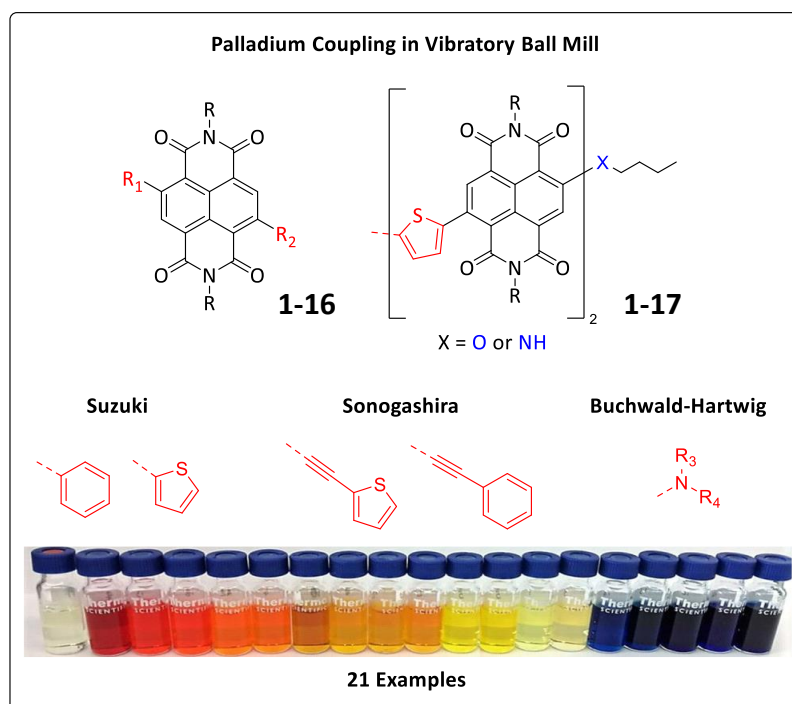
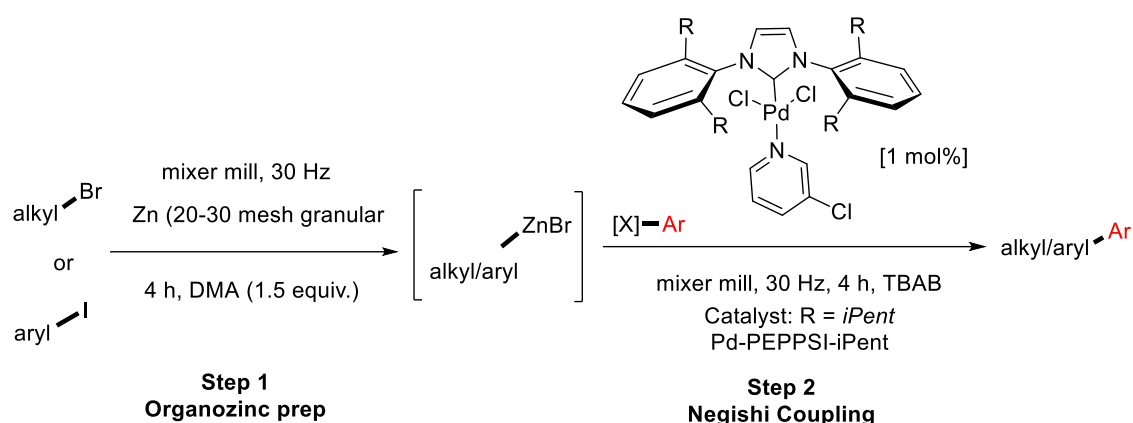
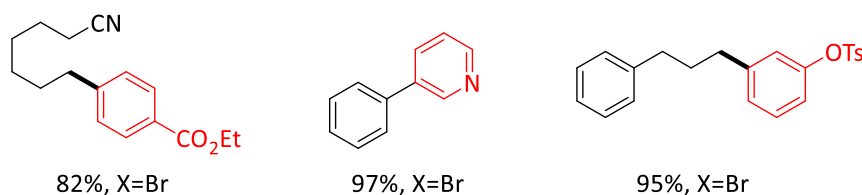


Figure 1-10 Greenland group's three Palladium coupling reactions in VBM, picture adapted from⁵⁷

Good to excellent yields were also reported for the 2-step Negishi coupling using a palladium catalyst, Browne⁵⁹ et al. were able to demonstrate that these reactions had broad substrate scope for both C(sp³)-C(sp²) and C(sp²)-C(sp²) couplings and that this form of the synthetic process is tolerant to many important functional groups.



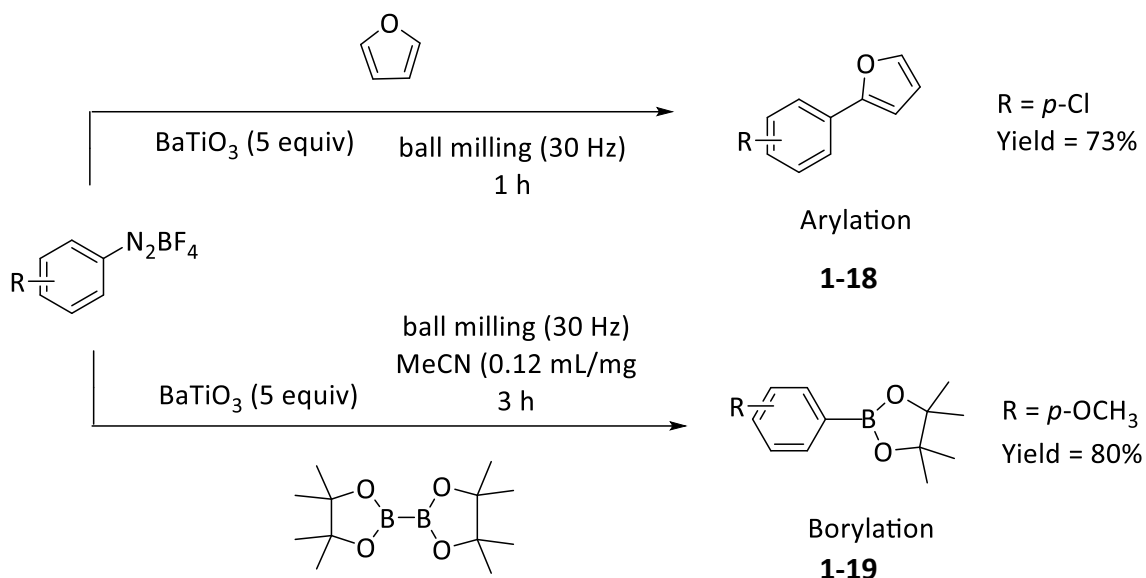
41 examples with quantitative yields including:



Scheme 1-8 Negishi Cross-Coupling in 2 steps using VBM

A survey of ball-milling in 2017 by Achar *et al.*,⁶⁰ concerns only small organic molecules, keeping to a single subject area of chemistry was sufficient to furnish a 25-page review. Beyond the mechanosynthesis of small organic molecules are a vast number of reported reactions that can be organised according to the materials produced. Reports of ball-milled materials by 'Mechanoredox,'⁶¹⁻⁶³ were discussed by Kubota⁶⁴ *et al.* As well as successful arylation **1-18** (yield 73%) and borylation **1-19** (yield 80%) in VBM they were able to recycle the BaTiO_3 catalyst.

It is not just small molecules that can be synthesised in the ball-mill, but also polymers that are designed as useful or functional materials.⁶⁵⁻⁷¹



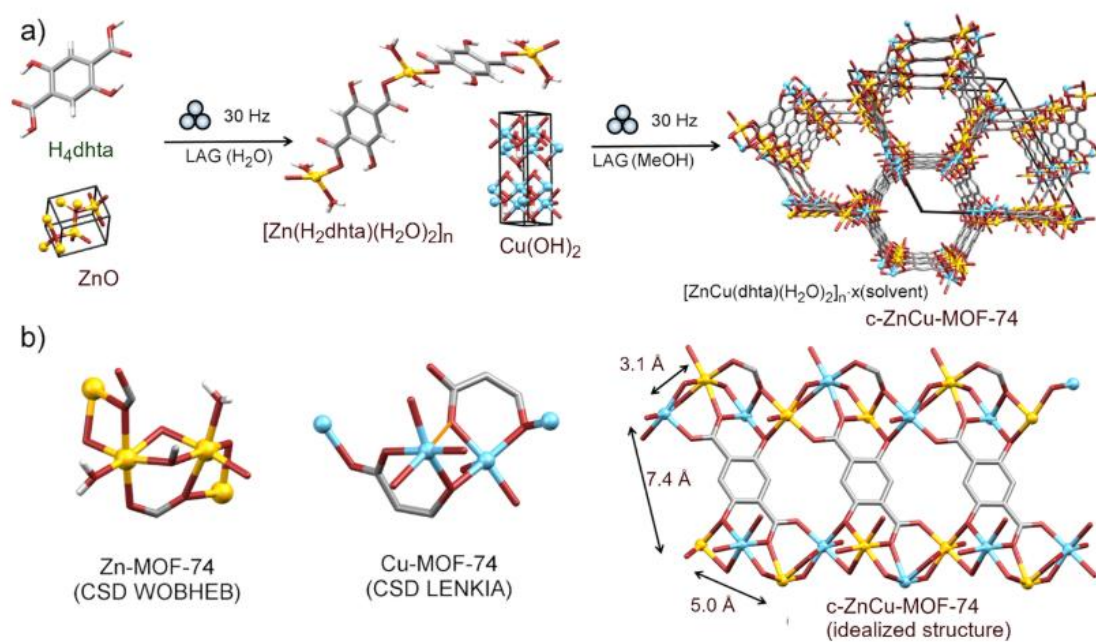
Scheme 1-9 Arylation and Borylation in VBM, scheme adapted from⁶⁴

1.6 Functional materials in mechanochemistry

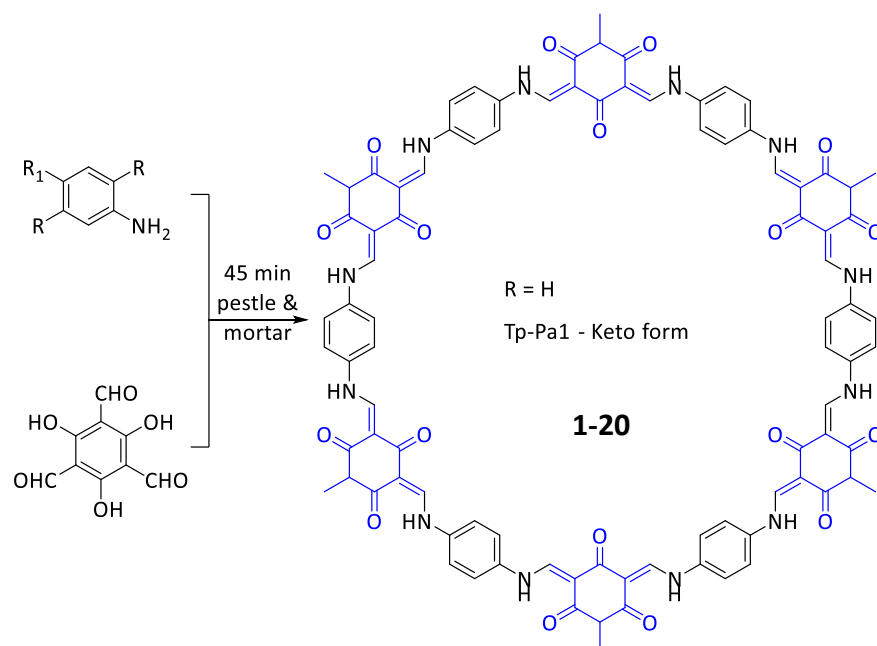
Developments in mechanochemical synthesis has expanded into a great number of areas tackling both known and novel species including covalent and metal organic frameworks (COFs and MOFs).^{18,72–75} An example by Stolar⁷³ and co workers is a MOF designed as a catalyst to remove the greenhouse gas, carbon dioxide, by reduction to methanol. In design, intent and manufacture, this ticks a great number of boxes in the list of 12 Principles of Green Chemistry and all the more laudable for using ball-milling in two steps and minimal solvent.

Such reactions are well investigated in the solution, but solvent-free methods add a new dimension.^{76–81} Using a pestle and mortar, Biswal *et al.* synthesised covalent organic frameworks of the form **1-20**, shown in

Scheme 1-11 frameworks with these types of topography are known as isorecticular. It has been shown that organic ligands of different sizes, but with a common geometry/symmetry can be used to generate COFs (and MOFs) of related topologies, but with expanded pore sizes and volumes.⁸²



Scheme 1-10 Synthetic Route to the functional MOF-74 as a catalyst for a selective CO_2 reduction reaction to methanol, taken from⁷³



Scheme 1-11 A mechanochemical synthesis of Tp-Pa1 – Keto Form, **1-20**

1.7 Monitoring reaction progress

Most syntheses are done in solution, this is undesirable because the over-use of solvents is unsustainable and environmentally destructive. The manufacture of functional materials at scale, such as organic conducting polymers to satisfy global demand using greener methodologies could bring many benefits including reducing waste and saving time.^{83,84} An understanding of what is happening in the ball mill is key to developing experiments for novel chemical syntheses. Alongside successful syntheses, ingenious experiments have been undertaken to describe how the processes combine to effect a chemical transformation. A chemical reaction typically requires an activation energy to occur. In solution this is achieved by heating the sample either on a hotplate or in a microwave, for example. Traditionally reactions can be monitored in real time using TLC by sampling the reaction without needing to halt the process. However, using opaque vessels like the milling jars, it is not possible to monitor the progress of a reaction using standard techniques as access to the reaction mix requires stopping the reaction to take a sample. In doing so, this changes the reaction conditions. Optimising each experiment is usually restricted to changing milling time, frequency of oscillation (1-30 Hz) and the number/size of balls used in the vessel and only being able to sample the reaction at the end of a predetermined period. Efforts have been made to understand what is happening inside the milling jar while it is being activated, including in-situ studies achieved during milling.

Kulla⁶⁰ *et al.* combined their direct measurements of temperatures during milling with *in situ* monitoring using Raman Spectroscopy, **Figure 1-11**. The data showed that the mechanical impact produced only low increases in temperature (c. 4 K) when the sample milled was SiO₂ (grey trace) but reaction exotherms were responsible for the greater part of the temperature rise when theobromine **1-1** was milled with oxalic acid **1-2** (black trace) – a process which created conditions for cocrystallisation. The simultaneous recording of the Raman spectra during the milling shows the corresponding stretching of the C-C assigned to the oxalic acid **1-22**, and theobromine's **1-21** C-N and C=O bonds and their respective vibrational stretching bands. It also indicates the time of the start of the reaction at 11 minutes where, on both the temperature profile and the Raman spectra coincide.

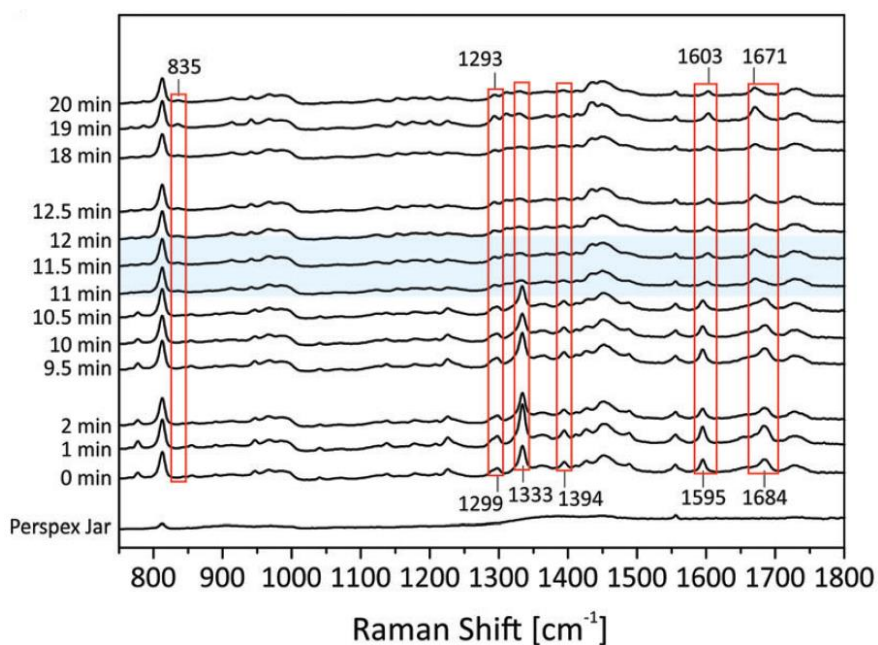
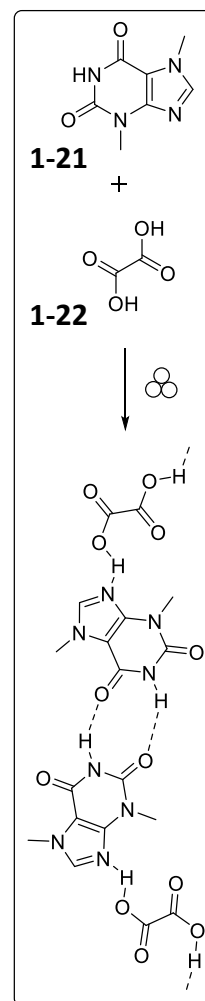
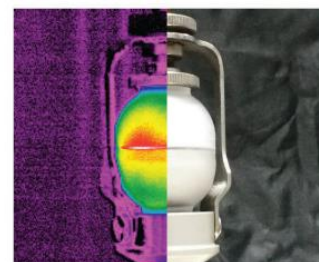
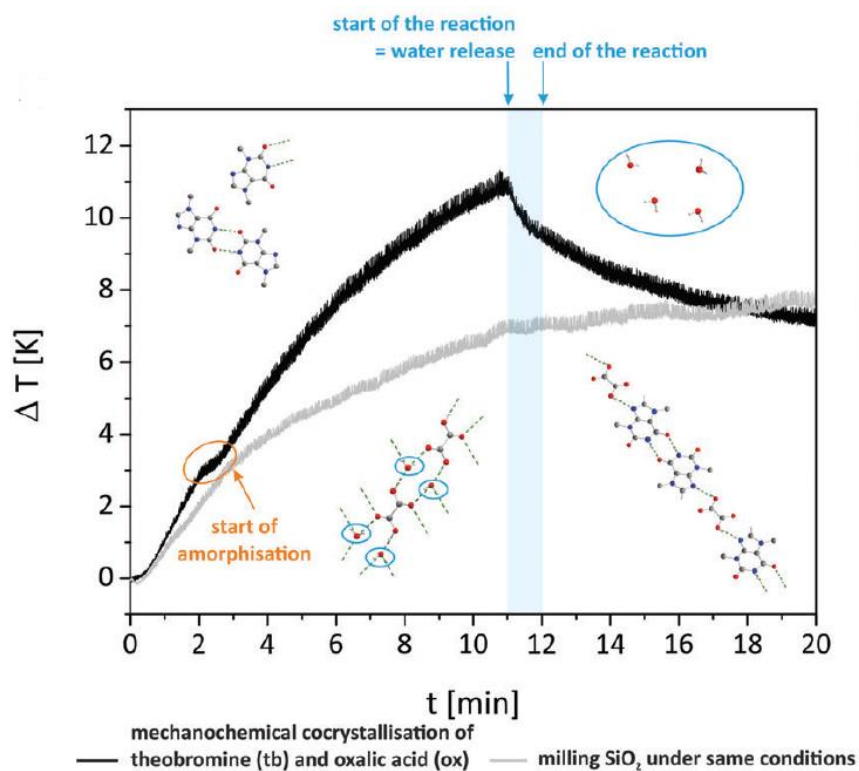


Figure 1-11 'Temperature development in ball mills during synthesis', pictures taken from⁸⁵

More recently Schiffmann⁸⁶ and co-workers used a home-built, solid state ¹H NMR probe fitted with a miniaturised milling vessel with internal volume of 0.5 mL, with capacity for ca. 150 mg of reagents and 50 x 1 mm \varnothing milling balls, **Figure 1-12**.

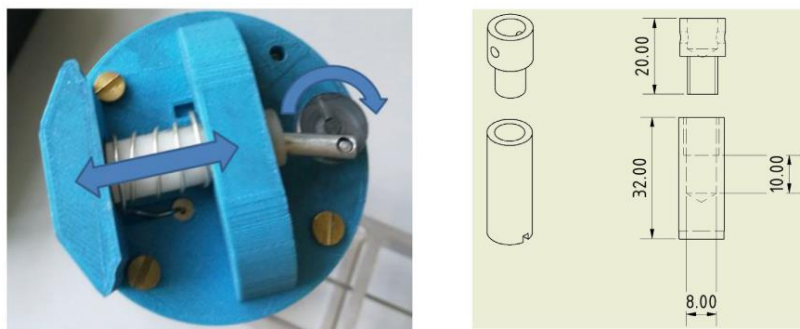


Figure 1-12 (L) 3D printed mini-milling jar fitted inside the NMR coil with eccentric wheel attachment and (R) the dimensions in mm of the milling jar, taken from⁸⁶

They were able to quantitatively follow the product evolution of the following metathesis reaction:



Using data showing conversion at different stages with solid state ³¹P NMR it can be seen that product formation is greater with increasing numbers of balls but there is not a linear relationship between product formation and number of balls; using 100 balls produced 15% more product than 50, by the end of the milling time.

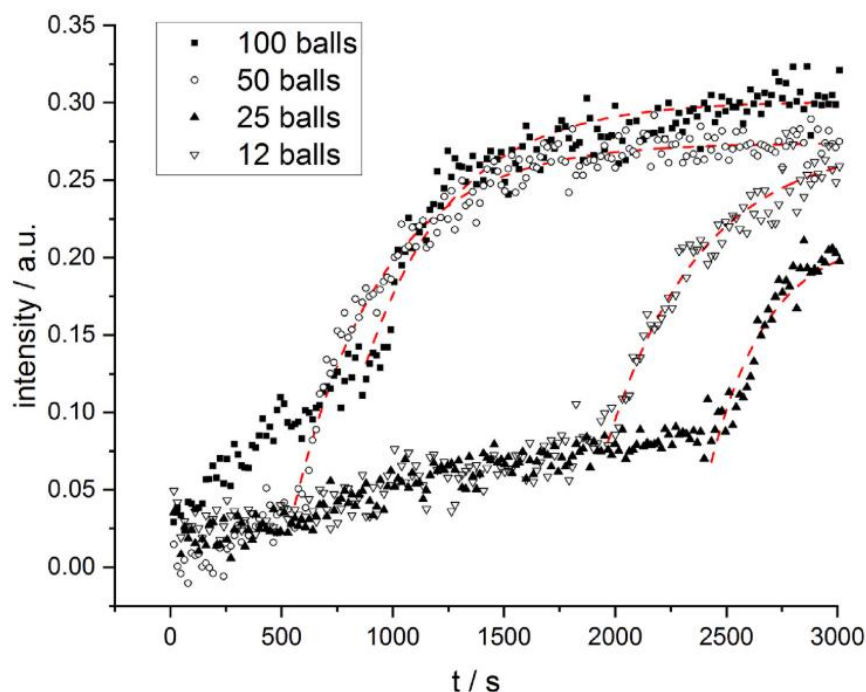


Figure 1-13 Product evolution as a function of time and vibrational frequency the number of balls was kept constant at 50. All curves were recorded through repeated single pulse acquisition measurements with a time resolution of 16 s. The rate constants of the exponential fits amount to 393 s^{-1} and 143 s^{-1} for 25, and 35 Hz, respectively, taken from⁸⁶

However, the rate of evolution of the product was faster using 50 or 100 balls compared with that of using 12 or 25 balls. After 1200 s of milling the 12 or 25 balls experiments showed a quarter of conversion compared to that of milling with 50 or 100 balls. In addition, MAS NMR investigations on the final reaction mixture confirmed a reaction yield of 89% in a typical example. Enthalpy and friction,⁸⁷ rheological studies, and work on cohesive states^{24,88} have all contributed to our growing knowledge of the processes occurring inside the ball mill. The scope of ball milling as a mode of chemical synthesis is considerable and growing but it is limited to volume capability defined by the size of the milling vessels in which they are conducted, much in the same way as batch processing in solution. Scalability through continuous synthesis of molecules and materials is the key to improved efficiency in solvent-free manufacturing processes.

1.8 Continuous reactive extrusion - twin screw (TSE) and single screw (SSE)

Continuous extrusion is a process that produces materials, such as polymers and small molecules, in an uninterrupted manner. Flow chemistry is also a continuous methodology; however, it is necessary for the reagents to be in the liquid phase for the process to work and this often requires solvent. Reactive extrusion⁸⁹ – was identified in 2019 by IUPAC as one of ten chemistry innovations that would change the world.

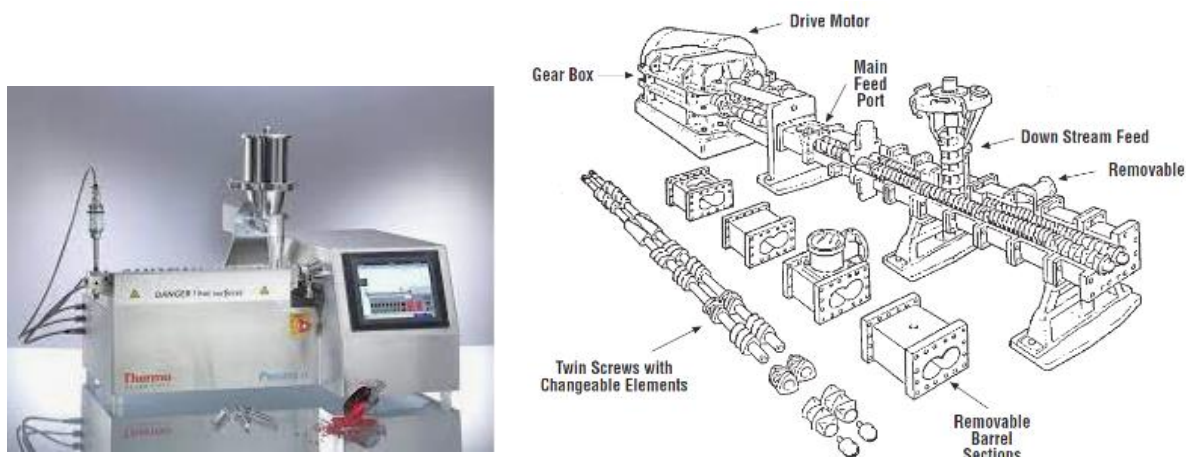
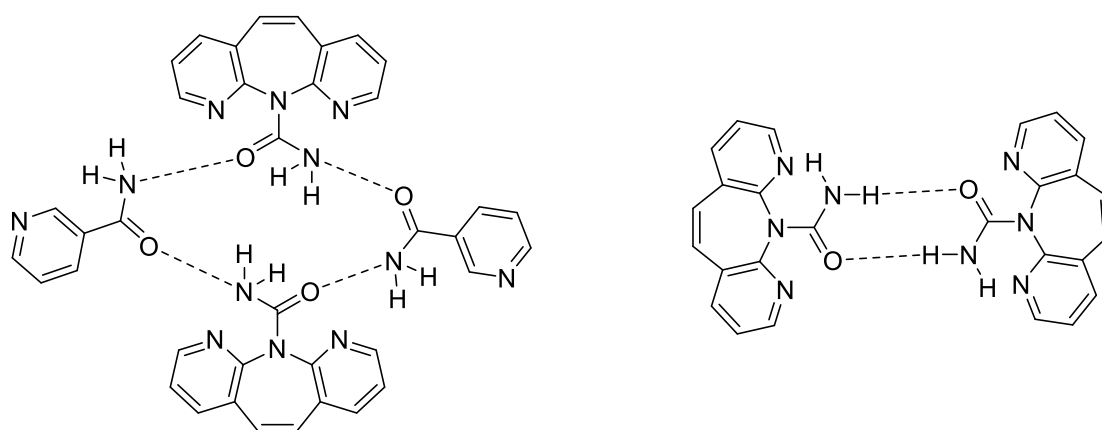


Figure 1-14 (L) ThermoFisher Process 11 Twin Screw Extruder, taken from⁹⁰ (R) Schematic for a twin screw types of extruder, picture from⁹¹

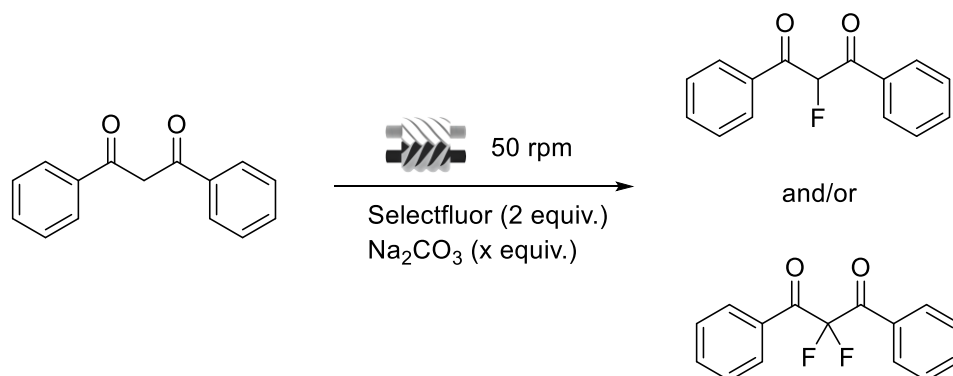
At the time of writing, this emerging field is sufficiently new that there are only a handful of academic papers published^{92–98} concerned with chemical transformation using an extruder. Therefore, mechanochemical reactions are well-placed for investigation using extrusion technology for the scaling-up of successful ball milling reactions. Establishing that mechanochemistry is scalable⁹⁹ in the form of extrusion brings additional benefits. Not only is the process solvent-free but also continuous. The limiting factor to transformation of starting materials to useful product/commodity being the how much starting material is loaded into the extruder. Extrusion technology is well established in the food and pharmaceutical industries,^{10,100–103} polymers^{104–106} and materials^{107–109} fabrication, producing many tonnes of product in shorter processing times, having been optimised the process to suit. The extrusion process itself has many significant advantages over traditional batch-type, non-continuous technologies and its prodigious use in fabrication reflects this. TSE is already widely used in pharmaceutical formulation but is mostly concerned with Hot Melt Extrusion.^{12,103,110–112}

Boksa¹¹³ *et al.* were able to demonstrate matrix-assisted cocrystallisation (MAC) where Carbamazepine (CBZ) was used as the model drug, nicotinamide (nic) is the coformer, and Soluplus[®] is used as the matrix. The product of extrusion contained 80:20 (w/w) cocrystal:matrix.



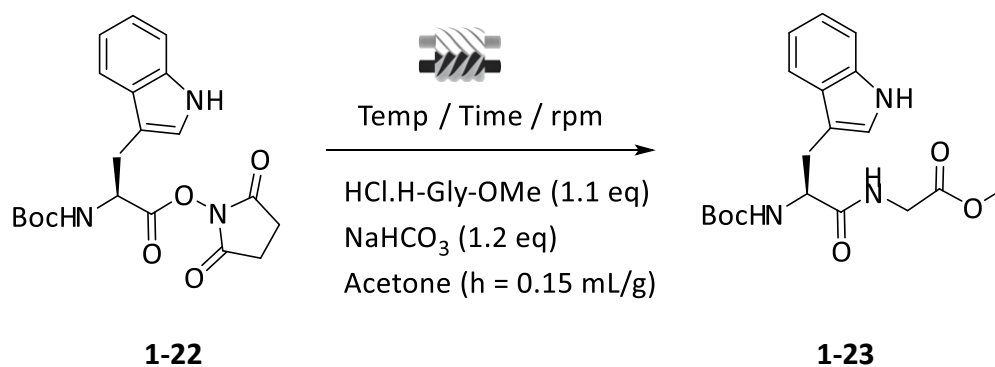
Scheme 1-12 Matrix-assisted cocrystallisation (MAC) in the simultaneous production and formulation of pharmaceutical cocrystals using HME. Hydrogen bonding (dashed lines) synthons for (L) the CBZ-Nic cocrystal and (R) CBZ, polymorphic form III

In contrast to published work using HME, there are but a handful of publications on Reactive Extrusion using Twin Screw Extrusion (TSE), these include Browne⁹⁴ *et al.*, which showed the first solvent-free organic fluorination synthesis.



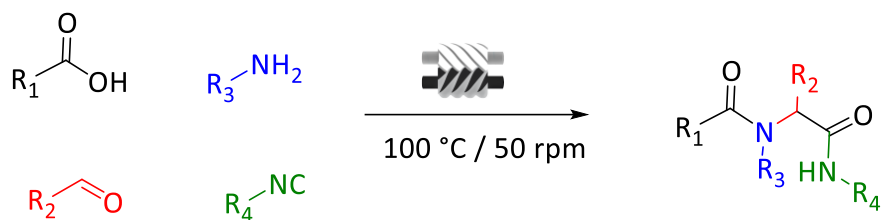
Scheme 1-13 Twin screw extrusion TSE fluorination with Selectfluor

Yeboue¹¹⁴ *et al.* with peptide couplings using TSE to couple HCl.H-Gly-OMe with sodium hydrogen carbonate and acetone to give the coupled peptide Boc-Trp-Gly-OMe **1-23** as described in **Scheme** 1-14. These reactions were not solvent-free but the extrusions were performed using reagents that are CMR-free (CMR = Carcinogenic, Mutagenic or Reprotoxic).

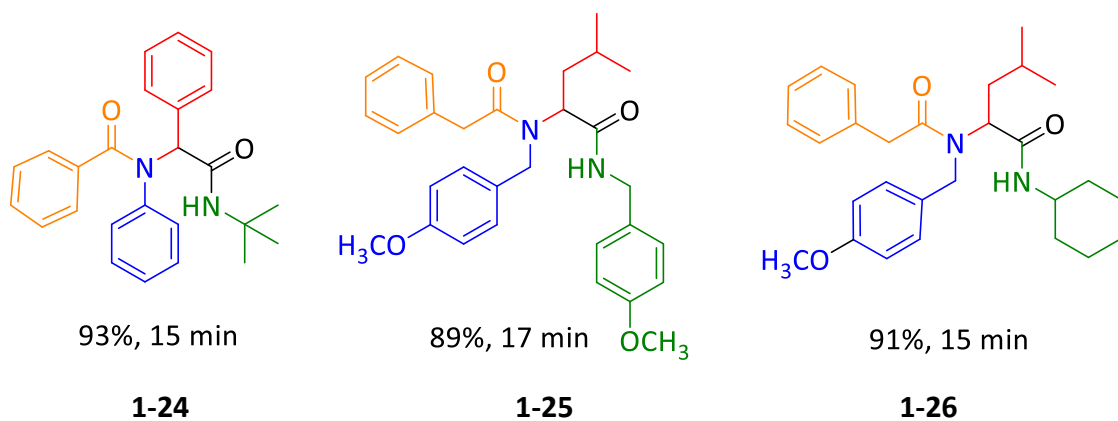


Scheme 1-14 Twin screw extrusion for a peptide coupling reaction

There is also the multi-component Ugi Reaction.⁹⁷ Their work describes the synthesis of the Ugi reaction of four components in one-pot. Using solvent and catalyst-free TSE they were able to show excellent yields for **1-24**, **1-25** and **1-26**.



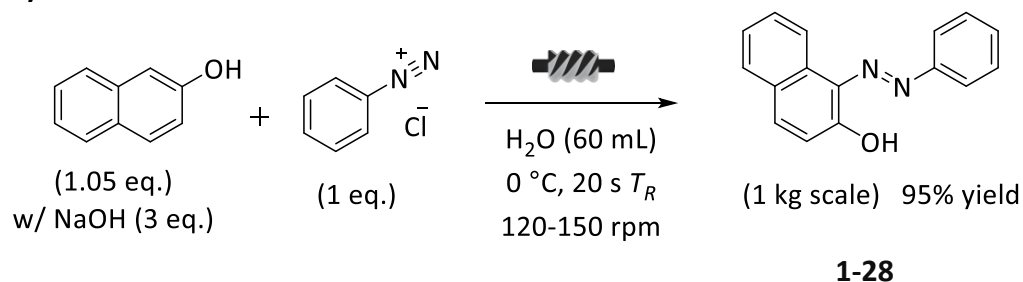
Three of the 9 Ugi products, with yields and reaction times reported by El-Remaily *et al.*



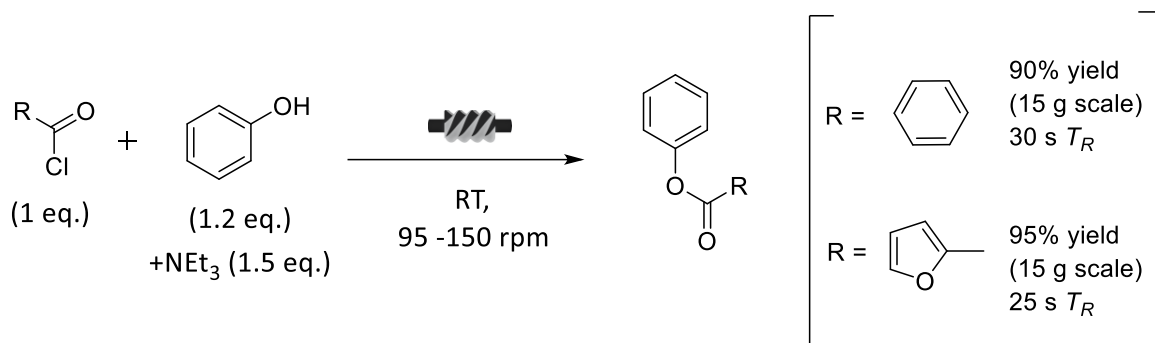
Scheme 1-15 Twin screw extrusion for the multi-component Ugi Reaction adapted from⁹⁷

These reactions have excellent atom economy and are a good example of Green Chemistry in practice as shown in the mechanism showing the reaction of three reagents, a ketone or aldehyde, an amine and an isocyanide to achieve the target bis-amide, **1-27**.

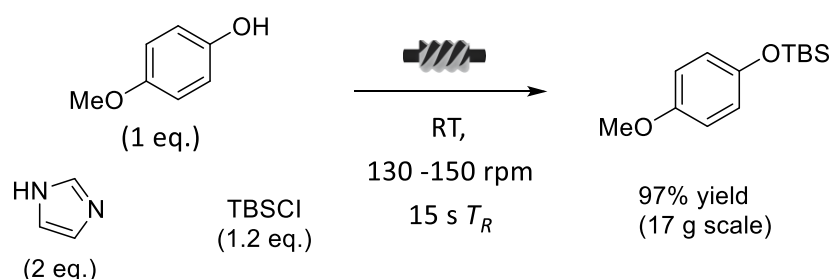
(a) Sudan dye



(b) Acylation



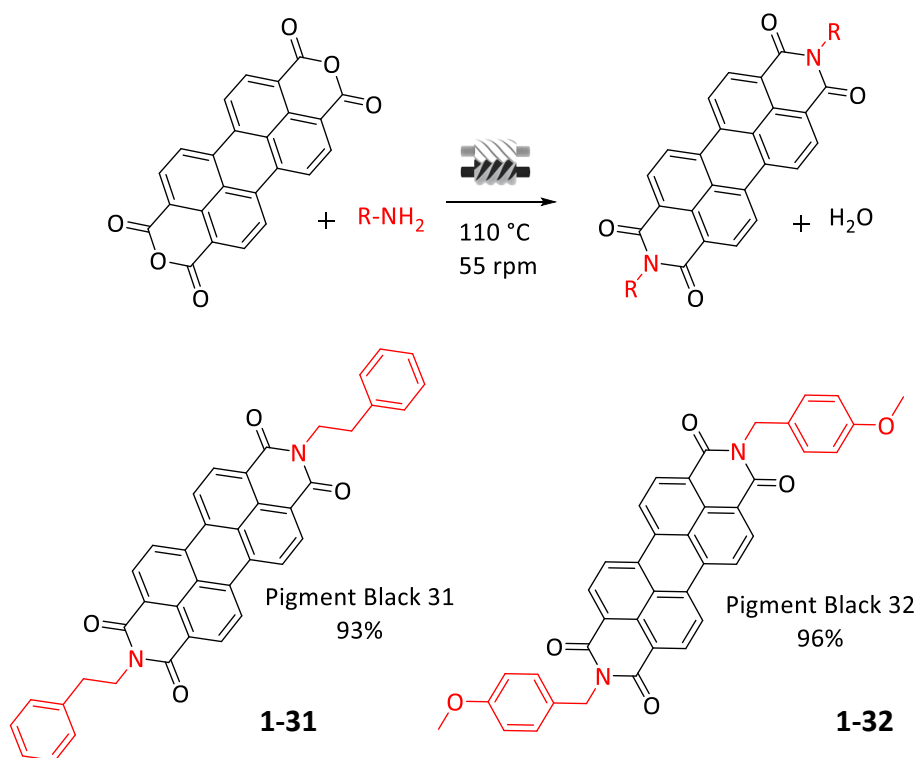
(c) TBS Protection



Scheme 1-17 SSE experiments for small organic molecule targets **1-28**, **1-29**, **1-30**

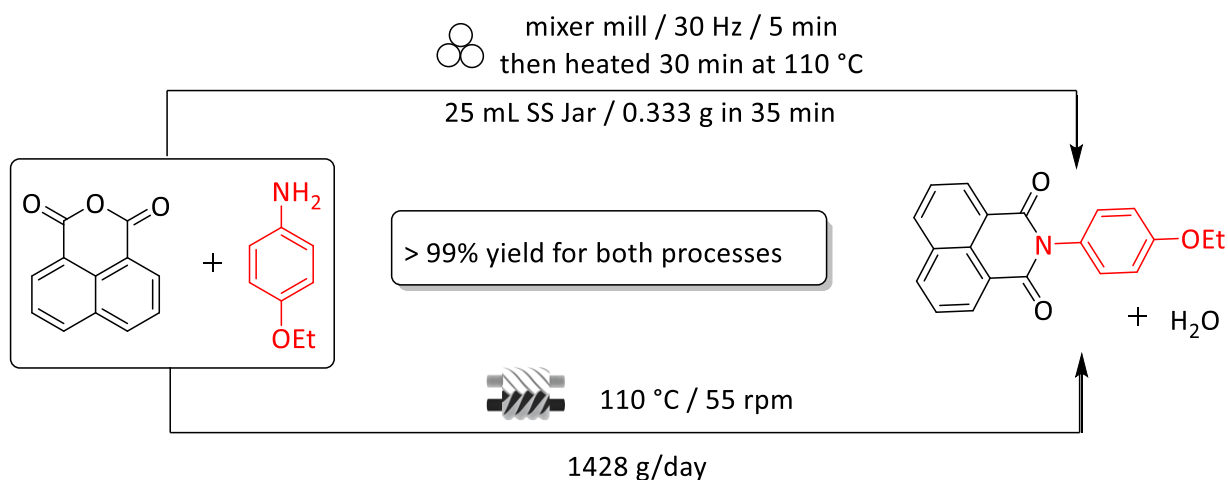
These are noteworthy firsts, not only for being a greener methodology for chemical synthesis, but innovations such as these are in their infancy. As such, this gives us opportunities to investigate more complex reactivities through extrusion which is an exciting proposition with a high possibility of fruitful outcomes. The transition from VBM to extrusion was made by James's Group⁹⁹ via MOF synthesis and batch processing.¹¹⁵ They followed this with a method for the synthesis of commodity dyes, namely various naphthalic imides and perylene diimide (PDIs). Water is the sole by-product generated and so the dyes were obtained quantitatively without the need for excess amine reactant or

purification. **Scheme 1-18** shows the commodity dyes manufactured were Pigments Black 31, **1-31**, and Pigment Black 32, **1-32** at a rate of 1.5 kg day⁻¹, which compared favourably to current solvent-based methods by 1-2 orders of magnitude. Twelve different perylene dyes were synthesised via TSE.



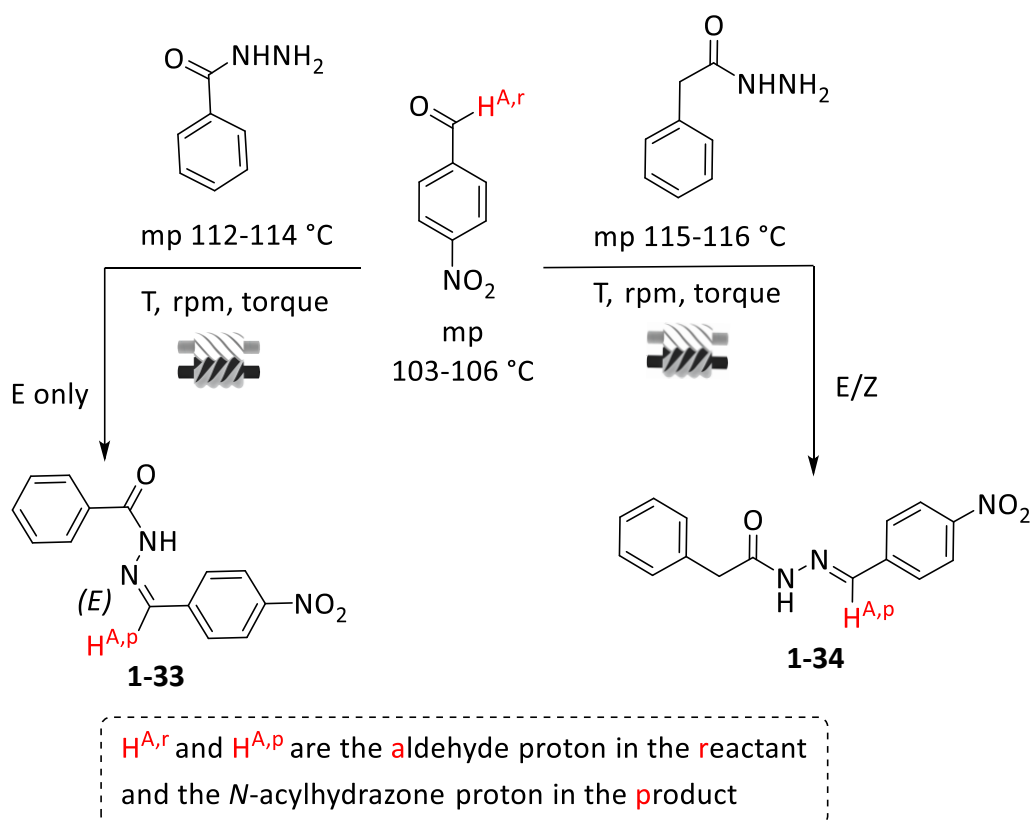
Scheme 1-18 General Scheme for the Twin Screw Extrusion of Perylene Dyes and the structures of Pigment Black 31, **1-31** and Pigment Black 32, **1-32**

They were also able to show the transference from ball mill to TSE in a set of experiments showing the relationship between temperature and conversion at different scales.



Scheme 1-19 The 'Beat and Heat' method from ball milling compared with Extrusion

In 2020 James⁹⁶ and co-workers were able to use continuous extrusion for the synthesis of active pharmaceutical ingredients (APIs). Twin-screw extrusion (TSE) was used to synthesize the hydantoin-based APIs **1-33** and **1-34** employing minimal or no solvent. Post synthetic work up was not required therefore solvent-heavy purifications were not an issue. This work is a first, demonstrating that solvent-free synthesis can be conducted in a continuous manner for pharmaceutical products.



Scheme 1-20 Model reactions for TSE synthesised hydantoin-based APIs **1-33** and **1-34**

Regarding scalability - although work on continuous methods of chemical synthesis is just starting, with throughput measured in kg/day.¹¹⁶ Extrusion techniques are a mature technology in many industries where they are used in polymer processing and food production on a tons/day scale.

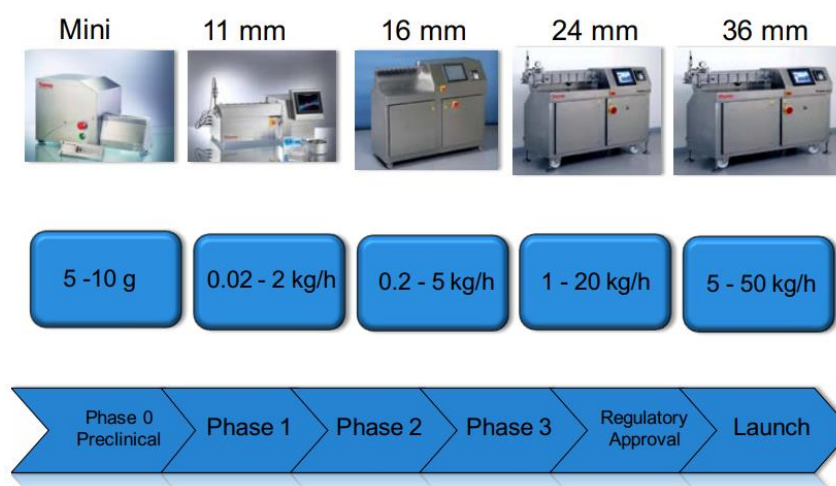


Figure 1-15 Thermo-Scientific™ Pharma twin-screw extruders for HME showing different screw sizes in mm, picture taken from¹¹⁶

Pertinent to this work are the combined discoveries of scale-up to 1.4 kg per day for the continuous extrusion of commodity dyes but also the reactive extrusion of APIs using this solvent-free technique. These are realities that make large advances towards sustainability were it to be translated into other areas of industrial-volume chemical synthesis, namely agrochemicals and polymeric materials.



Figure 1-16 Parallel Lima TSE Photos from¹¹⁷

Articulation of the Twin Screw Extruder has produced very sophisticated feats of chemical engineering, but complex mechanical processing may create more problems and so a consideration of simplified process could be a way forward. Published papers in chemical synthesis by extrusion are mostly of the TSE variant while Single Screw Extruders (SSE) have been used for the first time for reactive extruders as recently as 2019.⁹⁸ Innovations such as have been described in this chapter confirm that IUPAC had correctly predicted that

Reactive Extrusion is one idea that will change the world. This work considers all aspects of solvent-free synthesis, from feasibility, scalability all the way through to sustainability using standard borosilicate glassware, different materials in VBM and PBM and explores extrusion technologies in new ways.

1.9 New chemical targets - electro active materials by mechanochemistry

In the last fifty years, developments in the electronic properties of polymers have seen a proliferation of research in conductive organic scaffolds and this has stimulated the growth of diverse new technologies in material science. Discoveries that have driven progress include the idea – in the 1960s – that non-metals can be semi-conductors. However, the understanding that only metals are conductors of electricity while plastics are non-conductors persisted into the '70s until 1976 when Alan MacDiarmid¹¹⁸ and co-workers showed that Polyacetylene can conduct electricity almost as well as metallic copper. They reported on the high conductivity in iodine or bromine-doped Polyacetylene ushering in a new era with revolutionary ideas in conducting plastics. In 1990 Burroughs¹¹⁹ et al. published their discovery of light-emitting diodes based on conjugated polymers in Nature. Post-millennium, conducting polymers became central to a vast array of functional materials and technological advances; new applications ranges from bio-sensors in health settings through to consumable electronics, from screen displays, medical implants, solar cells, OLEDs to flexible electronic circuitry.

All structures in conducting organic polymers have fully conjugated units without this, electron charge cannot flow through an uninterrupted π -system. Some examples are shown in **Figure 1-17**. The fused heterocyclic structure of polyfluorene does not include fluorene atoms but the name is a reference to this polymer's interesting fluorescent properties.

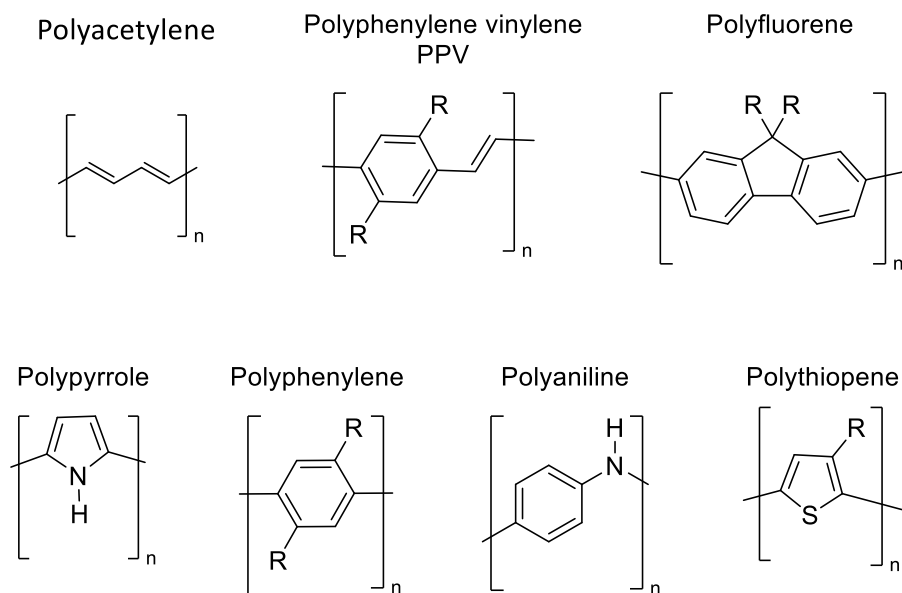
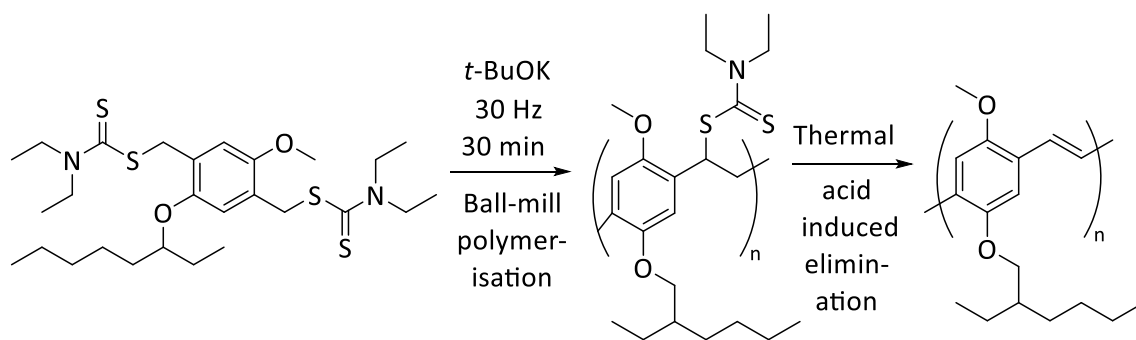


Figure 1-17 Monomers for a selection of fully conjugated polymer systems

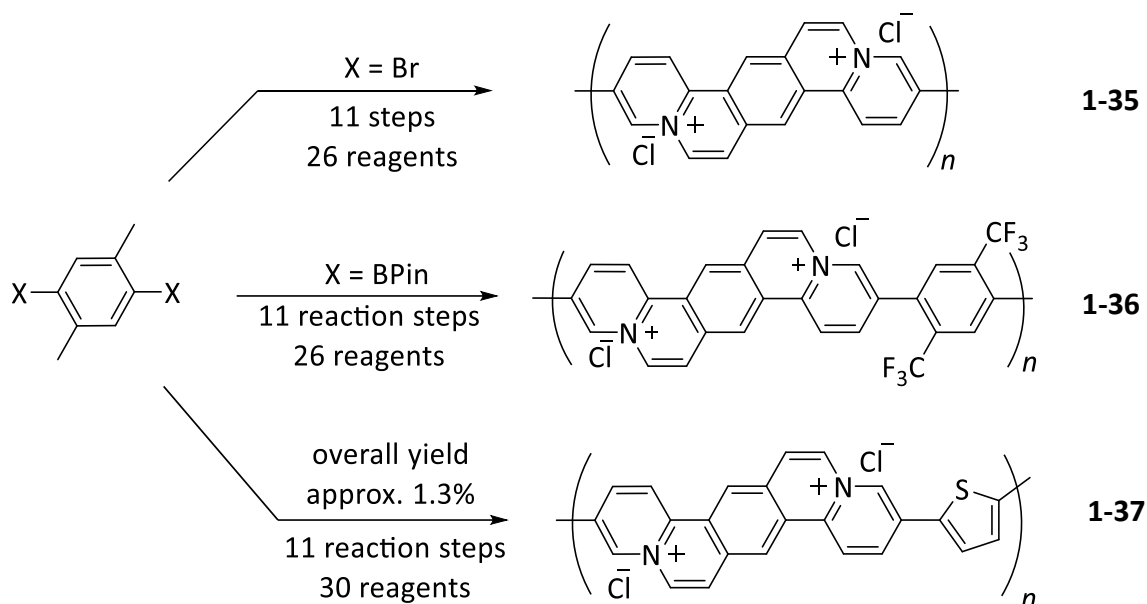
As discussed in the previous sections, presently, mechanochemistry has been restricted to medicinal chemistry applications, with materials synthesis less widely covered. Very recently, the areas of mechanochemical synthesis of polymers has been reviewed.^{83,84} However, the synthesis of electronically conductive materials remains underexplored. A notable exception to this is the work of Ravnsbæk¹²⁰ and Swager's investigation into the mechanochemical synthesis of Gilch¹²¹ monomers to a polymer with a maximum of $M_n \sim 40\text{k Da}$, using the ball mill.



Scheme 1-21 Gilch polymerisation by VBM¹²⁰

Preceding the ball-milling of the Gilch polymerisation, an extensive synthetic investigation was undertaken by Swager¹²² and Izuvara where they accessed conjugated polymers with high conductivity in the form of poly(pyridinium phenylene)s, **1-35**, **1-36**, **1-37** in **Scheme 1-22**. Using N-heterocyclic electron-deficient aromatics, this proved to be a time and

resource intensive process involving a 11-step solution synthesis beginning with an aryl halide.



Scheme 1-22 Solution syntheses of poly(pyridinium phenylenes) – a fully conjugated π system

The Greenland Group showed, **Figure 1-18**, that fully conjugated organic chains formed thin films with conductivities that increased with increasing molecular weight.¹²³

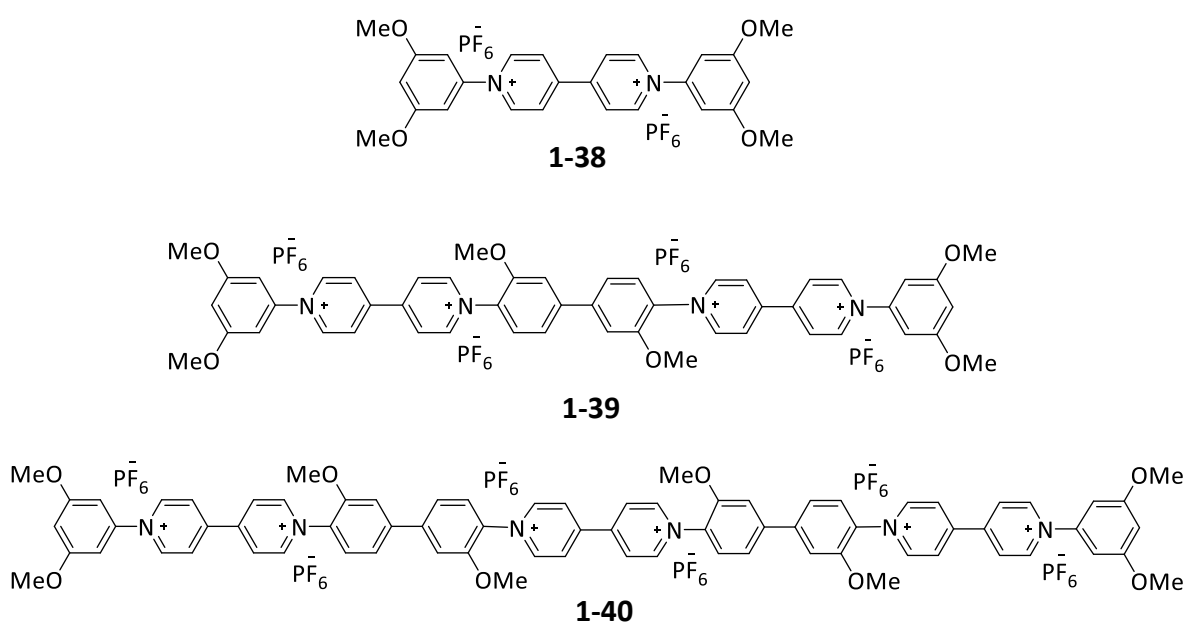
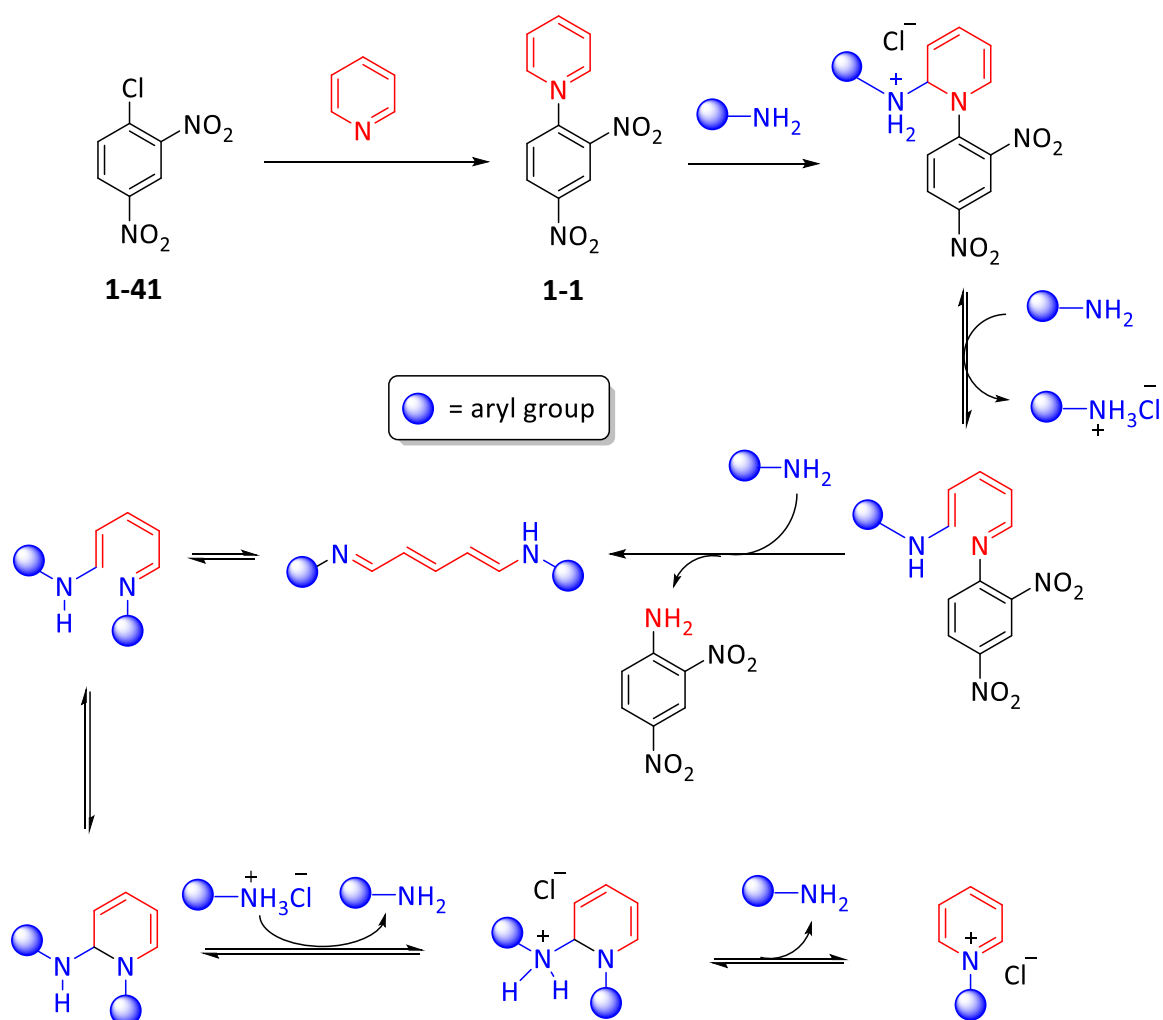


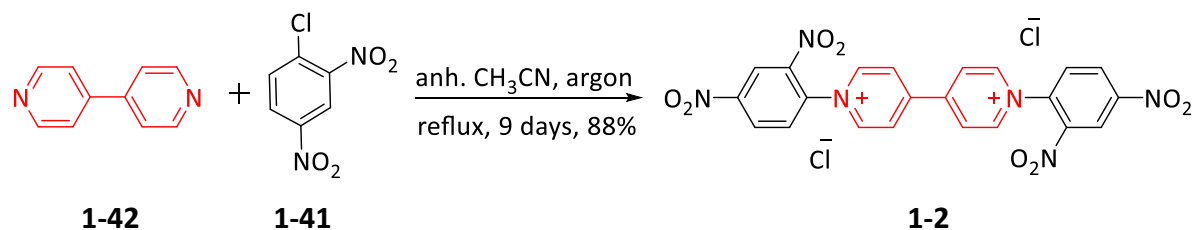
Figure 1-18 A unimer **1-38**, dimer **1-39**, and a hexacationic trimer **1-40**

The formation of these fully conjugated chains is made possible through the unusual mechanistic route known as the Zincke Reaction¹²⁴ which was discovered in 1904. It has been of interest to investigators for over a century because of its remarkable multi-step substitution reaction as shown in **Scheme 1-23**, which can be summarised as the Addition of the Nucleophile, Ring Opening, and Ring Closure in the nucleophilic attack on ring systems or A_NRORC .¹²⁵ This is best illustrated by colour-coding the heterocycles as seen in the scheme. The mechanism is unusual in that when completed, the nitrogen atom in the substituting aniline (blue) replaces the nitrogen atom in the pyridyl ring (red) of the Zincke salt **1-1**. For viologens, this mechanism can be used for bipyridine in place of the pyridine, giving the closed-ring product.



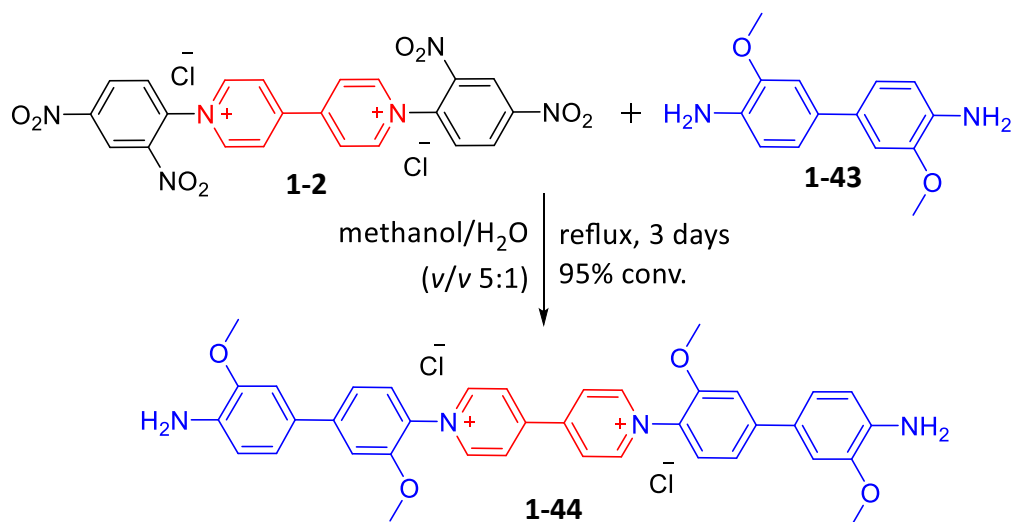
Scheme 1-23 Colour-coded Mechanistic Scheme for the Zincke Reaction

Greenland's oligomers were achieved through a set of sequential Zincke reactions, beginning with the di-Zincke **1-2** salt which can undergo substitution by nucleophilic anilines, its synthesis is shown in **Scheme 1-24**.



Scheme 1-24 Synthesis of the di-Zincke salt, **1-2**

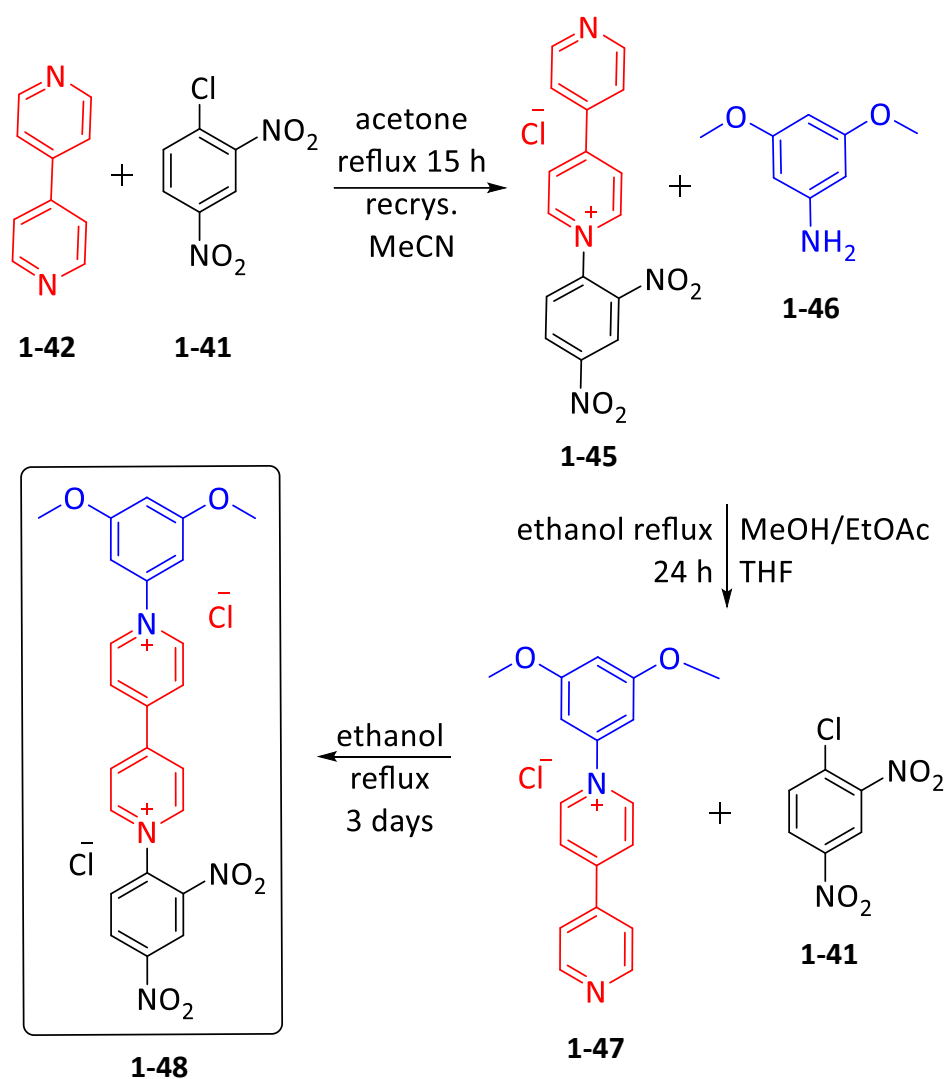
The di-Zincke salt **1-2** can undergo nucleophilic substitution with anilines, under reflux for 3 days in methanol and water to give **1-44** (95%).



Scheme 1-25 Reaction of the di-Zincke salt, **1-2** with the di-aniline **1-43**

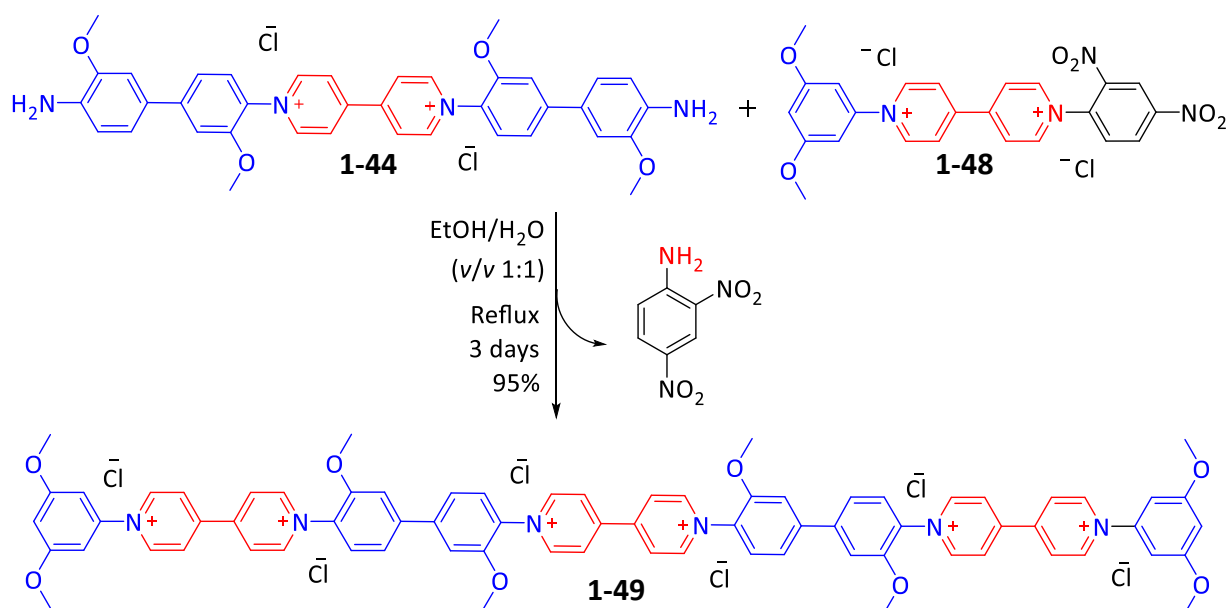
A 3-step reaction sequence is required for the formation of an asymmetric Zincke salt **1-48**. Its synthesis is shown in **Scheme 1-26**. First the bipyridine **1-42**, is reacted with an equimolar quantity of 1-chlorodinitrobenzene **1-41**. In solution this is achieved using acetone and heating under reflux for 15 h and the product **1-45**, is isolated by recrystallisation from

acetonitrile. **1-45** is then reacted with 3,5-dimethoxyaniline **1-46** under reflux in an ethanol solution for 24 h. A further S_NAr reaction of the purified product **1-47** with 1-chlorodinitroaniline **1-41**, in ethanol solution requires three days to achieve conversion to the desired asymmetric Zincke salt, **1-48**.



Scheme 1-26 Multi-step Zincke Reaction to give an asymmetric Zincke salt, **1-48**

A separate, fourth reaction step uses the di-amine **1-44** where both ends are nucleophilic and can substitute the dinitro-aryl group of the asymmetric Zincke salt **1-47**. When 2 equivalents of **1-47** are used, a double substitution is possible and gives **1-48**, a hexacationic species with full conjugation. Once again – it is a three day reaction under reflux in a bisolvent mixture of ethanol and water, to give **1-48**, **Scheme 1-27**.



Scheme 1-27 Formation of hexacationic species **1-49**

The route published by Greenland¹²⁶ and co-workers requires extended reaction times and significant quantities of solvent and excess reagents. Therefore the new solvent-free synthesis of a targeted set of monomeric, dimeric and trimeric viologen containing molecules were selected as the first target of this thesis.

1.10 Overview of the aims and scope of thesis

The two main objectives of the work in this thesis were principally to make useful molecules through their design and synthesis giving them desirable functionalities for specific commodities: solar cells and NIR imaging dyes. Secondly, to achieve their syntheses with as small a chemical footprint as possible so that they are sustainable in the long term, and to minimize both materials and energy resource requirements.

The Zincke Reaction – by dint of its unusual reaction mechanism - has been useful to exploit functionally for both electronic and fluorescent possibilities. Continuing the discoveries by Greenland Group using the di-Zincke salt **1-2** as the precursor for iterative substitutions to build chains of conjugated molecules with conductive properties **1-49**. In Chapter 2 we explore solvent-free, 'greener' methods of synthesis of the viologen unit and scope the steric and electronic effects of varying substrates.

An understanding of how reactions occur in the VBM was explored by the simple heating and stirring of the neat reagents, resulting in solvent-free synthesis for a range of reactions which included multi-gram scale ups for key starting materials. Attempted solvent-free synthesis for each molecule is shown with green dashed arrows in **Scheme 1-28**.

In Chapter 3 we discuss the mono-Zincke salt **1-1** and the formation of pentamethine or Cyanine 5 (Cy5) dyes and examine their molecular structures through X-ray crystallographic data. We develop the imaging dye possibility in Chapter 4, with a series of experiments using both the Cy5 and the mono-Zincke salt **1-1** to make a heptamethine or Cyanine 7 (Cy7) NIR dye.

Additionally, we explore the options for scale-up for our experiments deploying a Planetary Ball Mill (PBM), (125 mL) with a larger capacity than a Vibratory Ball Mill (VBM), (25 mL) before trying a reactive extrusion experiment, with the assistance of ThermoFisher, using their Process 11, a twin screw extruder (TSE). From our findings for the scalability using the reactions of the Zincke salt **1-1** we look at a different extrusion strategy for our work.

In Chapter 5 – we follow the successful synthesis of a Cy7 molecule by showing for the first time, the solvent-free synthesis of Indocyanine Green (ICG), an active pharmaceutical ingredient (API) and a commodity Cy7 dye, by using reactive extrusion in SSE. ICG is an FDA approved imaging dye and is used as an *in vivo* diagnostic tool. It is sufficiently important for IP to be currently sought for its continuous production.

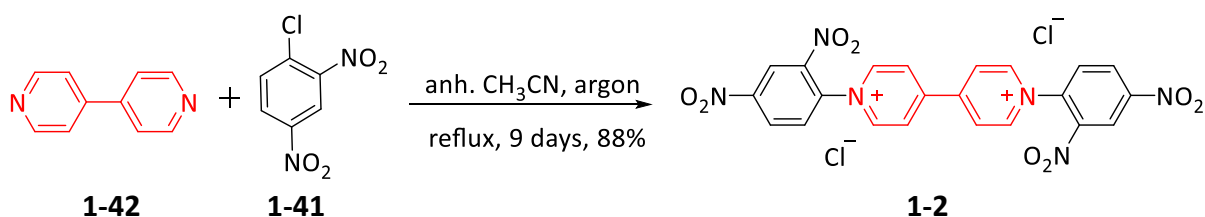
Chapter 6 concludes the thesis with full experimental details for all the molecules synthesised in this work. A bibliography and appendices are provided at the end.

Results and Discussion

2. Towards the synthesis of viologen containing oligomers

2.1 Synthesis of viologen containing molecules with varying end groups

The nucleophilic substitution of the di-Zincke salt has been successfully achieved using classical solution synthesis by Greenland and co-workers. The use of solvent-free methodologies had not been investigated and so initial VBM experiments were conducted to assess the feasibility of this approach. The key intermediate in the Greenland synthesis of molecular wires is the di-Zincke salt **1-2** by the reaction of equimolar quantities of 4,4'-bipyridine **1-42** and 1-chloro-2,4-dinitroaniline **1-41**. Attempts to make the di-Zincke salt **1-2**, using mechanochemistry were unsuccessful despite varying oscillating frequency, a change of reaction vessel and number of balls used. Therefore, it was decided to make a large quantity of **1-2** using a standard solution synthesis to provide enough material for further study.¹²⁷ The synthesis of **1-2** was conducted in anhydrous acetonitrile under reflux for 9 days, in an argon atmosphere. The resultant pale-yellow precipitate was filtered and washed with ethyl acetate twice, and then twice in acetone, producing an isolated yield of 88%.



Scheme 2-1 The solution synthesis of the di-Zincke salt **1-2**

The ¹H NMR spectrum of di-Zincke salt **1-2** dissolved in D₂O gave signals corresponding with the literature and the distinctive pattern of proton splittings, particularly for the dinitro group (H_{3'} d, 9.31 ppm, H_{5'} dd 8.83 ppm and H_{6'} d 8.20 ppm). The appearance (or absence) of these signals would aid assignment in future new syntheses. The proton labelled H₁ gives a normalised integrated value of 1.4 but there are 2 in the molecule.

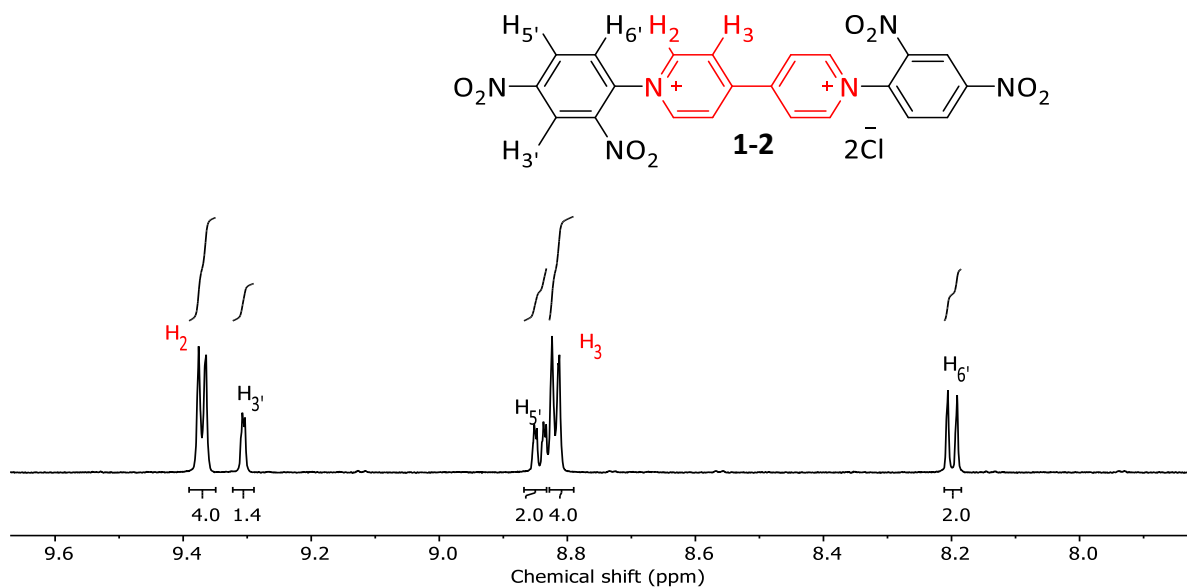


Figure 2-1 ^1H NMR spectrum for **1-2** with $\text{H}_{3'}$, d, 9.31 ppm, $\text{H}_{5'}$, dd 8.83 ppm and $\text{H}_{6'}$ d 8.20 ppm

The effect may be due to the way the free induction decay waveform data is collected from the proton that is labelled H_1 . It has no neighbouring ^1H s which affects the relaxation time between pulses. An experiment where selecting a different parameter by changing the relaxation delay from the routine default setting of 1 second to 25 seconds on the VNMR600 machine illustrates that changing this parameter gives the expected integration for $\text{H}_{3'}$, **Figure 2-2**.

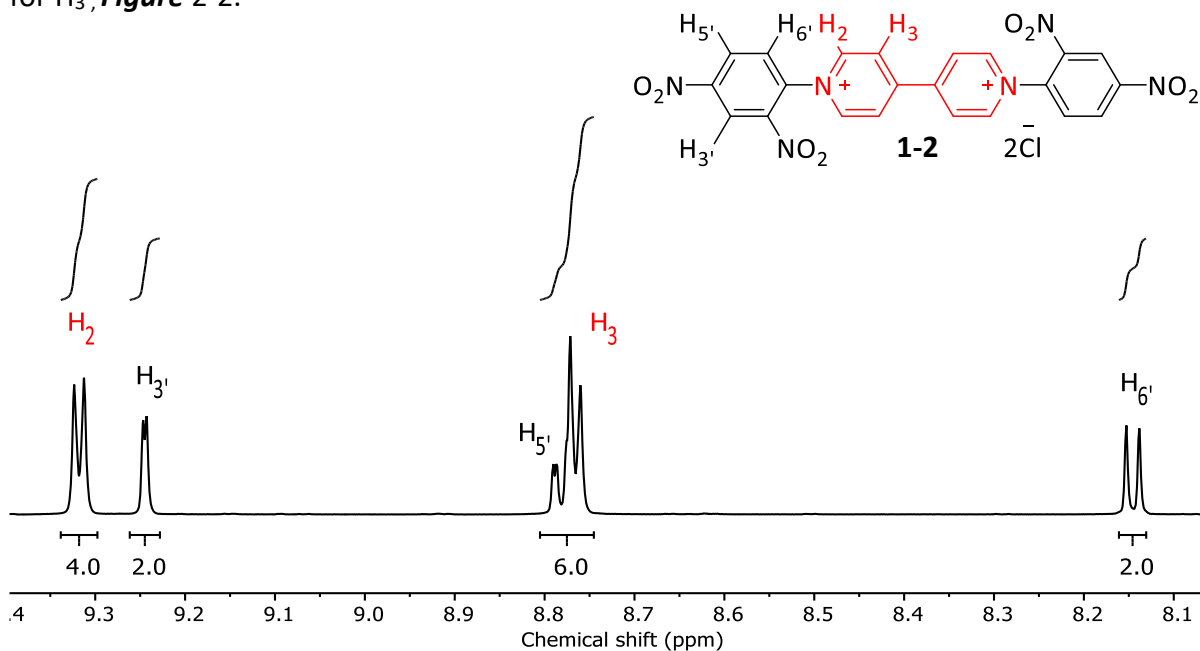
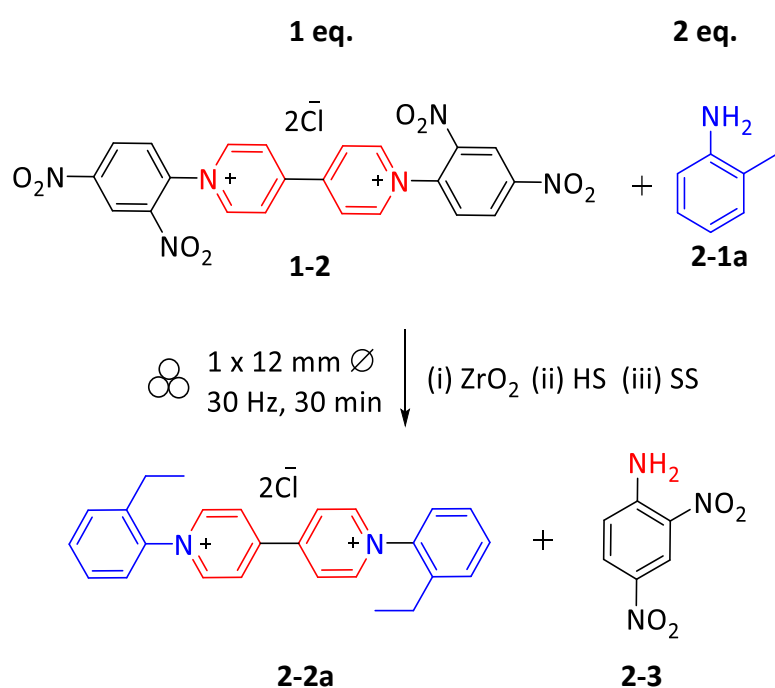


Figure 2-2 Time delay from 1 to 25 seconds gives correct integrated values for ^1H NMR spectrum of the di-Zincke salt, **1-2**

2.2 Mechanochemistry of viologens

A preliminary substitution reaction of the di-Zincke salt **1-2** was conducted with 2-ethylaniline **2-1a** to assess the feasibility of using solvent-free ball-milling as a route to the synthesis of viologens. Initial conditions were selected to be 30 Hz, for 30 minutes using 1 ball of 12 mm \varnothing , as shown in **Scheme 2-2**. A Retsch MM400 instrument was used, and the reaction was carried out in three different reaction vessels, composed of either hardened steel (HS), stainless steel (SS) or zirconium oxide (ZrO₂).



Scheme 2-2 Reaction between the di-Zincke salt **1-2** and 2-ethylaniline **2-1a**.

Figure 2-3 shows the ¹H NMR spectrum in *d*₆-DMSO of di-Zincke **1-2** starting material. The crude reaction mix from the ZrO₂ jars in spectra **B** does not contain the signals at 9.2, 9.0, 8.5 ppm, for the protons of the di-nitro aromatic residue **1-2** of the starting material, but it does contain signals for dinitroaniline **2-3** at 7.2, 8.2 and 8.8 ppm (one is highlighted in blue), the leaving group, as expected if a reaction has occurred (see **Scheme 2-2**).

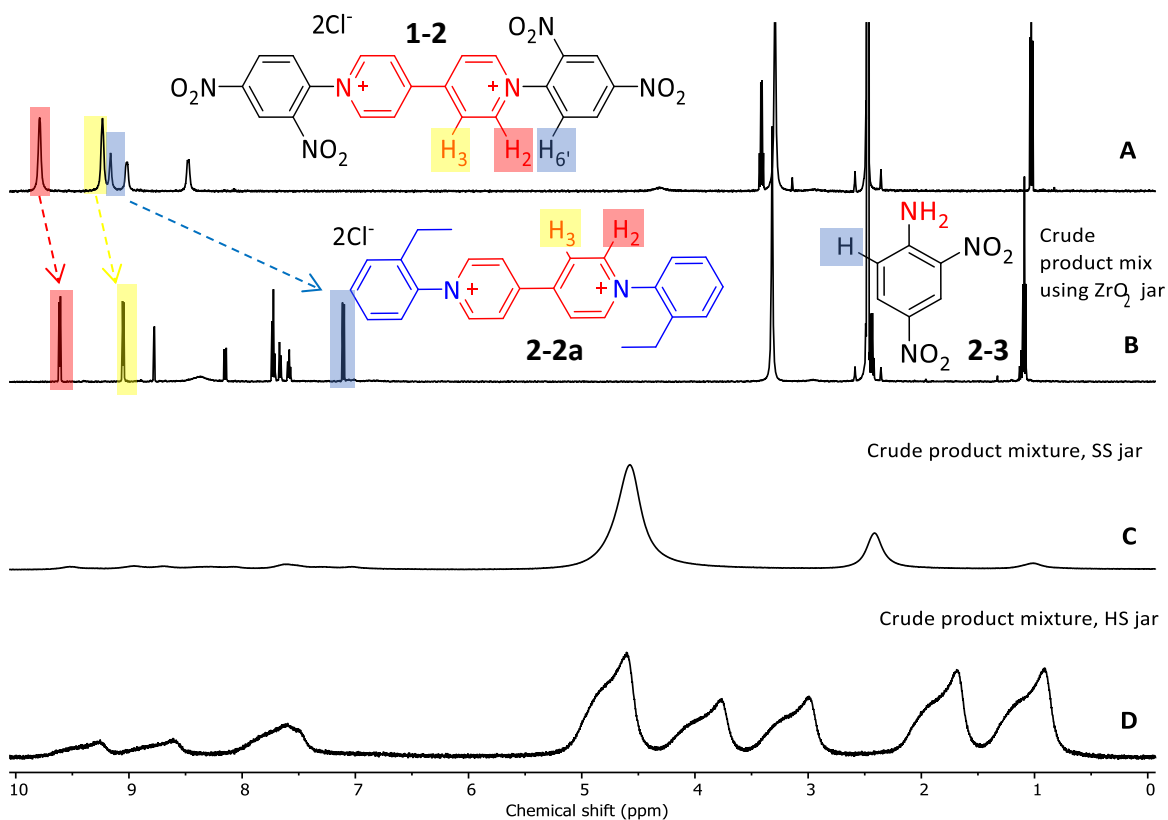
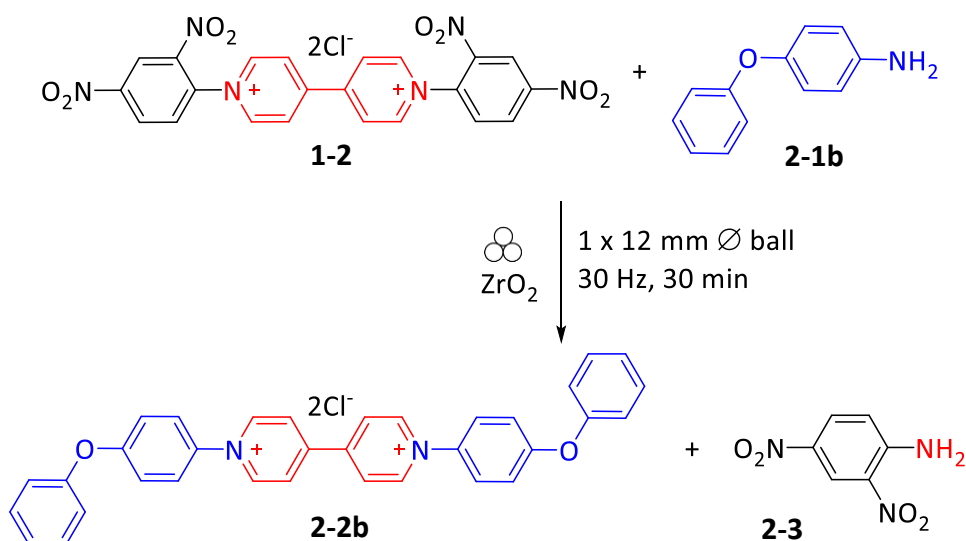


Figure 2-3 ¹H NMR Spectra for reaction between di Zincke salt **1-2** and 2-ethylaniline **2-2a** (A) di Zincke salt, **1-2** in d₆-DMSO (B) Crude reaction mixture from ZrO₂ jar (C) Crude reaction mixture from SS jar (D) Crude reaction mixture from HS jar.

Figure 2-3 shows the ¹H NMR spectra of the crude product samples taken directly after 30 min reaction time. Whilst the ¹H NMR spectrum (B) of the crude product from the ZrO₂ vessels show a well resolved spectrum, the signals in the ¹H NMR spectra for the other two conditions using steel vessels and balls (spectra C and D) can not be distinguished to make an attempt at meaningful analysis. Miklos¹²⁸ *et al.* used VBM to synthesise 2,2-disubstituted- and 2-spiroquinazolinones and reported their ¹H NMR spectra from products formed in both SS and ZrO₂. They showed similarly broad signals in their ¹H NMR spectra that occurred from using SS vessels and they proceeded to only use the ZrO₂ milling accessories for their subsequent investigations. It was therefore decided that all future experiments for the synthesis of viologens via mechanochemistry were conducted exclusively in ZrO₂. In addition, the signals corresponding to the four protons in the pyridyl heterocycle are in the product **2-2**. These are highlighted in red and yellow, and show that this reaction there was 100% conversion to our target molecule as evidenced by all the signals for starting material **1-2** in spectrum A being completely absent in the crude product mix shown in Spectrum B. These spectra clearly show that conversion can be readily

calculated from analysis of the crude ^1H NMR data after the reaction, this would prove very useful as the project progressed.

Experiments to investigate the scope of the substitution reactions of the di-Zincke salt **1-2** began with the use of a single milling ball of 12 mm \varnothing . Two equivalents of aniline **2-1b** were added to one equivalent of the di-Zincke salt **1-2** in a ZrO_2 jar (25 mL). The vessel was oscillated for 30 minutes at 30 Hz for the reaction, **Scheme 2-3**. Upon completion, the ^1H NMR spectra of the reaction mixture was taken, and the brown crude was worked up by removing the crude from the jar with minimum THF. It was then filtered and washed with EtOAc (100 mL), to give the isolated product as a yellow solid with a yield of 24%.



Scheme 2-3 VBM of di-Zincke salt **1-2** with 4-phenoxyaniline **2-1b** using 1 x 12 mm ball to give 24% isolated yield of **2-2b**

Figure 2-4 shows a stack of ^1H NMR spectra with the starting material **1-2** (spectrum A), the crude reaction mixture (spectrum B), and the phenoxyaniline starting material **2-4** (spectrum C). The ^1H NMR spectrum for the crude material does not show signals for the protons of the dinitro residue from the starting material **1-2** at 8.9 ppm (coloured red and yellow) and nor does it show signals from the phenoxyaniline starting material **2-1b** (coloured blue) at 6.9 ppm. Therefore, it is clear from this analysis that all the di-Zincke salt **1-2** (spectrum A) had been consumed and the conversion was essentially 100%. The isolated yield for this experiment was a disappointing 24% and likely to be because of losses incurred from multiple washings in THF and EtOAc to achieve as pure a product as possible,

despite the low solubility of the target salt in these solvents. There is also the possibility of another product formation with different solubility in the solvents used. However, we were at a sufficiently early stage in the project that it could be expected that we would develop improved isolation procedures of the crude products from this reaction.

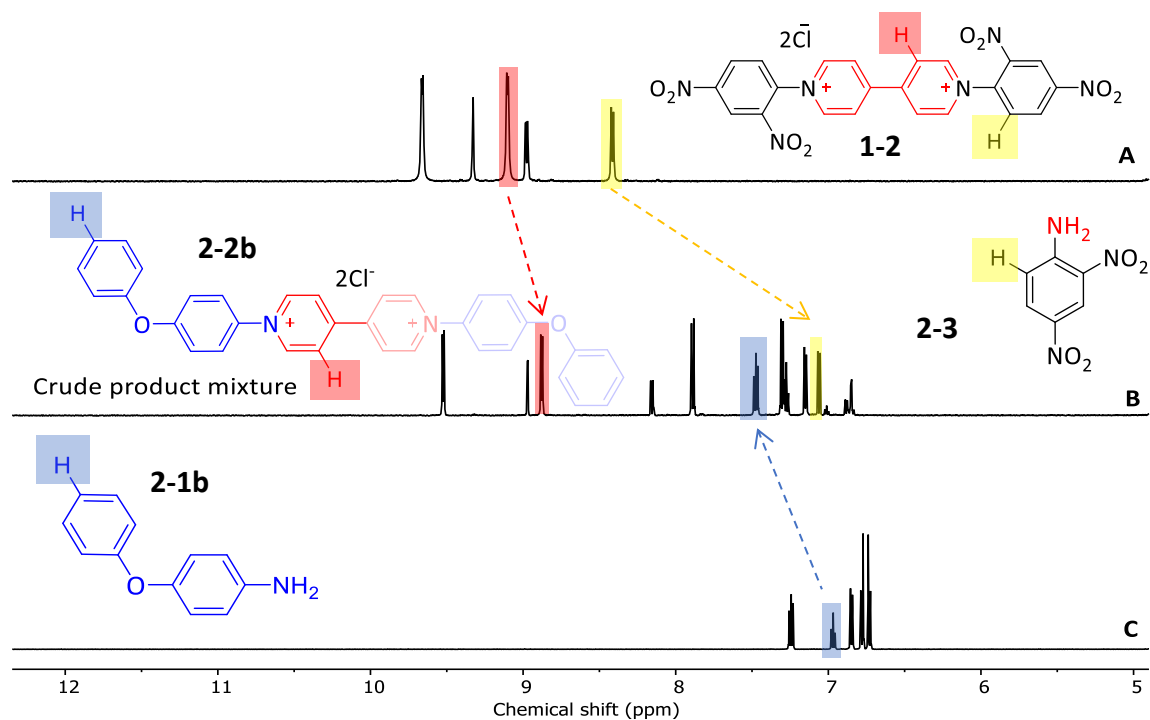
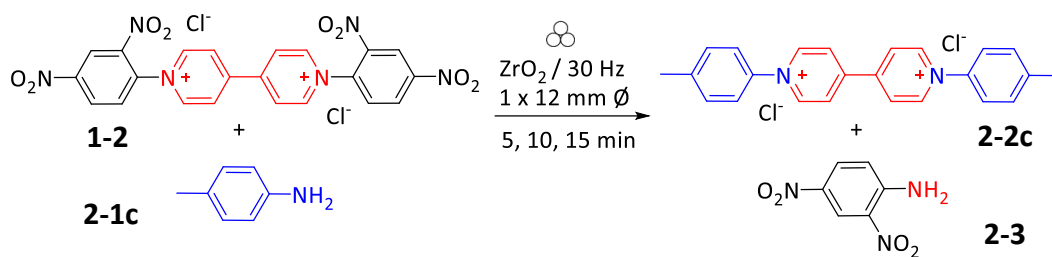


Figure 2-4 ^1H NMR stack of (A) di-Zincke salt **1-2** (B) crude product mixture and (C) 4-phenoxyaniline **2-1b**

A new experiment to establish the duration of oscillation (or milling) time that would give us the necessary conditions for the best conversion for these reactions. The reaction was monitored over fifteen minutes, with samples taken for ^1H NMR spectroscopy analysis every five minutes. For this monitoring experiment, 2 equivalents of *p*-tolyl aniline **2-1c** were reacted with one equivalent of the di-Zincke salt **1-2** in ZrO_2 jars (25 mL) using one ZrO_2 ball (1 x 12 mm \varnothing) at 30 Hz and samples were taken at 5, 10 and 15 minutes with their ^1H NMR spectra recorded immediately using ca. 10 mg of the crude.



Scheme 2-4 Reaction of the di-Zincke salt **1-2** and p-tolyl aniline **2-1c**

From the stack of ^1H NMR spectra for the reactions after 5, 10, and 15 minutes, it is possible to see the progress of the reaction and calculate the percentage conversion after each timed oscillation.

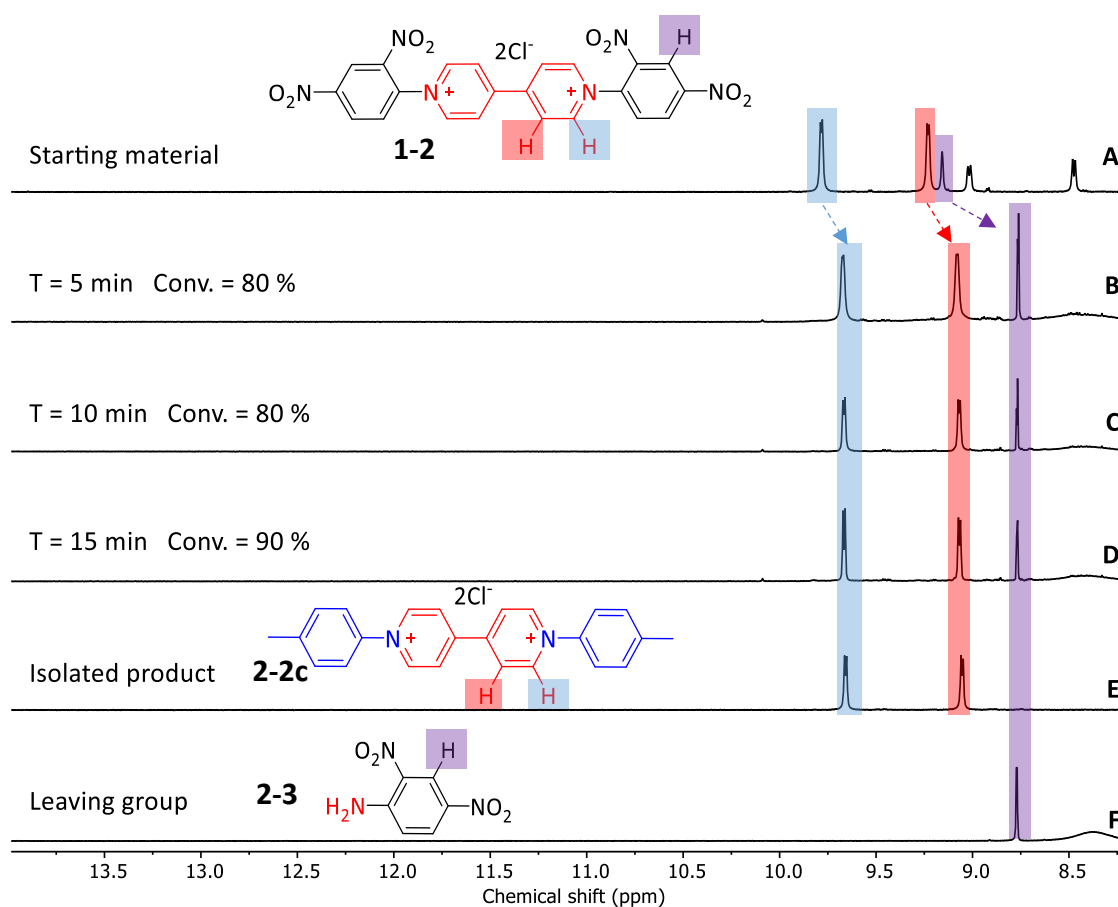
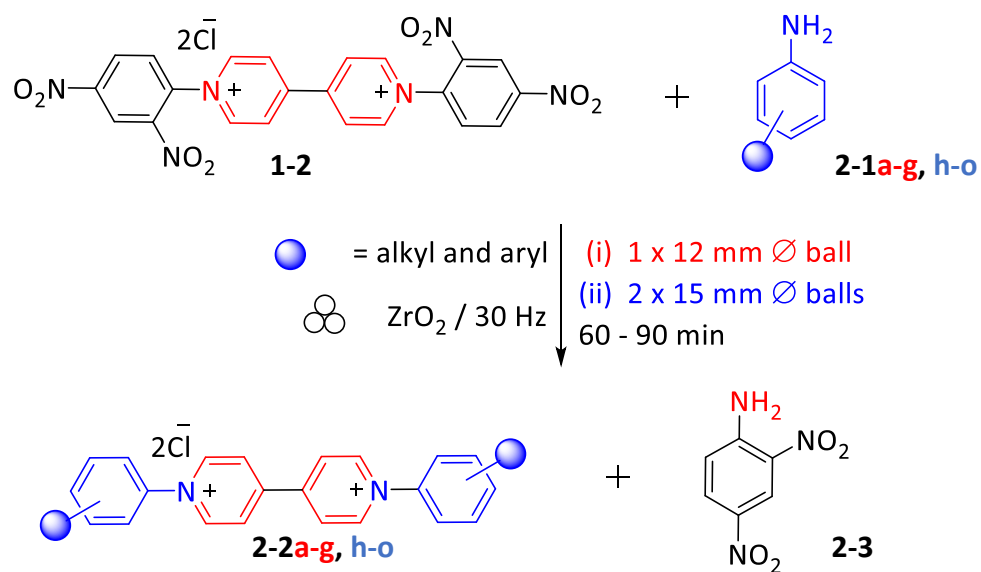


Figure 2-5 ^1H NMR spectra for reaction monitoring of the substitution of the di-Zincke salt **1-2** (A) di Zincke salt **1-2** (B) after 5 min (C) after 10 min (D) after 15 min (E) isolated product p-tolyl viologen **2-2c** (F) leaving group, dinitroaniline **2-3**.

After 5 minutes, 80% conversion was observed, after another 5 minutes, the conversion remained unchanged within the errors of the ^1H NMR spectrum analysis, but after a further 5 minutes conversion increased to 90% as seen in **Figure 2-5**. The difficulties of reaction monitoring for VBM experiments can be seen in this example; there is no possibility of taking a sample from the reaction *in situ* without disturbing the conditions. Stopping and starting the VBM to access a sample for analysis allows the mixture to cool. This may explain that the conversion after both 5 and 10 minutes is the same: 80%. Once a reaction has been set, the collisions in the vessel generate heat, sometimes sufficient heat to change the rheology of the reactants.²⁴ Setting off the machine again, the sampling intervention has changed the conditions and it is difficult to get a true picture of the course of the reaction. *In situ* monitoring^{86,129} is possible and has been discussed (Chapter 1, Section 1.7, p 21), however this was not investigated further for our reactions as we concentrated our efforts on the feasibility study. These experiments have established a set of conditions for the substitution of the di-Zincke salt:

- 25 mL Zirconium oxide jars
- 1 x 12 mm \varnothing ball
- Duration of oscillation should be at least 15 minutes
- Frequency of oscillation is set at 30 Hz

With rapid and easy analysis for the reaction by looking at the crude ^1H NMR spectra, it was now possible to examine the scope of the reaction using these conditions. A range of structurally related anilines were selected which varied by sterics and electronics. This would form a library of viologen units synthesised from the substitution of the di-Zincke salt **1-2** with aryl anilines **2-1**. These can be further used to establish their potential for creating linear, mono-disperse, conjugated chains.



Scheme 2-5 Reaction of the di-Zincke salt **1-2** and aniline

Entry	Mono aniline 2-1a-o	Bipyridinium salt 2-2a-g	Conv. (%)	Yld (%)	Entry	Mono aniline 2-1a-o	Bipyridinium salt 2-2a-o	Conv. (%)	Yld (%)	
a			100	53	h			62	15	
b			100	81	i			100	49	
c			100	24	j			48	88	
d			0	0	k			14	33	
e			100	50	l			31	0	
f			100	63	m			98	80	
g			18	0	n			0	0	
			<p>a-g Conditions 1 x 12 mm Ø ZrO₂ ball / 30 Hz / 30 - 60 min h-o Conditions 2 x 15 mm Ø ZrO₂ ball / 30 Hz / 60 - 90 min</p>							

Table 2-1 The substitution of the di-Zincke salt, 1-2 with a selection of anilines 2-1a-o in the VBM to give bipyridinium salt 2-2a-o

Entries **a-g** were carried out using the ZrO₂ jars (25 mL) and using one ZrO₂ ball (12 mm \emptyset). It can be seen that conversions were good for a range of substrates including more sterically hindered products e.g. Entries **b** and **f**. Surprisingly, the di-substituted aniline **d** which has electron-donating methoxy groups, and therefore may be expected to have increased nucleophilicity, gave zero conversion whereas the electron-withdrawing ester (**g**) showed some conversion (18%) but with reduced yield compared to **d** (0%). The reduced yields may be a consequence of insufficient energy being accessible to promote the reaction. Variables that can be changed to achieve more energy in the milling jar are (i) increasing the size and number of the milling balls and/or (ii) increasing the length of time the vessels are oscillates. For our reactions, the next step was to introduce larger (and therefore heavier) milling balls and to double the number used. Entries **2-2h-o** in **Table 2-1**, used the conditions ZrO₂ jars (25 mL) and ZrO₂ balls (2 x 15 mm \emptyset) with reactions times up to 90 minutes. The low yield (33%) for the *meta*- substituted 3-phenolaniline (**2-2k**) could be attributed to their varying substitution pattern compared with the more successful 4-phenolaniline (88%, **2-2j**). In this specific example using 3-phenolaniline, side reactions have been shown to occur when the ortho aminophenol is used as the nucleophile by Zeghib¹³⁰ *et al.* in their work on the nucleophilic substitution of the mono-Zincke salt using microwave activation and solvent.

They were able to isolate the major side product which was the diarylamine **2-4**. This may have formed from an S_NAr reaction – a consequence of the direct nucleophilic attack of the amino group on the aminophenol. Another route could be from the first substitution led by the hydroxyl group of the aminophenol which would give the intermediate diaryl ether **2-5**. It has been demonstrated that a Smiles rearrangement of **2-4** into **2-5** at room temperature and in the presence of water occurs.^{131,132}



Figure 2-6 Formation of major side product (i) diarylamine **2-4** which may also result from (ii) a first substitution by the hydroxyl group of the o-aminophenol giving the intermediate diaryl ether **2-5**

The results in **Table 2-1** for entries **2-2j** and **2-2k** (conversion 48%, yield 88%) and (conversion 14%, yield 33%) respectively, where percentage conversions were calculated from their crude ^1H NMR spectra. This gives values for the isolated yields that were greater than their percentage conversions which is incorrect. An explanation could not be directly gleaned from the ^1H NMR spectra of the product, shown in **Figure 2-7**. The compounds had been washed in THF and EtOAc, in which the products have very low solubility. If the sample had contained solvent residues, their signals would appear on the ^1H NMR spectra, of which there are none.

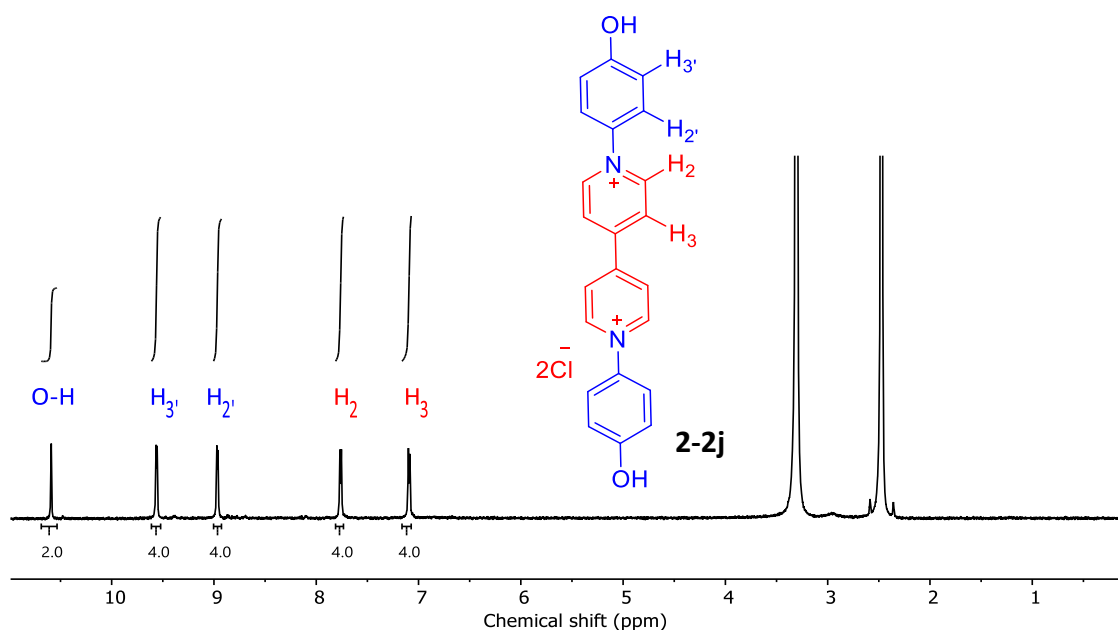


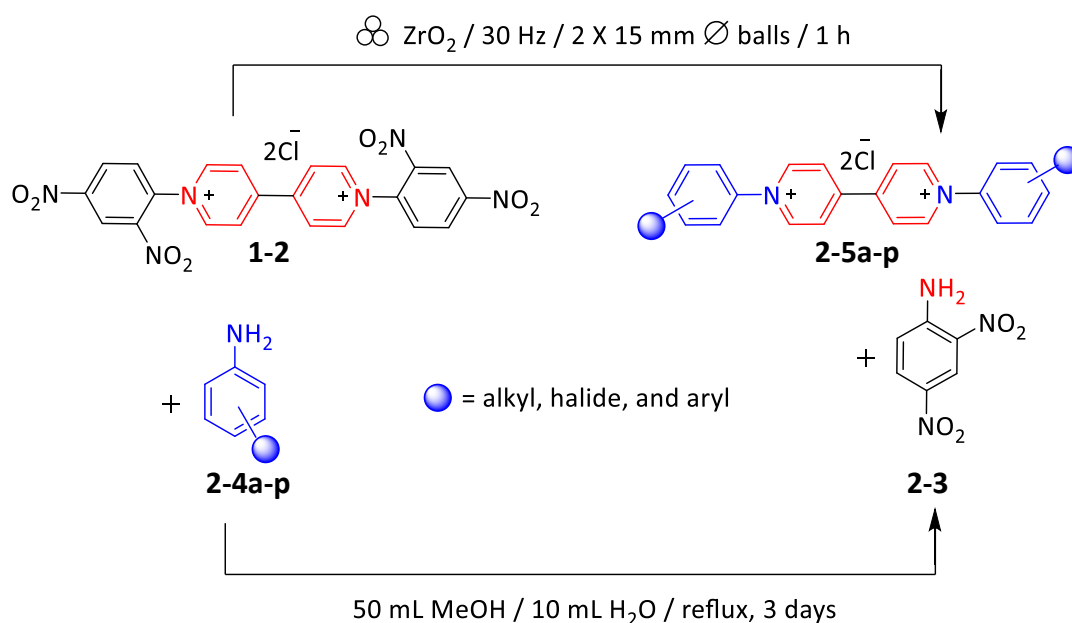
Figure 2-7 The ^1H NMR spectrum for **2-2j** in **Table 2-1**

Assignment of for all the protons H_2 , H_3 and H_2' , H_3' and H on the phenol group accounts for all the possible signals. The excess mass must therefore have come from material that is not observable in the ^1H NMR spectrum. It was hypothesised that the ZrO_2 , from the milling jars and balls may be responsible for the extra mass. Indeed, ICPMS showed low levels of Zirconium (ca. 3%) was present in the sample. However, this does not account for the large discrepancy, and the origin has yet to be established. There is a possibility of another species, perhaps a keto form, in the crude mixture but without isolating the compound, it was not possible to draw a conclusion. The confirmation of contamination from the milling balls and the lining of the jars served to do two things for future VBM experiments, (a) to use new milling balls for each experiment to mitigate against loss of material from the balls

falling apart through repeated use, and (b) to add a further purification step to all affected samples by filtering the solution through clean, tamped-down celite to remove the insoluble ZrO_2 .

2.3 Conclusion from VBM of the di-Zincke salt **1-2** with nucleophilic anilines

We have shown for the first time that using the Zincke Reaction to produce disubstituted viologen species can be achieved in VBM. The reactions used 2 equivalents of nucleophile for each di-Zincke salt **1-2** and thus demonstrating that it is stoichiometrically efficient in the solid state compared with Greenland Group's earlier work¹²⁷ in solution, where the SI shows their synthetic procedures to include up to 10 equivalents of aniline to 1 of the di-Zincke salt for same reaction. Conversion and the isolated yields achieved depended on the aniline used and its substrate, and range from 0 to 81%, depending on electronic and steric factors as well as the presence of competing reactions. One very positive outcome is, being solvent-free, the VBM is both time and energy-saving, reactions require just 1 h of oscillation vs 3 days of heating compared to classical solution methods.^{126,127}



Scheme 2-6 Scheme for the reaction between anilines **2-4a-p** and the di-Zincke salt **1-2** using ball-milling and classical solution methods

Although we were able to evaluate the efficacy of VBM on the Zincke Reaction, our results gave an incomplete picture and does not fully explain the lack of reaction with substrates that were electron-donating, e.g. Entry **d**, in **Table 2-1**, the dimethoxyaniline. The next

investigation was to use conditions that should improve the conversion of the di-Zincke salt **1-2** by maximizing the energy available for the reaction in VBM and by increasing the number and size of the balls used. Also, a systematic and consistent approach to comparing the substitutions can be achieved by using the same reaction conditions for each experiment, only then can we make fair comparisons.

2.4 Finding substrate scope using optimised conditions

A consistent set of reaction conditions comprising of 2 x 15 mm \emptyset zirconium oxide balls, ZrO₂ jars (25 mL), oscillated for 60 minutes at 30 Hz. A selection of anilines which have varying electron withdrawing group (EWG) or electron-donating group (EDG) substituents were chosen. Quantities used were one equivalent of the di-Zincke salt **1-2** with two equivalents of the aniline. Using ChemAxon software¹³³ available online, the calculated pK_a values of the aniline was plotted against the percentage conversion. This enables us to see the relationship, if any, between increasing basicity of the aniline and its reactivity in the Zincke Reaction. The results are collated in **Chart 2-1**.

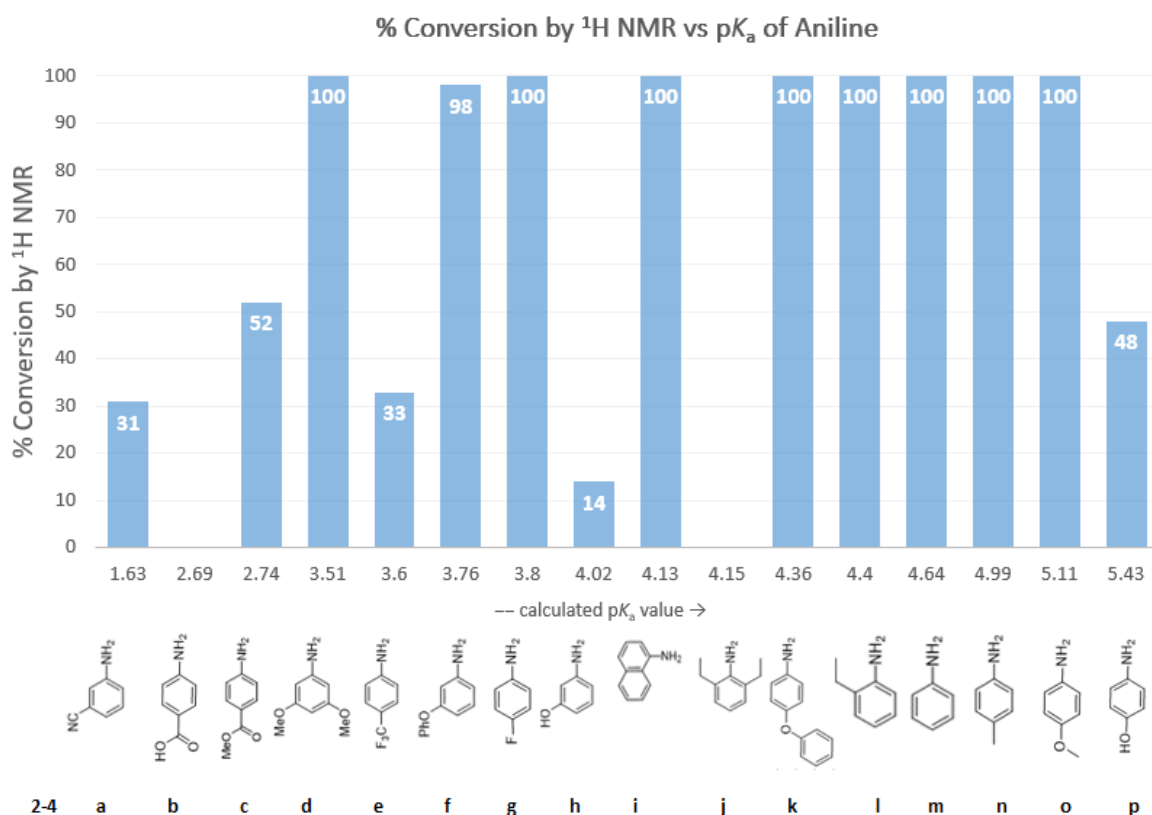


Chart 2-1 The % conversion of di-Zincke salt **1-2** vs the pK_a value of aniline **2-4a-p** using VBM

The reaction gave essentially complete conversion (as established by crude ^1H NMR analysis of **2-4 d, f, g, i** and **k-o**) for a broad range of substituted anilines with $\text{p}K_{\text{a}}$ values ranging from 1.63 to 5.43. Strikingly **2-4d** with the 3, 5 dimethoxy substrate shows 100% conversion using ZrO_2 (2 x 15 mm \emptyset) balls whereas there had been zero conversion using VBM with ZrO_2 (1 x 12 mm \emptyset). For the reactions that gave less than 100% conversions, these results may be rationalised starting with the zero-conversion due to steric hindrance, 2, 5 diethylaniline **2-4j**. There is also competing reactivity from the deprotonated $-\text{COO}^-$ group **2-4b**, and protonating the amine, forming a Zwitterion making the lone pair on the nitrogen no longer available as the nucleophile. Poor conversion is evident again with phenols because the $-\text{OH}$ group is a competing reactive site to the nucleophilic amine group as explained before (see Section 2-2, **Figure 2-6**). In general, electron withdrawing substituents on the aniline (entry **2-4c**) decrease the yield whereas electron-rich and donating $-\text{OMe}$ groups **2-4d** promote increased yield.

Yields achieved in these experiments help to show patterns in conversion and their determination can be made with the assistance of the calculated $\text{p}K_{\text{a}}$ values¹³³ of the aniline. Additionally, an understanding of substrates with steric, electronic, or competing reactive sites that may deviate the reaction from giving 100% conversion gives confidence in the utility of $\text{p}K_{\text{a}}$ values for solid state reactions and the nature of nucleophilicity of anilines in general.

Having established some of the chemical parameters that affect the conversion in VBM, attention was directed to whether the reaction was dependent on the milling balls and their grinding forces. Another factor could be the physical property of the starting materials (solid or liquid) and its impact to the success of the reaction; therefore, our next investigation was to explore these reactions when *no* milling balls are used.

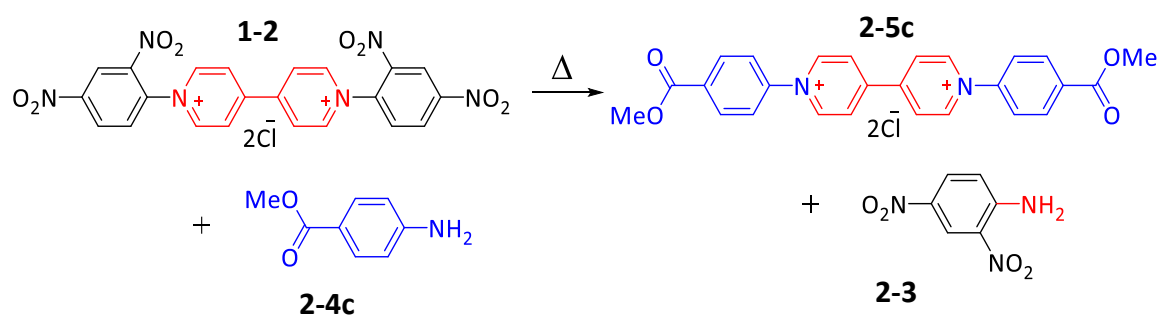
2.5 Effect of the melting point of anilines in 'heat and stir' experiments

There is now a body of work on the ball milling phenomenon; aspects considered include collision theory,¹³⁴ rates of reaction and rheology,⁸⁸ and *in-situ* studies for rates of conversion⁸⁶ which have been discussed in Chapter 1. These studies have all based on the

action of ball-milling and so it would be of interest to investigate our VBM substituted di-Zincke reactions in a different way – by not using milling balls at all. It was felt that a methodology for solvent-free synthesis that requires direct heating of the neat reagents in a suitable vessel that allows reagents to be mixed could be easily investigated.

Our hypothesis that the physical state of the reagents for the reaction may be an important factor in the reaction could be explored by choosing anilines with a range of low-medium-high melting points and stirring them with the di-Zincke salt and ramping the temperature over a series of time intervals. An initial reaction conducted was using **2-4c** the 4-aminobenzoate. It was selected because it failed to reach 100% conversion in VBM, stalling at 52% conversion after 60 minutes using ZrO_2 (2 x 15 mm \emptyset) balls. It is a good candidate for study because it has a melting point of 110 °C, and so by increasing the temperature of the reaction mixture over a period, it would be possible to sample at 3 different temperatures and easily see conversion for each temperature via analysis of their 1H NMR spectra.

As it has a high melting point, this starting material is a solid at room temperature and requires a temperature higher than 25 °C to change phase. In the VBM, access to increase in energy is through what is available from collisions, but when conductive heat energy is applied continuously to the reaction, we are able to see a change in phase through it melting. Molten reagents can move more easily and increases the likelihood of a reaction event. As with the VBM experiments, 2 equivalents of the aniline 4-aminobenzoate **2-4c** were added to 1 equivalent of the di-Zincke salt **1-2**, in a boiling tube.



Scheme 2-7 Heat and stir reaction of di-Zincke chloride **1-2** and 4-aminobenzoate **2-4c**

The reagents were stirred for an hour using a steel spatula at RT and sampled for analysis by ^1H NMR spectroscopy. The progress of the reaction was monitored by repeating the sampling after stirring for a further hour at 85 °C and 115 °C. The resulting stack of ^1H NMR spectra are shown in **Figure 2-8**.

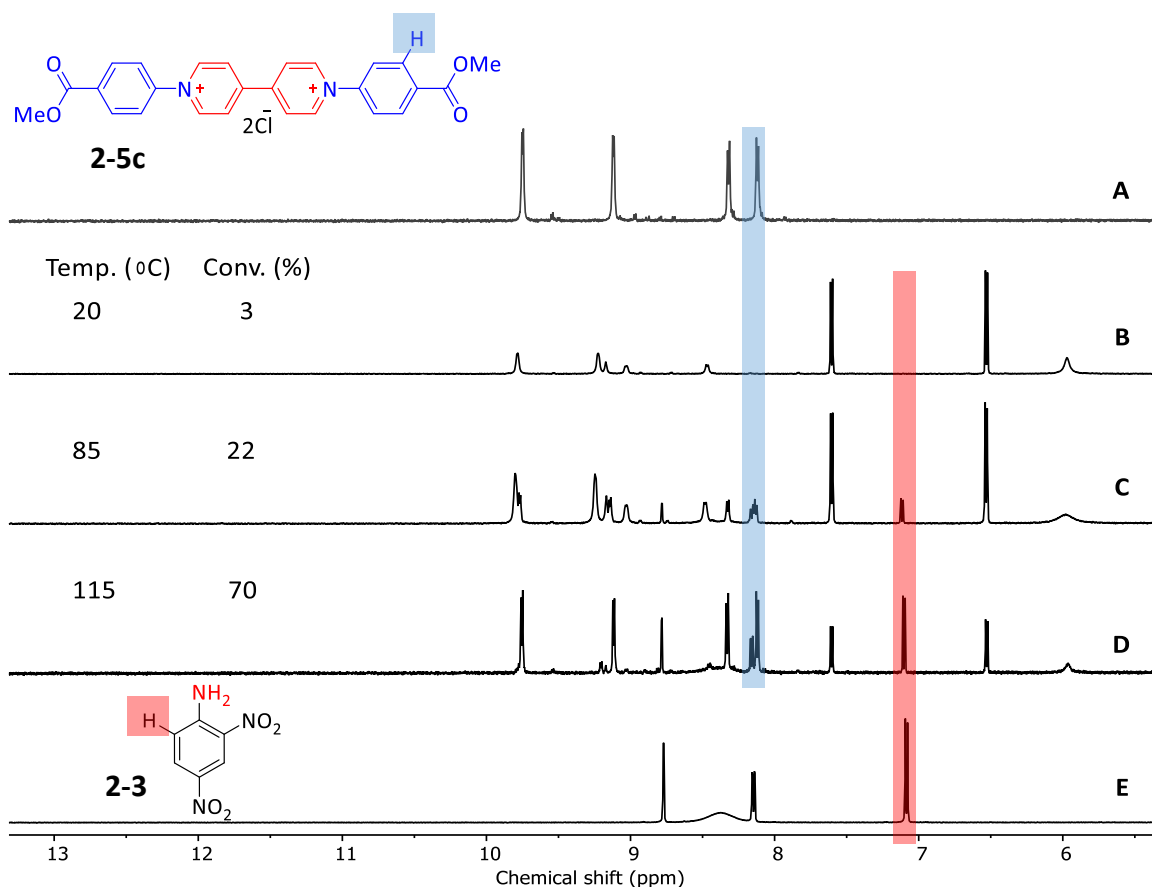


Figure 2-8 Stack of ^1H NMR of final product of (A) viologen **2-5c**, the crude reaction mixture sampled at (B) 20 °C (C) 85 °C and (D) 115 °C (E) the leaving group dinitroaniline **2-3**

^1H NMR spectrum (E) in **Figure 2-8** shows the dinitroaniline leaving group, (B-D) are the spectra of the crude, sampled after each hour of stirring at 20 °C, 85 °C and 115 °C. Spectrum A is the isolated product **2-5c**. The intensity of the ^1H signal highlighted in red and shown on the product **2-5c** can be seen to increase over the three temperatures (spectra B-D). Similarly, the evolution of the intensity of the blue ^1H of the leaving group in **2-3** is shown by raising the temperature. The conversions for this experiment as calculated by using the ^1H NMR spectra were 20 °C = 3%, 85 °C = 22% and 115 °C = 70%. 4-methylaminobenzoate **2-5c** has a melting point of 110 °C and changes phase, from solid to liquid, within the range of the temperature ramp in this experiment. Firstly, this has

demonstrated that the reaction occurs even when both reagents are below their melting points with conversion at 22% at 85 °C. At 115 °C, above the melting point of the aniline, the change of phase helps to promote the reaction further, giving 70% conversion. When a reagent is in the liquid state it is more able to form a homogenous mixture compared to when mixing two solids. It was observed that the conversion was 52% in VBM after 60 minutes of oscillation for this reaction. The result from the heat and stir method suggests that applying heat to the temperature of 115 °C to the reaction mixture may not have been accessible via collisions in the ball mill, however the timescale for ramping the temperature up to 115 °C was 3 hours. A direct comparison for conversion is therefore not possible.

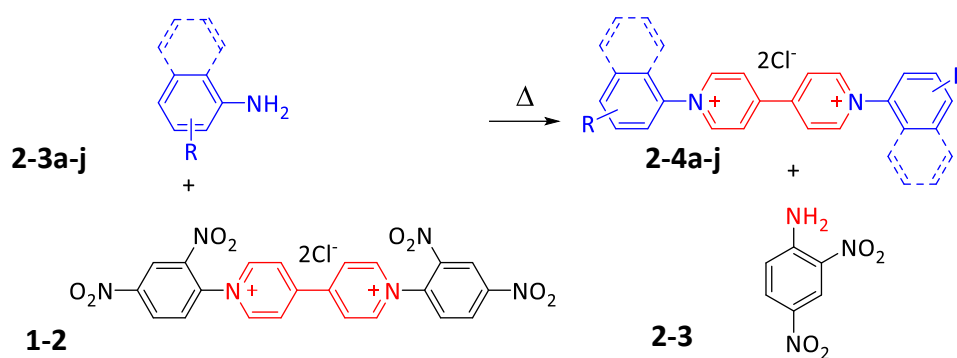
The result warranted an extension of the study to anilines with a range of melting points that would provide us with more information about their reactivities in relation to their physical states. The set-up for the 'heat and stir' experiments, requiring small quantities of *ca.* gram, and the most efficient piece of equipment to conduct this experiment was a carousel reactor, **Figure 2-9**.



Figure 2-9 Carousel reactor with 12 stations, picture taken from¹³⁵

The carousel reactor sits on a standard stirrer/hotplate and a water-cooled condenser is at the top of the apparatus. There are ports for 12 boiling tubes and lids are fitted with tubing to conduct reactions in inert atmosphere if required. For our set up, the boiling tubes were open to the air, reagents were weighed out in 2:1 molar equivalents of aniline: Zincke salt in weighing boats before being combined at the same time into each boiling tube. The magnetic stirrers that had been added to each reactor did not spin freely within the mixtures and so a pipette was inserted into each boiling tube and manually stirred for equal amounts of time. The strategy was to measure the conversion by ¹H NMR spectroscopy of reaction mixtures at three time points: after they have been stirred for 60 minutes at room temperature (RT), after a further hour at 85 °C and finally after 1 more hour at 115 °C. The

anilines selected for this experiment were purposely chosen to have a range of melting points to see how the physical state (i.e., were they a solid or liquid at a given reaction temp) of the starting material would affect outcomes for conversion. For example, the selected aniline with the lowest melting point of -44 °C was 2-ethylaniline and the aniline with the highest melting point that we used was 3-phenolaniline (122 °C), chosen because it was 7 °C above our maximum working temperature of 115 °C for the experiment (**Scheme 2-8**). Both these anilines have shown conversions using VBM and in solution to at least some degree and it would be insightful to see how they compared with ‘Heat and Stir’. The conversion data for each reaction is collated in **Chart 2-2**.



Scheme 2-8 Heat and stir experiment for the di-Zincke salt **1-2** with low melting point anilines

All the experiments show conversion at room temperature to varying degrees including the solid-solid combinations, where both starting materials had melting points well above room temperature, **2-6e-j**). Upon the application of heat, all show increased conversions with the exception of Entry **2-6a**. Further increases in reaction temperature (to 115 °C) did lead to significantly higher conversion for most compounds with mp above 57 °C. It is not clear if this is a straight function of the change in temperature or physical state, however.

It was noted that during the reaction the stirrer bars stopped spinning because the crude became too sticky, therefore the samples were mixed by hand. It is possible that when the reactions contain one component in the melted state, the chances of a reaction occurring between the reagents increase as the more homogenous the reaction mixture becomes.

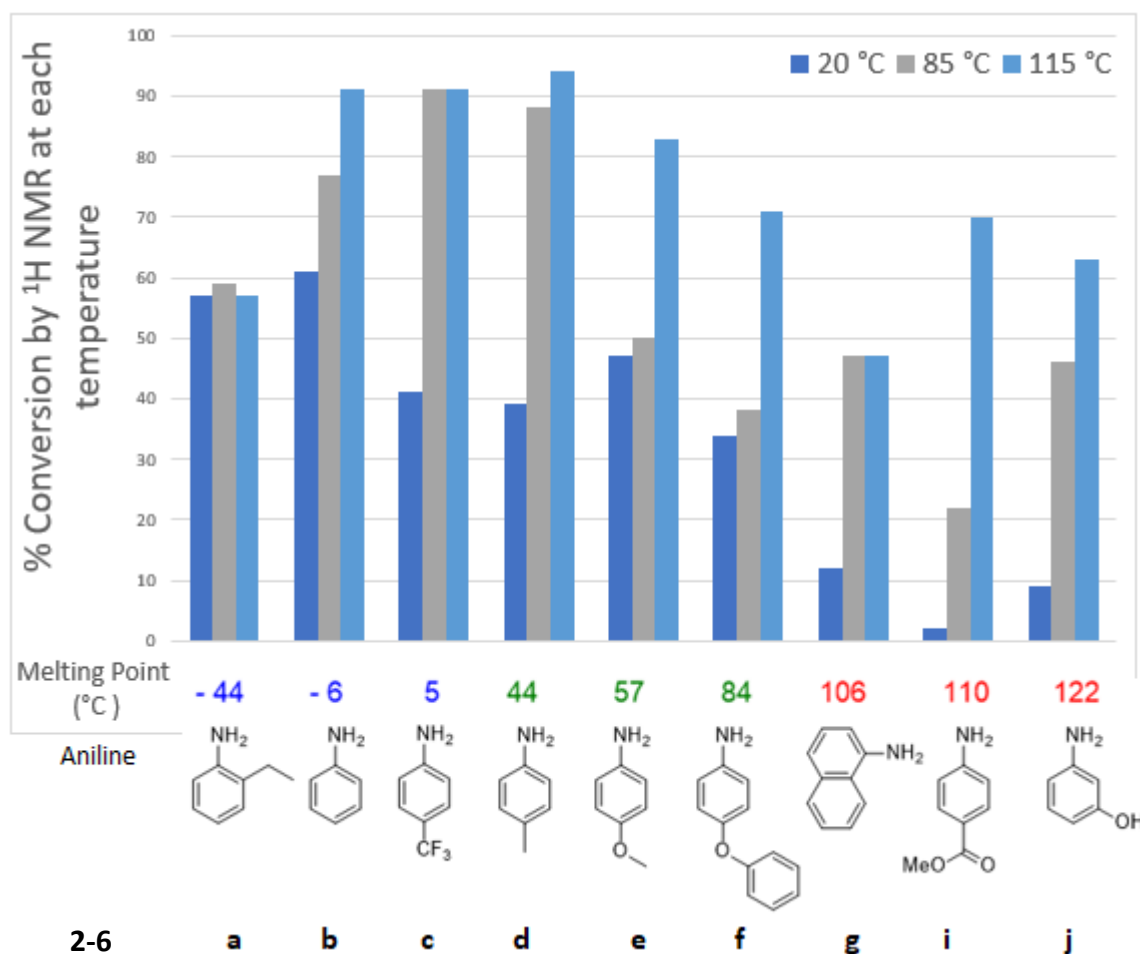
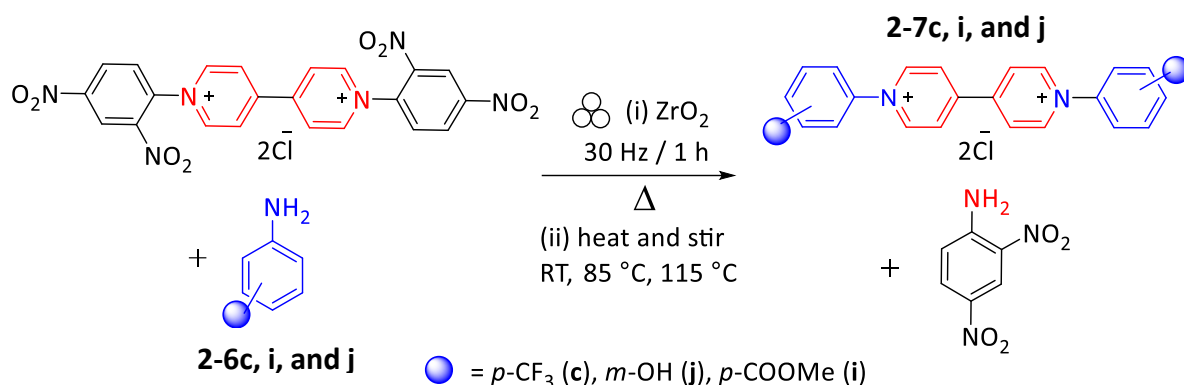


Chart 2-2 Solvent free synthesis of substituted viologen **2-7a-j** by heating and stirring of anilines **2-6a-j** with the di-Zincke salt **1-2**

Studies on ball milling have shown that shaking reaction mixtures with milling balls at high frequencies homogenizes the reactive mixture⁸⁸ to the point where complete conversions are therefore possible. This also explains why there are no 100% conversions with intermittent stirring with a pipette. Even with increased temperatures, manual stirring does not promote homogeneity of the reaction mixture as effectively as high-frequency ball milling at 30 Hz. A better system for stirring solids together would be to use an overhead mixer with rotary attachments, which are available for larger, single reactors but not for the 12-port carousel we used for this experiment. Anilines **2-6c, i** and **j**, gave low conversions in the VBM experiments (in the range 14 - 50%). However, in the heat and stir reactions these same 3 anilines give appreciably higher conversions (63 to 90%). The data are plotted in **Chart 2-3**. This could suggest that conversion in VBM is limited by

temperatures achievable by collisions of the milling balls and materials, and the exotherms generated from the reaction itself.



Scheme 2-9 Comparison of Heat and Stir vs VBM for low-converting anilines **2-15c, i and j**

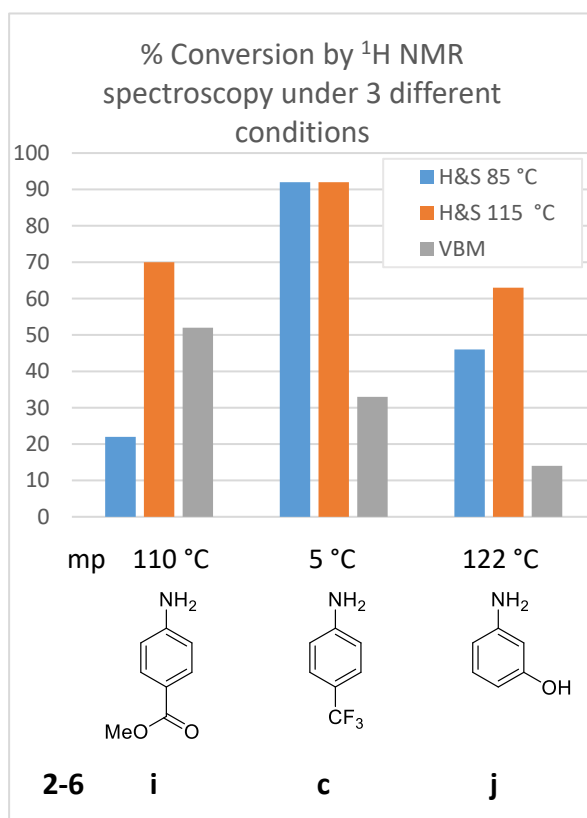


Chart 2-3 Comparison of conversion by ¹H NMR spectroscopy for select anilines **2-15c, i and j**

Despite the limitations of manually stirring all the heat and stir reactions and the likely inefficient mixing compared to VBM, solvent-free reactions between a range of anilines and **1-2** all gave appreciable conversions, even if both reagents are in the solid state. The principal result is that conversions of the di-Zincke salt **1-2**, does not require the action of

milling balls and their collisions in a VBM. We have shown that as a solvent-free technique in VBM, viologens may be produced with complete conversion for a range of anilines (see **Chart 2-1**). Extending the solvent-free method by using heating and stirring only, has shown that this technique provides an energy efficient and greener synthesis for di-Zincke substitution reactions.

2.6 Conclusion from the solvent- free substitution reactions of the di-Zincke salt

In summary, the investigations began with solvent-free synthesis of a series of viologens by utilising the Zincke Reaction and anilines with varying substrates. We showed for the first time that it is possible to carry out Zincke reactions in a ball mill which gave 100% conversions with pK_a value above 3.5. Where there were partial or no conversion, these could be reconciled by steric/electronic factors or side-reactions involving the substrate. The success of these syntheses led us to question the need for milling balls for the reaction. A set of experiments in a 12 reactor carousel showed that the application of heat and stirring were sufficient to effect conversions even when the reagents were solid at reaction temperatures. Therefore, the new syntheses of functional materials using 'heat and stir' has been shown to be a time and energy efficient methodology for the di-Zincke reaction and thus a 'greener' strategy. Manual stirring of the reaction mixture is demonstrably not the most effective method, particularly for larger scales of synthesis, however, commercial equipment may be adapted for this kind of use. For example, foodstuffs such as shaped pasta where the dough is mixed and cooked prior to being extruded into the desired product. Increasingly, fine chemical synthesis can look to other mechanical equipment for heating and mixing, rather than classical methods, to achieve solvent-free, kg/h output for suitable commodity chemicals.

2.7 Multi-step reactions of oligomers towards a hexameric viologen oligomers.

With conditions for carrying out the Zincke reaction in the solid state firmly established it was time to attempt the synthesis of conducting polymers based on iterative Zincke reactions (see p. 38). The multi-steps that are required for the complete sequence have been accomplished in solution, each step typically requiring up to 3 days under reflux followed by purification either through precipitation or recrystallisation¹²³ (**section 1.9**). The choice of diamine had already been established by the Greenland Group, who found that successful serial substitution required electron-donating groups in the diaromatic comonomer. A di-substituted benzidine, 3, 3'-dimethoxybenzidine **1-42**, was chosen that facilitated the reaction which featured the electron-donating methoxy group.

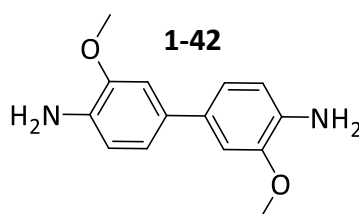
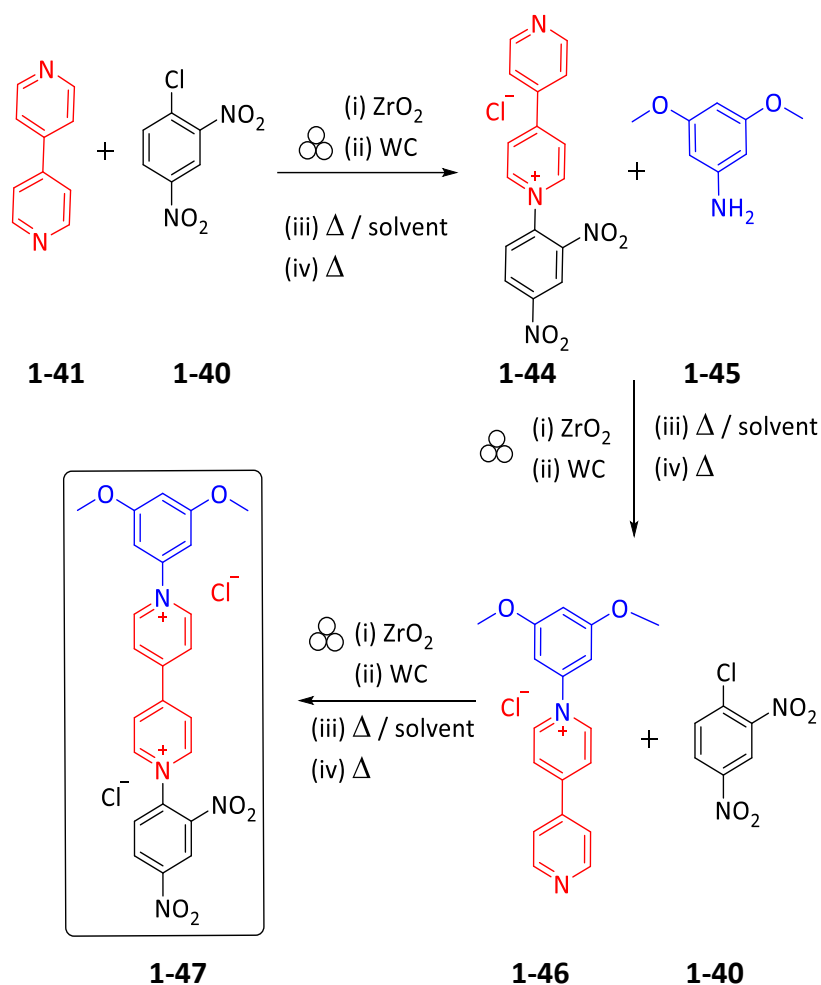


Figure 2-10 Diamine with electron donating methoxy groups, **1-42**

The aim of these experiments was to see if we could synthesise the series of oligomers through a stepwise synthesis using solvent-free techniques. The first target synthesis was to produce **1-47**, which was attempted using the 3-step procedure outlined in **Scheme 2-10**. The first intermediate, the bipyridyl Zincke salt **1-44** is synthesised from the reaction between bipyridine **1-41** and 1-chloro-2,4-dinitrobenzene **1-40** using 1 equivalent of each starting material. This is followed by the synthesis of the second intermediate **1-46** which is the product from the reaction of the Zincke salt **1-44** with the 3,5-dimethoxyaniline **1-45**, where the Zincke salt undergoes the nucleophilic substitution by the aniline.



Scheme 2-10 Three-step procedure of asymmetric Zincke salt **1-47** synthesis

Formation of the bipyridyl mono-Zincke salt **1-44**, was attempted using VBM with ZrO_2 and tungsten carbide (WC), classically in solution via the method of Nimkar,¹³⁶ and simply heating and stirring the reagents. Due to the volume of starting material being used for the heat and stir, the magnetic stirrer was immobilised and so a small amount of acetone (6 mL) was added to aid stirring, and effectively creating a concentrated solution. The reactions were followed using ^1H NMR spectra analysis as shown. Conversions for each method gave varying results which can be seen by the relative intensity of the signals highlighted by the ^1H (red) of the leaving group dinitroaniline and the formation of the product ^1H in (blue) using four different methods. Spectra D shows the experiment using ZrO_2 , it has 15% conversion after 60 minutes. In contrast, spectra B shows the crude spectra of the reaction after 15 minutes in 6 mL of acetone, where we saw 95% conversion. Therefore, we used a concentrated solution to produce **1-44** as it could routinely be used to generate 7 g of isolated product in 92% isolated yield.

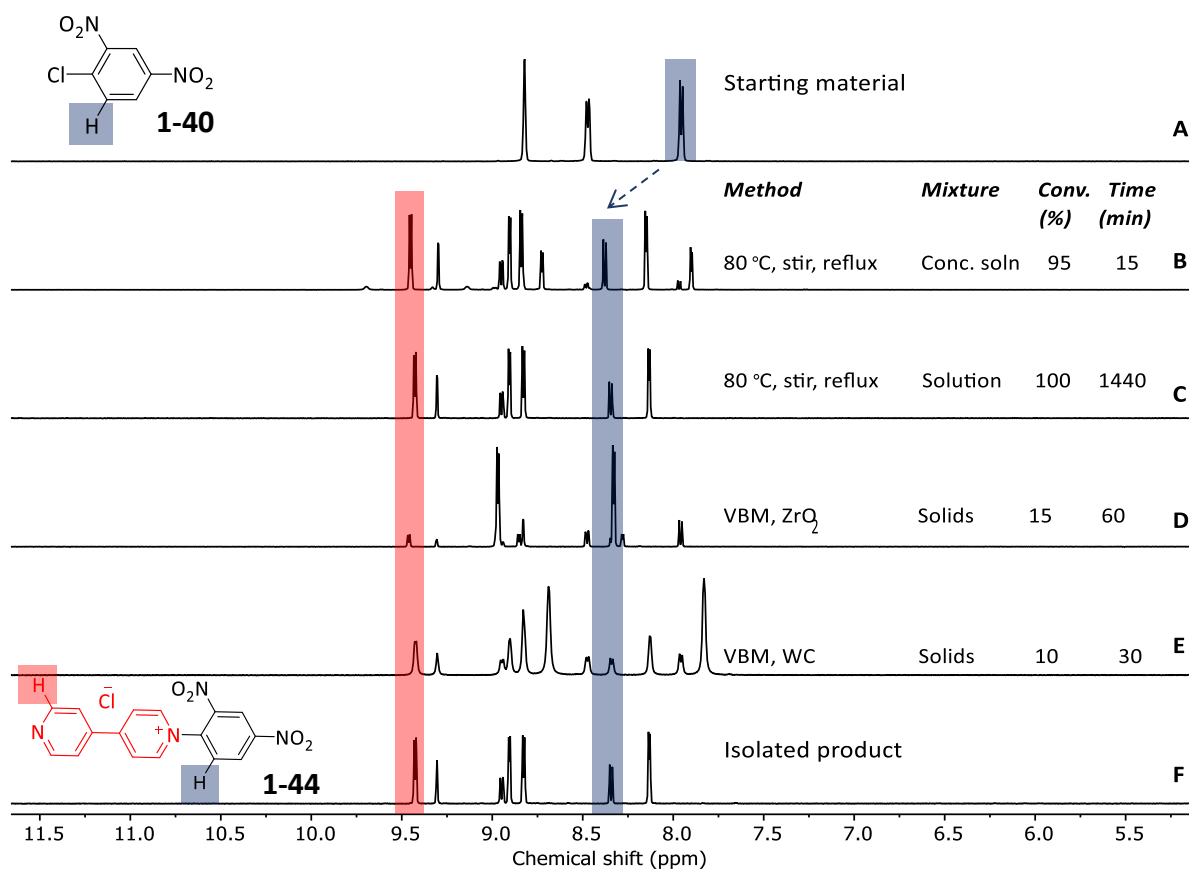
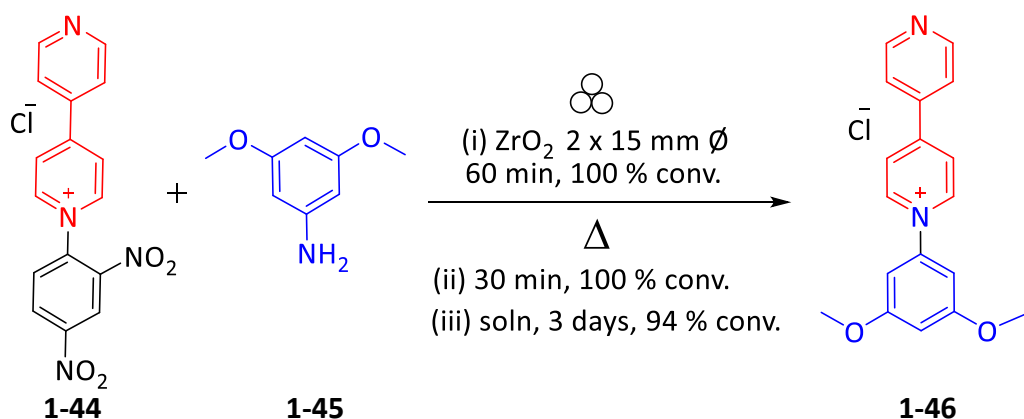


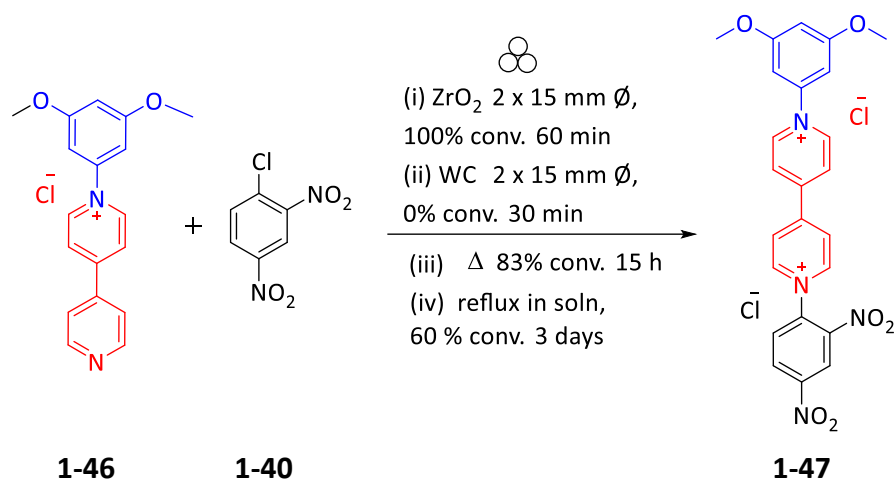
Figure 2-11 Four methods of synthesis **1-44**. ¹H NMR Spectra of (A) 1-chloro-2,4-dinitrobenzene **1-35** (B) Crude product mixture from heat and stir at 80 °C with minimal solvent to reflux (C) Crude product mixture of solution synthesis heated to reflux, at 80 °C (D) Crude product mix from ZrO₂ VBM (E) Crude product mix from WC VBM (F) Isolated product **1-44**

Synthesis of **1-46** was attempted in three of the four conditions previously discussed, shown in **Scheme 2-11**. It was found that, 100% conversions were achieved in 60 min using ZrO₂ in VBM. Heat and stir had a reaction time of 30 minutes, these were compared with 94% conversion in a 3 day solution synthesis.



Scheme 2-11 Synthesis of **1-46** from **1-44** by heat and stir and VBM

Transformation from **1-46** to **1-47** was attempted using four different methods **Scheme 2-12**. No conversion was observed using the WC vessels and milling balls, but once again we saw with ZrO₂ in VBM, 100% conversion after 60 minutes. Using Heat and Stir, there was 83% conversion after 15 h. Both were an improvement on the classical solution method which gave 60% conversion after 3 days under reflux.



Scheme 2-12 Synthesis of **1-47** from **1-46** using 4 different condition

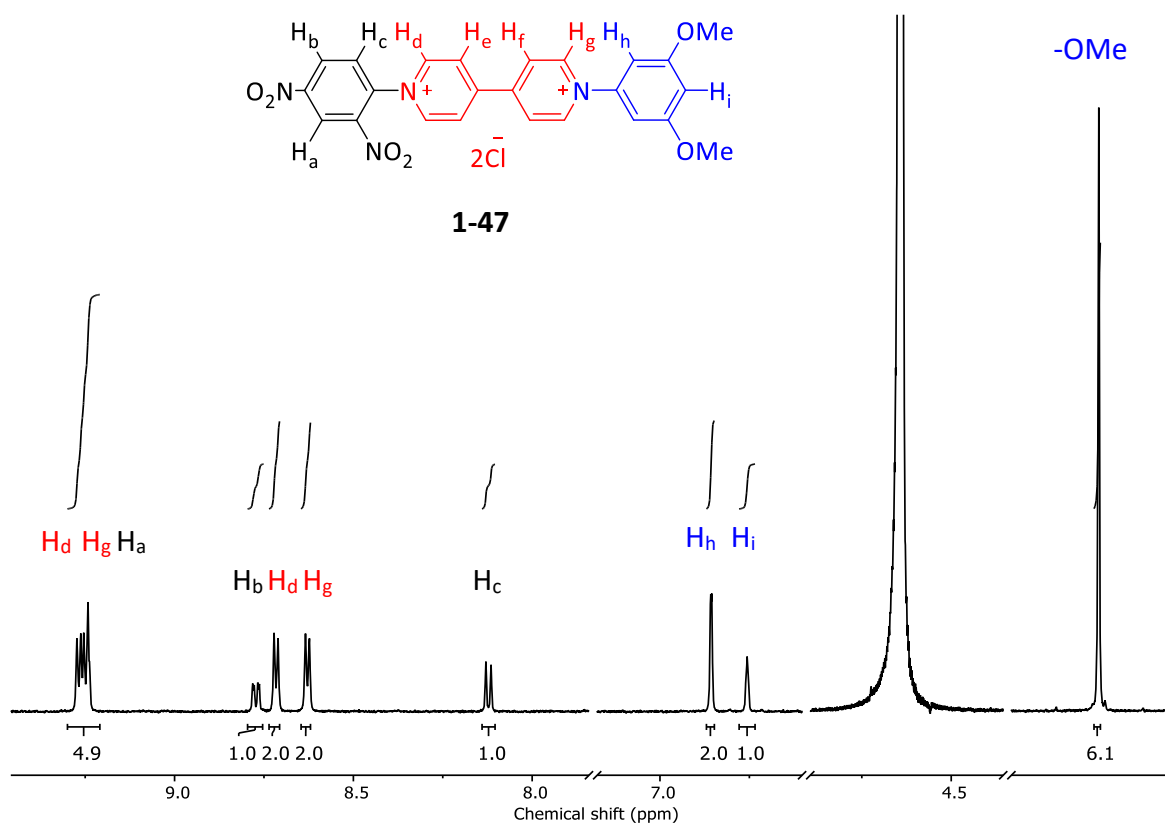
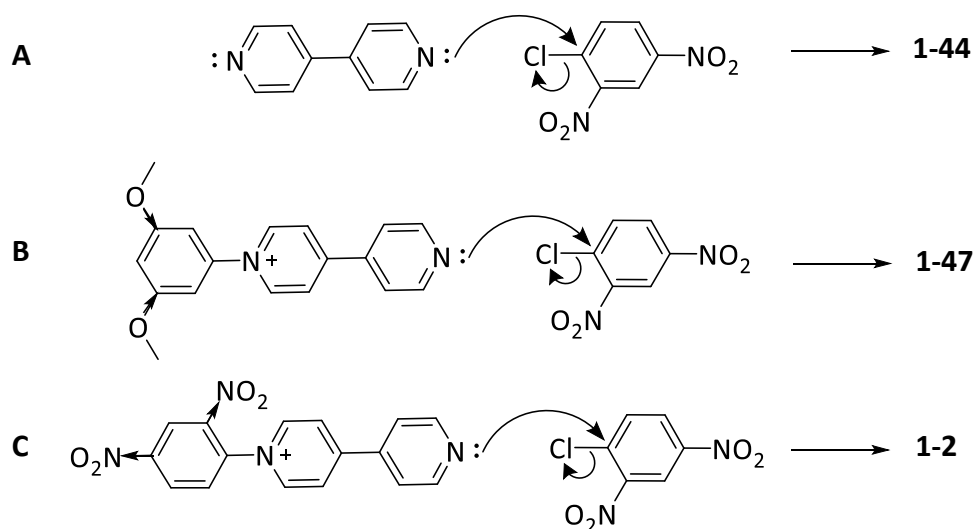


Figure 2-12 ¹H NMR spectra of purified asymmetric Zincke salt **1-47**, in D₂O

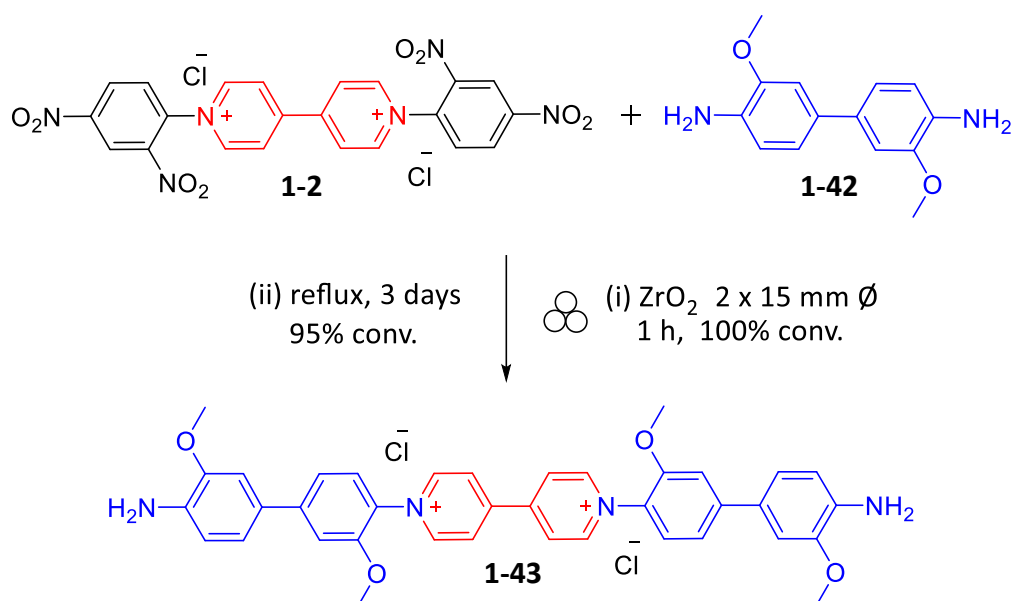
After purification the ^1H NMR spectrum of the asymmetric Zincke salt **1-47** in D_2O gave well-resolved signals, as shown in **Figure 2-12**. After assignment of the molecule's ^1H signals, it could be seen that the signals from the aryl group containing the 2,4- dinitro substituents gives integrals for H_a that are 10% under the expected value. We have seen this before with the ^1H NMR of the di-Zincke salt, **1-2** (**Section 2-1**), this is the same issue with the default relaxation delay set to 1 second on the VNMR600. This has been highlighted because it is a different molecule, but the same issue affects the integration of the proton between two nitro groups on the aryl.

Scheme 2-13 depicts three scenarios involving the bipyridyl component with the lone pair of electrons on the nitrogen atom behaving as the nucleophile in each case. **A** shows the bipyridine molecule, **B** is **1-45** containing electron-donating methoxy groups as a *p*-substituent and **C** the dinitro groups are EWGs acting on an already electron-deficient pyridyl group that is positively charged.



Scheme 2-13 Three scenarios for $\text{S}_{\text{N}}\text{Ar}$ reaction mechanism

It was interesting to note that the mono substitution occurred was essentially selective because of the different substituent effects upon the nucleophilic nitrogen in the bipyridyl unit. The proposed reaction mechanisms for the scenarios **A**, **B** and **C**, when conducted in solvent are in the order: **A** (1 day) is faster than **B** (3 days), is faster than **C** (9 days). For this $\text{S}_{\text{N}}\text{Ar}$ mechanism, **B** and **C** are slower than **A** because of the positive charges on both



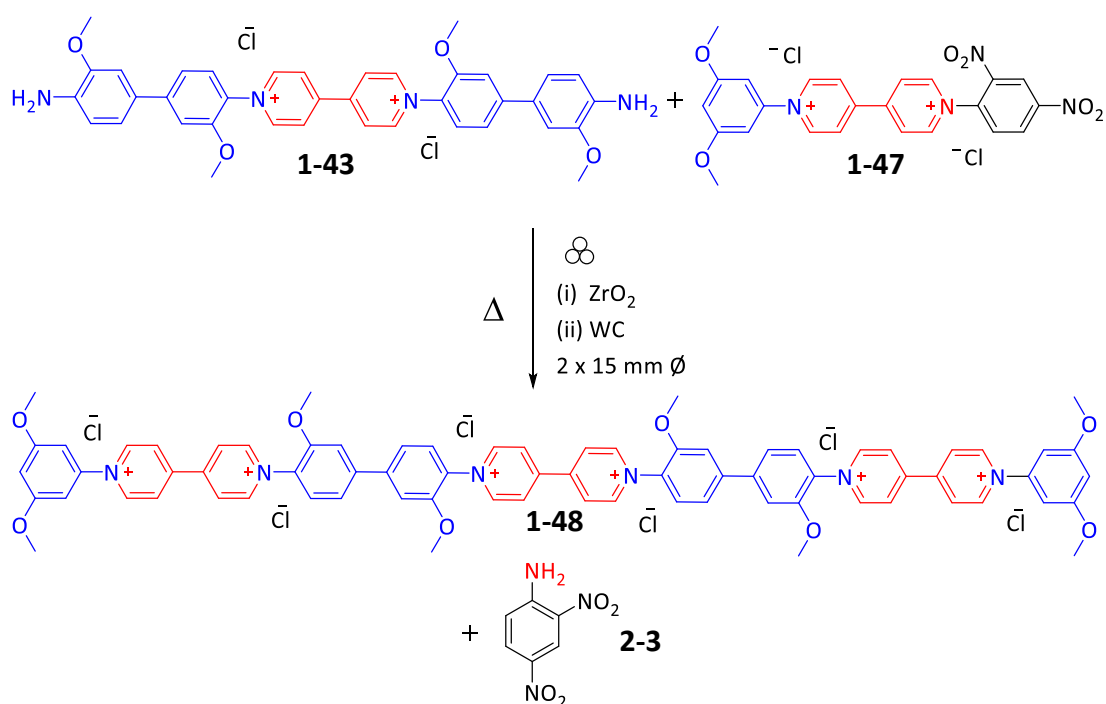
Scheme 2-14 The substitution of the di-Zincke salt **1-2** to form the diamine **1-43**

Each of the four reaction steps to form the compounds **1-44**, **1-46**, **1-47**, and **1-43** were conducted using 4 distinct conditions where quantities allowed

Molecule	Solution		ZrO ₂		WC		Heat and Stir	
	Conv. (%)	Time (min)	Conv. (%)	Time (min)	Conv. (%)	Time (min)	Conv. (%)	Time (min)
1-44	90	1440	15	60	10	30	100	15
1-46	94	4320	100	60	NA	x	100	30
1-47	60	4320	100	60	0	30	83	900
1-43	95	4320	100	100	NA	x	NA	x

Table 2-2 Comparison of 4 different ways to make the precursors for hexacation **1-48**

The summary, **Table 2-2** shows that WC - although giving more energetic collisions than ZrO₂ - gave only 10% conversion in the single experiment that showed any conversion. The ZrO₂ gave 100% conversions with 3 out of 4 of the reactions, but not as quickly as the heat and stir. Reactions conducted in excessive amount of solvent required a lot of heating time, with much of the energy applied being taken up by inefficiently warming the solvent instead of energizing the reactive reagents and promoting the reaction. With solvent being effectively the bystander in reactions, the inefficiency of its use in synthetic procedures can be seen from these experiments.



Scheme 2-15 Reaction to form the hexacation **1-48** (a trimer) via VBM

The two components required to produce the hexacation, using VBM with both the ZrO_2 and WC were now in place. A stack of the ^1H NMR spectra of **1-43** and **1-47** and their reaction in the ball mill shows that the formation of the hexamer **1-48**, **Figure 2-14**, was unsuccessful. Not only did the ^1H NMR spectrum of the crude comprise of broad signals that lacked definition to be useful for analysis, but their appearance suggested that there was contamination from the milling materials making WC unsuitable for this reaction. Despite being unable to create the polymeric hexacation trimer **1-48** the success of solvent-free, heating and stirring to synthesise the precursors had reduced the reaction time over the course of three of the necessary reactions from a total of 166 h in solution to 16 h – a tenfold saving in heating time. For industrial scale manufacturing processes, this would have immediate environmental and cost benefits, currently the best way to achieve these savings is through reactive extrusion.

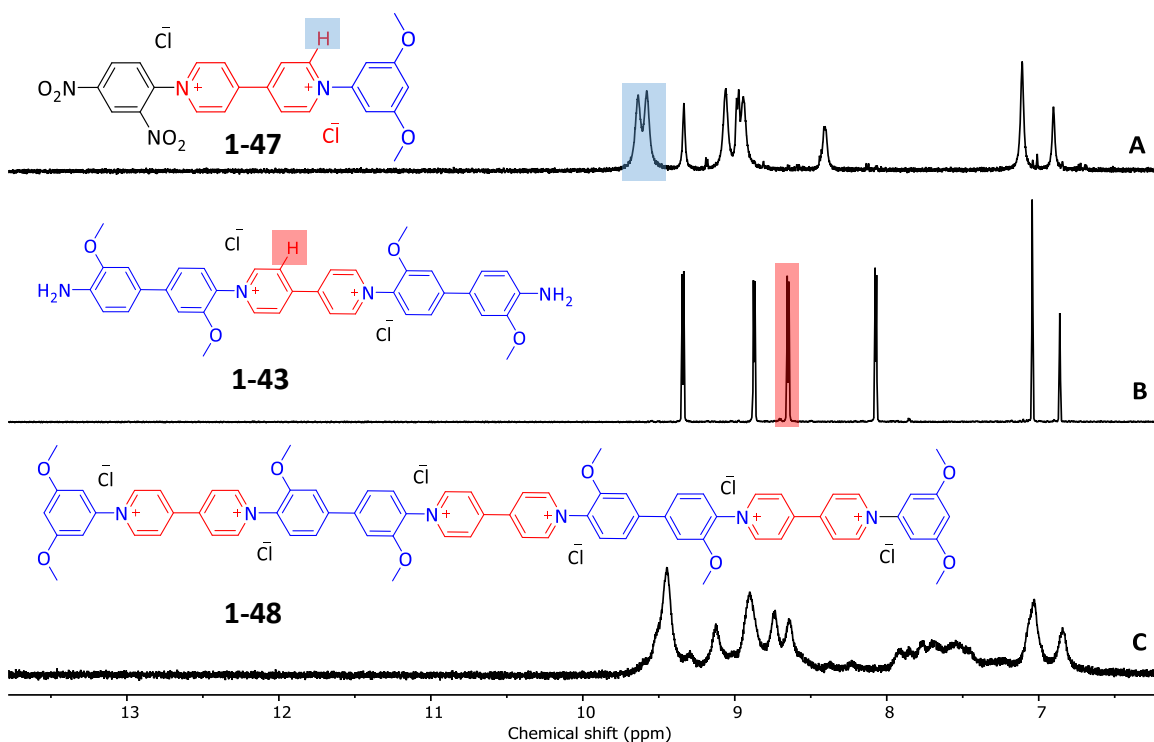


Figure 2-14 ^1H NMR stacked spectra for (A) asymmetric Zincke salt **1-47** (B) the diamine **1-43** and (C) the crude product after attempt from 30 min of VBM with WC, to make the hexacation **1-48**

These experiments have also shown that it is possible to increase the energy available for reactions by using the tungsten carbide (WC) jars, however the very broad peaks (spectra C) in the crude spectra indicate that contamination from tungsten carbide particles is a possibility. Experiments to synthesise **1-44** as seen in **Table 2-2** show that its synthesis is possible in all 4 conditions. This suggests that higher levels of kinetic energy through heavier balls increases the thermal energy available to push the reagents over their activation energy threshold using the VBM, more experiments and data would provide a better picture.

Another finding was that heat and stir experiments can also take hours and not just minutes on the hotplate. The reaction between chlorobenzene and the dimethoxy bipyridyl salt which required 15 h of heating and stirring, under argon, to achieve 83% conversion was the only reaction to require multiple hours of heating and was the longest solvent-free reaction at gram scale. This result is also in line with the discussion of $\text{S}_{\text{N}}\text{Ar}$ reactions for **Scheme 2-12** and the timescale becomes significant when considering scale-up quantities.

2.8 Conclusion

The reactions forming viologens in this chapter were concerned with the bipyridinium salt **1-2** and we were able to make a quantitative assessment of the relative reactivities of the substituting anilines. All of the reported experiments were performed using 2 equivalents of aniline to 1 equivalent of the di-Zincke salt. Observations from the iterative substitution reactions of Zincke salts are that solvent-free syntheses is possible and in multi-gram quantities using standard laboratory glassware, conductive heating and a magnetic stirrer bar. To overcome mixing problems with sticky mixtures, the addition of very small amounts of solvent to help mobilise the mixture and homogenise the reagents helps to improve conversion. Reactions conducted in this way gave target products in minutes as opposed to hours or days in solution.

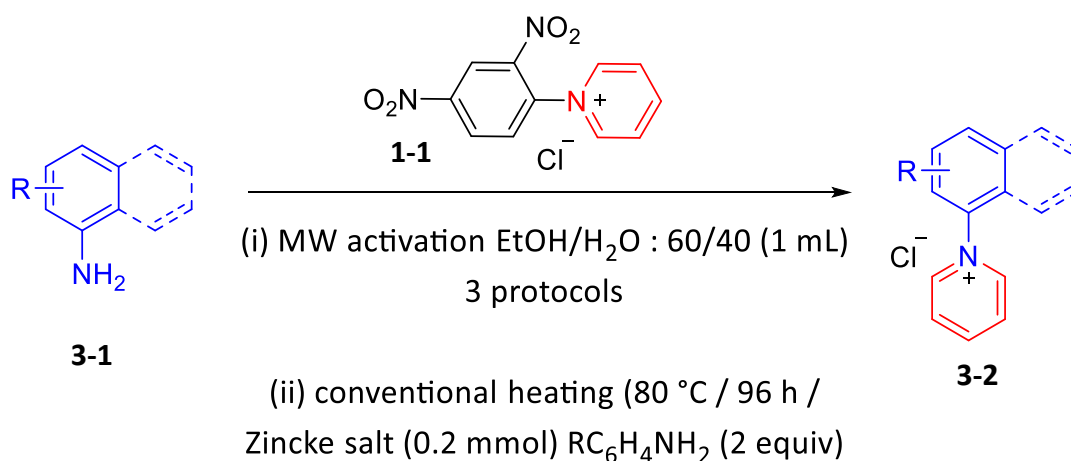
2.9 Further investigation of the Zincke reaction

Nucleophilic substitution reactions of the mono-Zincke salt had been scrutinised in the literature by Zeghib *et al.*¹³⁰ where they used microwave activation and solvent to show a number of phenomena including the relationship between pK_a and nucleophilicity of the aniline. Comparison of our VBM results to Zeghib's microwave with solvent experiments showed that all the di-Zincke reactions in VBM worked using the stoichiometrically-correct 2:1 aniline to di-Zincke salt **1-2**. Depending on the substrate, Zeghib reported using up to 12 equivalents of aniline to see a conversion for the mono-Zincke salt. This curious discrepancy was of sufficient interest to investigate having explored the Zincke Reaction in its bipyridyl form and the next chapter reports our work on the mono-Zincke salt's reactions with anilines in the VBM.

3. Mono Zincke salt and cyanine 5 dyes

3.1 Nucleophilic substitutions of the mono-Zincke salt

The reactions forming viologen derivatives in Chapter 2 were concerned with the nucleophilic substitution of di Zincke salts. We found that the conversion was related to the electronics, and sterics of the incoming nucleophile as well as any additional competing reactions (see **Fig 2-6**). However, it was clear that it should be possible to simplify our experiments further and examine the synthesis of mono-Zincke salts rather than di-Zincke salts using ball milling. Nucleophilic substitution reactions of the mono-Zincke salt as still of ongoing interest in the literature. For example, in 2016 as shown in **Scheme 3-1**, Zeghibib *et al.*¹³⁰ where they compared the yield and scope of Zincke reactions carried out under classical heating and microwave irradiation, in solvent, as shown in the scheme below.



Scheme 3-1 Zeghibib's microwave activation of the Zincke salt with anilines¹³⁰

When using classic heating they found that for anilines with pK_a values below c. 2.6 the conversion was poor (below 20%) even with an excess (c. 2 equiv) of nucleophile and extended reaction times (96 h). In contrast, when the pK_a of the aniline was over 3 the reactions essentially ran to completion (figure 3.1). In contrast to the classical heating results, when the same substrates were subject to MW heating, it was possible to observe good conversions (over 80%) even for reactions involving poorly nucleophilic primary amines (scheme 3.2).

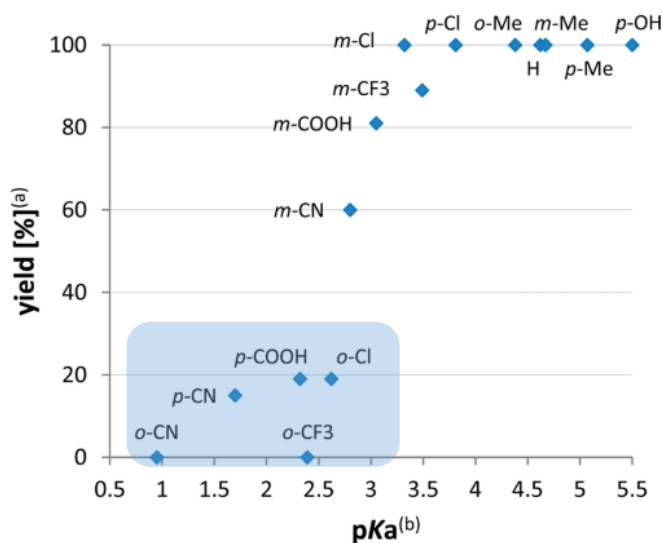
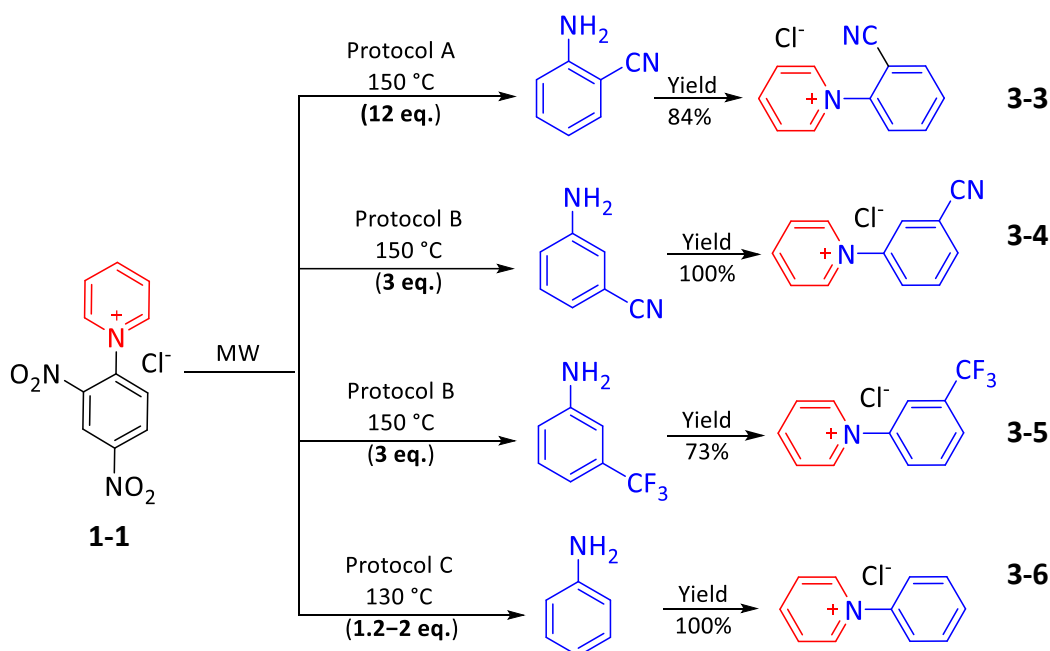


Figure 3-1 Reactivity study on aniline derivatives. Conditions: conventional heating (80 °C), 96 h, Zincke salt **1-1** (0.2 mmol), $\text{RC}_6\text{H}_4\text{NH}_2$ (2 equiv), EtOH/H₂O : 60/40 (1 mL). (a) Yields were measured by ¹H NMR spectroscopy in DMSO-d₆ in the presence of diethyl fumarate as external standard. (b) For pK_a values, see references.^{137–140} Figure with legends (sic) taken from¹³⁰

It should be noted that these reactions often required significant excess of nucleophile (for example 12 equivalents for complete conditions see **Scheme 3.2**) but the reactions were typically conducted for only 1h.

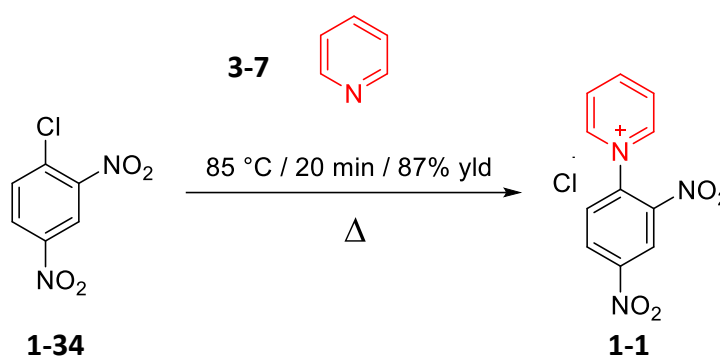


Scheme 3-2 Microwave activation conditions for substitution of the mono-Zincke salt **1-1**

During our work on viologen salts we had observed that the products were formed using 1:1 di-Zincke to aniline and were completed in less than 1 h in the VBM. We were therefore interested to see if the ball milling protocol could be transferred to mono-Zincke salts during this next phase of the work.

3.2 Solvent-free synthesis of the mono-Zincke salt

The need for multi-gram syntheses of the starting material, the mono-Zincke salt **1-1**, meant using the classical solution method instead of VBM. However we could still try a greener synthesis by not using solvent in the preparation. A literature search gave a synthesis by Robertson¹⁴¹ *et al.* that unusually did not use solvent, unlike 36 other separate entries in the ReAxys Database.



Scheme 3-3 Solvent-free synthesis of the Zincke salt **1-1**, 87% isolated yield

An initial attempt to make ca. 10 g of the mono-Zincke salt **1-1** using equimolar amounts of 1-chloro-2,4-dinitrobenzene **1-38** which is a solid with a mp 48-52 °C, in liquid pyridine (1 equiv.). Heating and stirring to 85 °C formed a homogeneous solution. Precipitation of the product appeared from the solution and after a further 10 minutes of heating, it was considered complete as the magnetic stirrer could no longer spin in the solid mass formed. The crude solid was broken up and stirred in acetone, then dried to yield 87% isolated product of the target compound **1-1**. The ¹H NMR assignment of the mono-Zincke salt **1-1**, as seen in **Figure 3-2**, shows again that the ¹H that is positioned between two nitro groups – H₆ – has an integrated value 20% below the expected value (spectrum A). As was shown for the ¹H NMR spectrum result for the di-Zincke salt **1-2**, (see **Fig 2-1**). Changing the

relaxation delay parameter on the VNMR600, this time to 10 sec, provided a spectrum with the expected integrated values (B).

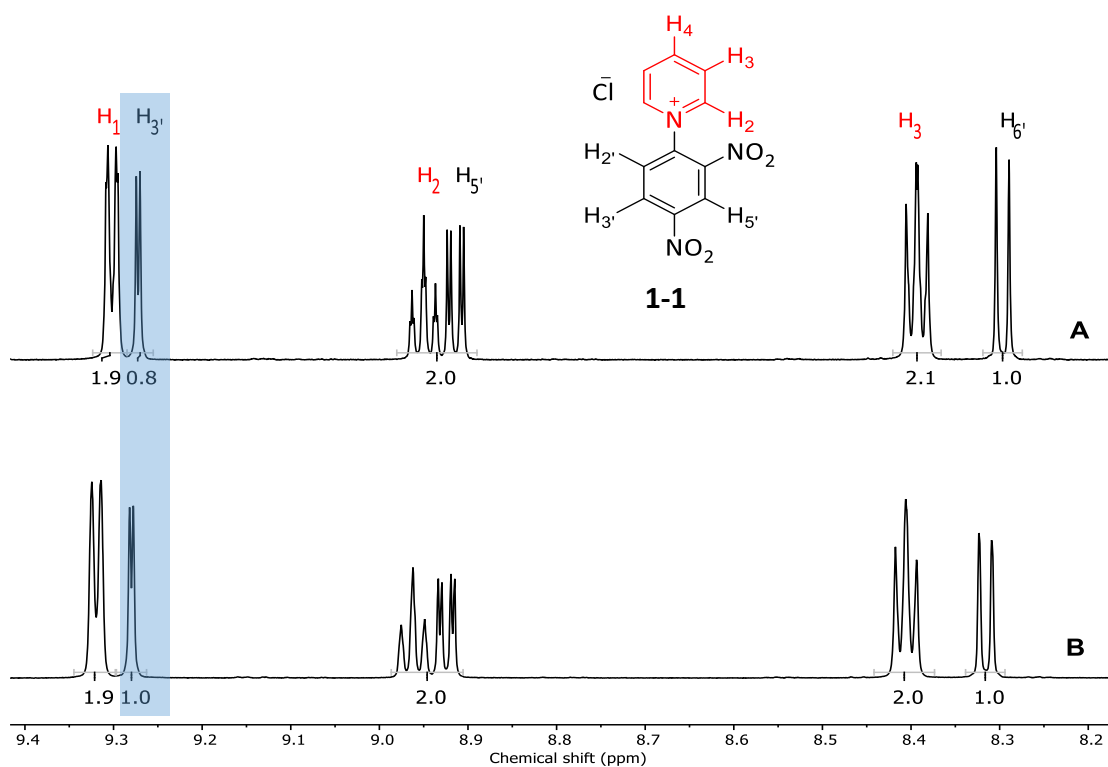
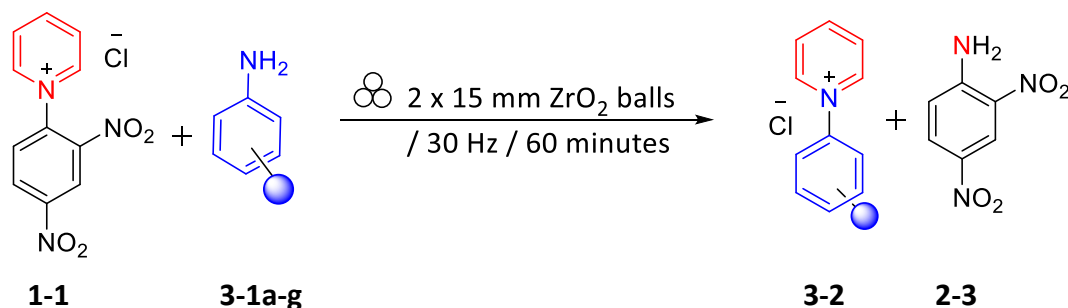


Figure 3-2 Assignment of the ^1H NMR for Mono-Zincke chloride **1-1** with (A) 1 sec and (B) 10 sec relaxation delay

3.3 Ball-milling the mono-Zincke salt with nucleophilic anilines

With enough of the mono-Zincke salt easily and quickly prepared, the first ball-milling experiment was to use it with equimolar amounts of the aniline – we began with *p*-toluidine as shown in the scheme below.



Scheme 3-4 A solvent-free route to substituted pyridinium salts, **3-2**

The mono-Zincke salt and *p*-toluidine were oscillated in 25 mL ZrO₂ vessels with 2 x 15 mm Ø balls, at 30 Hz for 45 minutes. Having only worked with the VBM using the di-Zincke salts to make substituted viologens, the expectation was for a crude product in some shade of brown as all previous experience had shown. Upon opening the milling jar, it was very surprising to find a vivid red powder. MS data on a sample of this gave a molecular ion peak at M/Z = 277.1705. This suggested the formation of the ring opened product **3-8a**. These are known in the literature as a class of compounds termed Cyanine 5 dyes (Cy5), Marvell *et al.*¹⁴² had reported the formation of red crystals upon the addition of the di-Zincke salt dissolved in aqueous ethanol to a solution of the aniline, also in aqueous ethanol.

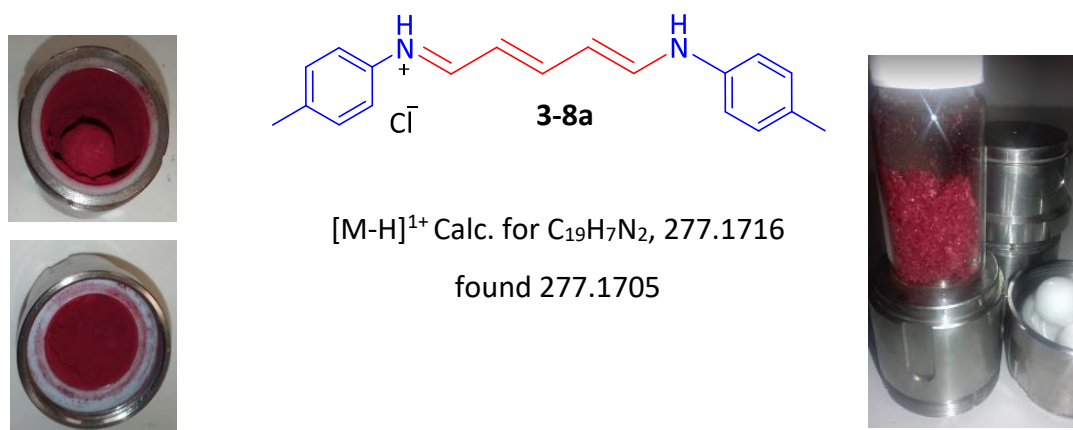


Figure 3-3 (L) VBM of the crude product mixture (Centre) Structure of *p*-tolyl Cy5, **3-8a** and (R) after recrystallisation

Analysis of ¹H NMR spectrum of this crude red powder, spectra (B) is shown in **Figure 3-4** along with the isolated product (A), *p*-toluidine (C), the leaving group dinitroaniline (D) and the mono-Zincke starting material (E). Using the data, we were able to identify the four compounds present in the crude reaction mix (B). With all the signals in the crude spectrum B attributable to each of Cy5 **3-8a**, aniline **3-1a**, mono-Zincke salt **1-1** and dinitroaniline **2-3**, there was no evidence for the formation of the closed-ring pyridinium **3-2** in the ball mill.

Spectrum (B) is the crude reaction mixture and shows that almost all the starting material *p*-toluidine **3-1a** has been consumed in the formation of the open-ring molecule **3-8a** (highlighted in green) whereas there is a much larger excess of the mono-Zincke salt **1-1**

(highlighted in red). We can also see that the expected leaving group, dinitroaniline (highlighted in blue) and shown in spectrum D, is present in the crude mixture.

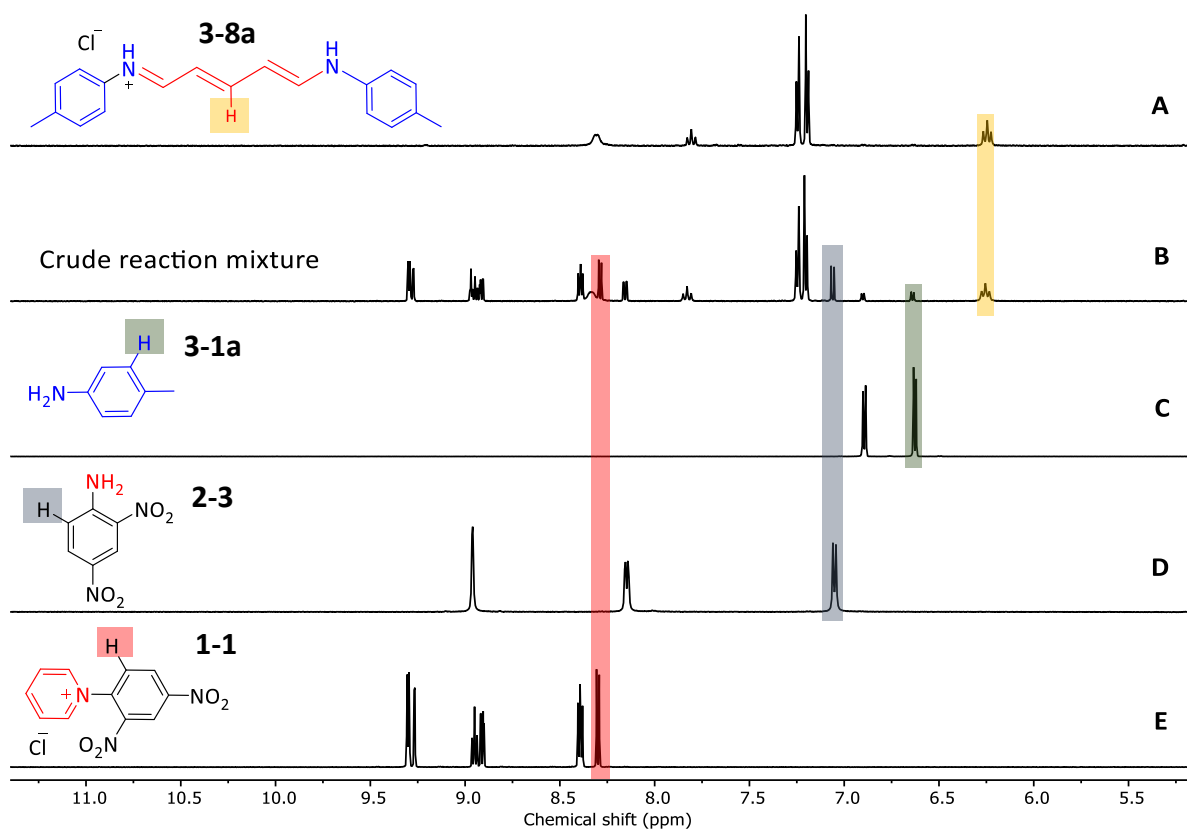
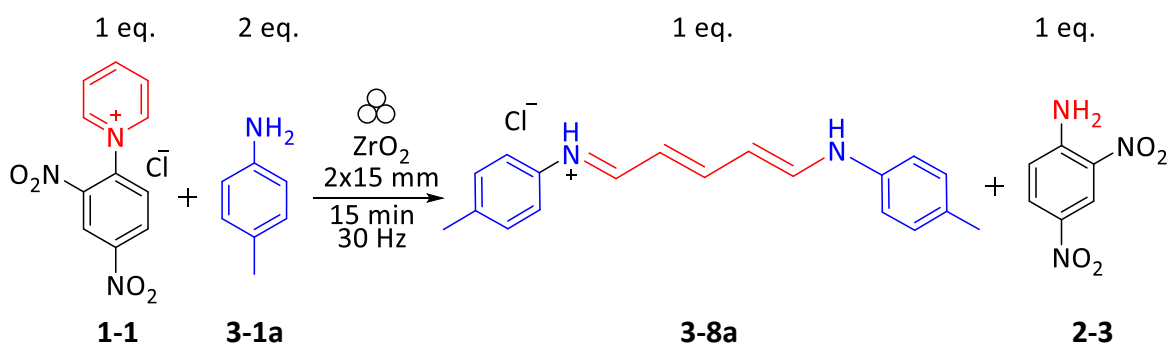


Figure 3-4 ^1H NMR stack of reaction between equimolar mono-Zincke salt **1-1** and *p*-toluidine, (A) isolated product **3-8a** (B) crude reaction mixture from ball mill (C) **3-1a** (D) **2-3** and (E) **1-1**

Assessment of the ^1H NMR spectroscopy data, as shown in **Figure 3-4** gave further useful investigative experiments to test the result. We sought to double the amount of aniline **3-1a**.



Scheme 3-5 Ratios of reagents to achieve Cy5 products from the mono-Zincke salt, **1-1**

This corresponds with the double substitution at both ends of the open ring and so a change in stoichiometry for this reaction by using 2:1 for aniline:mono-Zincke may give a more complete conversion of the Zincke salt **1-1**, **Scheme 2-5**. Therefore, this synthesis was repeated in VBM with the 2:1 ratio amounts and sampled at five-minute intervals for ^1H NMR spectra analyses so that we could evaluate the conversion as a function of oscillation time.

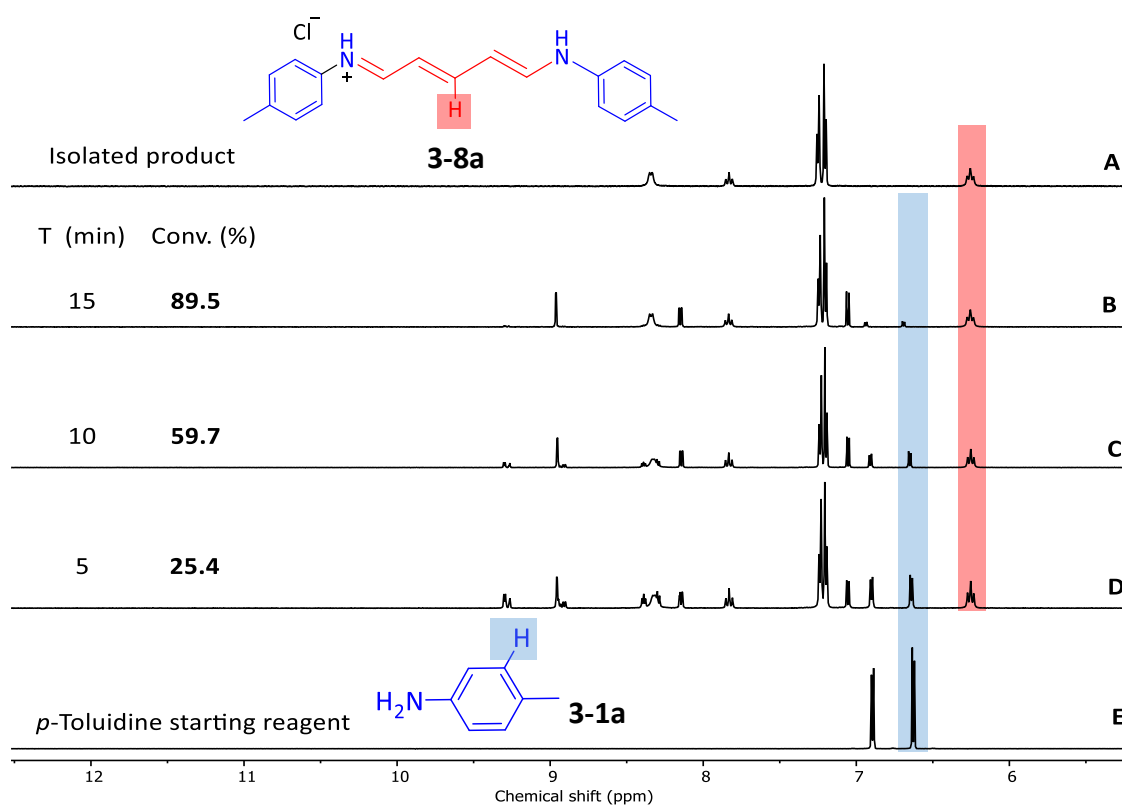
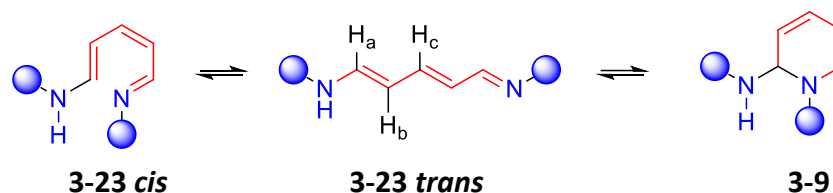


Figure 3-5 ^1H NMR spectra stack showing conversion as a function of time oscillated where spectrum (A) is isolated product **3-8a** (B) after 15 min (C) after 10 min (D) after 5 min of oscillation time and (E) starting material *p*-toluidine **3-1a**

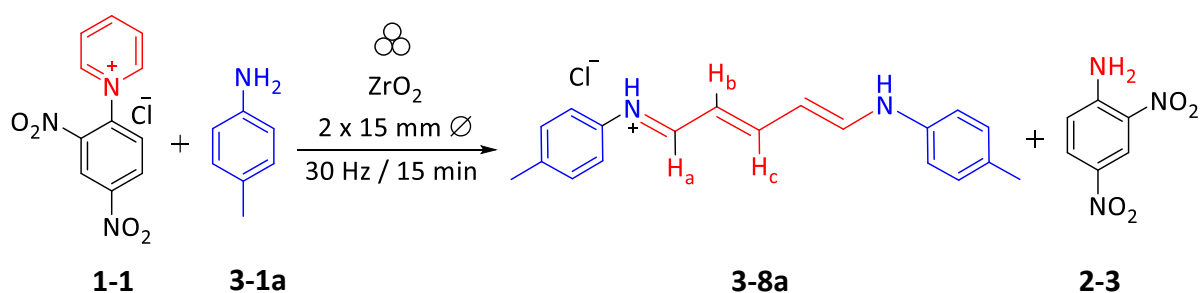
Using our stack of spectra ^1H NMR spectra in **Figure 3-5**. We can see that the intensity of the ^1H (highlighted in the blue) decreases from spectra D > C > B as more of the *p*-toluidine **3-1a** is consumed as the reaction proceeds. Less obviously, the intensity of ^1H signals (highlighted and shaded red) for the Cyanine 5 product **3-8a** increases over the 5 minute intervals in the VBM by 25, 60 then 90% . Comparison with **Figure 3-4 (B)** – which shows an excess of the Zincke salt, **1-1** – whereas **Figure 3-5 (B)** shows that the starting materials have been mostly consumed. The double-substituted intermediate that forms can take on both cis and trans configurations. The cis form allows a concerted 6π cyclisation giving **3-2**

under particular reaction conditions. Subsequent protonation/solvation of the amino leaving group gives the closed ring-pyridinium salt.



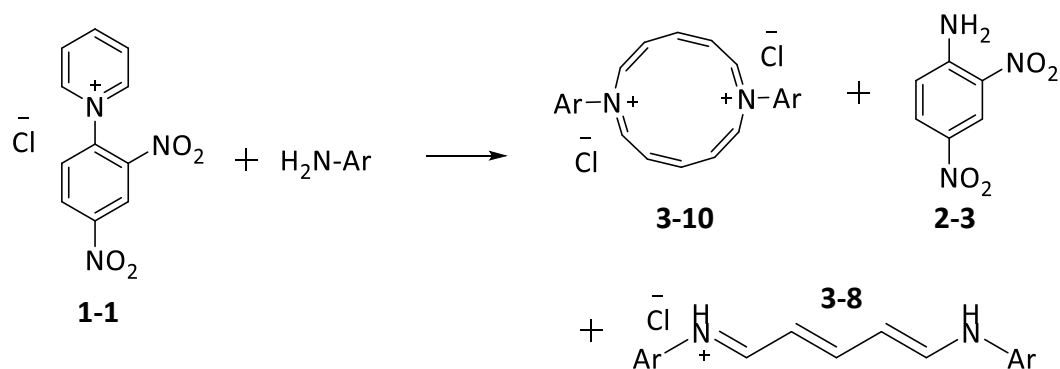
Scheme 3-6 Structures of the intermediates of the Zincke Reaction

With the Cy5 structure **3-8** identified and found in the literature,^{142,143} the ¹H responsible for the doublet is **H_a**, and the two sets of apparent triplets are **H_b** and **H_c**, in spectra **A (Figure 3-5)**. Their coupling constants are within the expected range (11-18 Hz) for vicinal *trans* ¹Hs.



Scheme 3-7 Reaction between mono-Zincke chloride **1-1** and p-toluidine **3-1a** via VBM

The pyridinium salt **3-2** and **3-8** the Cy5 are compounds discovered by Zincke^{124,143} in 1904, and their syntheses has been investigated in many different contexts. Its unusual reaction mechanism was explained in 1979 by Van der Plas.¹²⁵ However, the path of discovery has not been without controversy. Yamaguchi¹⁴⁴ *et al.* published their postulated formation of N-substituted diaza[12]annulenes, from the Zincke salt **1-1** which was later discredited but their work also gave details of the synthesis of a series of Cy5s. They reacted the Zincke salt, **1-1** with anilines and arrived at what they believed to be a 12-membered ring, an annulene.



Scheme 3-8 Yamaguchi *et al.* and their postulated reaction of the Zincke salt **1-1** with Anilines to give **3-10**

Their work was followed by Shi *et al.*¹⁴⁵ who based their theoretical calculations on the posited annulene structures **3-10** in search of useful surfactants **3-11**. Both papers were corrected after it was pointed out in a letter to *Angewandte Chemie* by Professor Manfred Christl¹⁴⁶ that it is the pyridinium salt that is formed. However, the counter-argument was that the data from the researchers' Electron Spray Ionisation experiment clearly showed a dimer. Christl remarked that association of molecular ions in ESI was a well-documented phenomenon but also highlighted the similarity of their NMR data and melting point analyses of $> 220^\circ\text{C}$ for the bromo phenyl pyridinium salt.^{147,148}

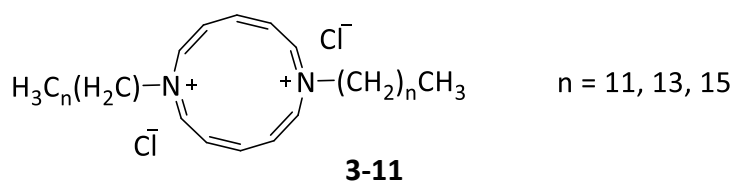
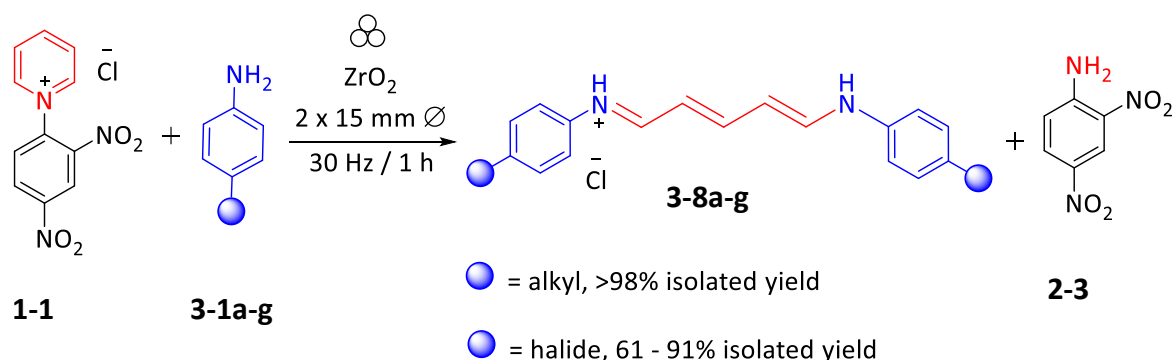


Figure 3-6 Shi *et al.* Structure of {12}Annulene gemini surfactants, **3-11**

UV-Vis studies of these highly coloured Cy5 compounds have been investigated by Van Dormael and Nys¹⁴⁹ and Marvell¹⁵⁰ *et al.* Further exploration of Cy5 can be found in the literature with the tri-ene motif, there are investigations into ring-opening reactions,¹⁵¹ and pyridinium salts used as a catalyst¹⁵² among many others.^{153–159} Using the expedient method of VBM we could quickly access these compounds and assess their utility for new or further applications.

3.4 General synthesis of cyanine 5 dyes in VBM

Although the formation of the ring opened product in solution is known,^{149,160} we were interested to see if the formation of Cy5 was a general phenomenon in VBM for a range of Zincke salts and anilines in the solid state. To achieve this efficiently, a rapid way of determining conversion for the reaction is required. This is exemplified for the reaction shown in Scheme 3-9, where the mono-Zincke salt **1-1** is added to an aniline **3-1a-g** in the milling jar along with 2 balls (15 mm \varnothing). This was also a good opportunity to investigate the reactions using a different milling material. We had found that steel was incompatible with these reagents (**Section 2-2**) and a further alternative to be considered was tungsten carbide (WC).



Scheme 3-9 VBM of mono-Zincke salt **1-1** with anilines **3-1a-g** using ZrO_2 and WC ball milling jars

WC is *ca.* 2.5 times denser than ZrO_2 , it is therefore likely to impart more energy during collisions in the ball mill. With our first experiments with WC (**Section 2-2**), it was decided to oscillate for less time in order to mitigate against material from the milling balls and vessel linings being potentially incorporated into the reaction mixture. Therefore the tungsten carbide jars were oscillated for 15 or 30 minutes depending on the substrate but the ZrO_2 vessels were oscillated for 60 minutes at 30 Hz.

The percentage conversion was readily established by ^1H NMR spectroscopy analysis after the completed reactions as shown with the ^1H NMR stack of spectra in **Figure 3-7**. The crude mixture is shown in spectrum **B**, along with the isolated products of the phenyl Cy5 (**A**) and dinitroaniline (**C**). The ^1H signals shaded red (**A**) and blue (**C**) are both represented in the crude mixture (**B**) and shows essentially 100% conversion.

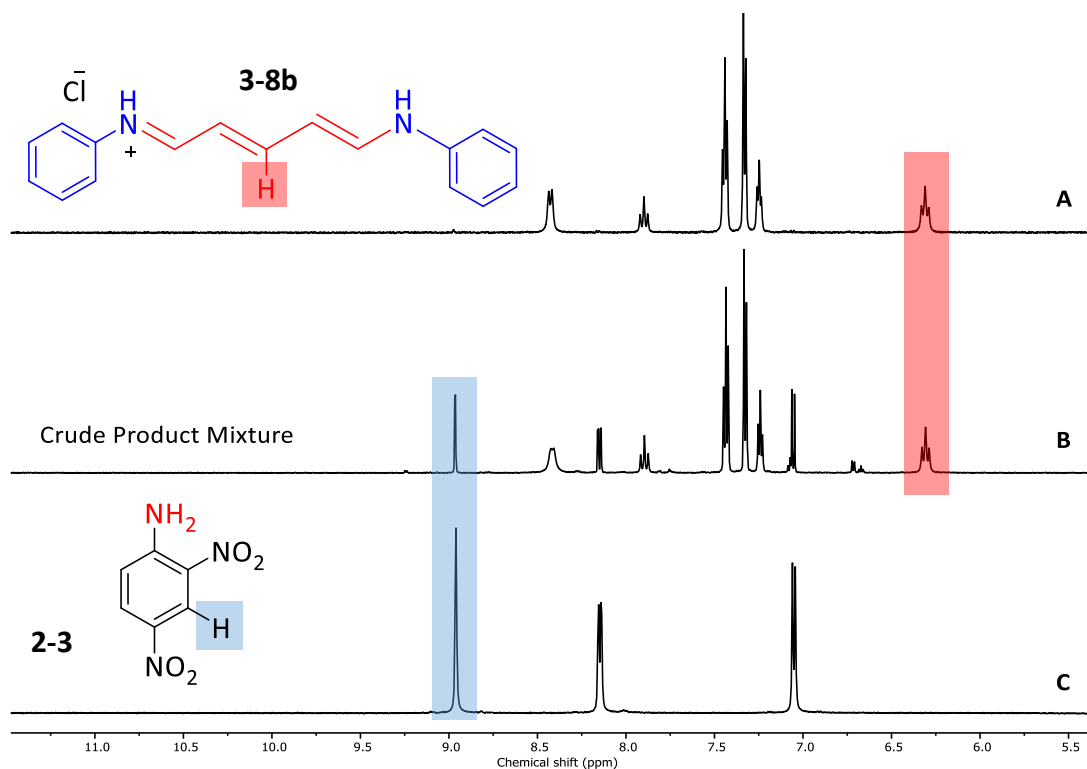


Figure 3-7 ^1H NMR spectra stack of the products of the mono-Zincke salt **1-1** and aniline **3-1b** reaction in VBM where spectrum (A) Cy5 **3-8b** (B) the crude product mixture and (C) the leaving group **2-3**.

With this conversion analysis established a full substrate scope could be readily carried out using 2 equivalents of aniline **3-1a-g** with the mono-Zincke salt **1-1**. Each resulting crude mixture was removed from the milling jar by dissolving in methanol. The leaving group, dinitroaniline **2-3**, is soluble in diethyl ether but the Cy5 **3-8a-g** is insoluble, and so our product was readily precipitated from warm diethyl ether, **Figure 3-8**.



Figure 3-8 (Left flask) Crude product dissolved in methanol, (Right flask) precipitation into warm diethyl ether

The experiment was repeated using a range of anilines **3-1a-g** and the mono-Zincke salt in different conditions, WC-Co and ZrO₂, details are shown in **Table 3-1**.

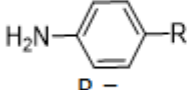
Entry	Aniline  R =	25 mL WC Jars			25 mL ZrO ₂ Jars		
		Time milled (min)	Conv. By NMR (%)	Isolated yield (%)	Time milled (min)	Conv. By NMR (%)	Isolated yield (%)
a	-CH ₃	15	100	87	60	100	99
b	-H	15	100	85	60	100	98
c	-OCH ₃	15	100	91	60	100	98
d	-OPh	15	93	84	60	99	98
e	-F	30	100	70	60	100	99
f	-Cl	30	56*	45	60	67	66
g	-Br	No data	No data	No data	60	61	61

Table 3-1 VBM of Mono-Zincke salt with anilines, *damaged balls

Two sets of data were collected, all reactions in the zirconium oxide vessels were oscillated for 60 minutes with new balls each time. Five entries **3-8a-e** gave near complete conversions as shown by ¹H NMR spectra analysis and also gave excellent isolated yields. **3-8f** and **3-8g** gave 66 and 61% isolated yields respectively. It should be noted that all the Cy5 products are vividly coloured, ranging from vermilion to deep maroon **Figure 3-9**.



Figure 3-9 Photograph of the Cy5 **3-8a-g** products showing the range of vivid red powders produced

The problem of milling accessories falling apart during the VBM process was shown to dramatic effect after dissolving the crude from the tungsten carbide (WC) vessel. Although

the red product was made (some residue is seen on the top of the filter funnel), the filtrate passed through tamped down celite leaving a layer of fine black powder. The powder was attracted to the magnetic stirrer bar retriever, and although tungsten carbide is not ferromagnetic, the manufacturer's specifications for the jars and milling balls show that the composition of the more accurate WC-Co includes 6% cobalt which is used as a matrix-binder in its manufacture. This therefore suggests that the black powder is that of finely milled alloy of cobalt and tungsten carbide.



Figure 3-10 (L) The result of filtering the crude through celite after activation in WC vessels, and (R) the magnetic property of the filtered solid with a magnet retriever

We had used ICP-MS to find the zirconium ions present in the crude mixture after milling with ZrO_2 balls, however after the WC-Co balls were cleaned, they were visibly degraded and pitted and likely that the tungsten carbide had come away and contaminated the reaction mixture. Although WC-Co works well for this reaction, it sheds material into the reaction mixture and therefore is not the best choice for this reaction. We can confirm that conversion of the reagents occurred in the WC-Co vessels, and that the vessels are too hot to touch after 15 minutes oscillation, however we surmised that it was WC-Co in the crude mixture because of its magnetic behaviour but the pitted and molten appearance of the damage observed on the balls looked unlikely to be solely due to impact forces. On the other hand, WC-Co has a melting point of $2870\text{ }^\circ\text{C}$ a temperature which may be attained by the Thermite Reaction (see **Figure 1-9**) where we have witnessed sparks from collisions. However, the formation of acidic halide, e.g. HCl, in the crude mix could be responsible for the smooth-edged indentations seen on the WC-Co milling ball **Figure 3-12 a and b**. through the degradation of cemented carbides (including tungsten) in acidic conditions.¹⁶¹

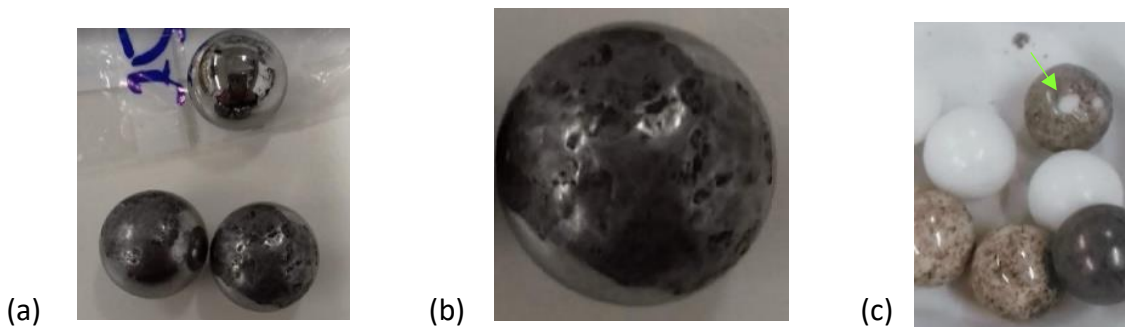


Figure 3-11 (a) damaged WC 15 mm diameter balls compared with the unused ball at the top of the picture. (b) enlarged picture of damaged WC ball (c) a chip of zirconium oxide that had come away from a stained ZrO_2 milling ball

This reaction in VBM confirmed that ball-milling is a successful, quick, and solvent-free route to the ring-opening of the mono-Zincke salt, **1-1** to give the intercepted intermediate, a Cy5 dye **3-8a-g** containing a fully conjugated methine chain. During the standard work-up of each product it was noticed that they were crystalline in nature, therefore efforts were made to grow single crystals of these dyes as discussed in the next section.

3.5 X-ray crystallography of compounds 3.3 a-g

Single crystals for X-ray structure determination for all the Cyanine 5 compounds, **3-8a-g** were grown by slow diffusion of diethyl ether into a methanol solution. The resulting molecular structures shown in

Figure 3-12, revealed the correct *trans* regiochemistry of the product and, therefore the substitution pattern of **3-8a-g** are confirmed to be the same for each molecule. Crystal packing for the compounds with halide substrates **3-8a-c**, gives a monoclinic crystal system with P21/n space group. The only other structure in this collection that shares the same monoclinic crystal system as the halides is **3-8a**, which is the *p*-tolyl, its solid state structure has been determined showing Z=2, with the stacking being very different to single molecule stacking. Similarly, **3-8g** was also found to be Z=2 but its structure could only be partially elucidated from the dataset. In contrast, the phenyl substrate, **3-8d** is orthorhombic with space group Pbc_a and finally **3-8f** has the methoxy substrate and has a tetragonal crystal

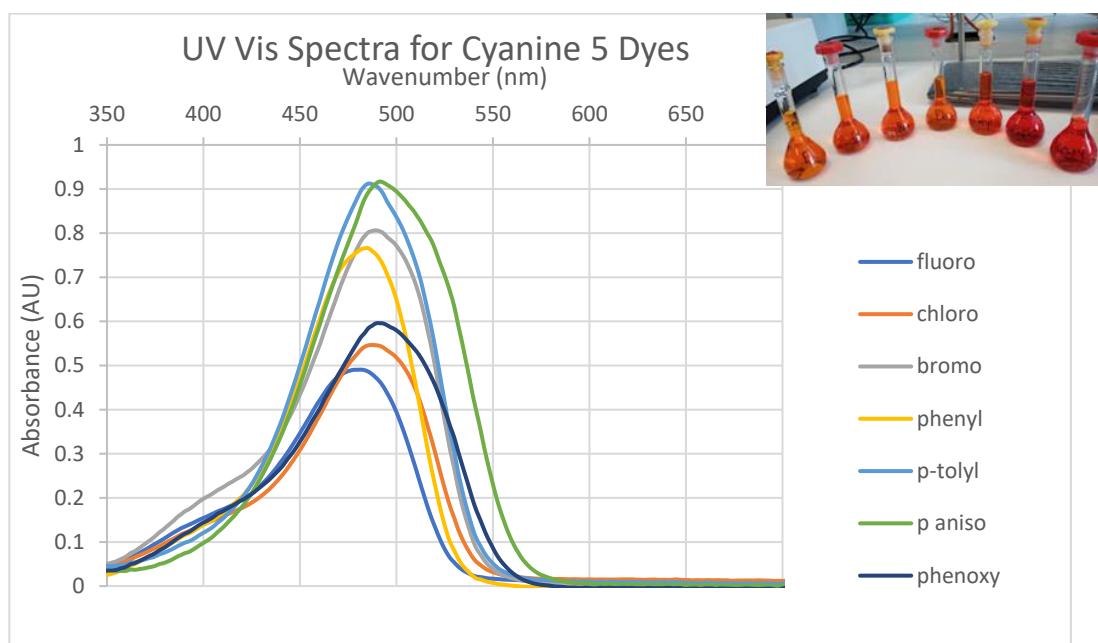
system with space group $I4_1/a$. With the data sets that are available for the structures, we were able to examine the bond lengths for each compound and the data is provided in the Appendix 2.



Figure 3-12 X-ray crystallography of compounds with counter-ions removed for clarity, **3-8a-g** showing solid state structures for methoxy substrate **3-8c**, p-tolyl substrate **3-8a** and phenyl substrate **3-8d** which were determined $Z=2$.

3.6 UV/Vis absorption properties of cyanine 5 dyes

The UV-Vis spectroscopic data for all the Cyanine 5 are presented in **Figure 3-13**. The λ_{\max} values for the Cy5s were found to exhibit λ_{\max} values between 481.6 – 491.2 nm.



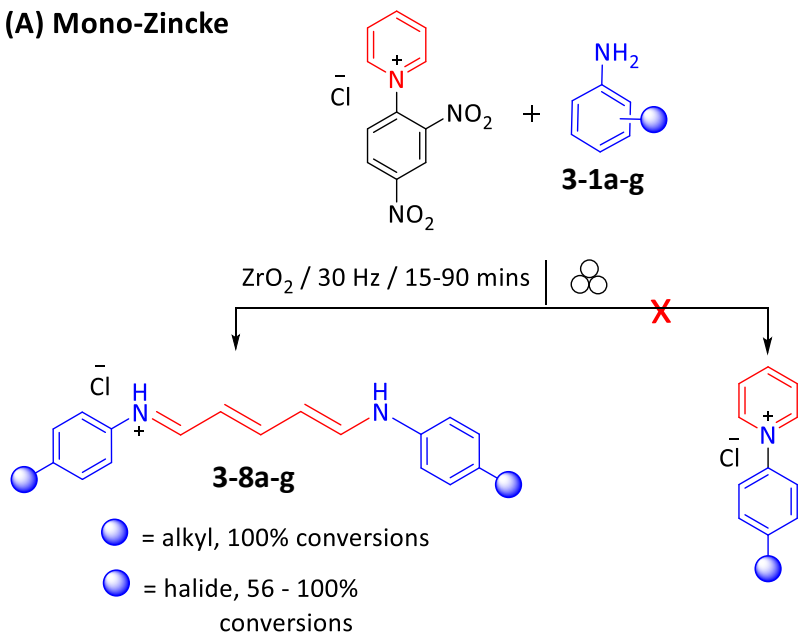
	p-tolyl	phenyl	p-aniso	phenoxy	fluoro	chloro	bromo
	3-8a	3-8b	3-8c	3-8d	3-8e	3-8f	3-8g
ϵ ($M^{-1}mol^{-1}$)	201000	132000	107000	203000	110000	122000	169000
λ_{\max} (nm)	485.4	485.4	491.2	491.2	481.6	487.4	489.3

Figure 3-13 Photophysical data of cyanine 5 compounds as observed using UV/vis absorption spectroscopy (4.5 μ M, methanol) for **3-8 a-g**

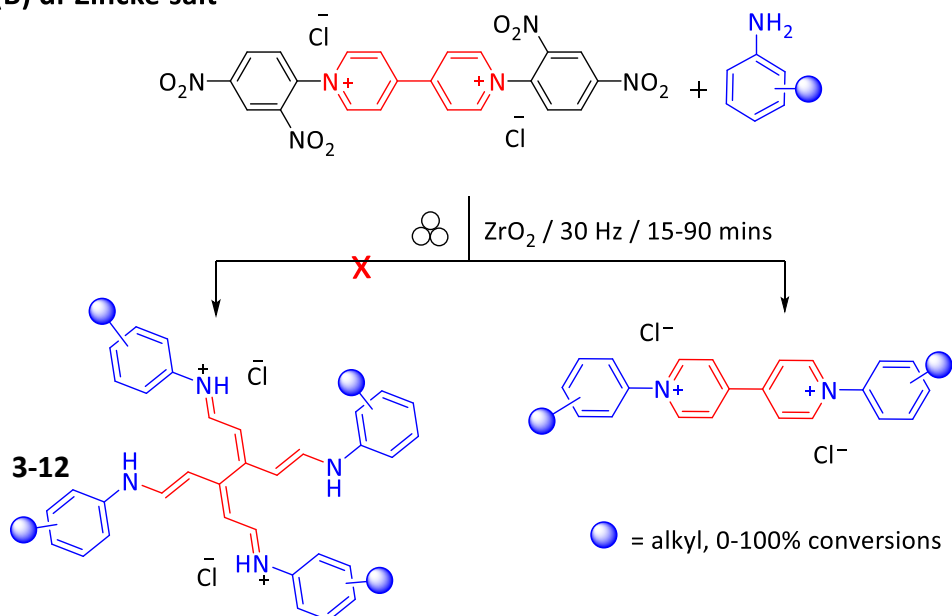
3.7 Synthesis of *p*-substituted pyridinium Zincke salts

The unanticipated and high yielding VBM synthesis of the ring opened Cy5 produced (Section 3.4) is in stark contrast to the predominance of the ring closed structures observed during the synthesis of viologen derivatives (Chapter 2) see **Scheme 3-10 (A)** and **(B)**.

(A) Mono-Zincke



(B) di-Zincke salt



Scheme 3-10 (A) Cy5 from reaction between mono-Zincke Salt **1-1** and anilines **3-1** and (B) di-Zincke salt **1-2** and anilines, the leaving group dinitroaniline **2-3** is not included for clarity

The difference in the propensity for the reaction to give ring-opened and ring-closed products prompted us to investigate the structural features that would lead to these different outcomes. We speculated that the difference in formation of ring-closed versus ring-open products could be a consequence of the substitution at the para position on the

pyridinium salt. Therefore, we planned syntheses of mono Zincke salts substituted at the *para*- position to see how this would affect their substitution with anilines. The objective for making **3-13** was to see if, like the pentamethines – the ring-open intermediate were favoured and double substituted - then we would see another Cy5 **3-14**. If the ring-closed, *cis* intermediate was preferred we should see the ring-closed pyridinium salt.

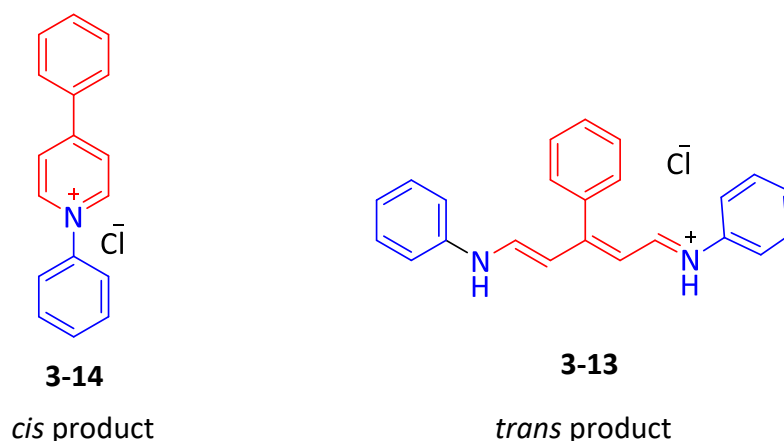
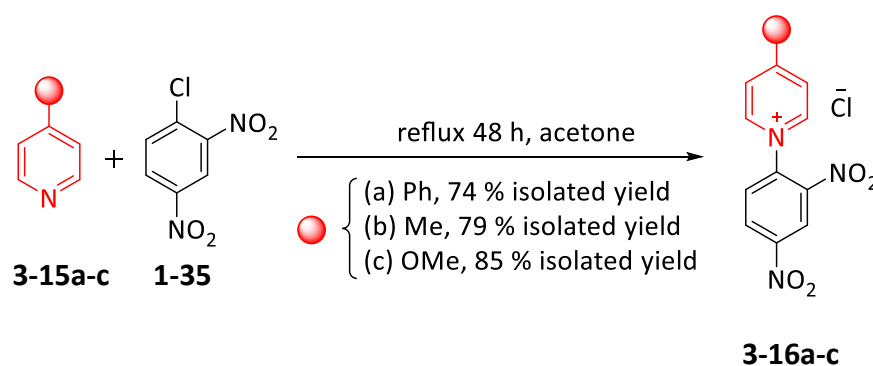


Figure 3-14 Possible structures from the substitution of the Zincke Salt

We selected substrates -Ph, -Me and -OMe as our *para* substituted pyridinium Zincke salts. Multi-gram quantities of each modified Zincke salt were obtained to investigate the scope of its substitution by aniline. The Zincke Reaction using substituted pyridines proceeded in solution, **Scheme 3-11**, and following the method of Steinhardt.¹⁶² 4-phenyl pyridine (**3-15a**) in equimolar amounts with 1-chloro-2,4-dinitrobenzene **1-35**, were added and dissolved in acetone then heated under reflux and stirred for 24 hours. The precipitate was washed with acetone and dried giving a 74% isolated yield, **3-14a**.



Scheme 3-11 Reactions for substituted pyridyl Zincke salts, **3-16a-c**

A set of ^1H NMR spectra shows a stack where spectrum **B** shows the isolated product, **3-16a** and its starting materials **1-35** (spectrum **A**) and **1-34** in (spectrum **C**) are given in **Figure 3-15**.

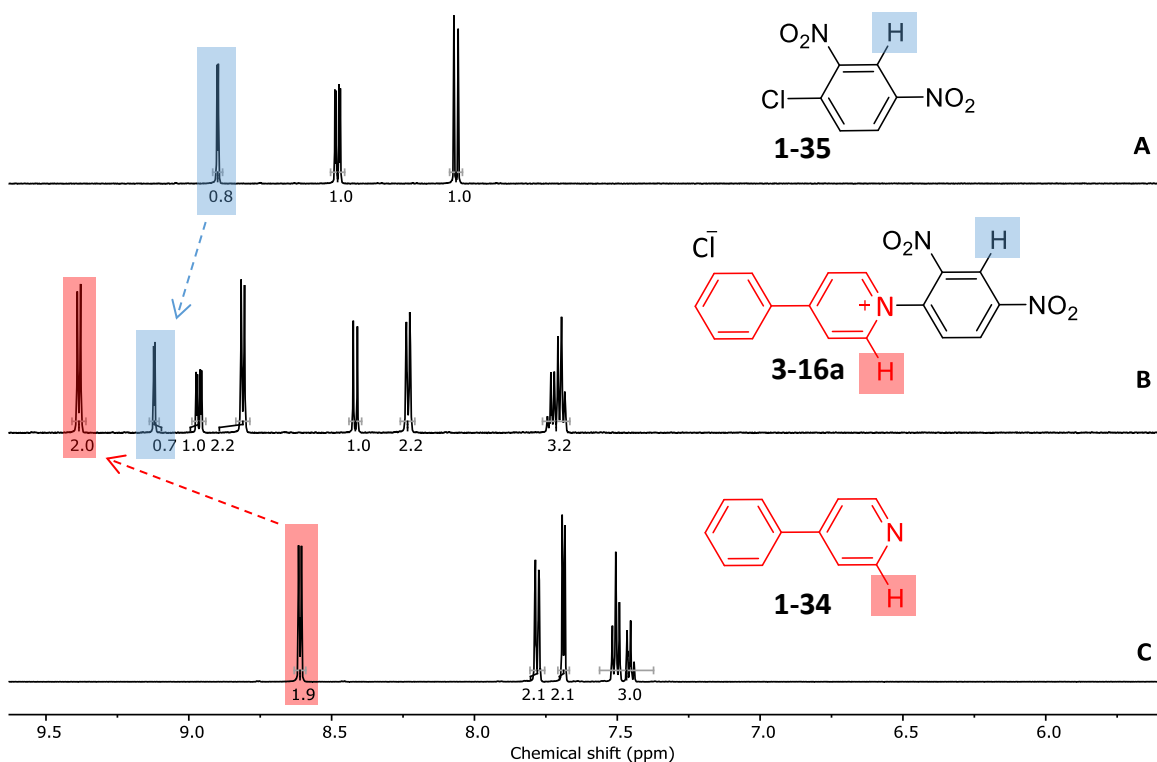
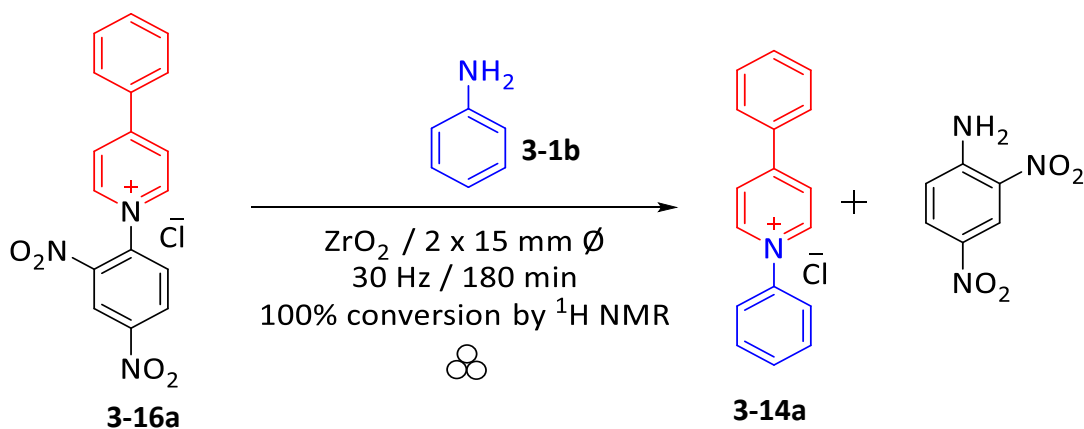


Figure 3-15 Stacked ^1H NMR spectra (**B**) Zincke salt **3-14a**, and (**A**) **1-38** and (**C**) **1-37**

The signals for the ^1H s highlighted in red and blue clearly show that the chemical shift values of the starting materials change significantly in their transformation via $\text{S}_{\text{N}}\text{Ar}$ into the Zincke salt **3-16a**. Without setting the relaxation delay time to 10-25 seconds for collecting the fid data, the integration for the ^1H located between the two nitro groups shown in ^1H NMR spectrum A for **1-38** integrates to 0.8 and in spectrum B for **3-16a** to 0.7 - these values are 20-30% below the expected value. Experiments for showing this was conducted using the mono-Zincke **1-1** and di-Zincke **1-2** samples (in Chapter 2) and has consistently featured in all ^1H NMR spectra involving the 2,4-dinitro aryl group because the default relaxation delay on the VNMR600 is set to 1 second.

Using 2:1 equivalents of the aniline and the Zincke salt **1-1**, a VBM experiment was conducted with samples taken at 30, 90 and 180 minutes. Conditions used were 2 x 15 mm \emptyset balls and with a frequency of 30 Hz.



Scheme 3-12 Reaction of 4-phenyl Zincke salt **1-1** with aniline **3-1b**

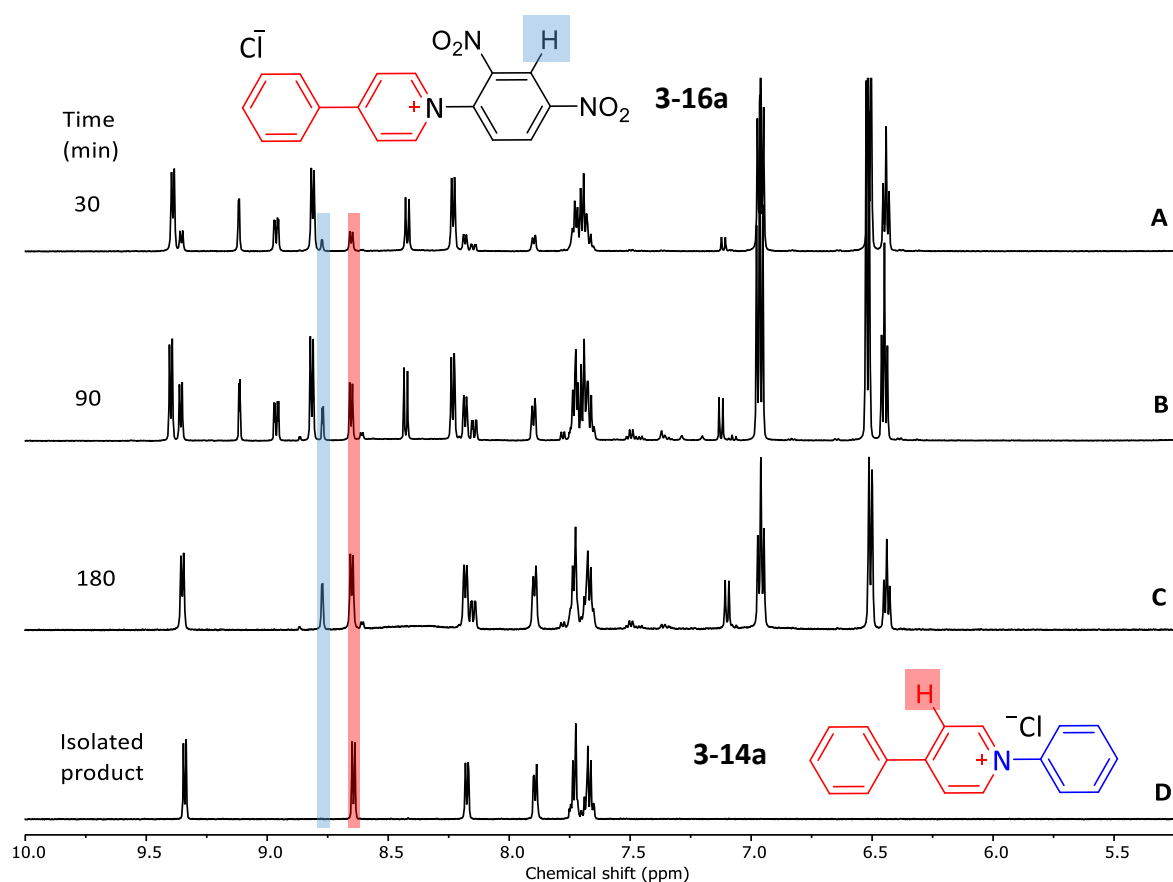
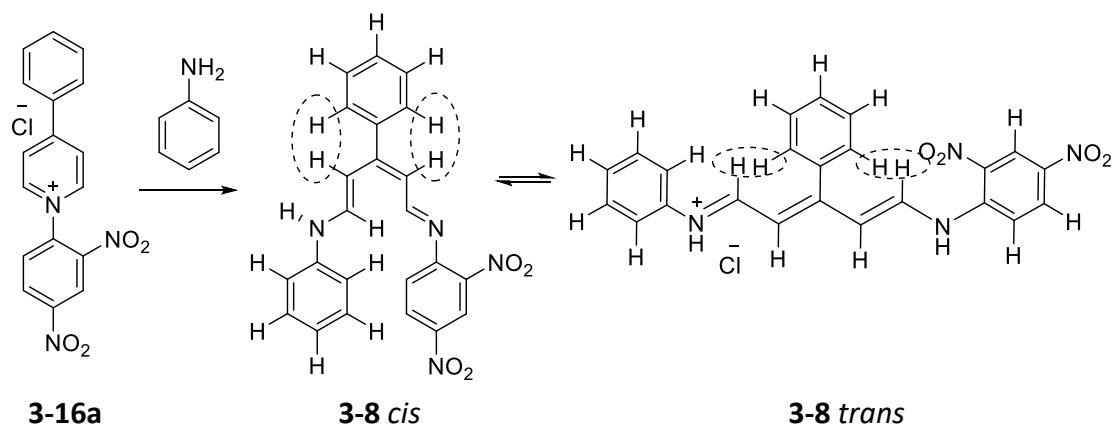


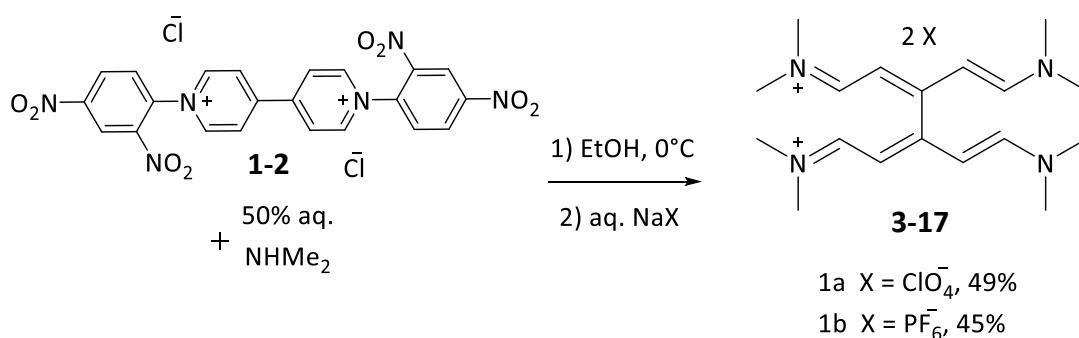
Figure 3-16 Evolution of substituted pyridinium salt **3-16a** over 180 minutes milling time using ^1H NMR stacked spectra to analyse for conversion (A) crude product mixture at after 30 min milling time (B) 90 min (C) 180 min and (D) the isolated product **3-14a**

Opening the jars, revealed a red powder but the idea that this may be a new Cy5 was not supported by the ^1H NMR data for the crude product, analysis of which showed 100% conversion after 180 minutes VBM of **3-14a** with **3-1b**. Despite the 100% consumption of **3-16a**, the isolated yield was very low (approximately 70 mg, 3%). The experiment was conducted with a 2:1 ratio of aniline **3-1b** to Zincke salt **3-14a**. As can be seen in **Figure 3-16** the ^1H NMR spectrum of crude mixture shown in spectrum (C) contains signals for the excess aniline **3-1b** but the Zincke salt **3-14a** has been completely consumed and only the ring-closed product is seen. The 4-phenyl pyridyl Zincke salt experiment helps to establish that the Zincke reaction mechanism, i.e. the nucleophilic substitution reaction is affected by the phenyl in the *para* position on the pyridyl ring and we can rationalize this finding by considering the steric arrangement for each type of resultant molecule.



Scheme 3-13 Cis and trans forms of the open ring Zincke intermediate, **3-8**

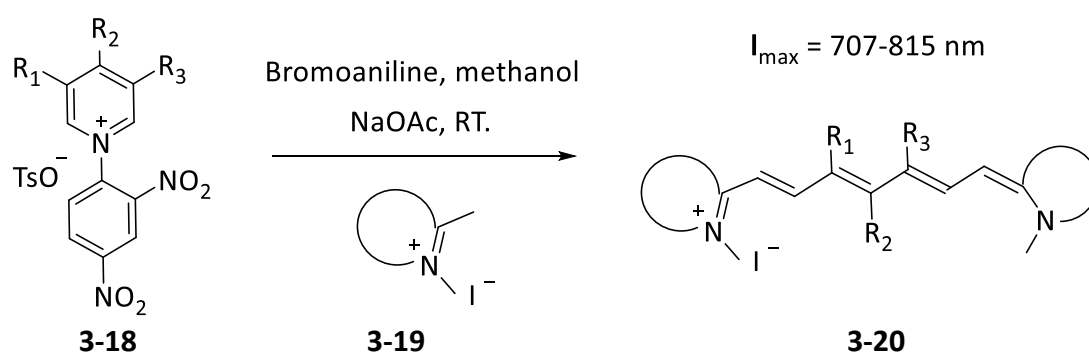
The *trans* conformation has protons on the aryl rings abutting, as shown in **Scheme 3-13** and are sterically unfavourable compared with those in the *cis* position. Therefore, the ring-closing that has to occur for the synthesis of the di-Zincke salt, **3-14a** is better understood from these considerations.



Scheme 3-14 Katoh's synthesis of pentamethine dimers, **3-17**

This is not to say that the open-ring molecule formed from the di-Zincke salt does not exist. **Scheme 3-14** shows the perpendicularly-linked pentamethinestreptocyanine dimers, **3-17** with the two cyanine moieties linked at the centre carbon atoms of the methine chains were prepared in solution by Kato *et al.*,¹⁶³ and was accessed via a secondary amine, with the bipyridine. The secondary amine, once it forms the doubly substituted intermediate **3-17** with no ring-closure, forms the streptocyanine.

The VBM study with the methoxyaniline and the picoline (methyl) substituted Zincke salts **3-16b** and **3-16c** did not show any conversion to the Cy5 salt and we were unable to isolate these compounds. However, the VBM crude mixtures showed conversion to the ring-closed species using ¹H NMR spectroscopy analysis. Copious evidence for the ring-open intermediates is provided in the work of Štacková¹⁶⁴ *et al.* where the Zincke Reaction mechanism is exploited to form Cy7 (heptamethine) dyes, in solution, by using a series of variously substituted Zincke salts, **Scheme 3-15**. They used a variety of Zincke salts **3-18** with substitution at the *-meta* and *-para* positions of the pyridine heterocycle (R₁, R₂, and R₃). They were able to show that syntheses of Cy7 **3-20** with a variety of R groups, can change the values of the absorbance, λ_{max} for their prepared analogues. Bromoaniline is used in sub-stoichiometric amounts, where it functions as a catalyst in the reaction with indolium iodide salts **3-19**. Štacková and co-workers' reaction required 16 h to accomplish yields of **3-20** of up to 94%.



Scheme 3-15 Štacková¹⁶⁴ *et al.* - Approach to a substituted heptamethine cyanine chain by the ring opening of Zincke salts

An interesting result is that they report only one aryl substitution on the methine chain, a phenyl group at R₃ and not at R₂ corresponding with our result that shows when R₂ is an

aryl group, the pyridinium salt is produced and not the intercepted trans intermediate Cy5. In the 17 examples of **3-20** that they give, none have an aryl in the 4-position and our study would suggest that aryl-substitution at the *para* position forces ring-closure. The complete Zincke reaction mechanism involves several steps prior to the pericyclic rearrangement seen in Marvell's experiments. The complexity of the reaction sequence means the relationship between substrates and the efficacy of the aniline requires further study, as does Štacková¹⁶⁴ *et al.*'s route to Cy7 using the Zincke Salt as the starting reagent which has yet not been attempted in the solid state. With the Cy5 salts to hand, their X-ray analysis gave us the data to verify bond-lengths in the polymethine chain.

3.8 Electronic symmetry in Cy5 salts

Our focus on looking to synthesise conductive organic materials had taken an unanticipated new direction: the synthesis of polymethine dyes from the ring-opening of the Zincke salt with anilines. The confluence of the two different electro-physical and photophysical properties is neatly summated in recent work by Anderson¹⁶⁵ *et al.* who made use of polyenes to form a cyanine series of the form –

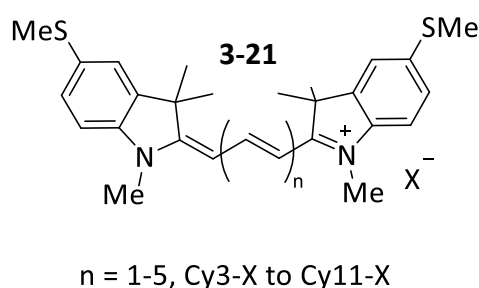


Figure 3-17 A series of long polymethine molecular wires

Electrical conductance in discrete molecules is of particular interest in a variety of applications requiring the transport of charge over several nanometres with minimal losses.^{166,167} In polymethine cyanine dyes which have structures featuring long conjugated chains, we can think of them as molecular wires. It has been shown by Anderson¹⁶⁵ *et al.* that up until Cy9 there is bond-length alternation, after which, there is distortion with the positive charge at one end away from the π -system in the extended chain. Charge distribution where Bond Length Alternation (BLA) is non-zero resembles behaviour found in solitons of polyacetylene, as seen in Heeger's doped poly-olefin.¹⁶⁸ De-localisation of

charge in polymethines between Cy3 and Cy7 is symmetrical and their electronic structure resembles a one-dimensional free-electron gas. However, Cy9 and Cy11 is found to undergo a symmetry breaking Peierls transition and they are sensitive to the polarity of the counterion.¹⁶⁵

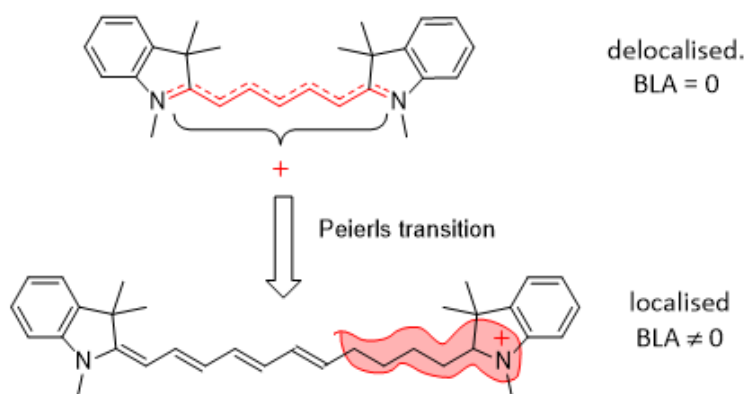


Figure 3-18 A symmetry breaking Peierls transition

With the acquisition of the crystal structures for all our Cy5s, the data set has all the calculated bond lengths and a comparison of each structure's BLA across the series would show whether their electronic symmetries were consistent. It is noted that for their series of BLA calculations, Anderson's methine chains have a heterocyclic nitrogen atom in the conjugated system whereas in the Cy5 molecules, the nitrogen is in a polymethine chain.

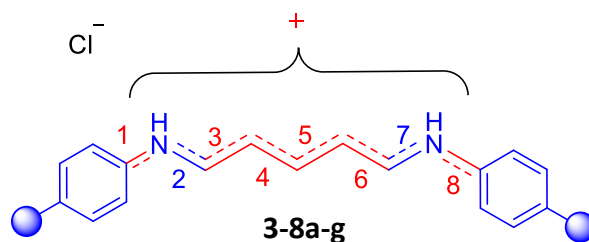


Figure 3-19 Bond lengths in the Cy5 methine chain

These values are consistent with expected bond orders of 1.5 for alkenes where each carbon has 2 electrons in the sigma bond but share an electron in the π -bond. The overall charge for the molecule is +1 and is delocalised across the length of the chain, resulting in a Bond Length Alternation (BLA) of 0. Establishing this for Cy5s gives an insight into the electronic behaviour of longer polymethine chains, Cy7-Cy11, as molecular wires as explained in the work of Anderson *et al.*¹⁶⁵

Understanding the conducting behaviour of molecules capable of transporting charge makes us better equipped to design a synthesis to improve the intended functionality. Greenland Group have demonstrated this, showing that conductivity increases with chain length of organic oligomers.¹²³

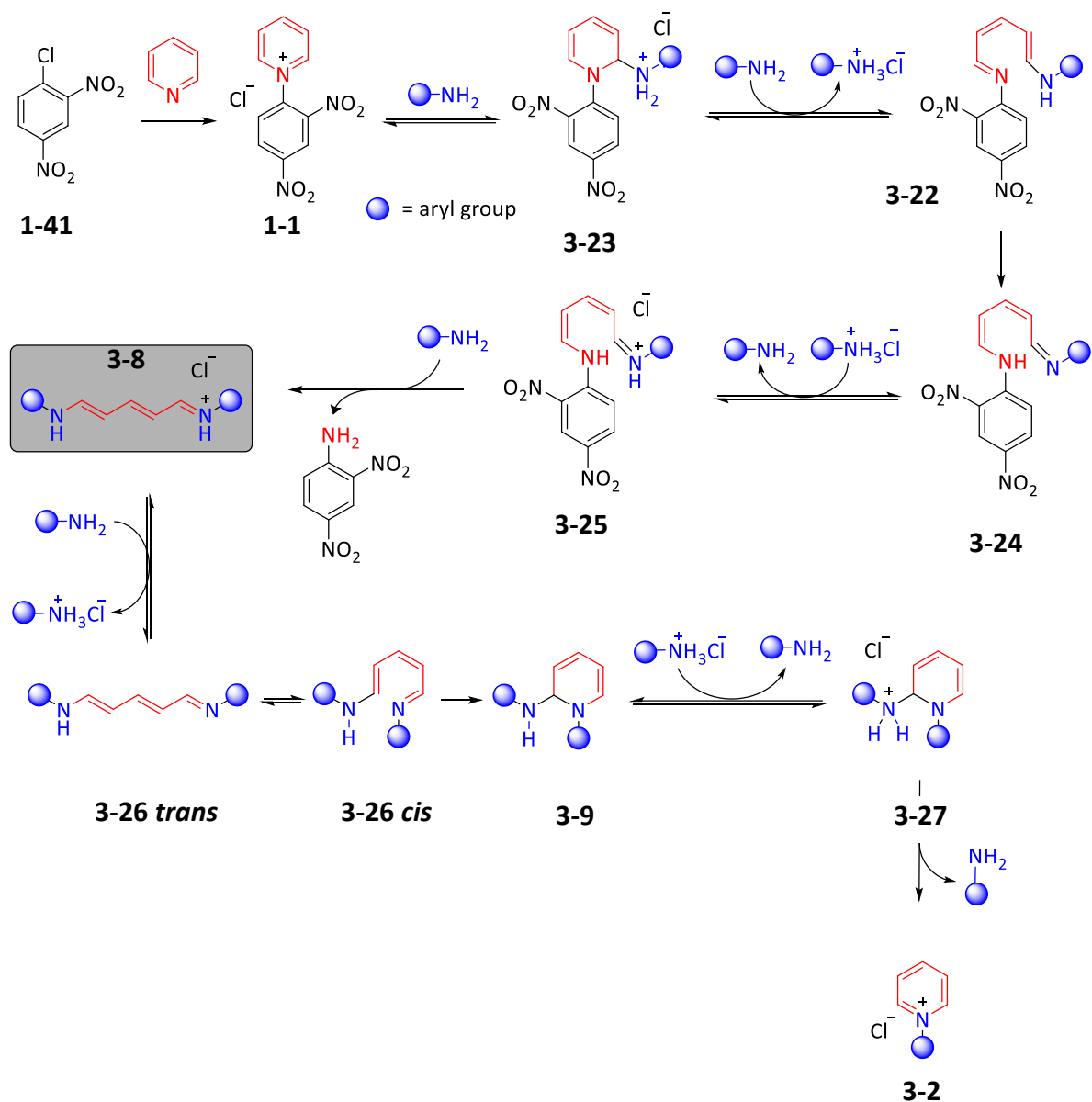
3.9 Understanding the Zincke reaction mechanism

The origins of the Cy5 from the mono-Zincke salt **1-1** is understood to be the intercepted intermediate **3-8** in **Scheme 3-16**. The full mechanism describing the Zincke reaction, concluding with the pyridinium salt has been explained and described in the literature^{125,170} along with reviews of reactions of the Zincke salt and its gluconaldehydes.¹⁷¹⁻¹⁷⁴

The reaction mechanism's acronym A_NRORC descriptor, describes the process as a nucleophilic addition, ring-opening, and ring-closing. Sections **3-2** – **3-6** discussed the solvent-free synthesis, isolation, and characterisation of seven analogues of the ring-open intermediate Cy5 **3-8**. This is the half-way stage of a scheme that culminates with the pyridinium salt **3-2**. The conditions for ring-closing to form the pyridinium salt requires the *cis* arrangement of the Cy5 molecule **3-26**, in **Scheme 3-16**.

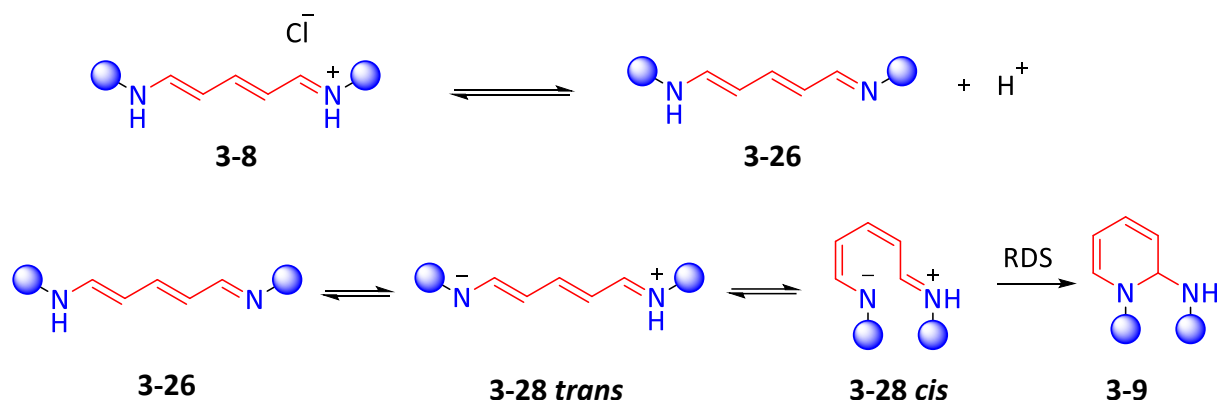
The equilibrium that exists between **3-26 trans** and **3-26 cis** is influenced by temperature and long reaction times (96 h) in solution or, as we saw in **Section 3-2**, through microwave activation¹³⁰ in aqueous solvent (30 min) by Zeghib¹³⁰ *et al.*

For the trans Cy5 molecule **3-8**, to undergo ring-closure, a cis arrangement is required, **Scheme 3-16**.



Scheme 3-16 The Formation of the Pyridinium Salt **3-2** requiring the neutral cis conformation of the Cy5 intermediate, **3-26**

The results of our X-Ray crystallography analysis confirmed that all the Cy5 molecular structures obtained from our crystals in the solid state contained the negative chloride counterion and gives the Cy5 molecule an overall positive charge, **3-8**, highlighted in the grey box in **Scheme 3-16**.

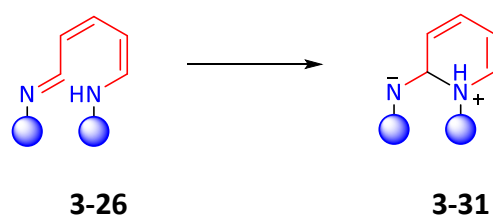


Scheme 3-17 Marvell's scheme accounting for the pH-independent behaviour in the basic region and for the reduction in rate of cyclisation with increasing acidity in solution

Marvell *et al.* had shown that structures **3-8** and **3-26** are in equilibrium through their UV-Vis spectroscopy studies¹⁶⁰ and the requirement of the cis conformation of **3-28** to enable ring-closure. They reported that in the presence of excess trimethylamine the equilibria is pushed in favour of **3-28**.

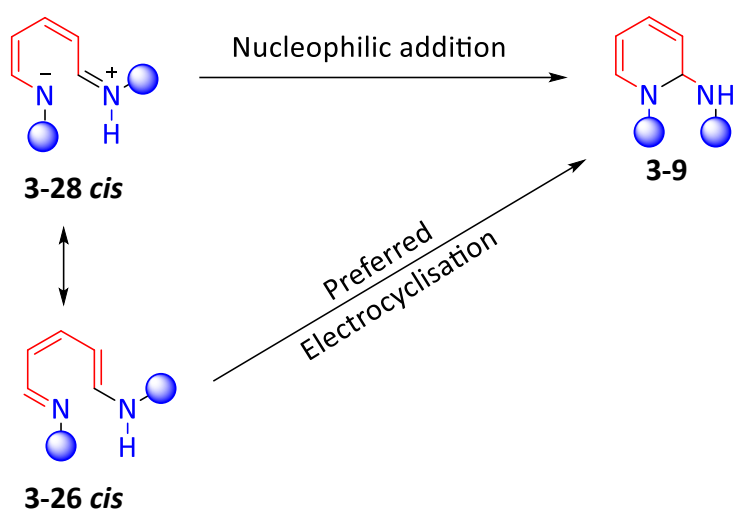
Marvell used three sets of experiments using solutions in methanol to investigate the influence of (i) base (MeO, Et₃N and Bu₃N), (ii) perchlorate salt and (iii) buffer, on the rate of cyclisation of **3-8** into the pyridinium salt **3-2**. To account for the pH-independent behaviour they found in their first investigation using the bases as in (i) - their rationale is given in **Scheme 3-18**.

For a nucleophilic addition **Scheme 3-8**, this involves the conversion of a neutral molecule into a dipolar species. The electron-poor, unsaturated, C=N double bond in **3-26** forms a covalent bond and is responsible for the cyclisation to give **3-31**. This gives a negative charge on nitrogen external to the heterocycle and a positive charge on the pyridyl nitrogen in the new closed-ring system.



Scheme 3-18 Suggested ring closure to **3-25** by nucleophilic addition

They attributed the reduction in rate of cyclisation to the protonation of the nitrogen to give **3-8** (as seen with Cy5) and they report that **3-8** reacted more slowly since it is stabilized as a symmetrical resonance hybrid. Thus, the process for ring-closure depends on the resonance-form of the intermediate contributing to the ring-closing process, **3-26**. Marvell's comprehensive investigation, using three sets of conditions, concludes that the ring closure of the *non-polar* resonance form **3-26** is preferred, **Scheme 3-18**. Electrocyclisation is the route from the non-polar transition state **3-26** and not nucleophilic addition.¹⁴²



Scheme 3-19 Suggested electrocyclisation from the non-polar transition state **3-26 cis**

Recent work has shown that the ring-closed pyridinium can be readily achieved in solution using microwave activation,¹³⁰ where EtOH/H₂O solvent was used in their reactions. Also from the literature is an example of using sonication¹⁷⁵ to form the pyridinium salt, where Zhao *et al.* reported using 80% EtOH solvent.

In conclusion, a rationale as to why only **3-8** was formed in the VBM could be that the equilibrium was unfavourable towards **3-26** under these conditions. In the solid state and in the absence of solvent, the reaction of mono-Zincke **1-1** with neat aniline meant that the conditions did not lead to the formation of the ring-closed pyridinium salt **3-2**. Consequently the formation of the thermodynamic product prevailed and so we saw only the Cy5 **3-8**.

4. Heptamethine or Cy7 dyes

Full characterisation and elucidations of the structures of Cy5 **3-8** by X-ray crystallography had provided us with a set of seven molecules with which to investigate further synthetic uses. Our next investigation looks at the suitability of **3-8** as precursors for heptamethine or Cy7 dyes, in solvent-free conditions.

4.1 Introduction

Cyanine dyes are a class of dyes that absorb light in the Near Infrared region (700-1000 nm) of the electromagnetic spectrum. This is a useful property for imaging dyes and has wide-ranging applications. Besides fluorescent microscopy^{176,177} these types of dyes can function as molecular probes,¹⁷⁸⁻¹⁸⁰ and for targeting cancerous tumours¹⁸¹⁻¹⁸⁴ security markings¹⁸⁵ and lithography,¹⁸⁶ OLEDs¹⁸⁷ as well as applications in solar cell technology^{188,189} where they may be used for increasing power conversion efficiencies.¹⁹⁰ Our investigations into the synthesis of Cy7 dyes has been focused on finding the most efficient route to a specific Cy7 dye called Indocyanine Green or ICG **4-1**.

Absorbance in the NIR region allows for many possible transitions between energy states that can occur in molecules such as shown in **Figure 4-1**, these are able to phosphoresce and fluoresce. The transitions occur because of their molecular structures and the bonding arrangement within them. In these five examples, the cyanines can be seen to contain a fully conjugated system and have uninterrupted resonance/delocalisation from one end of a polymethine chain to the other. Two of the examples, ICG **4-1** and Cyanine **4-2**, contain a *heptamethine* chain, also known as a Cy7.

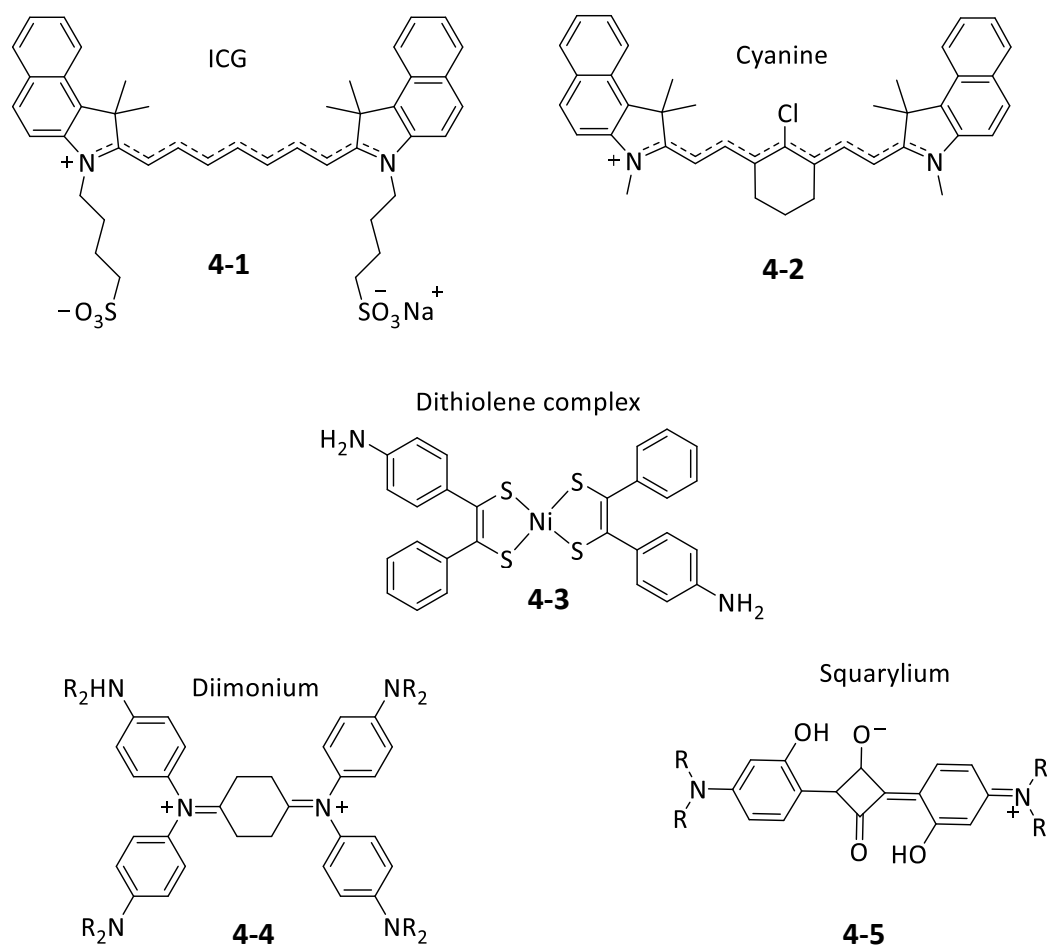


Figure 4-1 Molecules that have NIR properties and delocalisation in the heptamethine chain for **4-1** and **4-2**

These are but a few examples of the photophysical behaviours in molecules that give rise to their absorbing in the NIR region but what happens afterwards, the output, is what we can derive many useful applications from.

4.2 Processes leading to fluorescence in NIR dyes

Energy transfers that give rise to fluorescence can be shown in a Jablonski diagram, **Figure 4-3**. It depicts what happens when molecules absorb photons and the subsequent pathways and the timeframes for how absorbed energy can transfer in the system. When an electron in a molecular orbital, atom, or nanostructure, in the ground state (S_0) absorbs energy from an external source (blue arrow) it is elevated to a higher energy singlet state (S_1). It then relaxes back to its ground state (green arrow) by emitting a photon from an excited singlet state.

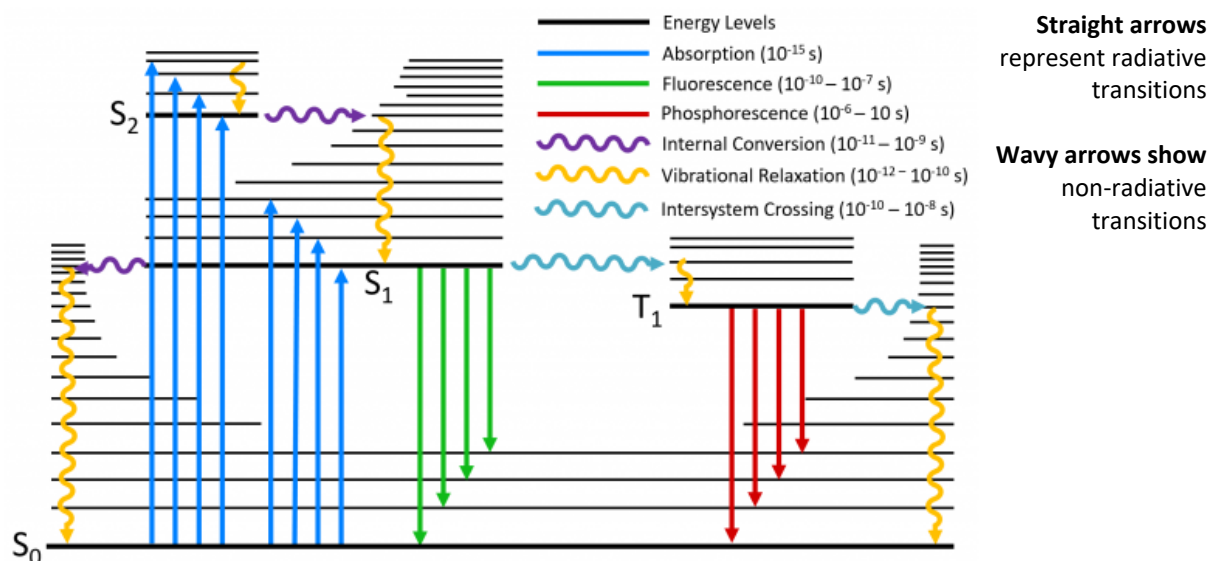
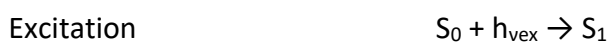


Figure 4-2 A Jablonski diagram showing all the possible radiative and non-radiative transition, diagram adapted from¹⁹¹

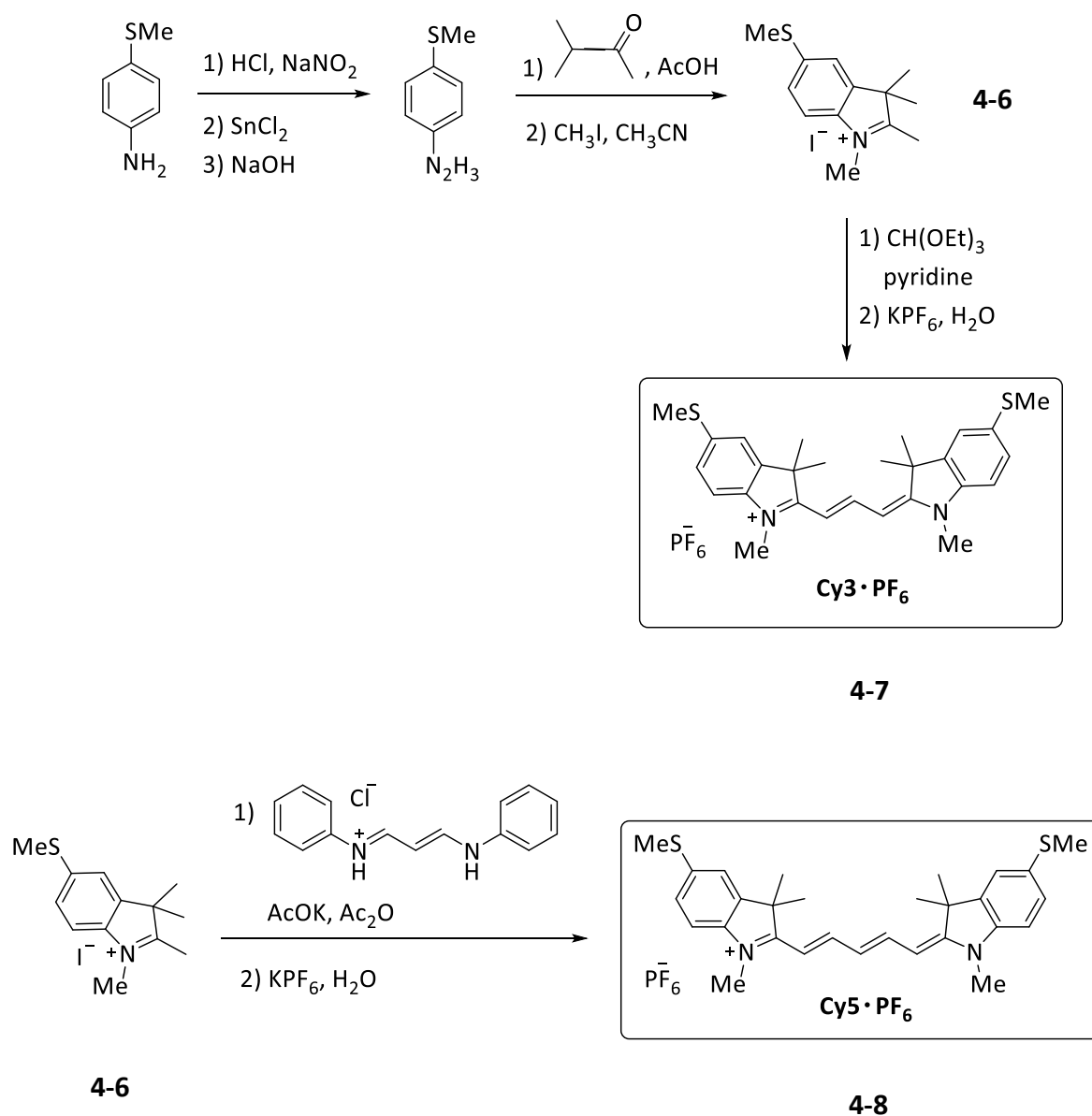
Excitation and emission may be expressed by the following notation:



Where h is Planck's Constant and ν is the specific excitation and emission frequencies depend on the system. In the Jablonski scheme, S_0 is the ground state and S_1 is the term given to the first electronically excited state of the fluorophore (the fluorescent molecule). In addition, a fluorophore that is in S_1 can relax in a variety of competing pathways, including non-radiative relaxation in the form of heat or through vibrational relaxation (wavy arrows) which is taken up by the solvent. Phosphorescence (red arrows) can occur from S_1 to T_1 via Intersystem Crossing (aqua wavy arrows) and vibrational relaxation (yellow wavy arrows). However Intersystem Crossing (i.e., phosphorescence) is in competition with the depopulation of other S_1 transitions such as fluorescence and internal conversion and is also too slow for the transitions to be relevant for most purely organic molecules. Thus, the ability to fluoresce is promoted in molecules with cyanine and highly conjugated structures which have these enhanced spectroscopic features.

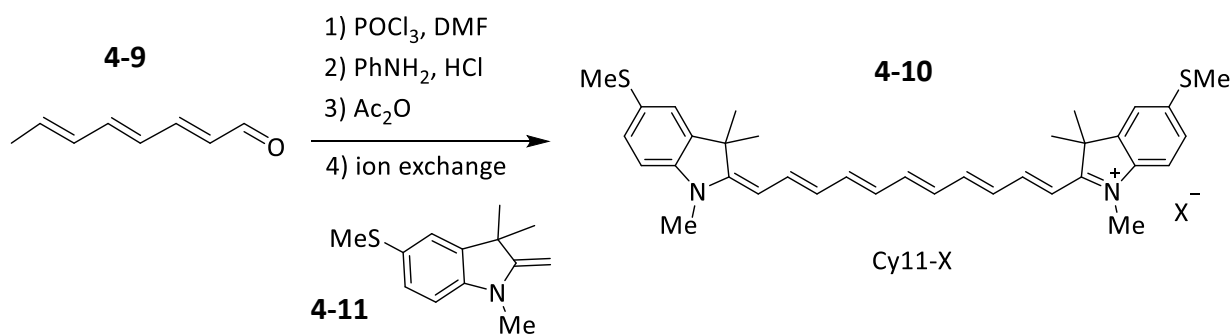
4.3 Heptamethine dyes – from Cy5 to Cy7

The conjugate addition of indole-type compounds such as **4-6**, with suitable polymethines is a well-established strategy for increasing methine chain length. It would be of interest to try a new methodology and to consider a solvent-free route to Cy7 dyes, using VBM.



Scheme 4-1 Synthetic routes for the Cy5 to Cy7 transformation

The transformation of Cy5 to Cy7 is interesting for us to investigate having achieved the syntheses of Cy5s using the Zincke salt and aniline. We shall discuss how this can be achieved in the solid state. Anderson *et al.*'s syntheses of both Cy5 and Cy7 were based on procedures reported by Gunasekaran.¹⁹² These involved solvents where the indole is reacted with the cyanine via the acyl intermediate formed with anhydride. Their synthetic route to Cy11·PF₆ was achieved from the aldehyde **4-9** as shown in **Scheme 4-2** using the Vilsmeier formylation; reaction with aniline, and condensation with Fischer base, 1,3,3-trimethyl-2-methyleneindoline **4-11**.



Scheme 4-2 Synthetic route using aldehyde **4-9** to form Cy11-X **4-10**

They reported that the reaction gave a complex mixture of products and Cy11·PF₆ could only be isolated in 4% yield, but a similar route gave Cy9·PF₆ with 42% yield. Their difficulty in finding a route for efficient yields indicated the challenges ahead for the formation of molecular wires using this synthetic strategy **Figure 4-4** shows the general structure of polymethine dyes, **4-12**. We have shown in Chapter 3 that Cy5 **3-8** has five methine carbons in a conjugated chain and is thus a pentamethine. A change in end groups to iodoliums, gives the Cy5 **4-14** and the Cy7 **4-13**. Heptamethine dyes absorb at λ_{\max} 756 nm, an increase of *ca.* 100 nm, from 646 nm, for Cy5 **4-13**. Hexamethylindotricarbocyanineiodide (HITCI),¹⁹³ **4-14**, is commercially available molecule It is typically used as a fluorophore for a laser dye, and is marketed for its ability to be used in pulsed or continuous wave operation and is tuneable at around 840-860 nm.

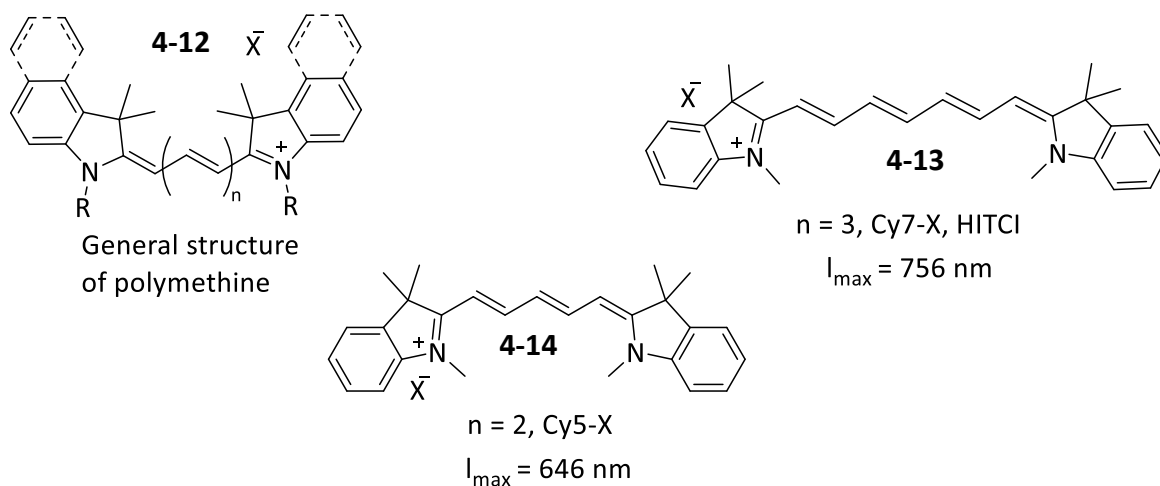
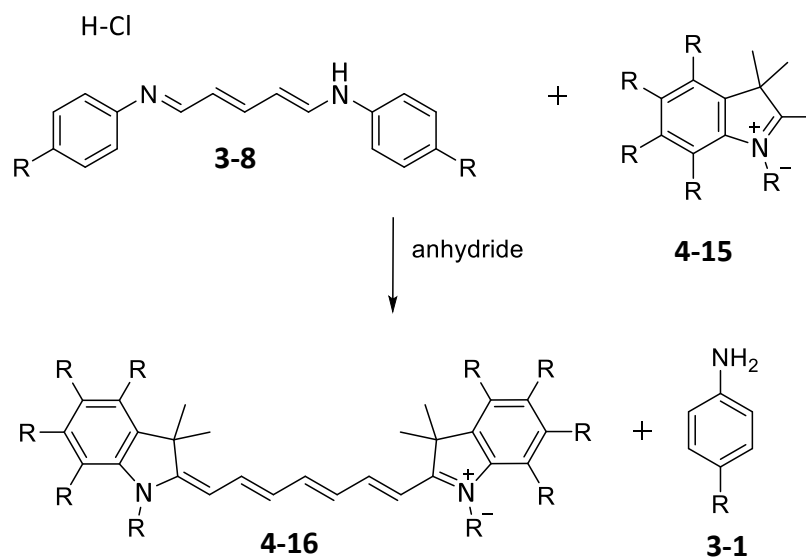


Figure 4-3 Cyanine Homologous Series **4-12** and target Cyanine **4-13**

There are many instances of the synthesis of Cy7 dyes directly from the **3-8b** (**3-8**, R=H) in the literature^{194–198} but far fewer involving substituted Cy5 molecules as synthesised in Chapter 3. The synthetic route utilizes the conjugate addition of an indole to each end of the methine chain to form the Cy7 with the aniline as the leaving group.

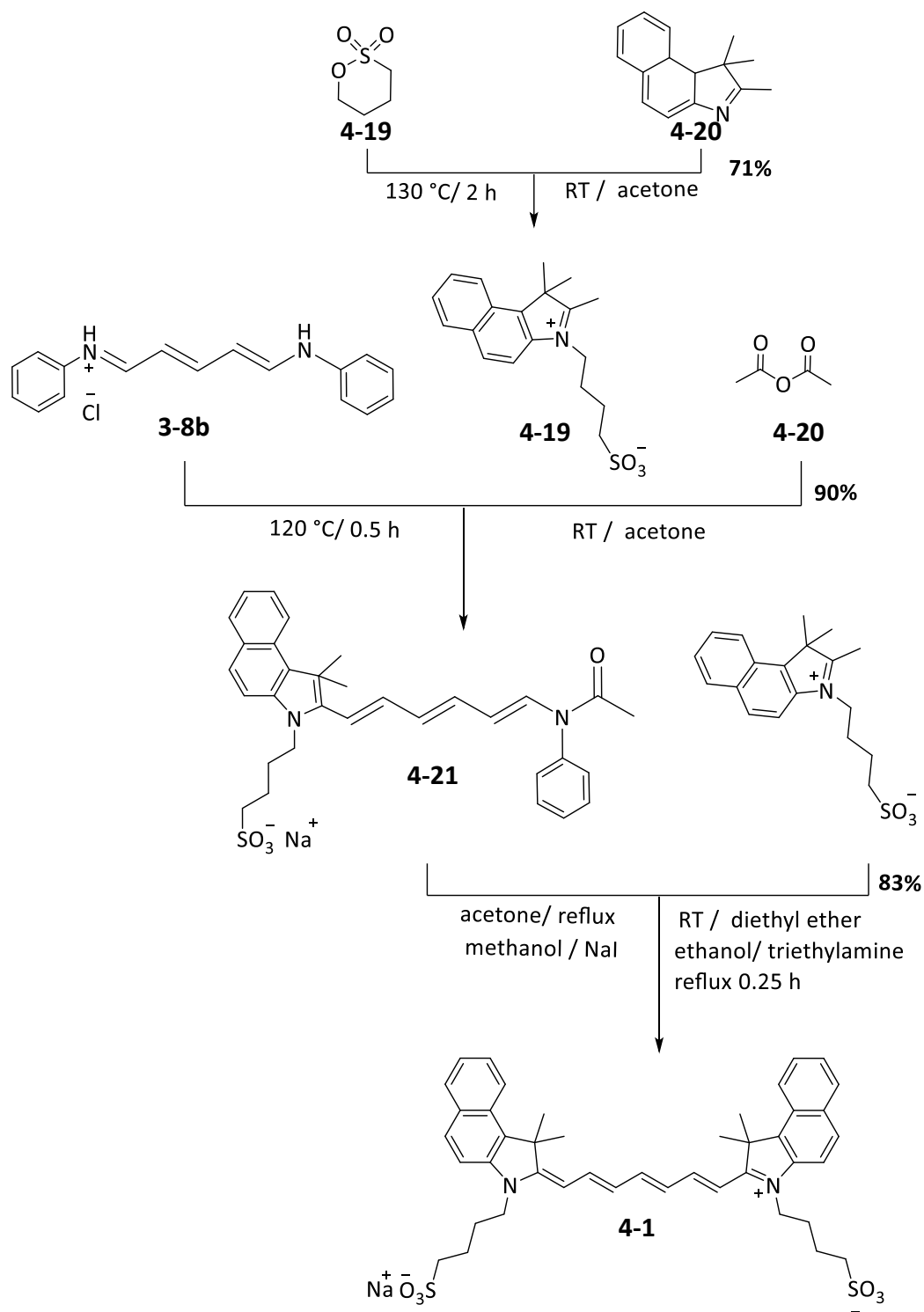


Scheme 4-3 Conjugate Addition of Cy5 **3-8** to form Cy7 **4-16**

4.4 First patented route to Indocyanine Green **4-1**

Heseltine and Brooker¹⁹⁹ working at Kodak, devised a synthesis which begins with heating 1,4-butane sultone **4-17** with 1,1,2,3-tetramethylbenzo[e]indol-3-ium **4-18**, under reflux for two hours to form a quaternary salt **4-19**. This was subsequently treated with the Cy5 **3-8b**, also known as glutaconaldehyde dianilide hydrochloride in equimolar quantity, and finely powdered fused sodium acetate was added and boiling acetic anhydride **4-20**. The reaction mixture was heated for twenty minutes under reflux, to give **4-21**. It was then poured into a cold water solution (1 L) containing sodium iodide (10 g). The crude dye was filtered and washed on the filter with water. Hot acetone was then added to dissolve the crude product, which was filtered again, and the filtrate was treated with more sodium iodide (10 g).

After chilling overnight, the iodide **4-1** 6.5 g (41%) was collected on a filter and dried. The iodide salt was converted to the chloride using silver chloride. The yield of the conversion of the halide salts was 90%. **3-8b** is also used as an intermediate in Kodak's 1957 patented *Scheme 4-5* to produce the Cy7 dye Indocyanine Green or ICG **4-1**.

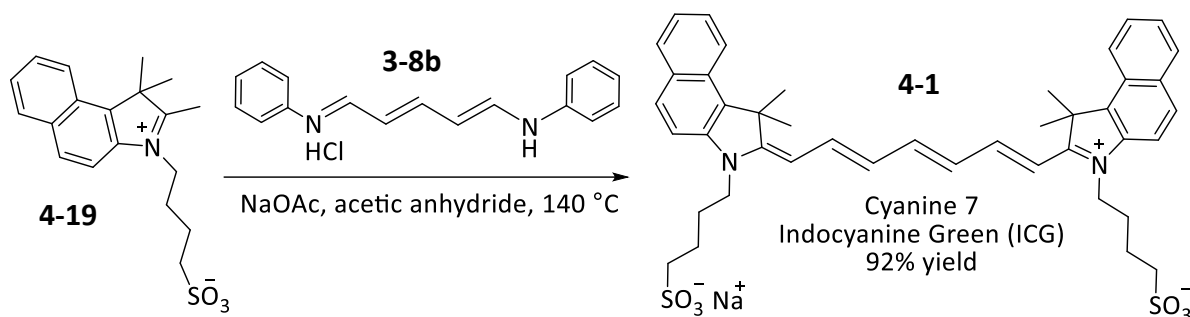


Scheme 4-4 Kodak's synthesis of ICG **4-1**

The dye was used by Kodak primarily for photographic chemicals where silver salts were used for those purposes. The development of ICG **4-1** as a medical imaging dye was instigated by Irwin Fox at the Mayo Clinic who used it to study blood flow in cardiology

using dilutions of his version 'FoxGreen' **4-1**. The Kodak patent reveals a multi-step synthesis requiring hours of heating and several purification steps.

Efficiencies have been found since then including a very recent one-pot condensation reaction.

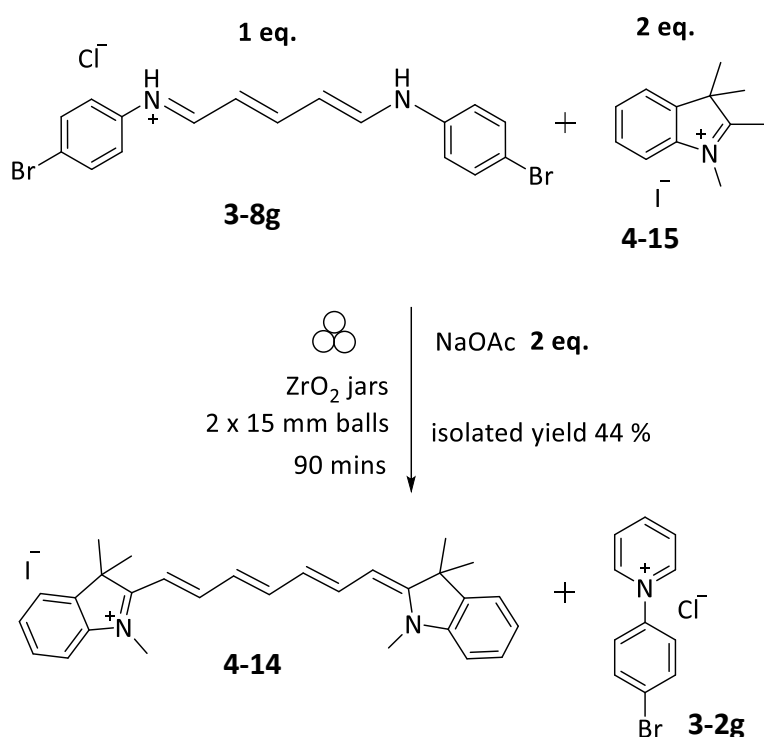


Scheme 4-5 A one-step condensation reaction to ICG **4-1**

In 2021, Fang²⁰⁰ *et al.* were able to show an improved process for the conjugate nucleophilic addition of a heterocyclic cation to Cy5 **3-8b** to make ICG **4-1**, in solution. This highly efficient reaction was reported to give greater than 95% purity and 92% yield. However, this is only the final step in the synthesis of ICG **4-1** and requires only 30 minutes under reflux. If the syntheses of **3-8b** and its precursor, the Zincke Salt **1-1**, were included in a complete scheme then the data reported for all the synthetic steps in solution, it gives an overall yield of 18.5% for ICG **4-1** with a total reaction time of 33 hours. The conjugate addition of indole-type compounds with suitable polymethines is well established and we shall consider this as a route to Cy7 dyes but without solvent and using VBM as a new methodology. A further consideration would be to assess the ring-closure of the Cy5 to its pyridinium salt, this is an undesirable outcome as we are looking to efficiently synthesis Cy7 **4-14**. All the Cy5s that were formed in **Chapter 3** were arrived at by the double substitution of the Zincke Salt **1-1**. The successful synthesis of the Cy5 compounds put us in a good position to form Cy7 dyes. A survey of the literature gives many examples of syntheses of Cy7 from **3-8b**.^{149,151,161-162} Instances of the use of the *substituted* Cy5s however, were not found and we were interested to understand which of our Cy5 compounds would give the greatest conversion to the targeted Cy7 dyes.

4.5 Route to Cy7 using substituted Cy5 **3-8a-g**

We began the investigation with the Bromo Cy5, **3-8g**, shown in **Scheme 4-7**. In this first attempt, bromo Cy5 **3-8g** was added to two equivalents of the indole **4-14** and two equivalents of sodium acetate in a ZrO₂ jar (25 mL) with two balls (15 mm Ø). They were oscillated together for 90 min at 30 Hz. The resulting maroon solid was dissolved in methanol and the target Cy7 compound was isolated by recrystallisation overnight, from diethyl ether at -20 °C to give very fine, vibrant green needles with a yield of 44%.



Scheme 4-6 VBM of bromo Cy5 **3-1g**, 44% isolated yield Cy7 **4-14**

Examination of the Cy7 ¹H NMR spectra shown in **Figure 4-4**, showed similar features to that of the Cy5 molecules in that the -CH₂ units give rise to poorly resolved signals.

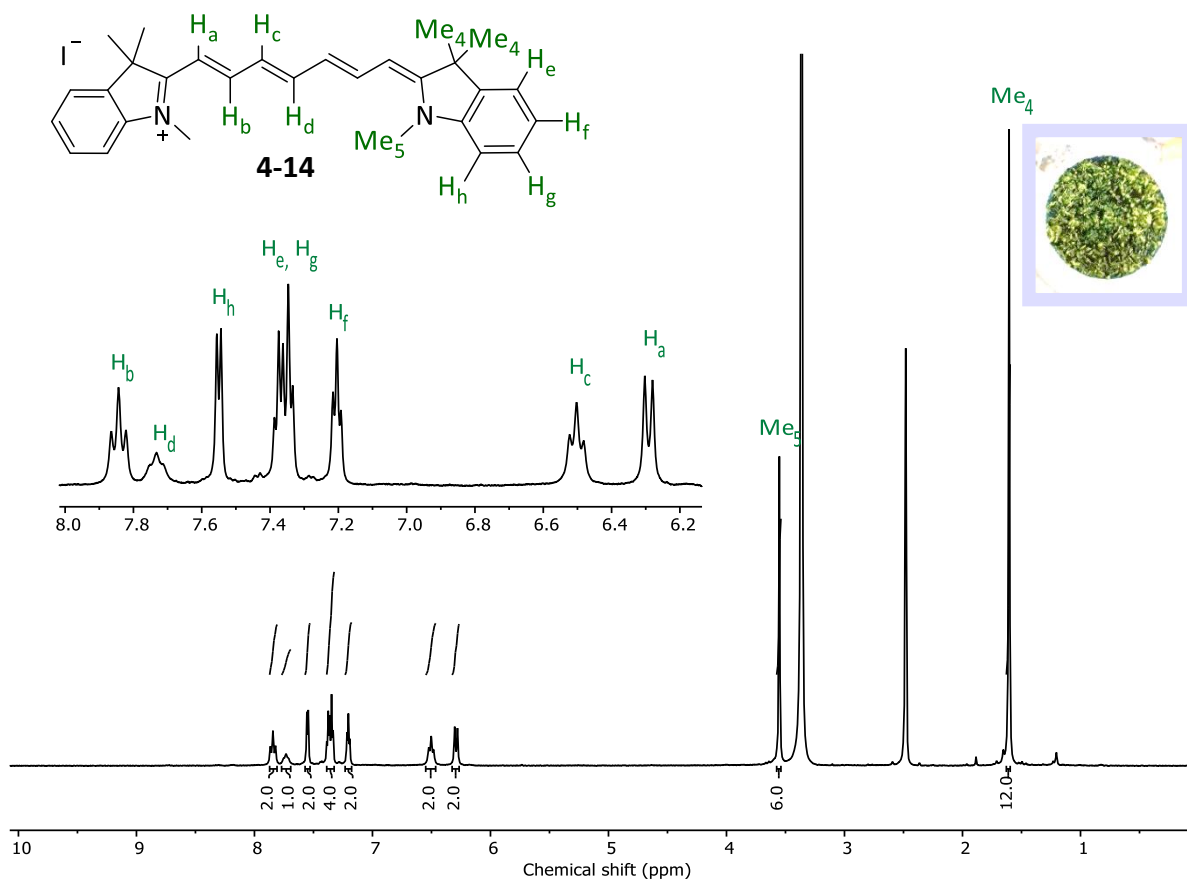


Figure 4-4 ¹H NMR spectrum for Cy7, 4-14

The central proton H_a is not well-defined but is a genuine triplet as it has C₂ symmetry on the central carbon in the chain. The resonances for H_b and H_c also have poor resolution, but they are in non-symmetrical environments and the resulting signal should be a doublet of doublets with very small J values but in the spectrum, they appear to be triplets. To make this distinction they may be reported as ‘app t’ (meaning ‘apparent triplet’) and the J-coupling constants should then be approximate to the same value of 12 Hz for these couplings. An interesting effect occurs when the methine protons are in an all trans environment where other processes can cause signal broadening in ¹H NMR spectroscopic studies. The J-coupling values for cis ¹H (7-8 Hz) and trans ¹H (11-13.5 Hz) observed in both Cy5 and Cy7 molecules are consistent in those conformations, examples of both for prepared Cy5 and Cy7 are shown in **Figure 4-5**. This effect was noted by Rüttger *et al.* in relation to their studies of HITCI **4-27** and ICG **4-1**.²⁰³ They report all methine protons have exclusively *trans* coupling constants (³J_{trans} ≈ 13 Hz) attributed to two environments.

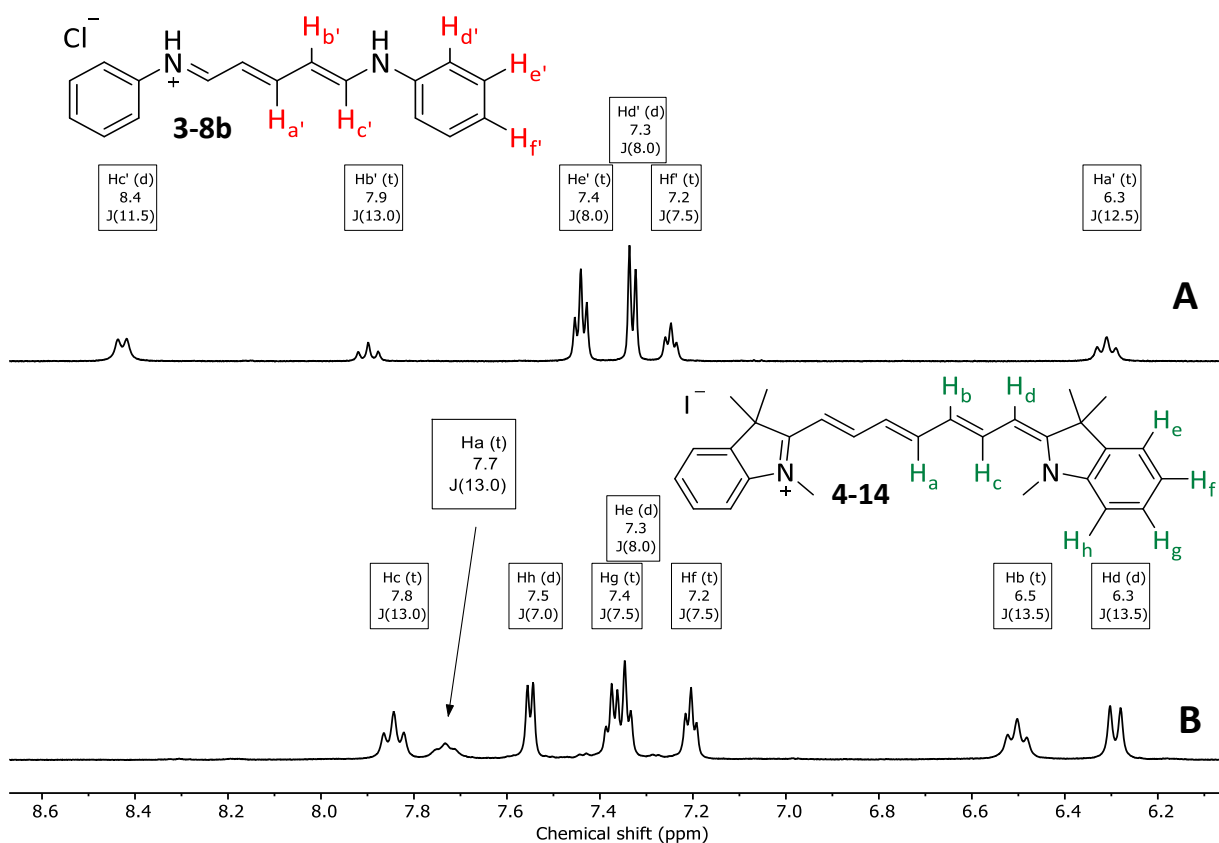


Figure 4-5 Comparison of J_{HH} of the methine protons in Cy5 **3-8b** and Cy7 **4-14**

In spectrum **A** (for Cy5), the ^1H NMR data, show values for J_{HH} of the methine protons $\text{H}_{a'}$ - $\text{H}_{c'}$ **3-8b** are 40-50% greater for than the protons in the aromatic systems $\text{H}_{d'}$ - $\text{H}_{f'}$. Similarly in spectrum **B** (for Cy7), the values of J_{HH} for H_a - H_d in **4-14** are 40-50% greater than H_e - H_h . The resonance for H_a is especially flat and while this is consistent with J_{HH} values for *cis* and *trans* protons, a number of other issues can cause broadening in ^1H NMR signals. For example, inhomogeneity of the sample solution from poor mixing or paramagnetic effects. For polymethines, the poor resolution of these peaks has been attributable to the typical dynamic equilibrium involving a low-populated second species (a *cis* isomer)²⁰⁴. The phenomenon was observed by Rüttger *et al.* where they found a weak (approximately 3% relative intensity of the *cis* isomer located between the H_2 - H_3 bond in **4-14**). Using multi-temperature analyses of NOESY/EXSY spectra confirmed the signals assigned to an isomer with a *cis* confirmation of the H_2 - H_3 bond. The signals showed interchange with that of the main (all-*trans*) isomer, this process has also been studied computationally by Abergel *et al.*²⁰⁵

With the Cy7 successfully isolated from the first VBM of bromo Cy5 to Cy7 experiment, the process of identifying the remaining compounds that are present in the crude product mix is much simplified.

Figure 4-6 shows the stacked ^1H NMR spectra for (A) the indolium salt **4-15** starting material, (C) target Cy7 molecule **4-14** and these can be compared with (B) the crude product mix. The identification of the target product **4-14** and the conversion was quantified via the intensity of the signals. It is apparent from the aliphatic signals between 1.00 and 4.00 ppm showed that the methyl groups on the indolium **4-15** (Me_1 and Me_2) were not completely consumed and that the target Cy7 molecule **4-14** was present. The percentage conversion was 61% as evidenced by the ^1H NMR from which an isolated yield of 44% for the Cy7 **4-14** was achieved.

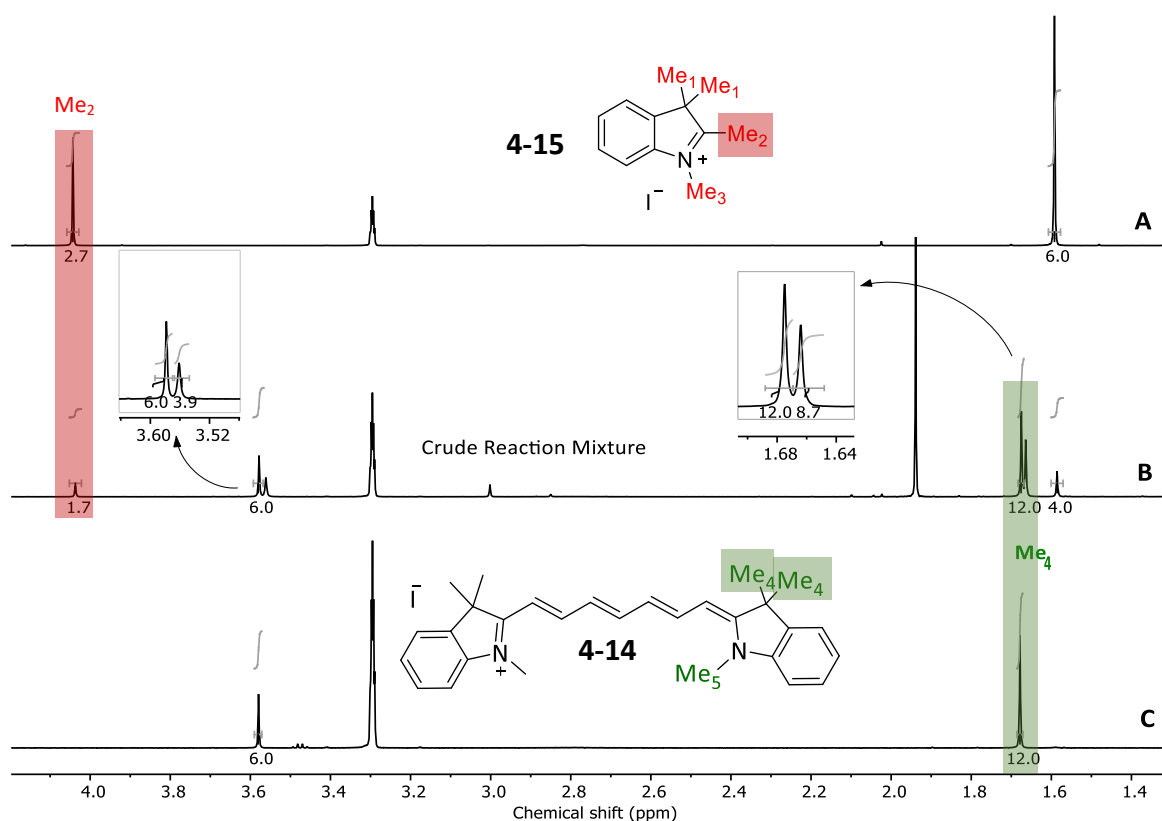


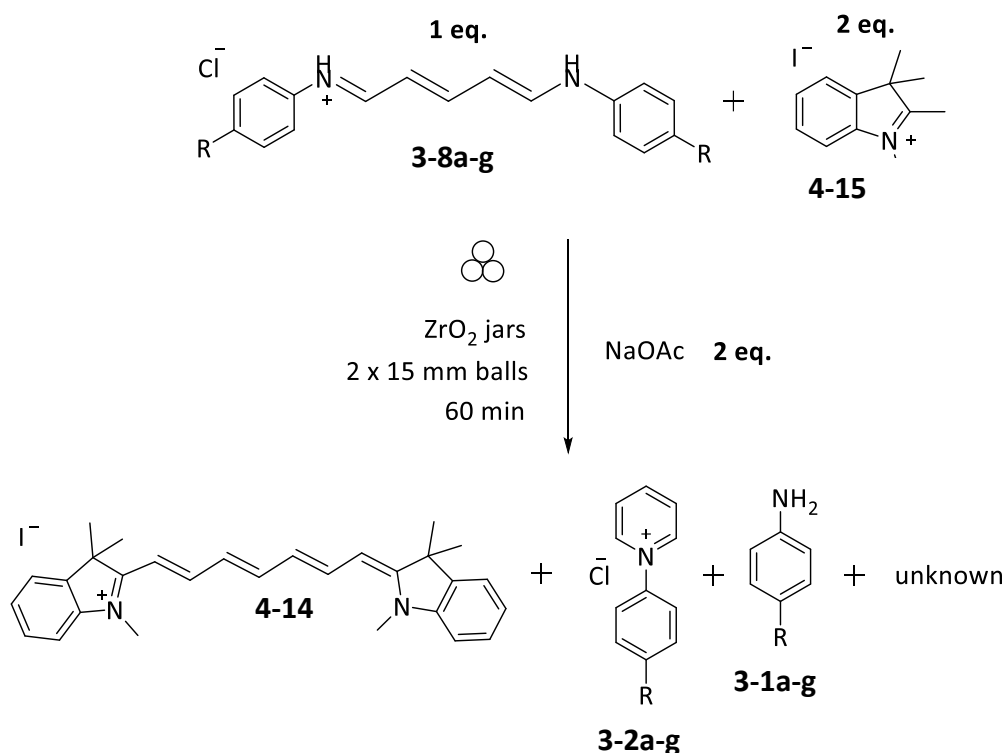
Figure 4-6 Stacked ^1H NMR spectra (aliphatic region) showing (A) indole **4-15** starting material, (B) the crude product mixture and (C) the target Cy7 molecule **4-14** using Bromo cy5 **3-8g**

Of interest were the smaller of the signals at Me_4 and Me_5 , which are 0.02 ppm upfield, integrated to a very similar ratios, (6:3.9) and (12:8.7) suggesting that another molecule is

in the mixture. Unfortunately, we have insufficient information to draw any further conclusions from this data. Although there are at least four different molecules in the crude product mix, a 61% conversion to the target Cy7 molecule is a sufficiently sound result with which to proceed with a series of experiments for attempting all seven Cy5s to find the most efficient Cy5 to Cy7 transformation.

4.6 Cy5 transformation to Cy7 in the VBM

Each of our prepared Cy5 **3-8a-g** was added to 2 equivalents of Indolinium salt **4-15** in a ZrO₂ jar (25 mL) with two ZrO₂ balls (15 mm \emptyset) along with 2 equivalents of sodium acetate. The vessels were oscillated at 30 Hz for 60 minutes and each crude product mix was sampled and analysed using ¹H NMR spectroscopy directly after the completed experiment, **Scheme 4-7**.



Scheme 4-7 Reactions of Cy5 **3-8a-g** with the Indolinium salt **4-15** in the VBM

Analyses of the ¹H NMR spectra showed that reducing the reaction time from 90 to 60 minutes had a deleterious effect on conversion, for the bromo Cy5 there was a 51% reduction in conversion. The decision to change from the exploratory 90 minute

experiment using Bromo Cy5 **3-8g** to 60 minutes for all seven cy5 compounds **3-8a-g** was based on the most efficient method of completing each experiment and sampling their crudes within a workable timeframe. The conversions for this suite of experiments are shown in

Table 4-1.

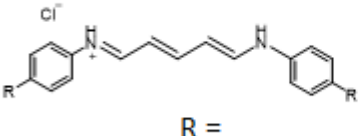
Cyanine 5, 3-8a-g		ZrO ₂ Jars (25 mL)	
 R =		T (min)	Conv. By NMR (%)
3-8a	-Me	60	0
3-8b	-H	60	20
3-8c	-OMe	60	9
3-8d	-OPh	60	0
3-8e	-F	60	20
3-8f	-Cl	60	30
3-8g	-Br	60	10

Table 4-1 Percentage conversions for substituted Cy5 **3-8a-g** to Cy7 **4-14** using VBM

The poor conversion after 60 minutes oscillation time fits with the work on kinetics in the ball mill as described in James²⁴ *et al.*'s work, *Feedback Kinetics in Mechanochemistry: the Importance of Cohesive States*. They describe the 'snowball effect', a phenomenon described as then the initial free-flowing powders in the reaction vessel dramatically changes to cohesive 'rubber-like' state encasing the ball. In their experiments they had observed that the reaction mixture returned to powder again with further oscillation. As this change cannot be witnessed through opaque reaction vessels, a change in the sound of the collisions in the mixer mill accompanies the change in the cohesive state of the reactants and their products.

For all the experiments shown in **Table 4-1** – each result after 60 minutes oscillation gave the encrusted ball as described in James' paper, **Figure 4-7** the result of the **3-8b** reaction.



Figure 4-7 Cy5 **3-8b** reaction with Indole **4-15** after 60 minutes oscillation in the MM400 forms a sticky coating on the ZrO₂ balls.

Purification of a small sample of the same crude that gave us the first Cy7 **4-14** was conducted using a silica flash column. The chromatogram had overlapping broad peaks which corresponds with observed streaky TLC plates, this was problematic for distinct separations and only a small quantity (*ca.* 40 mg) of colourless compound **3-2** that was clearly not Cy7 was isolated. This was sufficient quantity to analyse using ¹H NMR spectroscopy, **Figure 4-8**.

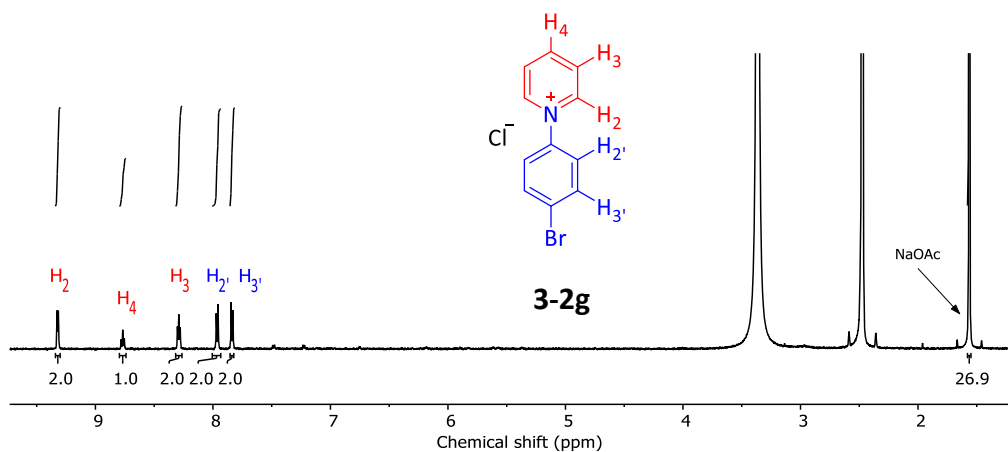


Figure 4-8 ¹H NMR of the isolated 4-bromophenyl pyridinium salt, **3-2**

Comparison of the ¹H spectra and with the literature¹⁴⁷ showed it to be consistent with N-4-bromophenylpyridinium chloride molecule **3-2**, the *ring-closed* product of the Zincke Reaction. Sodium acetate is also present in the spectra, verification was possible by addition of more sodium acetate to the sample in the NMR tube and observing an increased

integral for the signal. Assignment of another set of signals shown in **Figure 4-8** are highlighted in red. This was possible by comparing with the ^1H NMR spectra of bromoaniline **3-1g**. Bromoaniline was not a starting material in the reaction and its appearance in the crude product mixture indicates that it is the leaving group in this reaction. There is also a possible fourth, unknown molecule, as the remaining signals could not be assigned as they were not isolated.

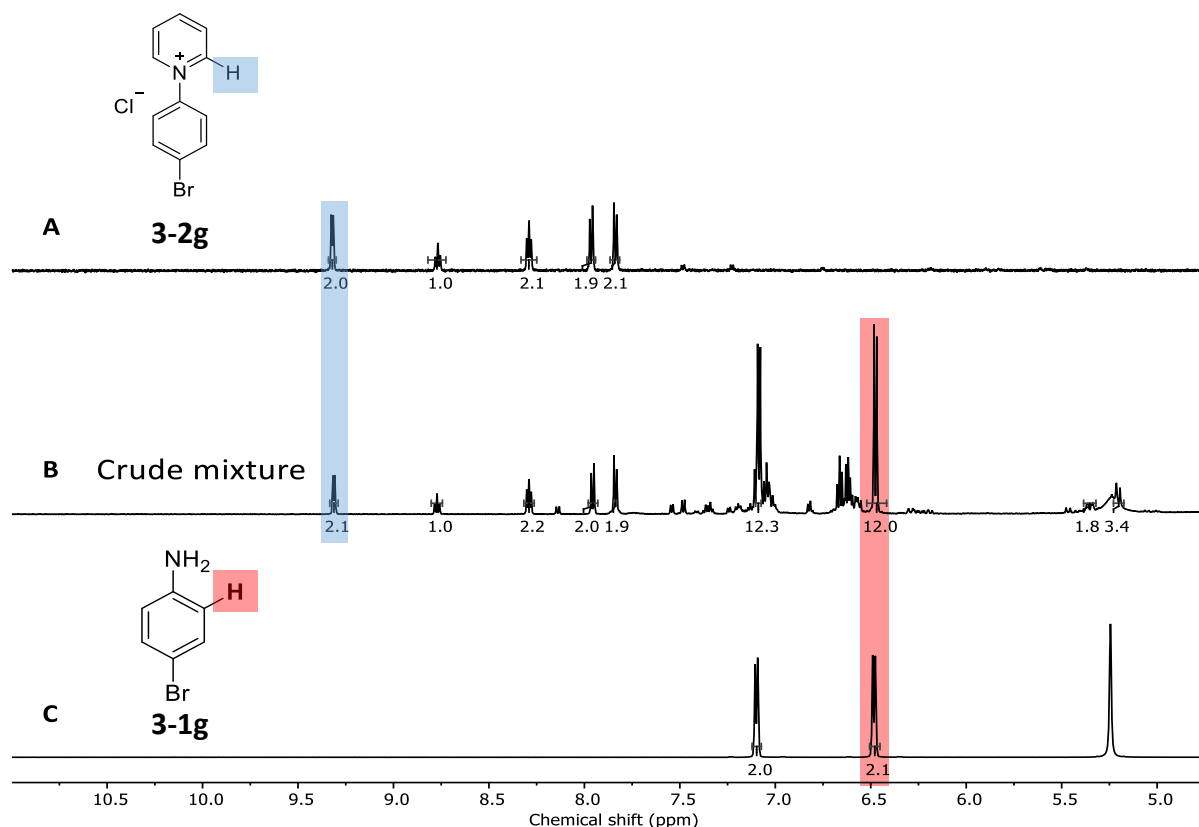


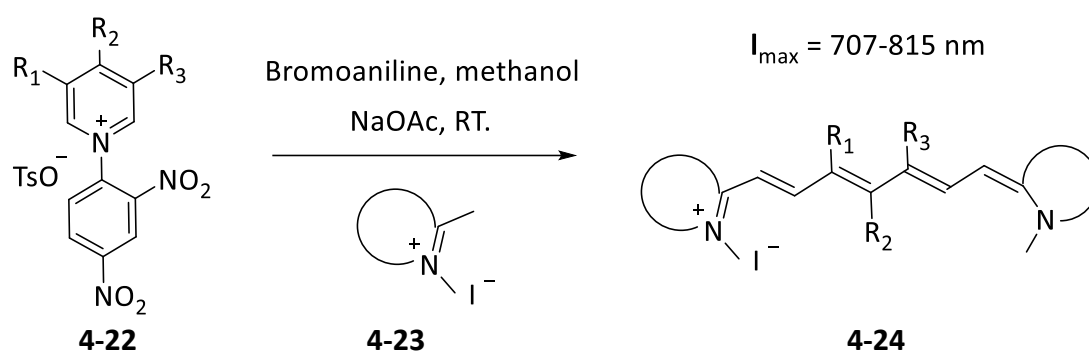
Figure 4-9 Assignment of the ring-closed product, the pyridinium salt **3-2g**, from a ^1H NMR spectroscopy analysis where **(A)** 4-bromopyridinium salt **3-2g** **(B)** Crude product mixture for **Entry 4-4 c** and **(C)** bromoaniline **3-1g**

Calculating conversions in a crude ^1H NMR spectra where only the target molecule and a leaving group appears is straight forward. The crudes for all the substituted Cy5 to Cy7 reactions contained at least 4 species and so integrals from the known molecules were identified and their values normalised for ease of comparison. The appearance of small amounts (*ca.* 10%) of the closed ring product in the crude, requires further analysis of the mechanistic routes. This new reaction, taking the Cy5 **3-8b** which is an intermediate in the Zincke Reaction mechanism, to a closed ring product is understood. However, reacting it with an indolium salt **4-15** in a basic medium using sodium acetate sets up different

reaction conditions to the initial Cy5 experiments (mono-Zincke salt **1-1** and anilines **3-1a-g**). As discussed in **Section 3-9** the ring-closing of the Cy5 intermediate is susceptible to acidic conditions. In this reaction, the presence of sodium acetate shifts the equilibrium between the different resonance forms of the intermediate, making it more favourable towards the ring-closing intermediate, and giving the pyridinium salt.

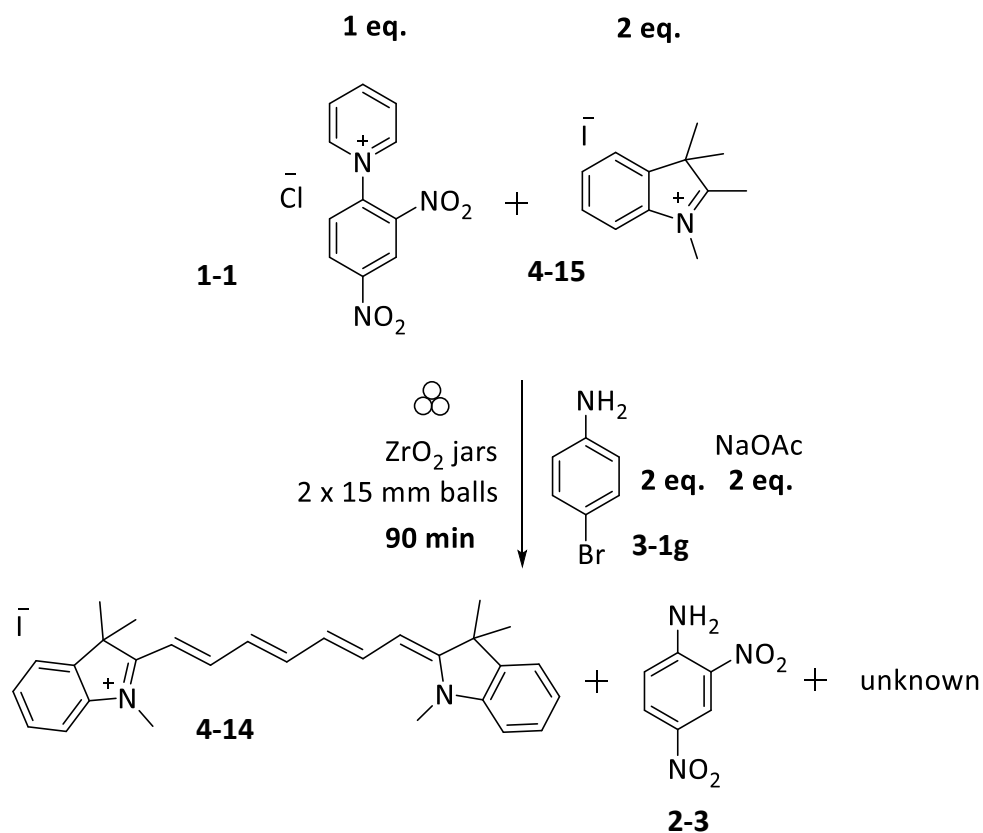
4.7 From Zincke salts to Cy7

Štacková's findings¹⁶⁴ - *Approach to a Substituted Heptamethine Cyanine Chain by the Ring Opening of Zincke Salts* (Section 3.7), **Scheme 3-14** reproduced below.



Scheme 3-14 Štacková *et al.* - Approach to a Substituted Heptamethine Cyanine Chain by the Ring Opening of Zincke Salts

Our attempted syntheses of Cy7 **4-14** from Cy5s **3-8a-g** in the solid state completed, a new set of experiments to see which aniline would perform the best for ring-opening in the VBM was investigated. Again, bromoaniline **3-8g** was chosen as the first experiment. 2 equivalents of the mono-Zincke salt **1-1** were added to 1 equivalent of indolium salt **4-15** in a ZrO₂ jar (25 mL) with two ZrO₂ balls (15 mm Ø) with 2 equivalents of sodium acetate. The vessels were oscillated at 30 Hz for 90 minutes and the crude product mix was sampled and analysed using ¹H NMR spectroscopy directly after the completed experiment.



Scheme 4-8 VBM of the Zincke Salt **1-1** with Indole **4-15** using Bromoaniline **3-1g** as a catalyst

Conveniently, as for all the previous examples, making a stack from the crude product mix and comparing it with the indole starting material and the target Cy7, the percentage conversion may be calculated. As before, the ^1H NMR spectra of the crude product mixture, contained the signals for **4-14**, **Me₁** and **Me₂** are reduced showing that it has been consumed relative to the appearance of the product signals **Me₄** and **Me₅**.

The **Me₃** signal is coincident with the water peak in the ^1H NMR spectrum, this was verified using a HSQC experiment in NMR spectroscopy to check for couplings between the C and H atoms. A cross peak is seen at $\delta 4.86$ ppm and it was found to be consistent with the literature.²⁰⁶ The calculation for percentage conversion using the integrals shown give 66% for our target product.

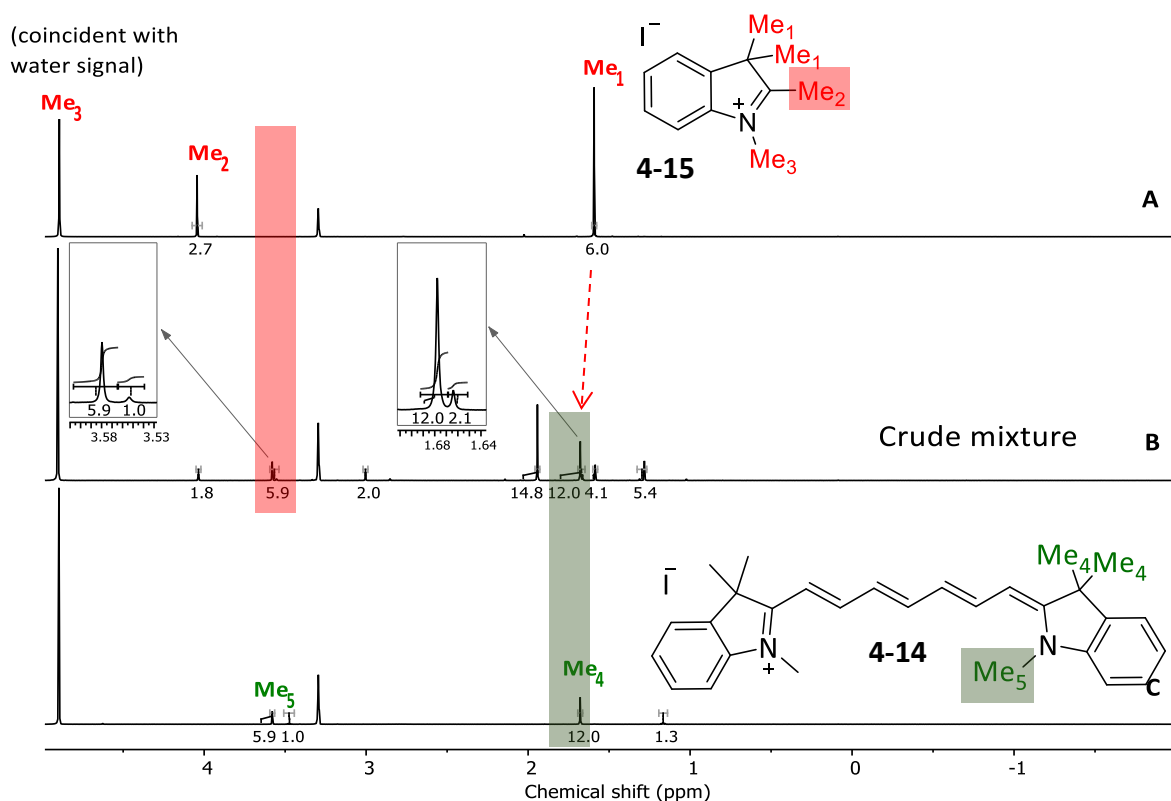
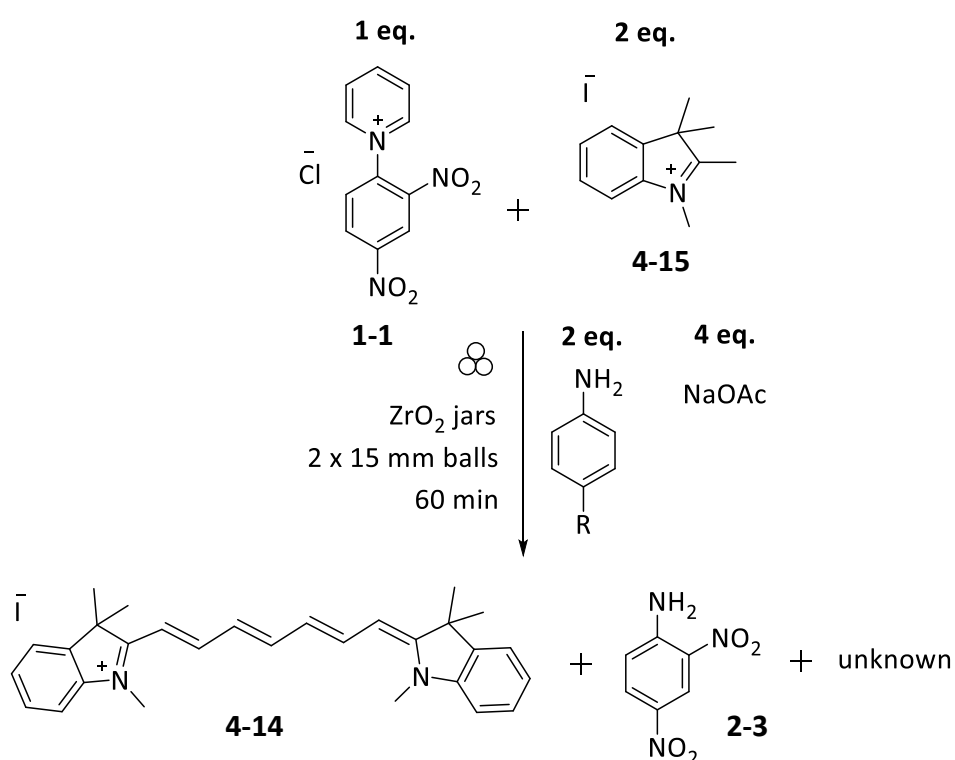


Figure 4-10 VBM of indole and Zincke Salt **1-1** with Bromoaniline **3-1g** as catalyst, Stacked ¹H NMR spectra (aliphatic region) showing (A) indolium salt **4-15** starting material, (B) the crude product mixture and (C) the target Cy7 molecule **4-14**

On further analysis of the crude product mixture ¹H NMR spectrum, both signals **Me₄** and **Me₅** comprises two peaks separated by 0.02 ppm and are therefore have ¹Hs that are in two different environments as they have different chemical shifts. The relative integrals for the Cy7 molecule **4-14** are 12 (**Me₄**) and 5.9 (**Me₅**), i.e 2:1. Interestingly, the signals that are 0.02 ppm upfield of both, approximate to the same ratio 2.1:1.0 as shown in **Figure 4-10**. These integrals suggest that another, very similar, molecule(s) is in the crude mixture. When preparing crudes from the experiments for separation in a column, the markings obtained on the TLCs were streaky rather than discreet spots. After the column, this subsequently translated to mixtures of molecules appearing in each fraction as determined by their levels of UV-vis absorption from which the auto-column. The analyser is able to take readings and displays the data collected. Good separations of the Cy7 crude mixtures were a challenge, and there remains the puzzle about the unknown molecule(s). This result

gave cause to see how the mono Zincke Salt **1-1** would perform with different anilines. A series of new experiments for each aniline were undertaken. It was noted that Štacková had used *six* equivalents of sodium acetate for their studies in solution. For the VBM, it was of interest to see if doubling the amount of base, we had used previously (**Schemes 4-7, 4-8 and 4-10**), to 4 equivalents for the series of experiments could improve upon the 49% conversion from our preliminary experiment shown in scheme **4-8**. We had to restrict the base to 4 equivalents compared to Štacková's using 6, because loading conditions were prescribed as one-third balls, one-third space and one-third space.



Scheme 4-9 VBM of the Zincke Salt **1-1** and indolium salt **4-15** with a selection of Anilines **3-1a-g**

As for the previous set of experiments, analysis of the ¹H NMR spectra of the crude product mixture for each experiment facilitated rapid assessment of the conversion to the target Cy7 **4-14** product. This is exemplified in **Figure 4-11** which shows a stack of starting material, target product **4-14**, and the crude product mix with aniline catalyst, **3-1a-g**.

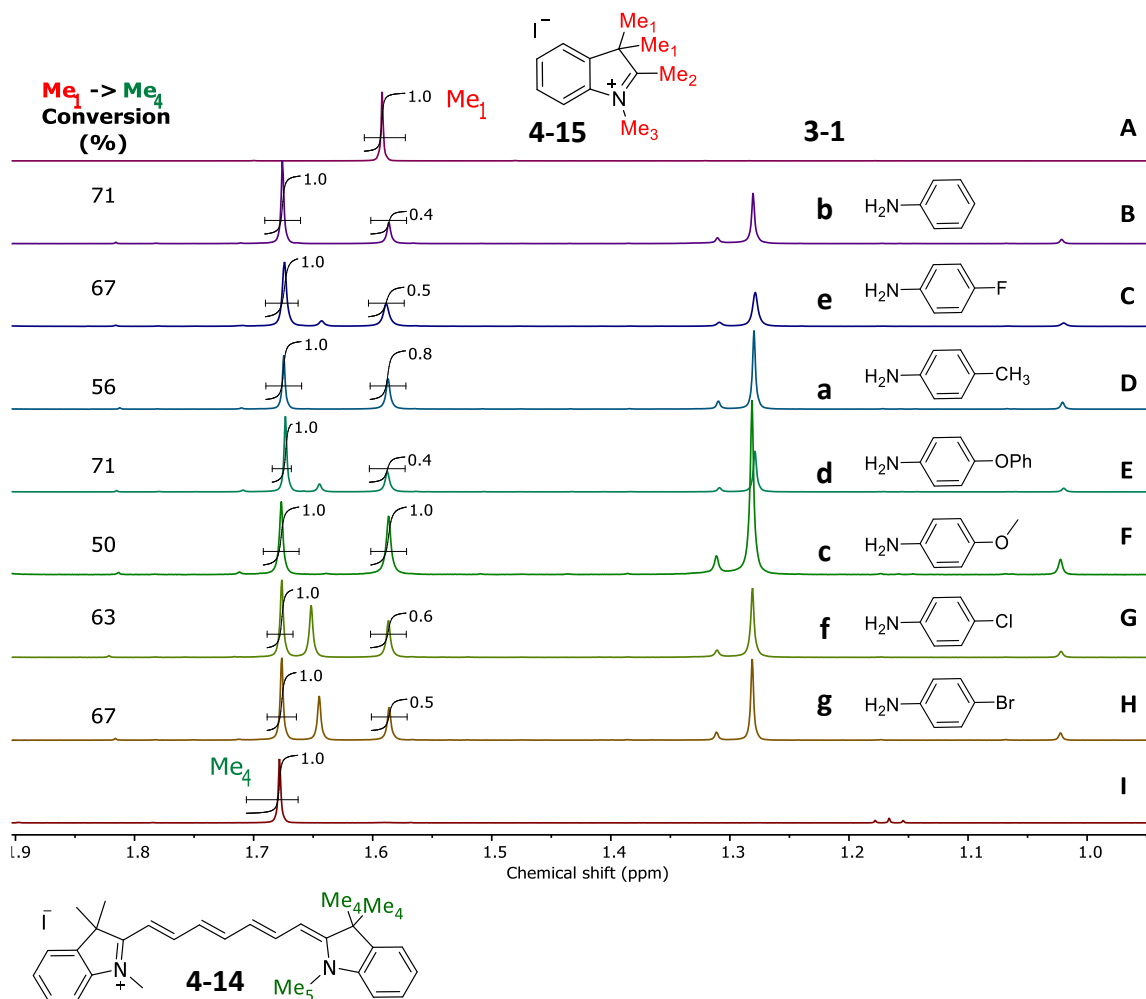


Figure 4-11 Assignment of methyl groups Me_1 from the starting material Indole **4-15** and Me_4 from the target compound Cy7 **4-14** in experiments using a range of substituted anilines **3-1a-g**. ^1H NMR Spectra for (A) indole **4-15** then crude reaction mixtures (B) aniline **3-1b** (C) 4-fluoroaniline **3-1e** (D) p-tolyl aniline **3-1a** (E) 4-phenoxyaniline **3-1d** (F) p-aniso aniline **3-1c** (G) 4-chloroaniline **3-1f** and (H) 4-bromoaniline **3-1g** (I) Cy7, **4-14**

Percentage conversions are based on the signals Me_1 of the indole, and Me_4 on Cy7. The signal for Me_1 at 1.6 ppm diminishes significantly in the NMR of the crude product in comparison with the signals in the series for each crude product mix in the NMR stack. A summary of the conversions is set out below. Interestingly, the doubling of the sodium acetate from 2 to 4 equivalents for this suite of experiments shows that for the bromoaniline catalyst, conversion increased from 49% to 67%.

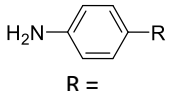
Aniline		25 mL ZrO ₂ Jars		
 R =		Calc. <i>pK_a</i>	Time milled (min)	% conv. a - d
a	Me	4.99	60	57
b	H	4.64	60	75
c	OMe	5.11	60	53
d	OPh	4.36	60	73
e	F	3.80	60	67
f	Cl	3.49	60	65
g	Br	3.83	60	66

Table 4-2 (top)% Conversion by ¹H NMR spectroscopy from the Zincke salt **1-1** to Cy7 **4-14** with aniline substituted aniline catalyst **3-1a-g**

A plot of each aniline against its calculated *pK_a* value gives a correlation that shows a ‘bump’ which gives the pattern of reactivity of the variously substituted anilines, peaking between 3.5 and 5.2 for this series of experiments. All the Zincke Salt **1-1** starting material gave moderate to good conversion to the targeted cy7 **4-14** residues depending on the catalyst/aniline. It is apparent that the ‘tipping point’ value for the *pK_a* should be no greater than 4.70, the point in the chart when the percentage conversion dips below 60% as seen in **Figure 4-12**. However, it is noted that the differences in conversion are small.

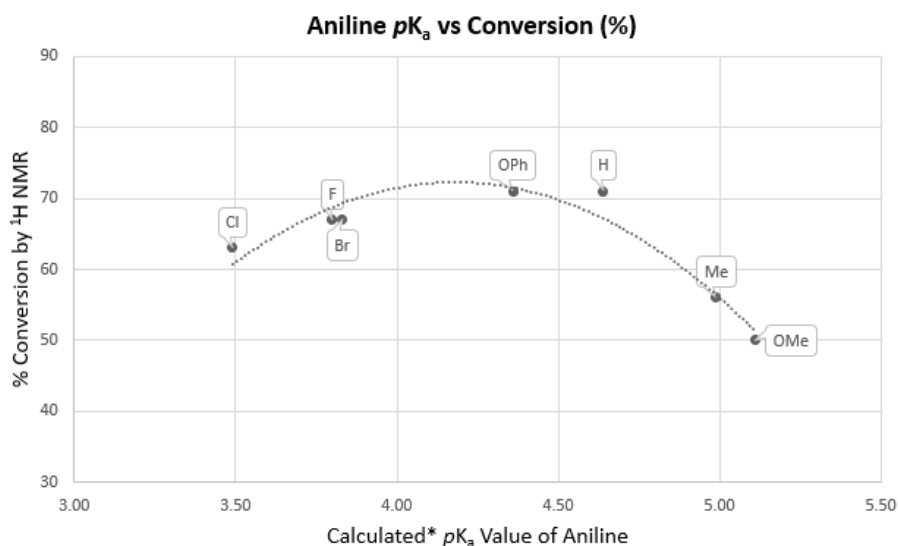


Figure 4-12 Plot of Aniline *pK_a* vs percentage conversion

To summarise, in Chapter 3, the formation of seven Cy5, **3-8a-g** compounds using VBM gave excellent yields for all anilines (63 - 98+%). The Cy5s **3-8a-g** were then used to

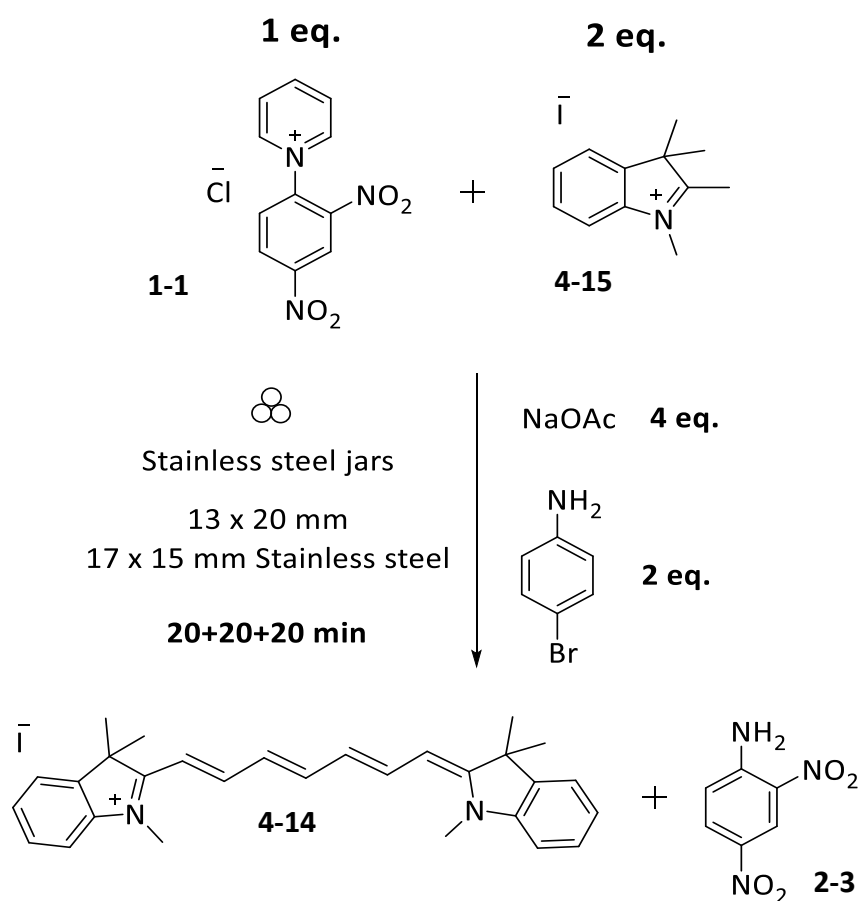
investigate as a route to Cy7 **4-14** using VBM. To find the best Cy5 for conversion, 1 equivalent of the Cy5 **3-8a-g** salt were added to 2 equivalents of indolium salt **4-15** in a ZrO₂ jar (25 mL) with two ZrO₂ balls (15 mm Ø) and oscillated at 30 Hz for 60 minutes using 2 equivalents of NaOAc. These experiments showed decidedly poor conversions (0-30%) to the target Cy7 molecule **4-14** with a strong possibility that these experiments needed more time in the VBM, 90-120 min rather than 60 min.

A new set of experiments in VBM were conducted to find the best *aniline* to convert the Zincke salt **1-1** into the targeted Cy7 **4-14**. The reaction conditions were 1 equivalent of the mono-Zincke salt **1-1** added to 2 equivalents of indolium salt **4-15** in a ZrO₂ jar (25 mL) with two ZrO₂ balls (15 mm Ø) and oscillated at 30 Hz for 60 minutes using 4 equivalents of NaOAc. This gave a contrasting table of conversions which ranged between 51-71% for conversions. A plot of conversion against pK_a indicated potential candidates for the scale-up of this reaction. Maximising the amount of reactive reagent in the mixer mill was preferred over optimising for the amount of base due to the limited volume/space available in the reaction vessel. Study of the stacked ¹H NMR spectra shows that although all the indole *and* starting material are consumed as evidenced by their absence from the crude product mix in the ¹H NMR spectra, it had not been used up to form the Cy7 product **4-14**.

The final selection of aniline would be down to the physical state at room temperature – a solid is preferred over liquid aniline for ease of processing and practicality. Another consideration is the melting point of the aniline used (cf heat and stir experiments in Chapter 2). A low melting point solid would be advantageous in the ball mill because without the ability to use conductive heat, the collisions in the ball mill help to generate sufficient thermal energy for melting. The more liquid the mixture becomes; the better conditions are for it to become homogenised. In combination these help improve conversion to the desired product. Therefore, the best aniline, with a melting point of 60-64°C for this process, is bromoaniline **3-1g**.

4.8 Scale-Up of the Zincke to Cy7 in the Planetary Ball Mill

The two sets of experiments were intended to inform the best conditions for a scaled-up reaction in a Planetary Ball Mill (PBM). The four highest yielding anilines from the data in **Table 4-2** are aniline **3-1b**, 4-phenoxyaniline **3-1d**, 4-bromoaniline **3-1g** and 4-fluoroaniline **3-1e**. We discounted both the aniline **3-1b** and the fluoroaniline **3-1e** as both are liquid at room temperature. Bromoaniline **3-1g** is a solid at room temperature and is preferred over the phenoxyaniline **3-1d** as it is more efficient from the 'atom economy' point of view but is also costs *ca.* 40% of the price, this makes it the greener and cheaper of the two remaining options.



Scheme 4-10 Reaction scheme for the PBM of heptamethine Cy7 **4-14** from Zincke salt **1-1** and Indolium salt **4-15**

With an increased volume of the reaction vessel to 125 mL, using a stainless steel jar, this meant that the ball charge could be greater. In the event we used a mixture of sizes of steel

balls and used the recommended 1:1:1 ratio for balls: space: reagents for optimum milling conditions. Reaction monitoring by sampling the ^1H NMR was conducted every 20 minutes with a total milling time was 60 minutes. The resulting crude mixture bore no resemblance to the pale or colourless powders prior to the PBM experiment, **Figure 4-13**.



Figure 4-13 Top: the starting reagents Bromoaniline **3-1g**, sodium acetate, Zincke salt **1-1** – the indole is in the jar at the rear – it is a pale pink crystalline solid. Bottom: (L) The 125 mL Stainless Steel PBM and milling balls and (R) the crude reaction mixture after 60 minutes in the PBM

As for all previous experiments to synthesise Cy7 **4-14**, a stack of ^1H NMR spectra of the starting material **4-15** the sampled crude product mix, and the target Cy7 **4-14** molecule, is shown in **Figure 4-14**.

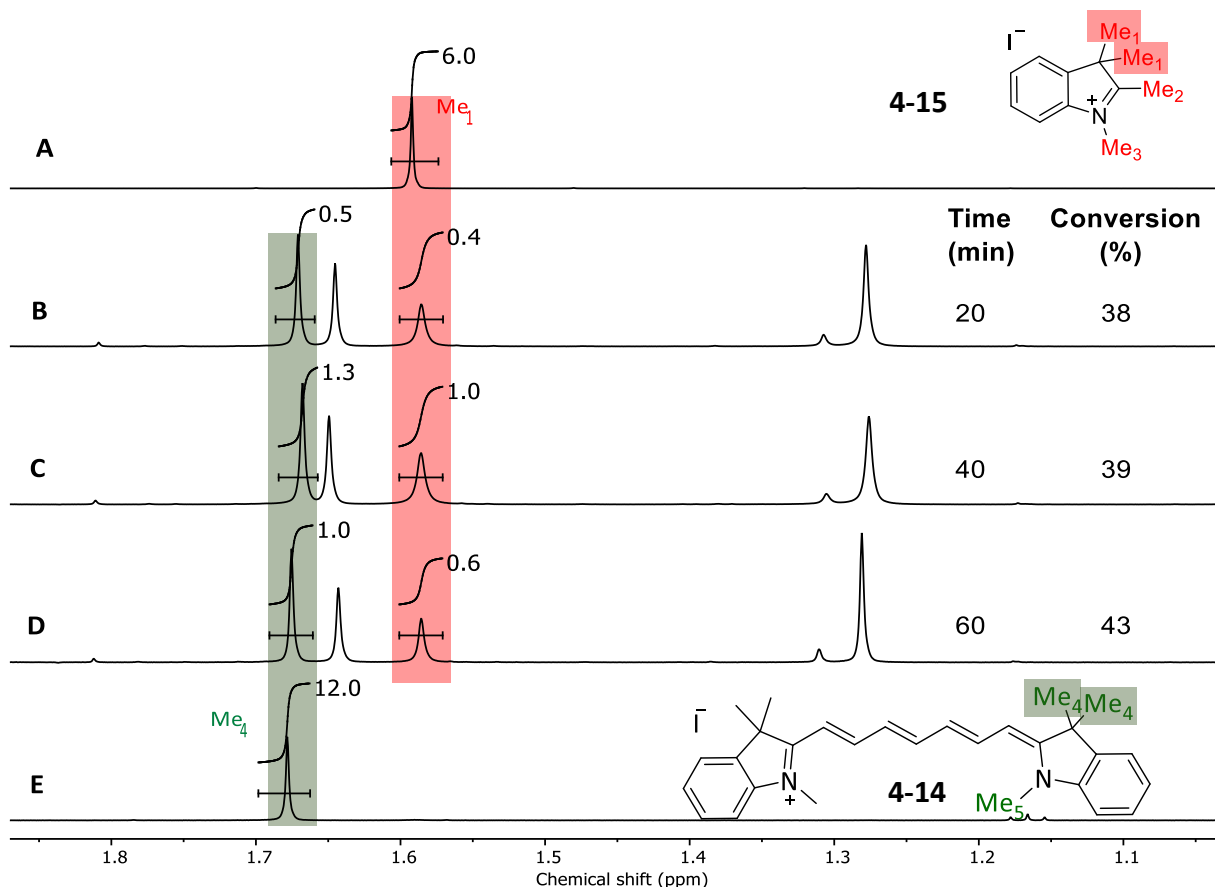


Figure 4-14 Stacked ^1H NMR spectra for sampled crude from PM100 to make Cy7 where (A) indole starting material, **4-15** (B) Crude product mixture at $T = 20$ min (C) Crude product mixture at $T = 40$ min (D) Crude product mixture at $T = 60$ min (E) Isolated Cy7, **4-14**

The percentage conversions were calculated and showed that over a third of the indole had been consumed (38%) within the first 20 min of planetary rotation. After a further 20 min conversion crept to 39% and the experiment was halted after 60 minutes with a final conversion of 43%. We understand from studies into the reaction kinetics in the ball mill, that stopping the experiment for reaction monitoring purposes interferes with the progress of the reaction. The inevitable cooling that occurs when heat-generating collisions are interrupted, means that when the reaction is re-activated for the next 20 minutes, the temperature in the vessel will not have been a continuation from the point at which the experiment was paused. Nevertheless, the next 20 minutes sees an increase in conversion, but just by 1%. It was also noted that using stainless steel equipment with the mono-Zincke compound **1-1** did not give the same problems as the di-Zincke salt **1-2** with ^1H NMR spectroscopy analysis (**Section 2-2**). The spectra from the sampled were well-resolved with none of the broadened resonances as was seen with the viologens. This was good news for

future experiments in scale up using extrusion methods as extruders are often equipped with steel components, and so the knowledge that this would not be a handicap for this reaction was a useful outcome. Examination of the stacked ^1H NMR spectrum of the crude mixture (A) reveal the main products are the target Cy7 **4-15** molecule but there is also the expected leaving group, dinitroaniline **2-3** and negligible if any amounts of the closed-ring side-product spectrum (B), **Figure 4-15**.

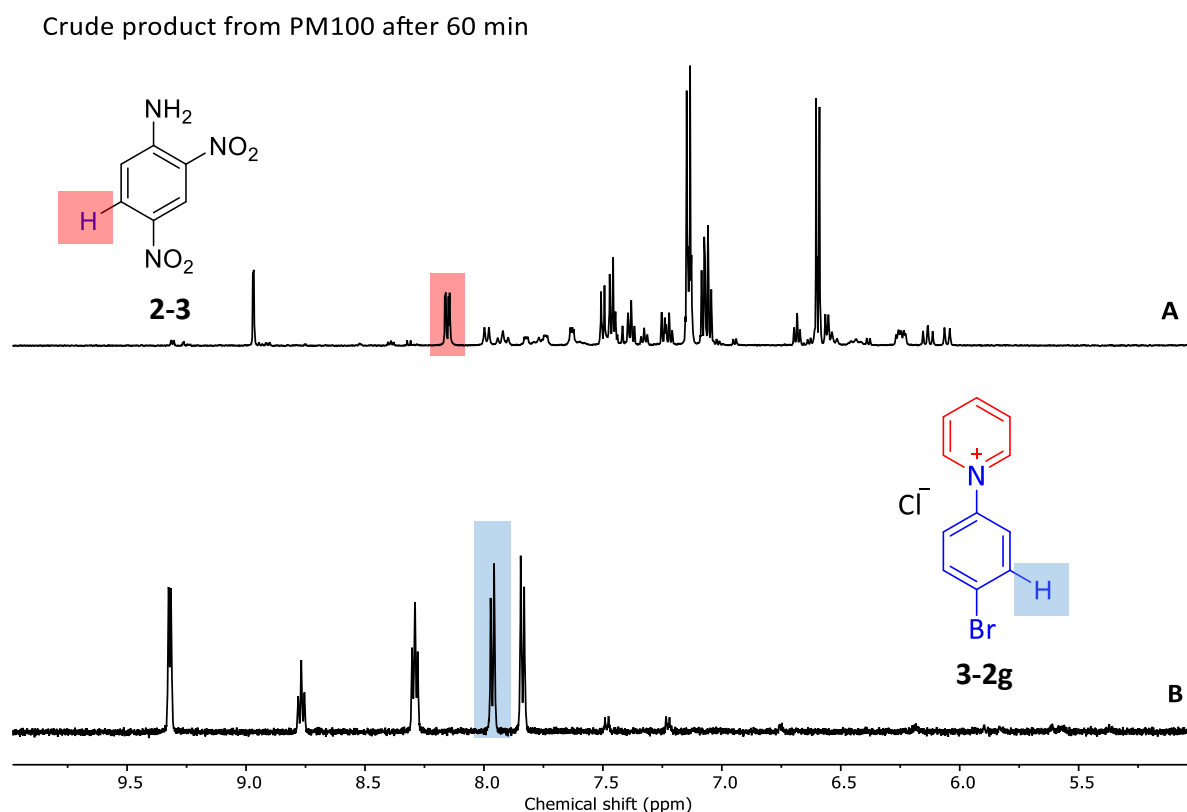


Figure 4-15 Stacked ^1H NMR spectra for (A) crude product of Zincke salt **1-1** with indolium salt **4-15** after 60 min in the PM100 (B) the closed ring bromopyridinium salt **3-2g**

This ^1H NMR spectroscopic result is consistent with the previous two series of experiments with the scale-up. Purification was achieved by dissolving the crude product mixture in methanol and recrystallising from diethyl ether over 1 week. Upon filtering and washing the solid with distilled water a glittery *red* solid was recovered, (6.85 g, 35% yield), as shown in **Figure 4-16 (a) and (b)**. A second crop of larger crystals formed in the filtrate which had been left to precipitate out giving *ca.* 2mm long crystals, **Figure 4-16 (c)**

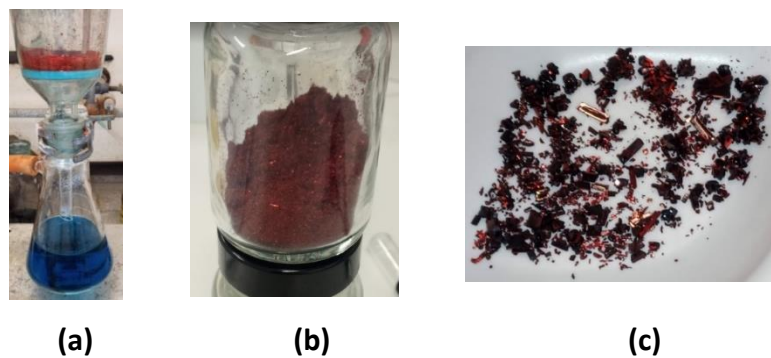


Figure 4-16 Filtration of the opaque green mixture gave a red glitter **4-14.2-3**.

We had expected to see intensely green needles of the Cy7 **4-14** as was isolated previously (*Section 4-3*).

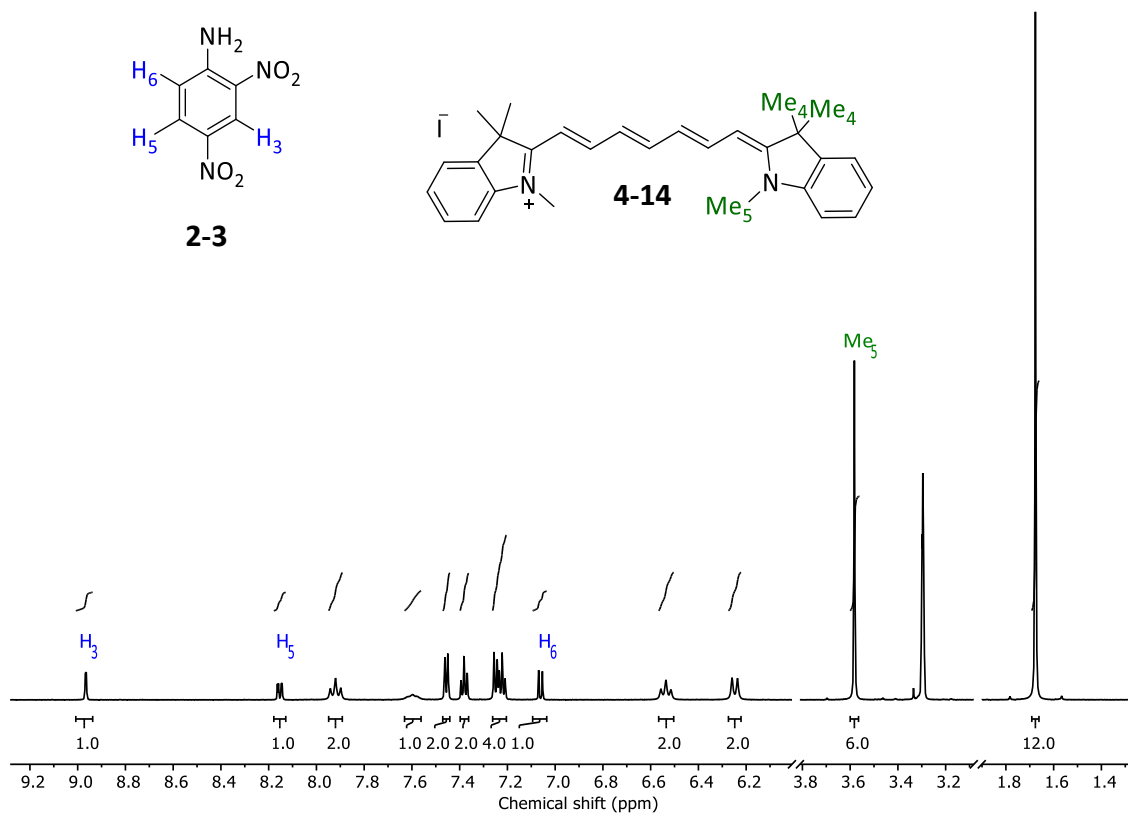


Figure 4-17 The ^1H NMR of the red cocystal and the assignments of the two molecules present.

A sample of red crystal dissolved in deuterated methanol for ^1H NMR spectroscopy analysis gave a deep green solution. Analysis of the ^1H NMR spectra revealed a second set of signals

belonging to the leaving group dinitroaniline **2-3** in equal intensity to the Cy7 molecule **4-14**, shown in **Figure 4-17**.

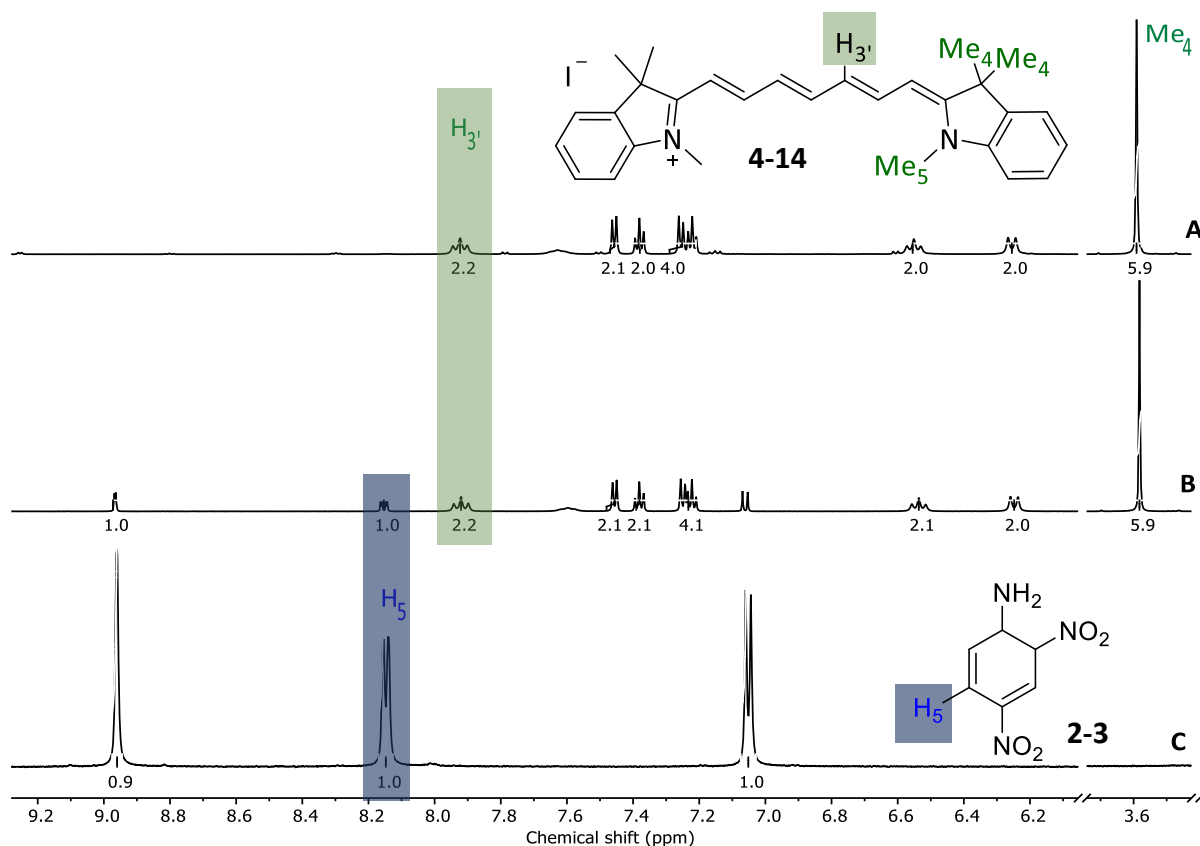


Figure 4-18 Stacked ^1H NMR spectra (A) of Cy7 **4-14** (B) cocrystal Cy7 **4-14** and dinitroaniline **2-3** (C) dinitroaniline **2-3**

The ^1H NMR spectrum, once fully assigned, showed equal amounts of our target Cy7 **4-14** but also the leaving group, dinitroaniline **2-3** – there was a strong possibility that a cocrystal of the two molecules had formed, **Figure 4-18**. Further identification came from an X-Ray crystal structure showing the electron-deficient dinitroaniline positioned adjacent to the electron-rich environment of the polymethine chain. Another interesting feature shown in the structure is that the indoles on either end of the polymethine are not lying in the same plane and it is a very twisted molecule with the dinitroaniline. The shortest distance between the two molecules is 3.4 Å, there are 4 cocrystals per unit cell which are packed in a classic herringbone with a calculated point group $P2(1)/n$, giving us the monoclinic crystals that are observed in our sample.

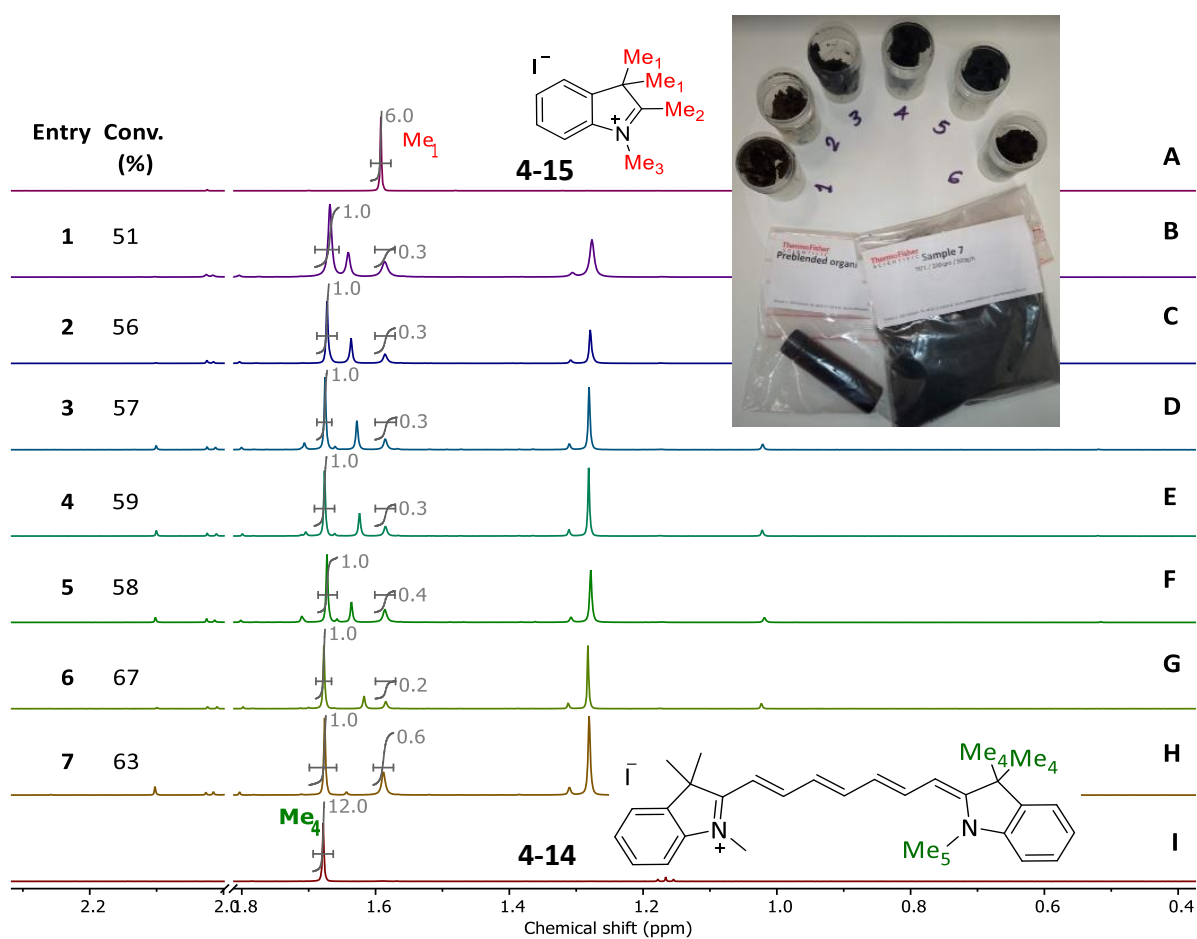


Figure 4-21 Percentage conversion using signals Me₄ and Me₁ for Twin Screw Extrusion Experiments using ¹H NMR spectroscopy where spectra (A) indolium salt **4-15** and the Twin Screw extruded crude products for Entries **1-7** (B)-(H), (I) the isolated target molecule Cy7 **4-14**.

¹H NMRs were taken for each sample to see which set of conditions worked best in the extruder. As with all the previous conversions calculated, the signals used to calculate conversion were **4-15** Me₁ from the starting material and Cy7 **4-14** Me₄ of the target molecule.

There were resonances that could not be assigned in each spectrum for an unknown molecule which is present in sizeable quantities.

Entry	Barrel temp. (°C)	RPM	Torque (%)	Feed Rate [g/h]	Conv. Me ₁ -Me ₄ (%)
1	40	100	13	200	51
2	70	100	5	200	56
3	120	100	3	200	57
4	120	100	4	500	59
5	120	400	5	500	58
6	25	100	48	200	67
7*	70	200	31	500	63

* on Entry 7 in the table denotes reduced amount of sodium acetate used in experiment.

Table 4-3 Extruder conditions and the percentage conversions to **4-14** for each.

The result from the table shows that all combinations achieved over 50% conversion, but we cannot meaningfully compare each experiment against the other as there were four different variables of which two were changed for each experiment. However, here was sufficient evidence to conclude that the Zincke Salt **1-1** route to Cy7 **4-14** with bromoaniline as a catalyst was feasible using extrusion as a methodology and we were very excited to use this result as a springboard to a synthesis of another Cy7 **4-14** molecule, the imaging dye Indocyanine Green, **4-1**.

An important photophysical property of Cy7 dyes is its ability to fluoresce in the near infrared region (**Section 4-2**), experiments to help verify that synthesis from the mono-Zincke salt had produced the Cy7 molecule were needed. This would give us confidence in proceeding to the next set of experiments: the continuous extrusion of Indocyanine Green **4-1**.

4.10 UV-Vis and fluorescence studies of Cy7

A set of UV-Vis measurements of Cy7 **4-14** at various dilutions in methanol were taken which are in agreement with the findings in the literature.¹⁶⁴ A fluorimetry analysis of the same sample gave a value of 29 nm for the Stokes Shift for the Cy7 **4-14**, **Figure 4-21**.

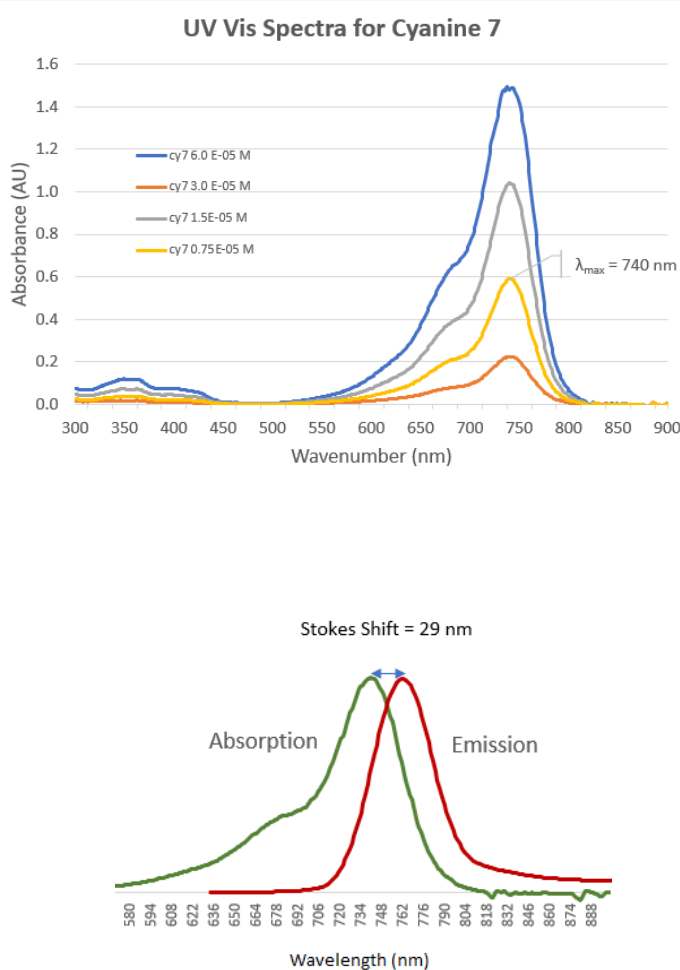


Figure 4-22 (Top) UV-Vis absorption spectra for **4-14** and (bottom) measurement of the Stokes shift fuorimetry for Cy7 **4-14**

While this UV-Vis study on the molecule gives further veracity to the synthesis of Cy7 accessed via the mono-Zincke salt, further interesting work conducted by Štacková *et al.*²⁰⁷ showed the effect of EDG and EWG on the methine chain, **Figure 4-24**. A single substitution on the polymethine chain (R_{1-3}) enabled the modulation of absorption maxima in the range of 693–805 nm. They also discovered that photophysical properties that the quantum yields of singlet-oxygen formation (1O_2 , Φ_Δ), decomposition (Φ_{dec}), and fluorescence Φ_F or affinity to singlet oxygen Φ , were within 2–3 orders of magnitude.

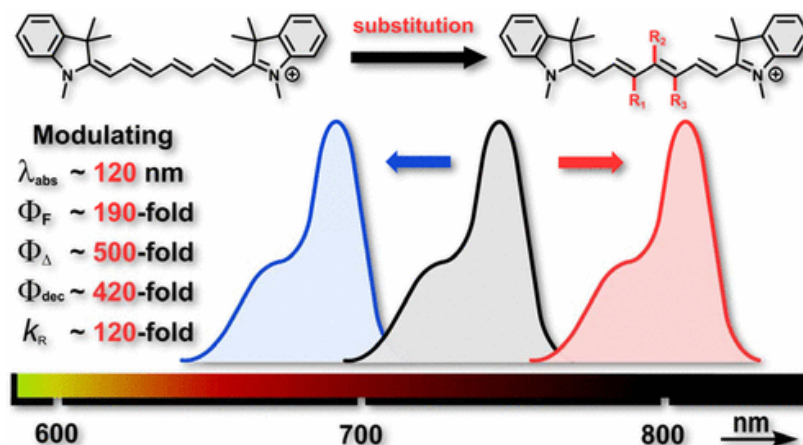
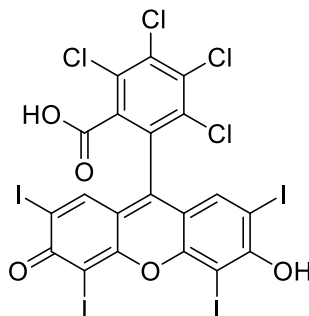


Figure 4-23 UV-Vis Investigation by Štacková *et al.* 'Deciphering the Structure–Property Relations in Substituted Heptamethine Cyanines,' figure from²⁰⁷

In order to calculate the rate bimolecular rate constant, they used Rose Bengal dye (**4-16**) as an auxiliary $^1\text{O}_2$ generator to determine the bimolecular rate constant (k_{R}) of the reaction of cyanines and assessed the effects of individual substituents. Surprisingly, they found the same substituent occupying different positions on the chain often had distinctly a contradictory effect.



4-25

They concluded that the design of Cy7-based dyes for applications would be dependent on the type and position of the substituent. Using their experimental results alongside quantum-chemical calculations helps build an understanding the structure–property relationship and help to develop cyanines useful for applications in fluorescent probes and sensors such as singlet-oxygen detection and PDT.

4.11 Conclusion

In Chapter 4 we have examined the synthesis of a Cy7 molecule **4-14** by reacting the indolium salt **4-15** with the mono-Zincke salt **1-1** in the solid state, initially with VBM and then scaling up to PBM. With both methods giving conversions up to 73% and 43% respectively, to our target molecule. Samples of all the starting reagents, the mono-Zincke salt **1-1**, bromoaniline **3-8g**, indolium salt **4-15**, and sodium acetate, were sent for exploratory experiments using a twin screw extruder (**TSE**) at a facility in Germany using ThermoFisher's Process 11. These experiments confirmed that the reaction can proceed via extrusion with conversions ranging from 51-67% were seen via analysis of ^1H NMR spectroscopy of the seven extruded samples that were returned to us. This combined evidence supported our proposal to produce the very useful NIR imaging dye, ICG **4-1** using the solvent-free, continuous, reactive extrusion, which is discussed in Chapter 5.

5. Indocyanine Green: a new process for synthesis by SSE

We have demonstrated the successful synthesis of a Cy7 molecule using the mono-Zincke salt **1-1** as precursor for the conjugate addition by an indolium salt, with sodium acetate and seven different aniline catalysts. Evidence that the reaction is viable in the solid state using both VBM (**Section 4-5**) and TSE (**Section 4-8**) has also been established. One of the more useful Cy7 dyes that is in current mass production is Indocyanine Green or ICG **4-1**, (**Figure 5-1**) and the patent literature shows that its manufacture is currently based on synthetic methods in solution. The global market for ICG is predicted to grow to US\$64 M by 2028²⁰⁸ and is therefore a useful target molecule for a solid state methodology based on our findings.

5.1 Background of Indocyanine Green (ICG) **4-1**

ICG **4-1** was one of a number of dyes – initially developed for photographic use – presented to a cardiologist, Irwin Fox, at the Mayo Clinic from a grateful patient who was in the employ of the Eastman Kodak Laboratories.¹⁹⁹ Fox went on to develop the dye, testing it in circulatory-dilution experiments, and named the compound ‘Cardio- or Fox Green’, **4-1**.²⁰⁹ In 1960, Kodak filed another patent establishing indocyanine green as a fluorescent imaging dye¹⁹⁹ used for surgical imaging²¹⁰ applications. ICG **4-1** along with Methylene Blue **5-1** remain to date the only two Near Infrared (NIR) fluorescent dyes approved by the FDA for clinical use.²¹¹

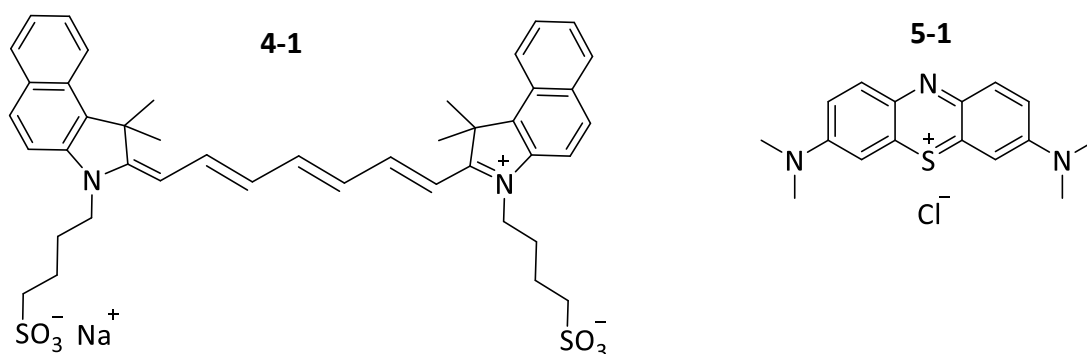


Figure 5-1 The structures of ICG **4-1** and MB **5-1**

Common to both structures of ICG, **4-1** and methylene blue, MB **5-1** are their extended systems of π -conjugation. This enables them to absorb higher energy radiation and through

a series of energy transfer mechanisms within their electronic states, to then emit lower energy radiation. Stokes observed this phenomenon when ultra-violet light was shone onto the mineral fluor spar in 1852, and gave it the term fluorescence.²¹²

5.2 Photophysical properties of fluorophores ICG 4-1 and MB 5-1

Of particular importance for applications of imaging dyes is their *Quantum Yield* (Φ), which is the value given to the number of times a specific event occurs per photon absorbed by the system in a radiation-induced process. For ICG 4-1 – Φ is 9.3% compared with MB 5-1's 3.8% - these dyes, while having low a percentage values, are considered to exhibit sufficient fluorescent properties to be useful *in vivo*.

Molecule	ICG 4-1	MB 5-1
Excitation Peak (nm)	807	670
Extinction Coefficient ($M^{-1}cm^{-1}$)	121000	71200
Emission Peak (nm)	822	690
Quenching Threshold (μM)	20	10
Quantum Yield, Φ (%)	9.3	3.8

Table 5-1 Photophysical properties²¹³ for ICG 4-1 and MB 5-1

Comparison of their other photophysical properties shown in **Table 5-1** show that Methylene Blue 5-1 is inferior to ICG 4-1 in categories relating to its utility as an imaging dye and thus limiting its use as a contrasting agent for imaging applications. Values quoted for the Quenching Threshold (μM) show that MB 5-1 is 50% that of ICG 4-1. An emission peak at 822 nm for ICG 4-1 is 132 nm longer wavelength than MB 5-1 meaning it is lower energy which places it in the NIR region of the electromagnetic spectrum. MB 5-1 at 690 nm falls into the IR region and has more energetic waves of higher frequency. Finally, the extinction coefficient for ICG 4-1 is 63% greater than MB 5-1 – this is the characteristic which measures how strongly the substance absorbs radiation at peak wavelength – a requirement for imaging applications.

Fluorescence spectroscopy (also known as fluorimetry) is the analysis of a type of electromagnetic spectroscopy measuring the degree of absorbance when an incident beam of light (usually ultraviolet) which excites the electrons in the sample then causes it to emit

light typically, but not exclusively, visible light. **Figure 5-1** shows the spectra that has been reported from a FLARE™ imaging system²¹³ using samples comprised of 5 μM MB **5-1** and 2.5 μM ICG **4-1**. This gives profiles as shown where the relative fluorescence profiles of ICG **4-1** and MB **5-1** may be compared. ICG **4-1** absorbs and fluoresces with approximately 90% more intensity; with concentration of samples being on a linear scale, the ICG **4-1** sample shown is half the concentration of the MB **5-1** sample. In practicality terms, not only does this make the ICG **4-1** dye more easily seen, it emits photons at longer wavelengths, 750-900 nm versus MB's **5-1**, 620-750 nm which means it is visible through greater depths of tissue. Both these attributes make ICG **4-1** a better candidate for biological imaging than MB **5-1**.

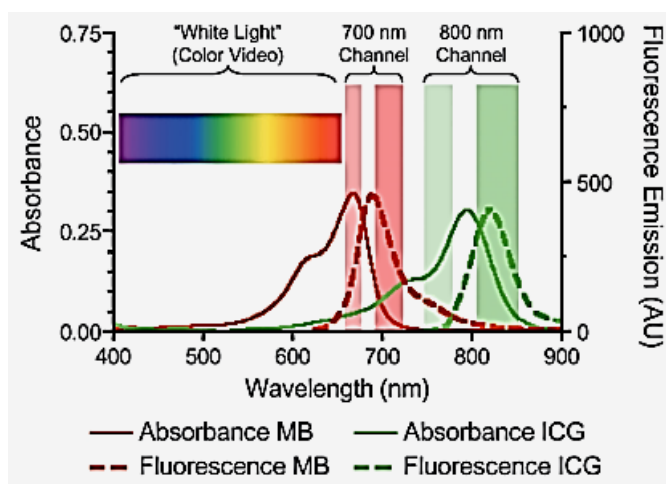


Figure 5-2 The absorption and emission profiles of indocyanine green **4-1** and methylene blue **5-1**, taken from²¹³

One useful feature is the difference in the maxima of the absorption and emission spectra of a molecule; it can be measured as the wavelength difference between the spectral maxima of the absorption (~780 nm) and the emission (~830 nm) curves as depicted in **Figure 5-2**. It would be advantageous to maximise the value of $\Delta\lambda$ because this counteracts molecular self-quenching.

The larger the value of $\Delta\lambda$, the more internal conversions and vibrational relaxation become possible, and these are the energy transfers that are required in the molecule in order for it to fluoresce. While this may be possible by designing a molecule to satisfying these criteria, when looking to use the probe *in vivo*, for example, it would need many other

attributes to be serviceable such as non-toxicity, photostability, and specificity to the target function, to name but three. Finding a molecular probe for a specific target, therefore, presents significant technical challenges.^{214,215} While outside the scope of this thesis, it is a very topical issue in that testing for specific viruses and their mutations is in continual development with Covid-19 pandemic. For example the WHO document²¹⁶ bringing together shared knowledge shows that a commonly used reporter dye (the fluorophore) 6-carboxyfluorescein (FAM), **5-2**, is covalently bonded with TaqMan, an oligonucleotide, at one end and a quencher at the other. This is the basis of the Polymerase Chain Reaction and is how PCR tests identifies the virus in an infected person.

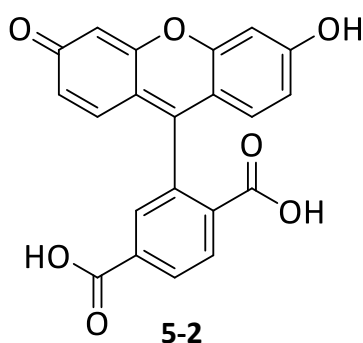


Figure 5-3 6-carboxyfluorescein (FAM), **5-2**

The combination of absorbance and fluorescence of a dye and its interactions with the biological mediums present has direct impact on the utility of the dye. This range is known as the ‘optical’ or ‘tissue’ window, **Figure 5-5**.

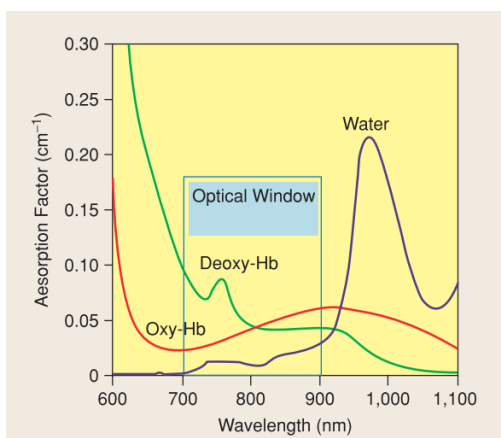


Figure 5-4 The ‘Optical Window’ – wavelengths where absorbance is lowest making imaging possible © [2007] IEEE, picture taken from²¹⁷

The emission spectral properties of ICG sits squarely within what is termed the NIR window – the region of the electromagnetic spectrum where wavelengths are between 700-900 nm, as seen in **Figure 5-5 (L)** where ICG's 4-1 emission profile is shown in red. Most biological tissues are relatively transparent to light in the range 700-900 nm, this makes ICG currently the most widely used NIR dye for surgical imaging. For the purposes of applications of this kind, where there are limited range of wavelengths.

The 'optical window' in **Figure 4** shows the absorbance of the main constituents of human tissue: water, oxygenated haemoglobin (Oxy-Hb) and de-oxygenated haemoglobin (Deoxy-Hb). The window is where the absorbance is lowest – this allows light to penetrate the tissue and facilitate imaging. Molecular oxygen is an example of a molecule that can very efficiently quench fluorescence of a molecule. This is because O₂, unusually, has a triplet ground state, **Figure 5-5** gives the molecular orbital arrangement of electrons in molecular oxygen were (A) shows the complete scheme for the O₂ molecule and (B) illustrates the p orbitals only and the two possible excited states (second and triplet) with the arrangement of the unpaired electrons in each orbital shown with red arrows.

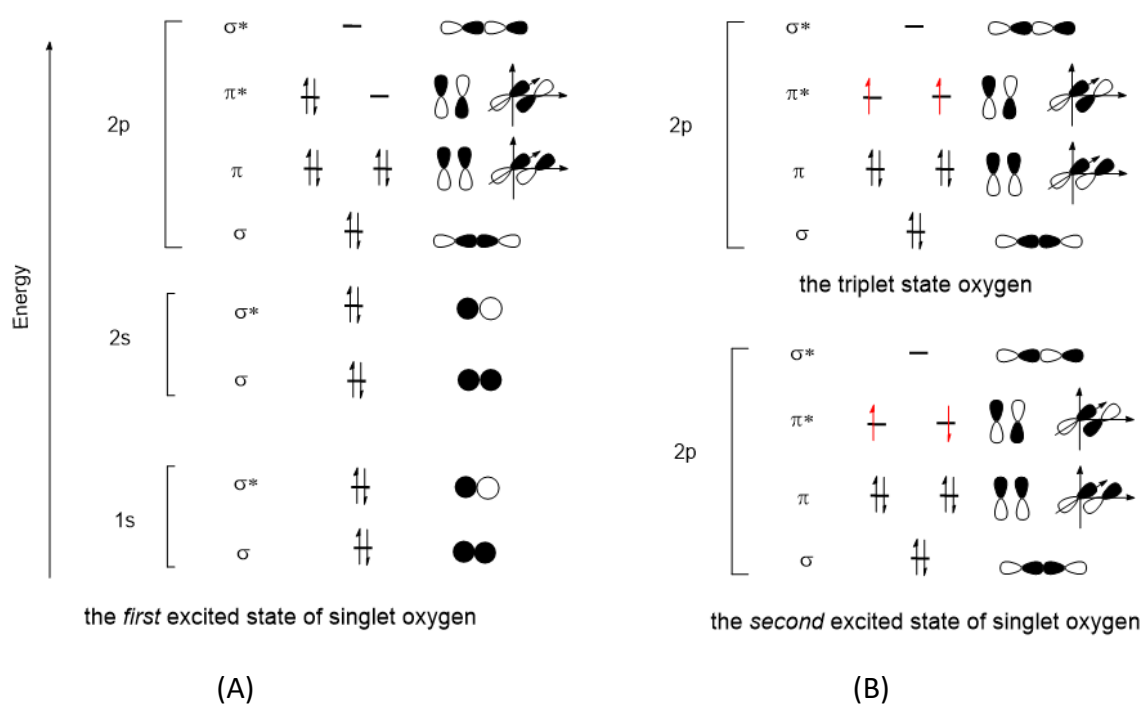


Figure 5-5 Energy diagrams for the different excited states of oxygen

Methylene blue **5-2** also has the fluorescent quenching effect of oxygen and can be useful for diagnostic purposes. For example, methylene blue may be used as a probe for the intracellular, excited singlet state oxygen, $^1\text{O}_2$, in Photodynamic Therapy.²¹⁸ When ICG **4-1** reacts with singlet oxygen, it decomposes and its absorption capability at 780 nm decreases with laser irradiation.^{219–221} The presence of singlet oxygen in the biological context signals the mediation of cell death and therefore is important for tumour diagnostics and is intensively investigated.^{222–225}

5.3 Patented synthetic routes to ICG **4-1**

There are many syntheses of ICG **4-1** in solution available in the academic literature but also a number that are patent protected by their inventors. **Figure 5-6** is a plot showing the number of patents as a function of year since 2002 for ICG **4-1** provided by the University's IP department.

The explanatory notes accompanying it state: *This chart shows the number of grants or issued patents resulting from applications filed in the same year. This is helpful for understanding the rate of applications over a period, whether the technology is recent, or whether it is heading towards stagnancy. The grant rate is useful to understand the date from which the technology protection is established and the rate of successful applications over a period. Blue represents the application trend and green represents the trend of issued patents resulting from applications of the same year. Example: if a 2012 patent application is issued in 2014, the issued patents will appear in 2012 in green.*

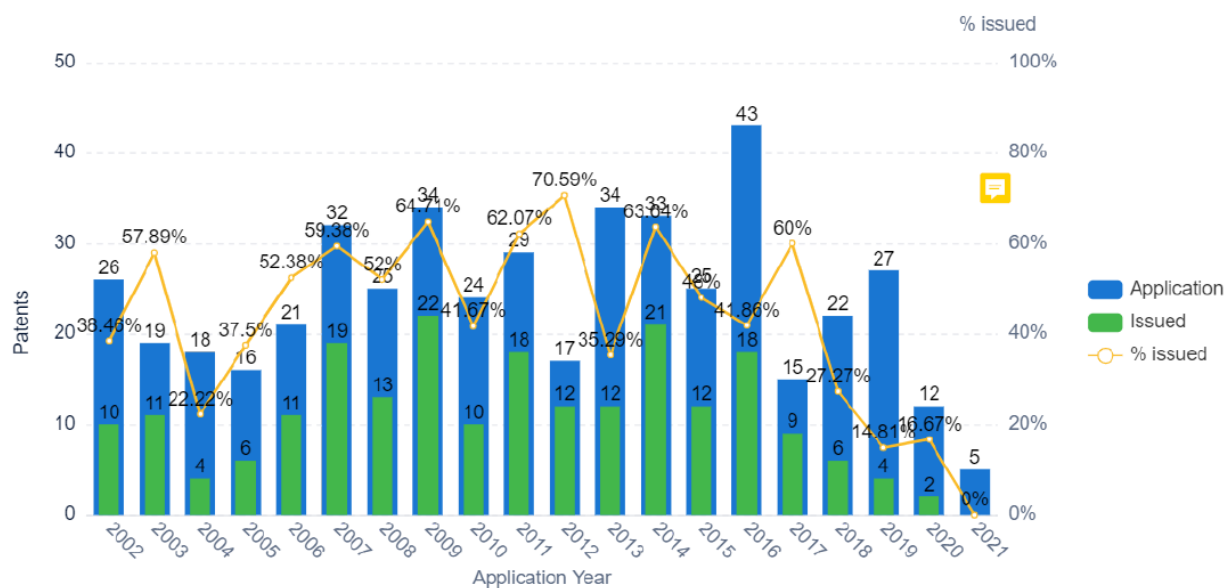
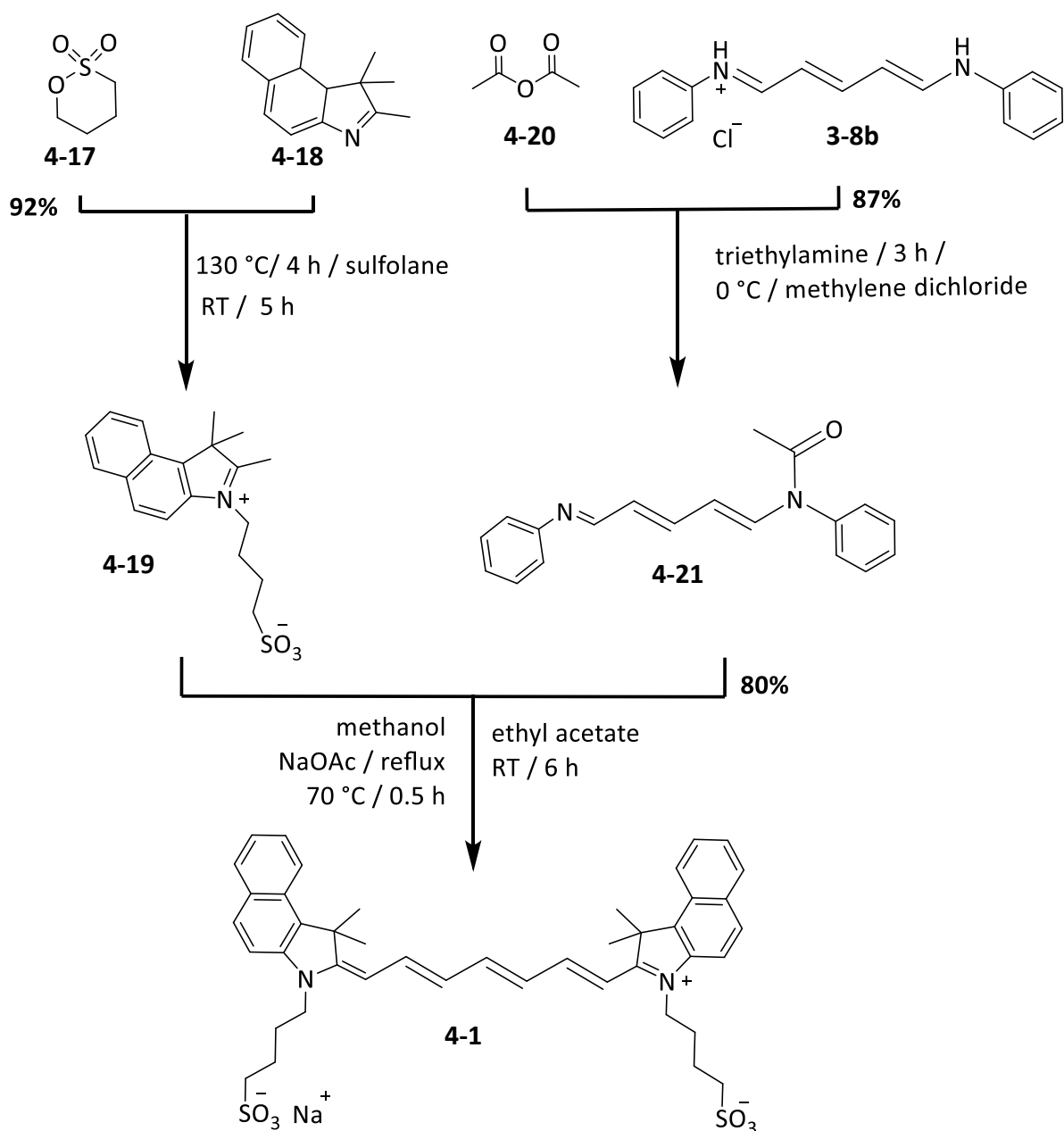


Figure 5-6 Patent search by the University of Sussex IP Department: Application and Issued Trend

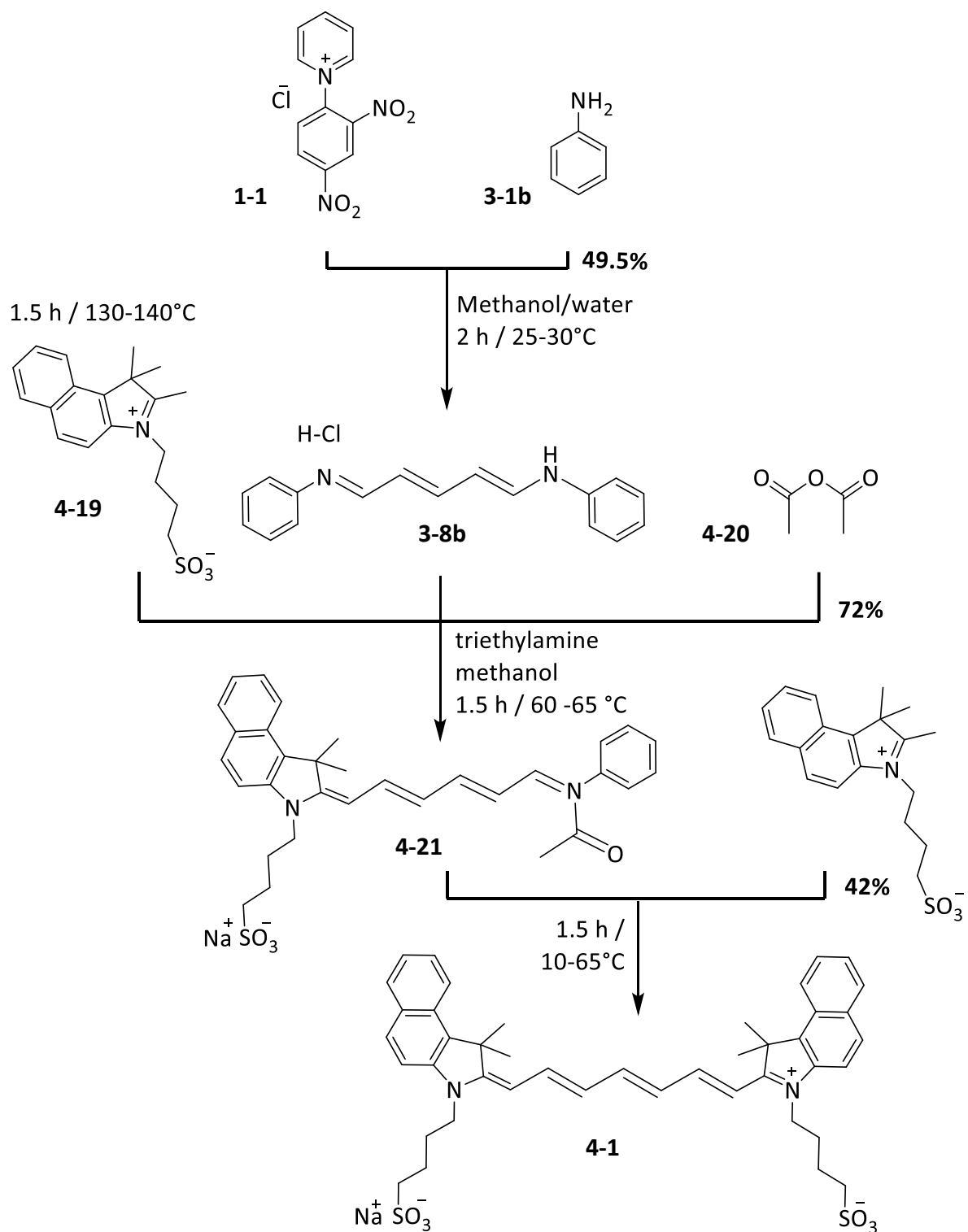
The disambiguation could suggest that patents filed and issued for the manufacture of ICG **4-1** have a roughly 4-year cycle and in 2021, because there is time lag for this information, we do not know a percentage issued. However, it would not exceed the number of applications (shown in blue) and so we see a decreasing trend from 2016. One interpretation of this could be that improvements have reached their pinnacle of optimisation in solution and so new methodologies could be an opportunity to begin a new cycle of innovation.

The differences in approach centres on the intermediate to produce ICG **4-1** in solution. In their 2016 patent filed by Dishman²²⁶ shown in **Scheme 5-1**, the Cy5 **3-8b** forms the polymethine chain with the anhydride **4-20** leading to an acyl amine **4-21** which is reacted with **4-19** to form **4-1**. The sole difference between the Eastman Kodak patent of 1957 (see p. 105) and Dishman in 2016 (**Scheme 5-1**), is that Dishman were able to show that a good yield (80%) can be achieved through the conjugate addition of the acyl amine **4-21** in a single step whereas in the Kodak scheme, it was performed in 2 steps.



Scheme 5-1 Dishman scheme for their ICG **4-1** patent²²⁶

The first patented use of the mono-Zincke salt **1-1** specifically, as a precursor for ICG **4-1** was filed by Biophore²²⁷ in 2019.



Scheme 5-2 Biophore India patent²²⁷ for making ICG **4-1** with the mono-Zincke salt **1-1** as a precursor

In the Dishman patent **Scheme 5-1**, the Cy5 **3-8b** does make an appearance but there is no indication as to its provenance in the patent and it is noted that glutaconic aldehyde

dianilide hydrochloride **3-8b** is widely available through a number of commercial vendors. A search on ReAxys gives several routes to Cy5 **3-8b** including its synthesis from the Zincke salt **1-1**. Although we have shown the reaction is facile in VBM, it cannot be assumed this is the only route to this intermediate. The Biophore patent in **Scheme 5-2**, once again uses solvents throughout the multi-step process. The synthesis takes a total of 6.5 hours and temperatures up to 140 °C and four different steps to produce, by their calculation, a total linear yield of just 15% (calculation = 0.495 x 0.72 x 0.42 from the Biophore patent **Scheme 5-2**).

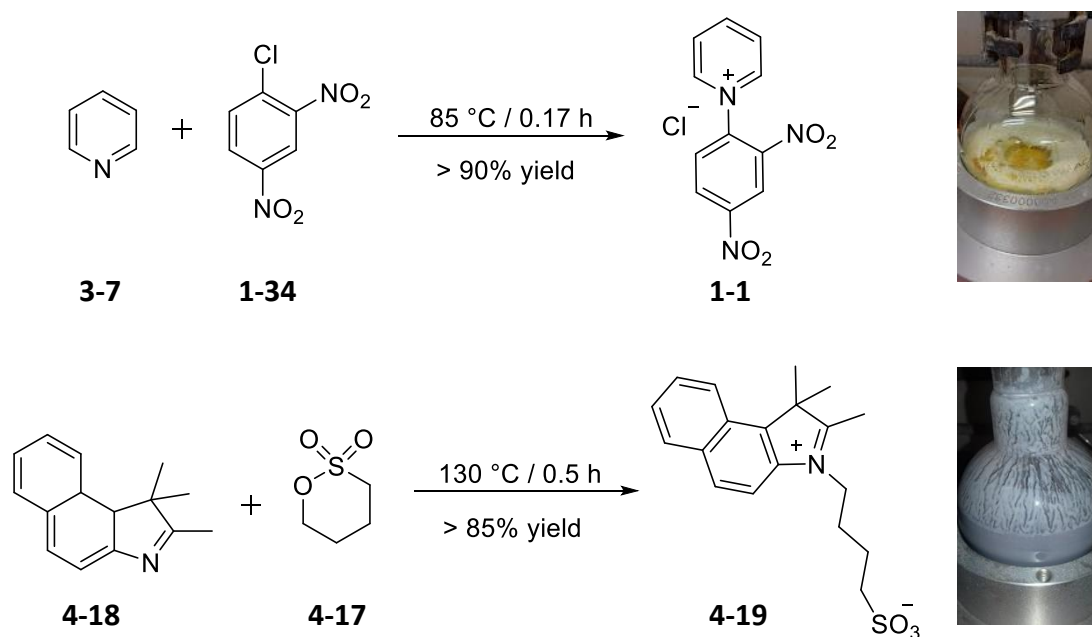
A potential improvement on these patented schemes is to react all the starting materials, the mono-Zincke salt **1-1**, indolium sulfonate salt **4-19**, bromoaniline **3-1g** and sodium acetate in one-pot to avoid purifications of the intermediate compounds as they can all be made *in situ* just as Štacková and co-workers did for their heptamethine dyes in solution as previously discussed (**Section 4.4**). The term telescoping synthesis²²⁸ is given to a sequential one-pot synthesis with reagents added to a reactor one at a time and without work-up. There are also cascade reactions which are sometimes referred to as domino or tandem reactions.²²⁹ This is when the final product has been arrived at through a series of consecutive reaction events. The process requires at least two sequential reactions where each reaction is a consequence of the chemical functionality formed in the previous step.²³⁰ The synthesis of ICG **4-1** using reagents in one-pot is therefore the obvious next step with the required starting materials being the mono-Zincke salt **1-1** and the naphthyl indolium sulfonate **4-19**.

5.4 Solvent-free synthesis of mono-Zincke salt **1-1** and the indolium salt **4-19**

The solvent-free syntheses of scalable and commercially available molecules are a major directive in this work, in both eliminating solvent use altogether in their synthesis and, where this is not possible, use sustainable solvents preferentially. The objective for searching for solvent-free, scalable methods using ReAxys was to access multi-gram amounts of both starting materials that are required for the scale-up production of ICG **4-1** by single screw extrusion.

These approaches were aided by starting material reagents pyridine **3-7**, and 1,4-butane sultone **4-17** being liquids at RT, because for these reactions, the liquid reagent functions as both solvent and reagent. Syntheses were conducted using 250 mL flask fitted with a Findenser™ - a condensing unit that is designed for heating under reflux without the need for coolant (usually a water jacket) and is another aspect of following the 12 Green Principles in chemical synthesis. 1-chloro-2,4-dinitrobenzene **1-38** were dissolved in equimolar quantity with hot pyridine **3-7** and stirred under reflux until the stirrer could no longer move due to the solid precipitate having been formed.

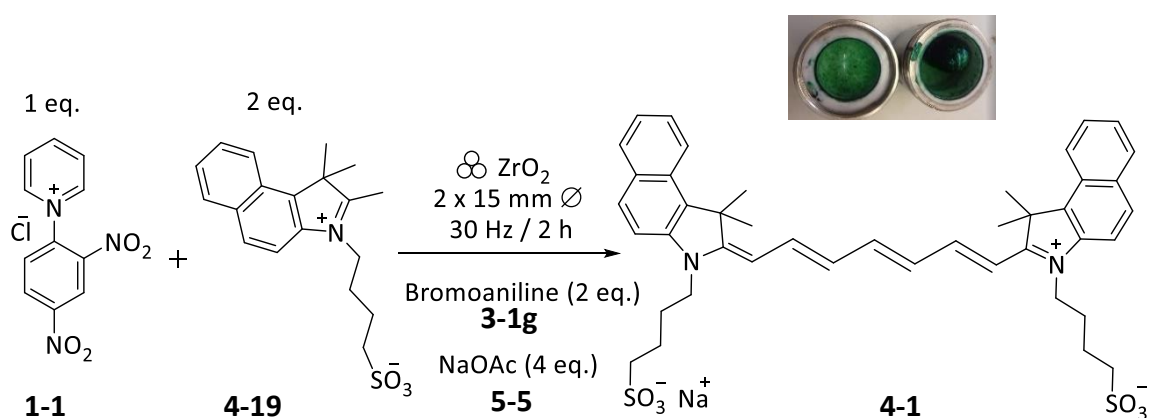
Similarly, for the synthesis of the naphthyl indolium sulfonate starting material, 1,1,2-Trimethyl-1H-benzo[e]indol **4-18** was heated with liquid 1,4-butane sultone, **4-17** under reflux for 30 minutes. Upon cooling, both the solids were stirred in acetone, filtered and washed with further acetone to give the mono-Zincke salt **1-1**, a yellow solid (20.3 g, 97% yield) and 2,3,3-Trimethyl-1-(4-sulfobutyl)-indolium inner salt **4-19** as a lilac-coloured powder (18.3 g, 88% yield). The mono-Zincke salt **1-1** can be easily prepared without solvent¹⁴¹ and based on the success of this, the indolium salt **4-19** was also synthesised with no solvent, **Scheme 5-3**.



Scheme 5-3 Solvent-free synthesis of the mono-Zincke salt **1-1** and the naphthyl sulfonate **4-19**

5.5 VBM synthesis of ICG, **4-1**

With a large stock of starting materials to hand we could now investigate whether the 'one-pot' synthesis of ICG, **4-1** was feasible. Two equivalents of the indolium salt **4-19** were added to 1 equivalent of the mono-Zincke **1-1** in a ZrO₂ jar (25 mL) and oscillated together with 2 eq. of bromoaniline **3-1g** and 4 eq. of sodium acetate for 2 h at 30 Hz.



Scheme 5-4 Synthesis of ICG **4-1** in the VBM

Of the four reagents that were used in the Twin Screw Experiment, the indolium sulfonate salt **4-19** is analogous to the indolium iodide **4-14**. The other three reagents, the bromoaniline, the Zincke salt **1-1** and sodium acetate are identical. After completion of the experiment, the reaction vessel was opened to reveal a vivid green product encasing the ZrO₂ balls (**Scheme 5-4**). A sample of this crude was taken and analysed using ¹H NMR spectroscopy and compared with the spectra of the starting materials and leaving group **Figure 5-7**.

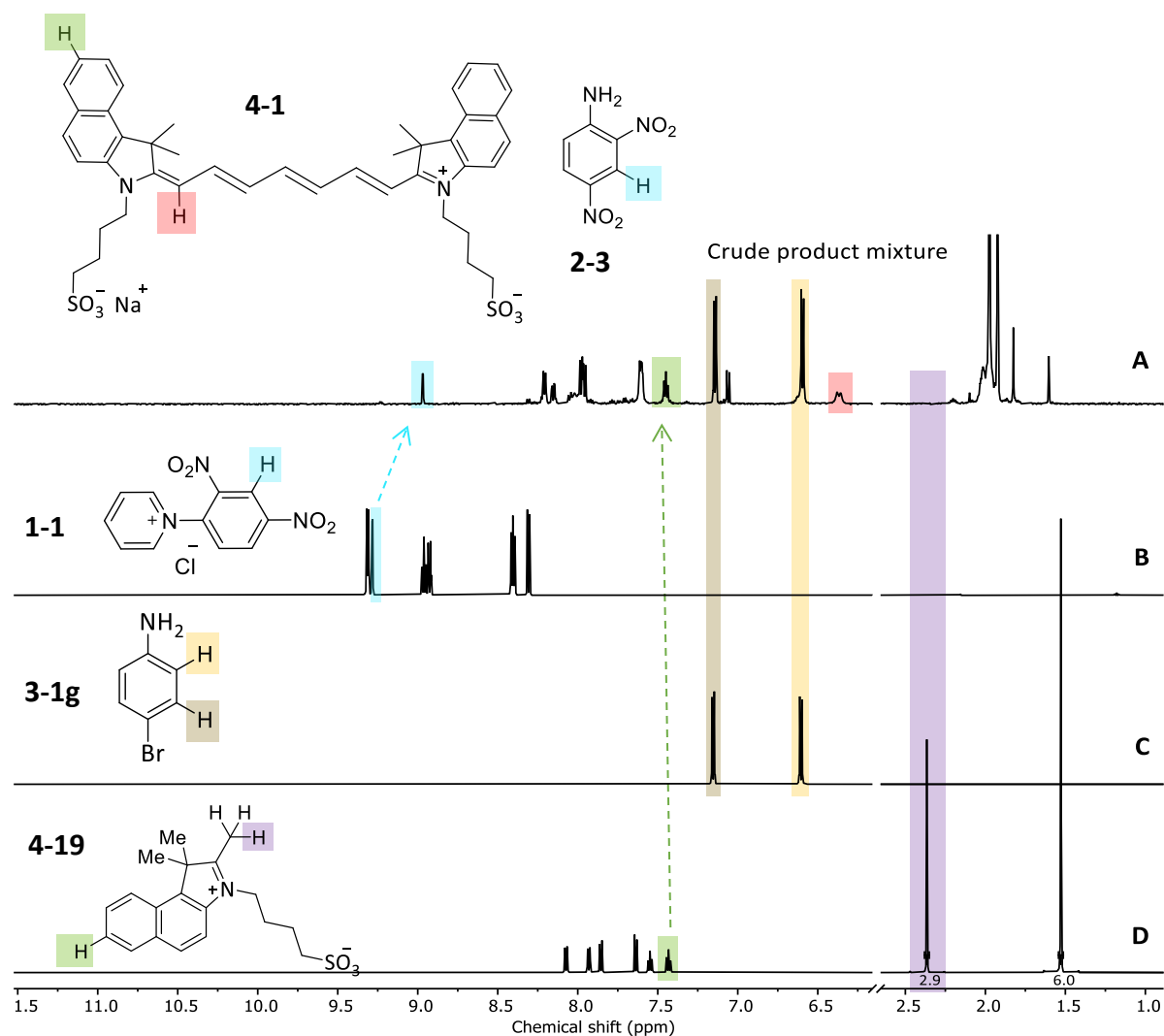


Figure 5-7 ^1H NMR spectroscopy spectra for (A) the crude product mixture with methine protons highlighted (B) the mono-Zincke salt **1-1**, with a methine proton highlighted (C) bromoaniline **3-1g** catalyst and, (D) **4-19** with a methyl proton highlighted

The data presented in **Figure 5-7**, shows 100% conversion of both the mono-Zincke salt **1-1** and the indolium sulfate salt **4-19** as neither are evident in the spectrum of the crude product mixture (**A**). The lack of starting material in the crude spectrum is highlighted by the proton (blue) from the mono-Zincke salt **1-1** (spectrum **B**) becoming part of the leaving group, dinitroaniline **2-3** in spectrum (**A**), which results in an upfield chemical shift of 0.5 ppm. It can also be seen that the resonances for the bromoaniline **3-1g** catalyst spectrum (**C**) appear in the same position in the crude mixture with the grey and yellow highlights. Charting the changes in the ^1H signals of the starting material, indolium salt **4-19**, and comparing its signals in spectrum (**D**) with the crude product mixture (**A**) shows that it had all been converted to the target molecule because the methyl ^1H signal, highlighted in

purple does not appear in the spectrum (**A**). From the same starting material, the ^1H highlighted in green, shows a methine ^1H with a triplet signal appearing in the crude product mix with a close to identical chemical shift value. Also new in the crude spectrum (**A**) is the proton highlighted in pink, which is a doublet, this corresponds with the methine on the chain with just one neighbouring proton.

In VBM there are no means by which to control temperature through external, conductive heating when using the Retsch MM400, as discussed in previously (**section 1-7**). Any heat generated would be through impacts and collisions inside the reaction vessel. The options for varying these are to change the frequency of oscillation with the maximum possible being 30 Hz. The other changeable variable is the size and number of milling balls. In this experiment we were using the maximum number and size of ball possible (2 x 15 mm \varnothing) for a ZrO_2 (25 mL) jar. The oscillation time was 120 min because we had seen that a longer experiment in VBM gives more conversion of starting material to desired product.

Attempts for the purification of ICG **4-1**, VBM product was through using a published method by Dishman.²²⁶ It involved dissolving the crude²²⁶ product in warm de-mineralised water, followed by the addition of acetone and heating the whole to reflux for an hour. The solution was allowed to cool and was stirred for up to 12 h then filtered and washed with more acetone. ^1H NMR spectroscopy was used to establish the condition of the purified sample. This process was repeated three times and the ^1H NMR spectra of the final sample is shown in **Figure 5-8** where, disappointingly, sodium acetate (highlighted in yellow δ 1.88 ppm) was present 1.5% by weight, in the sample after four cycles of recrystallisation.

While the removal of sodium acetate from the crude product was unsuccessful, we had established that the solid state synthesis of ICG **4-1** in VBM is possible and the transfer to larger scale with these starting materials was a viable proposition. In addition, minimising the use of solvent or using sustainable alternatives as per the 12 Green Principles, meant trying to restrict the types of solvent we use to water, acetone and methanol also became an objective.

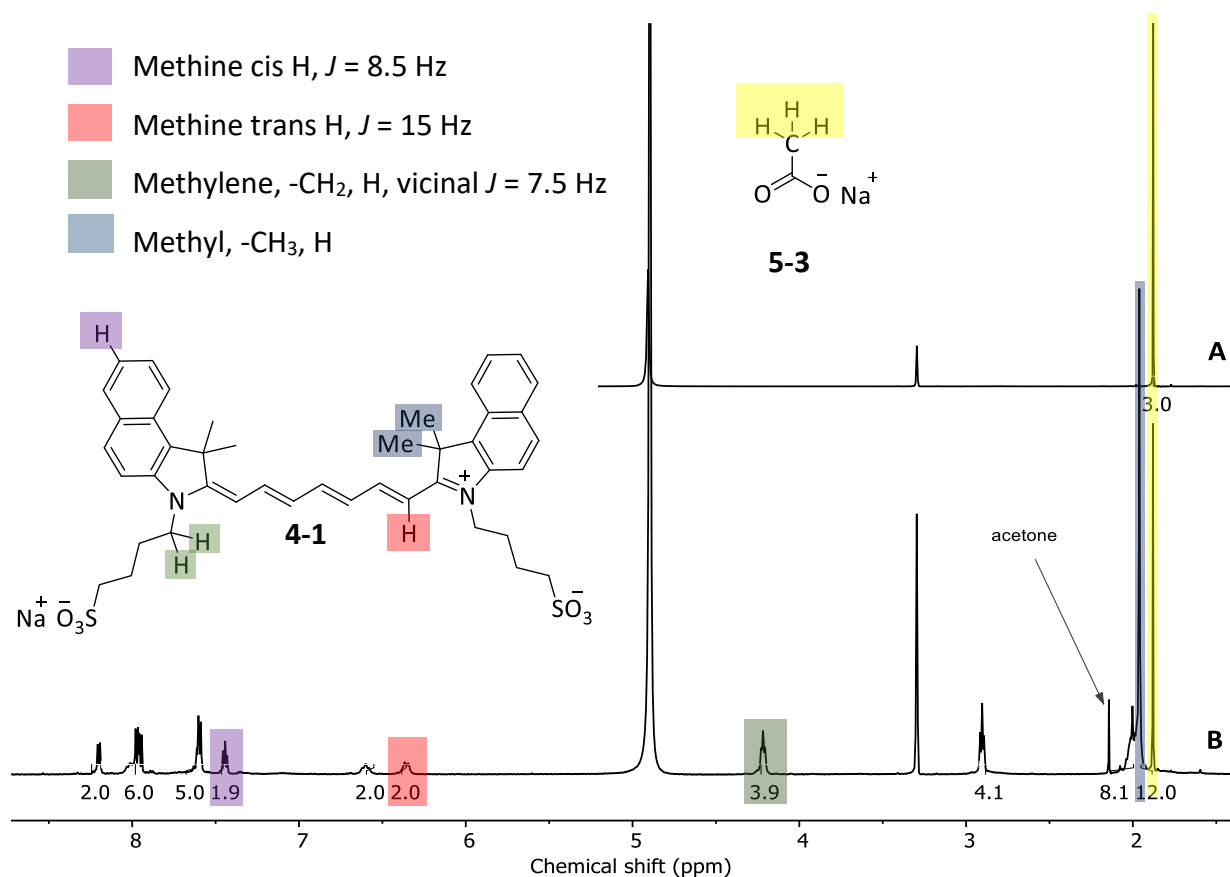


Figure 5-8 ^1H NMR spectrum of (A) sodium acetate, **5-3** and (B) four times recrystallised ICG **4-1** from water and acetone

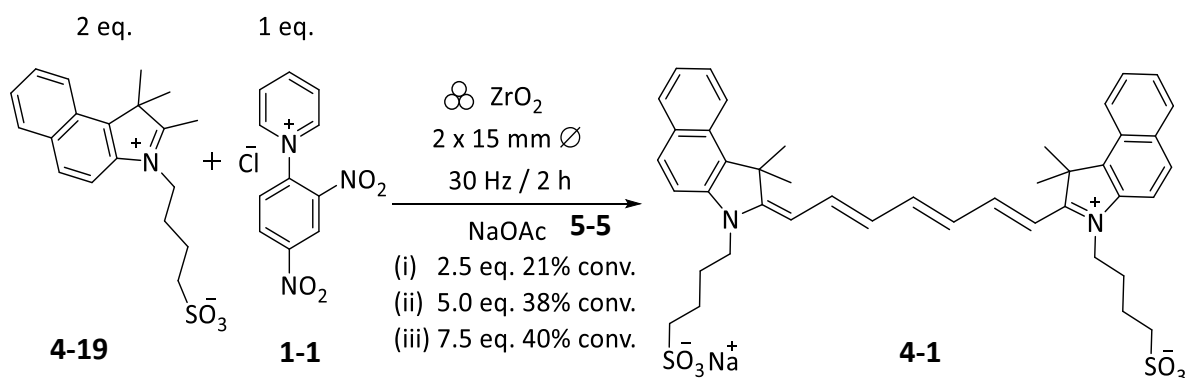
ICG **4-1** has within its structure several distinguishable types of proton, namely *cis*- (purple in **Figure 5-8**) and *trans*-methine (pink), methylene (green) and methyl (blue) giving rise to different coupling constants depending on vicinal or geminal protons and their stereospecific environments. These are indicated with colour-coding in **Figure 5-8** and the J values, where they apply, are within expected range to the nearest 0.5 Hz.

The successful synthesis of ICG **4-1** in VBM gave impetus to attempt this reaction using continuous extrusion methodology. We have large stocks of the starting materials for ICG **4-1** and a better understanding of solid state synthesis. It would therefore be advantageous to understand how the components of this cascade reaction fit together so that we can use this knowledge to perfect the procedure and quantities required. The next experiments were to see how the bromoaniline catalyst and the conjugate base, sodium acetate, participate in the reaction to form ICG **4-1** from the indolium salt **4-19** and the Zincke salt **1-1**.

5.6 Understanding the role of sodium acetate **5-5** in the synthesis of ICG **4-1**

In Chapter 3, we saw that the transformation from Cy5 to Cy7 in VBM produced poor conversions after 60 minutes of milling time compared with using the mono-Zincke salt **1-1** with an aniline catalyst (**Section 4-5**). In both sets of experiments, sodium acetate **5-5** was used but its role as a deprotonating agent was not obvious because anilines are also able to perform nucleophilic addition as the first step in the Zincke reaction mechanism (**Scheme 1-21**). If this could be separately identified, then we would have a better understanding of the reaction mechanism for the synthesis of ICG **4-1**.

Investigations into whether ICG **4-1** could be synthesised in VBM also included attempts *without* aniline. We used the same conditions, zirconium oxide jars and balls and oscillation times of 2 h, as we had for the successful VBM experiment. A series of three experiments which included increasing amounts of sodium acetate (2.5, 5.0 and 7.5 eq.) added to the mono-Zincke salt **1-1** and the indolium salt **4-19** as shown in **Scheme 5-5**.



Scheme 5-5 VBM of mono-Zincke salt **1-1** with naphthyl indole sulfonate **4-19**

Using ^1H NMR spectroscopy to analyse conversion to ICG **4-1** in **Figure 5-9**, we found percentage conversions for 2.5 / 5.0 / and 7.5 eq. to be 21, 38 and 40 respectively.

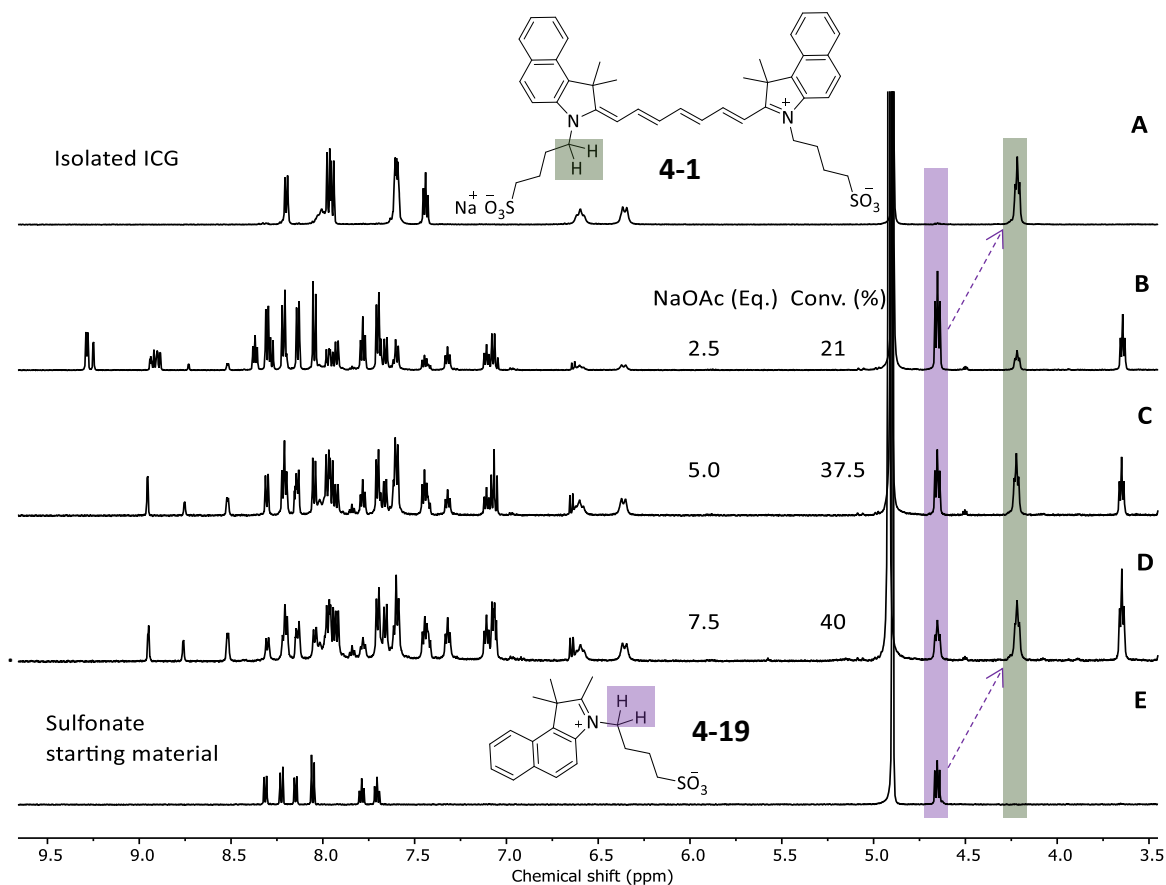


Figure 5-9 Sodium acetate optimisation for ICG Synthesis by VBM – stacked ^1H spectra of (A) isolated ICG **4-1** (B) VBM using 2.5 eq. NaOAc **5-5** (C) VBM using 5.0 eq. NaOAc **5-5** (D) VBM using 7.5 eq. NaOAc **5-5** (E) starting material **4-19**

Surprisingly, ICG **4-1** is formed despite the absence of aniline, this tells us that the sodium acetate **5-5** may deprotonate the indolium salt **4-19** to form the indolene salt **5-6**. The indolene **5-6** is able to perform conjugate addition at positions 2 and 6 on the *N*-pyridyl ring of the mono-Zincke salt **1-1** thus offering a new pathway to ring-opening that is distinct from the use of an aryl aniline as the nucleophile in the Zincke Reaction mechanism (see **Scheme 1-21**).

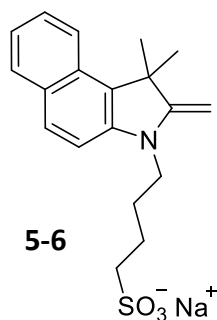
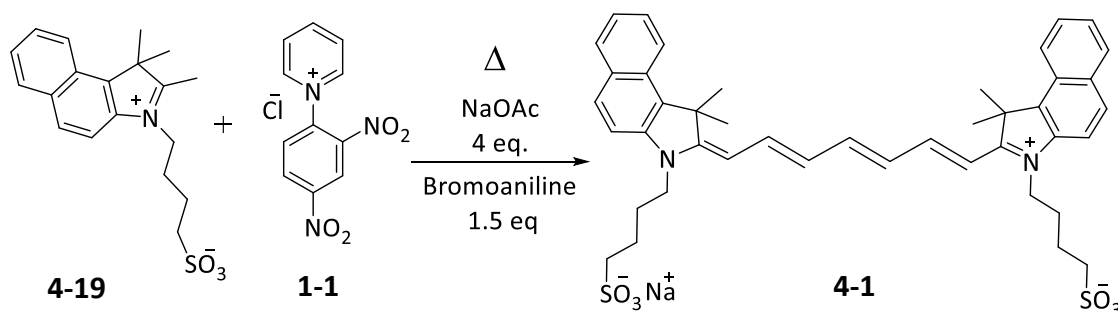


Figure 5-10 Suggested formation of sodium indolene **5-6** by deprotonation with sodium acetate **5-5**

It can then perform another conjugate addition of the intermediate to give ICG, **4-1**. The percentage conversions with sodium acetate **5-5** to ICG **4-1** were non-linear shown by an increase of only 2% conversion by ^1H NMR spectroscopy analysis, when the addition of sodium acetate went from 5 eq. (38% conversion) to 7.5 eq (40% conversion).

This result contrasts with conducting the reaction with the addition of bromoaniline **3-1g**. The formation of ICG **4-1** must therefore go by a different, more efficient, pathway to the target molecule. Using VBM, the conversion to ICG **4-1** for the same reaction was 100% through analysis by ^1H NMR spectroscopy of the sampled crude product (**Scheme 5-4**).

We have also established that a heat and stir experiment is a very efficient way to gather optimisation data and so the reaction to synthesise by heating and stirring the solid reagents to make ICG **4-1** using both sodium acetate **5-5** and bromoaniline **3-1g** was investigated. We found from the heat and stir experiments for synthesising viologens in **Chapter 2**, that increasing temperatures increases the conversion to products with the manually stirred small samples. A preliminary heat and stir experiment on a hotplate using small quantities of the four starting materials would therefore allow us to set reasonable temperature parameters for extrusion experiments.



Scheme 5-6 Heat and stir reagents for synthesis of ICG **4-1** on a hotplate

The reagents were combined in a 100 mL flat bottomed conical flask with a pivoted stirring bar and stirred on a stirrer/hotplate at room temperature. The heater was then switched

on to a maximum of 85 °C while continuously stirring. At 72 °C the stirrer stopped moving as the reaction mixture became sticky. Stirring was resumed manually with a metal spatula. After 4 minutes at 85°C, the flask was removed from the heat and allowed to cool. The ^1H NMR taken of the crude from this experiment showed 90% conversion, **Figure 5-11**.

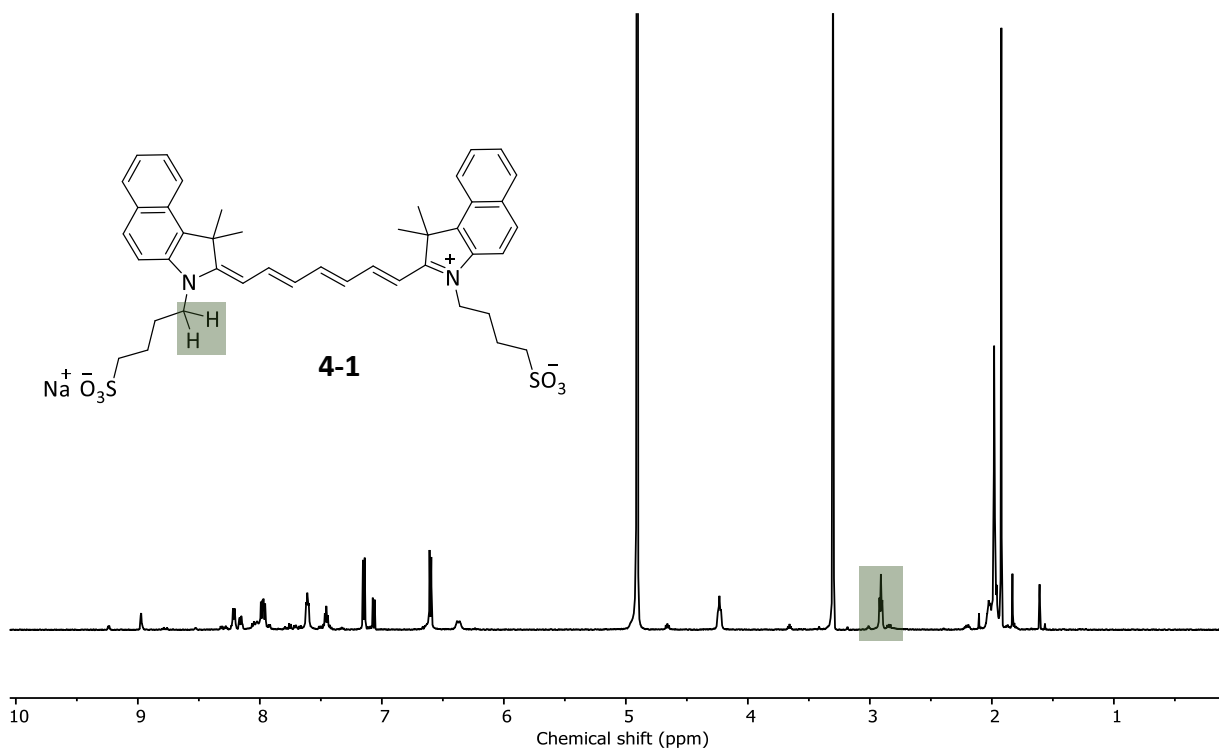


Figure 5-11 Crude ^1H NMR spectrum from heat and stir synthesis of ICG **4-1**

Purification of the crude product was conducted using a silica gel column using flash chromatography with a chloroform and methanol gradient yielded the title compound **4-1**, (0.501g, 72%). The ^1H NMR for the purified title compound is shown in **Figure 5-12**, with purity analysis by HPLC (UV) of 93%.

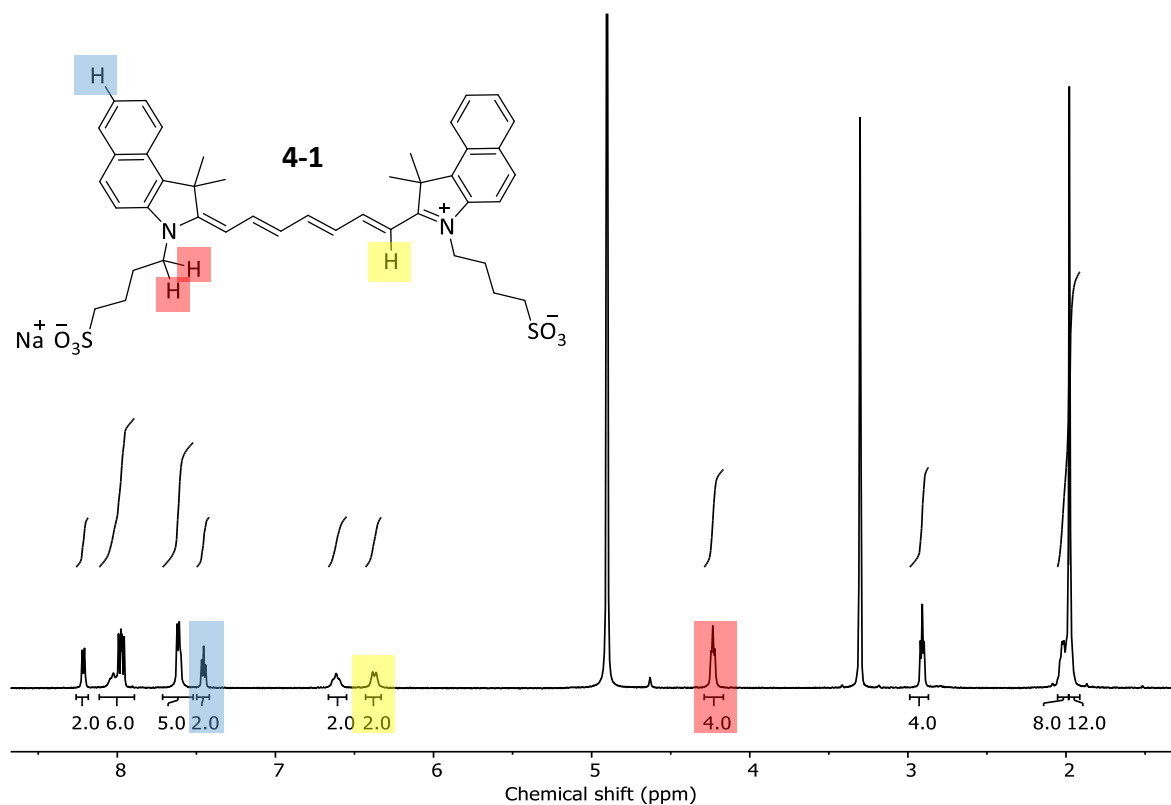


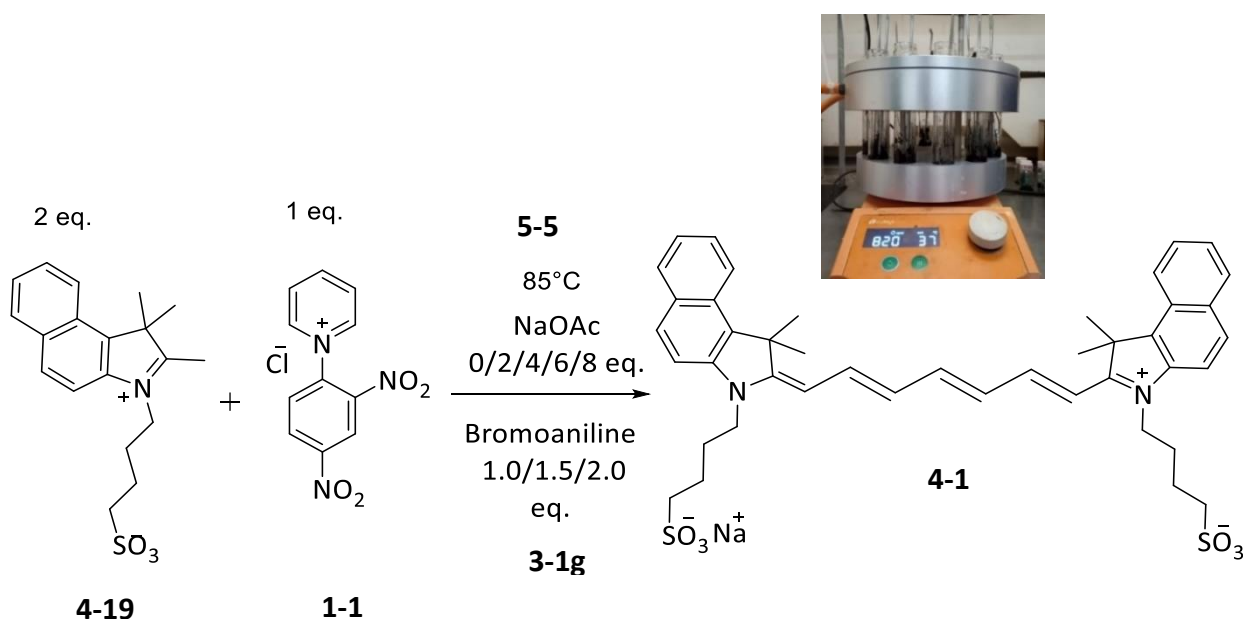
Figure 5-12 Heat and stir ICG **4-1**, purified by flash chromatography, yield 72%

With clearer information on the *temperature* required to give near full conversion (>90%) of starting materials to our target compound, an assessment of variable quantities of reagents suitable for scale-up experiments required a review of the contributions made by sodium acetate and aniline, in combination, to the overall effectiveness of the conversion to ICG **4-1**.

5.7 ICG **4-1** optimisation carousel - heating and stirring

Investigations in Chapter 2 with the 'heating and stirring' of viologens **2-12a-p** from the nucleophilic substitution of the di-Zincke salt **1-2** and the scope using a variety of substituted anilines gave us sufficient confidence to reproduce this methodology and we could therefore optimise the reaction to make ICG **4-1** very easily in a carousel, using different ratios of conjugate base, sodium acetate **5-5** and bromoaniline catalyst **3-1g**.

All reagents were measured out and each reactor was equipped with a stirring magnet and a 12 inch long steel stirring spoon. Once all the reactors were in position, the hotplate, which was set to 85 °C, was switched on and while it warmed to the set temperature, each reactor was individually manually stirred. All the reactors required manual stirring because the magnetic stirrers could not rotate in the tacky slurry that formed upon heating. Once the set temperature was reached, each reactor was manually stirred for a further 5 minutes before samples were taken from each reactor for immediate analysis by ¹H NMR spectroscopy.



Scheme 5-7 Heat and stir reagents for synthesis of ICG **4-1** in a carousel

The results are tabulated in **Table 5-2**, showing percentage conversion as identified from the crude spectra for each experiment, with their respective reagent compositions.

The table of data shows that without any sodium acetate **5-5** (Entries 1, 6 and 11), there is no conversion to ICG **4-1** observed in the ¹H NMR analysis of these samples, after 5 minutes of manual stirring at 85 °C. Of note, at the point of sampling, all reactors with all four reagents had achieved at least 51% conversion with 2-8 equivalents of **5-5** and 1-2 equivalents of bromoaniline catalyst **3-1g**. When the amount of catalyst **3-1g** present is constant in the reaction mixture, and the sodium acetate **5-5** increases, the results are variable and not easy to interpret but in two out of three cases, using 8 equivalents of **5-5** gives the best conversions (Entries 5 and 10). The optimum conditions for best conversion were found to be reactor 10 which used 8 eq. of the base and 1.5 eq. of the catalyst. Overall,

the synthesis is tolerant of a range of equivalents of base (above 4 equivalents) and catalyst (between 1 and 2 equivalents). The single experiment performed using a magnetic stirrer in a flat-bottomed conical flask gave 90% conversion.

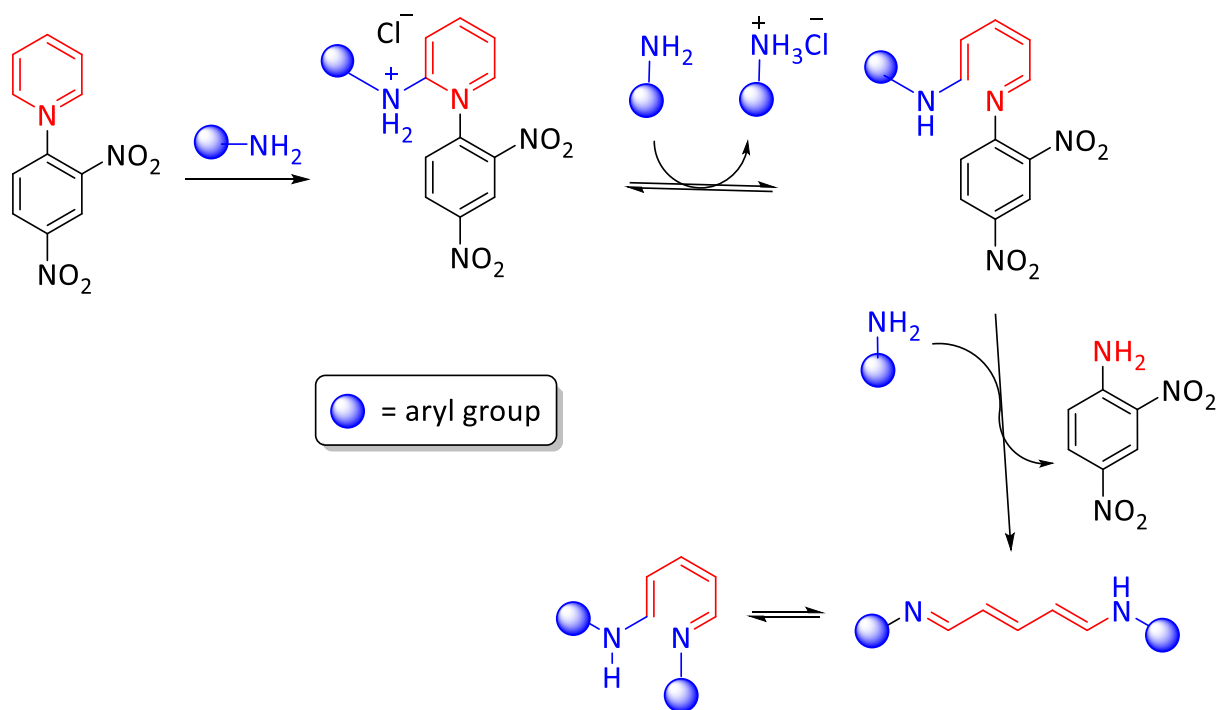
Reactor	No. Eq. 1-1	mass (g) 1-1	No. Eq. 2	mass (g) 4-19	No. Eq. 5-5	mass (g) 5-5	No. Eq. 3-1g	mass (g) 3.1g	% Conv. at 85°C
1	1	0.50	2	1.38	0	0.00	1.0	0.18	0
2	1	0.50	2	1.38	2	0.18	1.0	0.18	23
3	1	0.50	2	1.38	4	0.36	1.0	0.18	56.5
4	1	0.50	2	1.38	6	0.54	1.0	0.18	52.4
5	1	0.50	2	1.38	8	0.72	1.0	0.18	57.4
6	1	0.50	2	1.38	0	0.00	1.5	0.28	0
7	1	0.50	2	1.38	2	0.18	1.5	0.28	23
8	1	0.50	2	1.38	4	0.36	1.5	0.28	55
9	1	0.50	2	1.38	6	0.54	1.5	0.28	51
10	1	0.50	2	1.38	8	0.72	1.5	0.28	64
11	1	0.50	2	1.38	0	0.00	2.0	0.37	0
12	1	0.50	2	1.38	2	0.18	2.0	0.37	20
13	1	0.50	2	1.38	4	0.36	2.0	0.37	59
14	1	0.50	2	1.38	6	0.54	2.0	0.37	63
15	1	0.50	2	1.38	8	0.72	2.0	0.37	57

Table 5-2 Conversion to ICG 4-1 – the effect of changing variables of sodium acetate 5-5 and the catalyst, bromoaniline 3-1g

This high percentage conversion had not been matched in the manually-stirred carousel of boiling tubes. There was also 100% conversion to ICG 4-1 in VBM after 120 min; the best seen in the carousel with manual Heat and Stir was 64%. Both the magnetic stirrer bar and VBM results are highly suggestive that manual stirring is no match for oscillating the reagents with balls, 30 times per second or a freely spinning magnetic stirrer.

The experiments that show no conversion do not feature sodium acetate 5-5, this is evidence that it is necessary for the deprotonation of the indolium 4-19 to form the indolene salt 5-6 and initiate the cascade reaction. We have also seen from experiments in VBM (*Figure 5-9*) that with increasing the quantity of sodium acetate 5-5, that conversion to ICG 4-1 without a bromoaniline catalyst is limited, the maximum achieved was 40% by

^1H NMR spectroscopy analysis, using 7.5 equivalents. The Zincke Reaction Mechanism involving nucleophilic attack by primary anilines is well understood (see **Scheme 1-20**). The ring-opening steps involving only aniline are reproduced in **Scheme 5-8**.



Scheme 5-8 The ring-opening steps in the Zincke reaction mechanism with aniline

The 'one-pot' synthesis of ICG **4-1**, however, combines a primary aniline - bromoaniline **3-1g**, a conjugate base of acetic acid, sodium acetate **5-5**, the indolium sulfonate **4-19** and the Zincke salt **1-1**. The inclusion of a sodium acetate **5-5** in a one-pot reaction mixture that has a greater pK_{aH} than both the nucleophilic bromoaniline **3-1g** and the leaving group dinitroaniline **2-3** must therefore initiate the ring-opening, and not the bromoaniline **3-1g**. The mechanism of the ring-opening when both the sodium acetate **5-5** and the bromoaniline **3-1g** are in the reaction mixture to synthesise ICG **4-1** may be speculated from the observations we have made from our experiments for the synthesis ICG **4-1** using (i) aniline **3-1g** only (ii) sodium acetate **5-5** only, and (iii) both **3-1g** and **5-5** are present. In scenarios (ii) and (i) the possible intermediates formed by ring-opening are **5-7** and **5-8**.

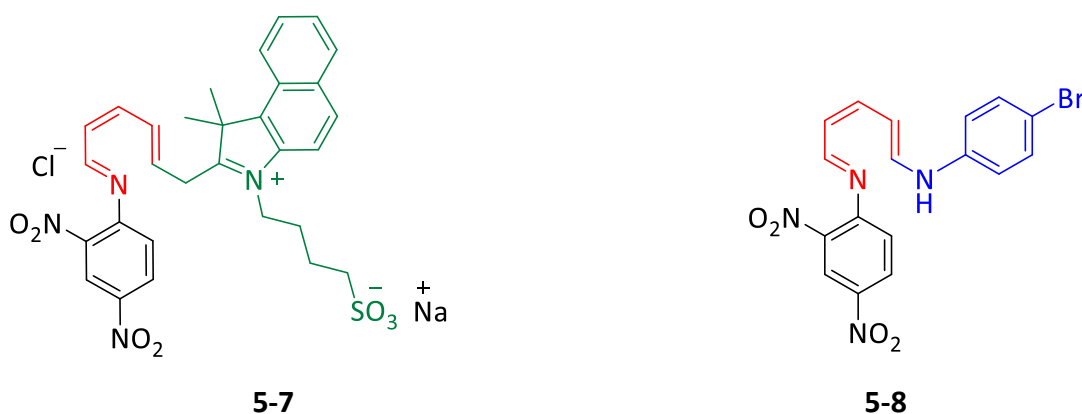


Figure 5-13 Intermediates **5-7** and **5-8** formed from ring-opening of the Zincke salt **1-1**

However our VBM experiments show that **5-5** on its own is not sufficient for 100% conversion of the Zincke salt **1-1**. The aniline **3-1g**, while not a part of the target molecule facilitated the process with the displacement of the leaving group, dinitroaniline **2-3**. The order of the mechanistic sequence – forming the cascade reaction – can be rationalised with reference to the pK_{aH} of the conjugate acid, or pK_{aH} , **Figure 5-13**.

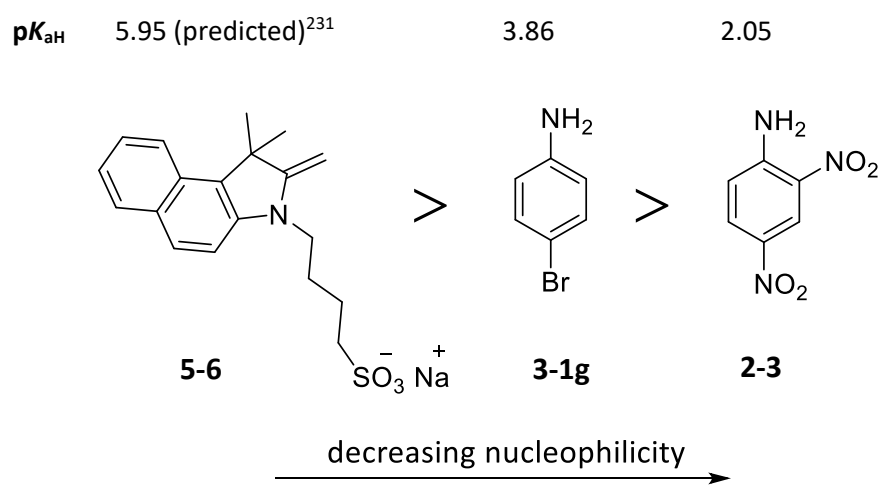
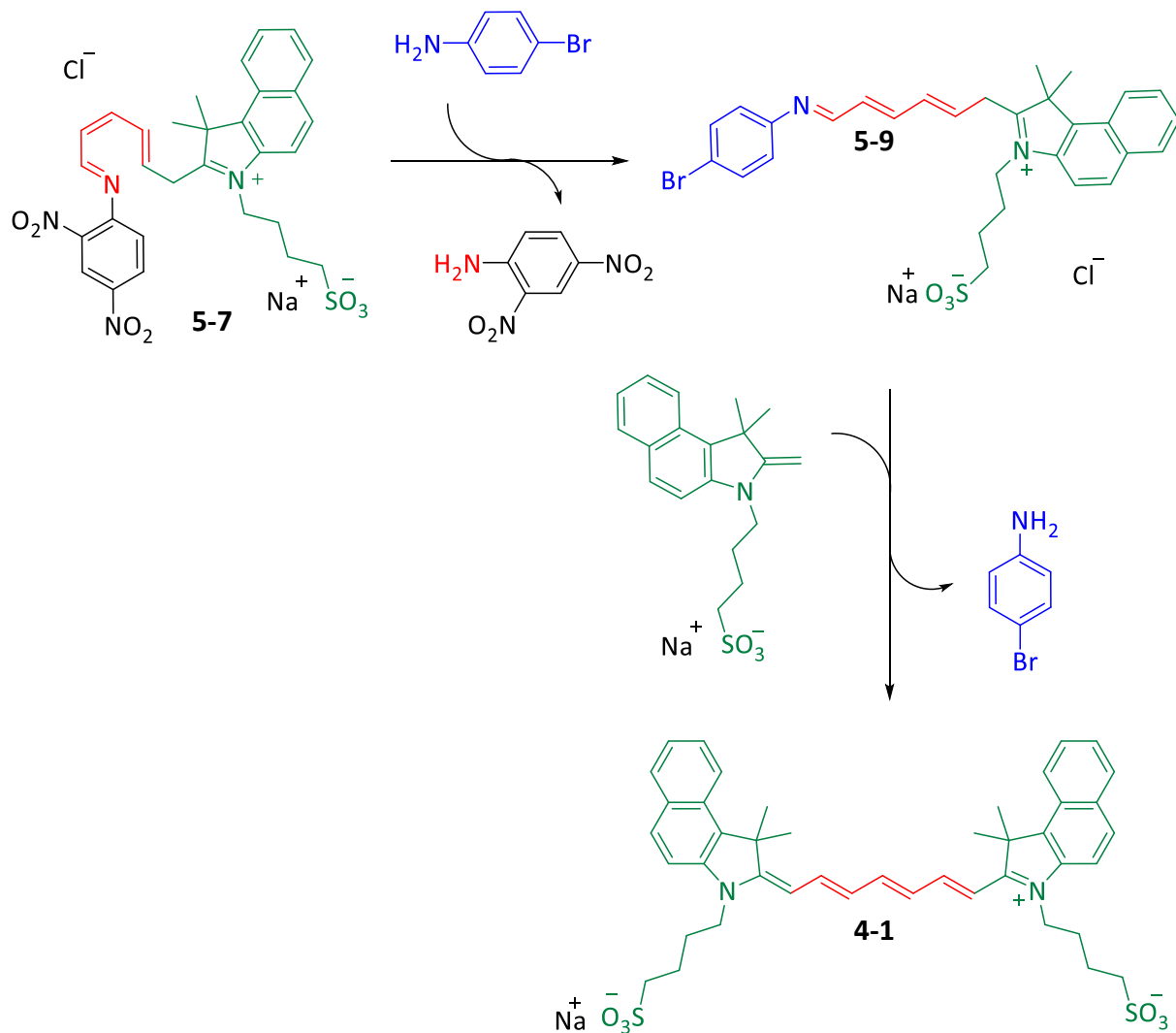


Figure 5-14 Cascade reactions follow from the nucleophilicity and pK_{aH} values¹³³ of competing species

The outcomes of the 'one-pot' ICG **4-1** synthesis that can be seen from the 1H NMR analyses of all the crude mixtures are because of the near complete conversion of starting materials **1-1** and **4-19** into the target molecule **4-1** – the remaining signals are attributable to the leaving group, dinitroaniline **2-3** and the catalyst, bromoaniline **3-1g**.

A proposal for the reaction mechanism following on from the initial ring-opening step giving the proposed intermediate **5-7** can therefore describe the process as shown in **Scheme 5-9**.

Scheme 5-9 A mechanism for the one-pot synthesis of ICG **4-1** from proposed



intermediate **5-7**

We have assembled large quantities of starting materials **1-1** and **4-19**, conducted optimisations, and assessed the possibilities for the solid state synthesis of ICG **4-1**. The next step was looking for the means to scale up to a continuous process of extrusion for this reaction. We have also shown that solvent-free synthesis can be easily explored by heat and stir as a standard procedure for small molecule, fine chemical synthesis.

5.8 Single screw extrusion

The use of a single-screw extruder (SSE) for synthesis has recently been successfully explored by Sharma *et al.*⁹⁸ in their solvent-free, continuous extrusion of a variety of organic transformations such as aldol condensation, acylation and coupling reactions using equipment they had designed, **Figure 5-14**.

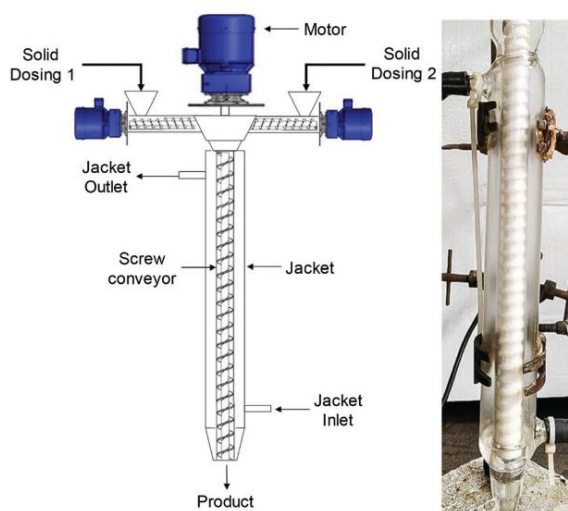


Figure 5-15 The general set-up for continuous solid reactor, picture taken from⁹⁸

The main feature comprises a motorised screw, in combination with feed ports for reagents which can be assembled in different ways according to the requirements of the extruded product. There is also the facility of a cooling jacket to help maintain a temperature suitable for the reaction.

Options are available in current extruder technology in diverse industries including food manufacturing, agricultural hardware, but also in packaging design and civil engineering where extruders fulfil different briefs depending upon the requirements for the product. Many can be multi-purpose and are also worth considering for continuous synthesis in synthetic chemistry. For our experiment to continuously synthesise ICG **4-1** we use of a single screw extruder (SSE) for this chemical transformation. The FilaFab 350 Pro EX is a SSE designed to produce filament for 3D Printing and has been adapted from specialist manufacturing equipment to a table-top filament extruder for the hobbyist and has

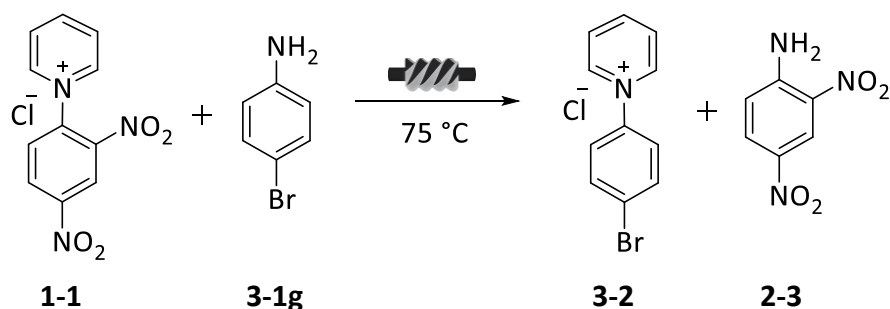
therefore seen a growth into new markets. Their popularity as a 'green' product is based on the fact that the SSE can recycle thermoplastics such as milk bottles made from HDPE and the biodegradable PLA to form spoolable filament which can then be used for printing.



Figure 5-16 The FilaFab 350 Pro EX, designed to extrude filament ready for 3D printing²³²

It is very compact, fits easily in the fume hood and with only temperature and rotation speeds to set, very easy to operate. A hopper feeds the pre-mixed raw material into a 20 cm long, 2.5 cm dia. screw with a barrel capacity of 40 mL, once the material is conveyed to the end of the screw the back pressure of the material in a full barrel is extruded through the nozzle. The barrel can be heated up to 250 °C and has variable screw rotation speeds of 5-30 rpm.

In this work we show that all these attributes are sufficient to produce *ca.* 300 g/hr of our crude product ICG **4-1**, which is approximately 100 times the output compared with the same reaction in a 25 mL vessel using the ball mill. Before committing large, multigram amounts of starting materials of all four reagents in the extruder, a preliminary experiment involving two of the four reagents would give us evidence that the SSE methodology is suitable for solvent-free reactions.



Scheme 5-10 Extrusion of mono-Zincke salt **1-1** and bromoaniline **3-1g**

Our first extrusion experiment was performed using 70 grams of premixed powders of the Zincke salt **1-1** and bromoaniline **3-1g** in molar ratio 1:2. An earlier experiment using a Kenwood Mini-Chopper to blend the mixture for 5 minutes using a bladed attachment to see if the Cy5 **3-8g** could be synthesised without VBM and no balls colliding, gave no reaction from ^1H NMR spectroscopy analysis, despite the colour change from yellow to dull red.

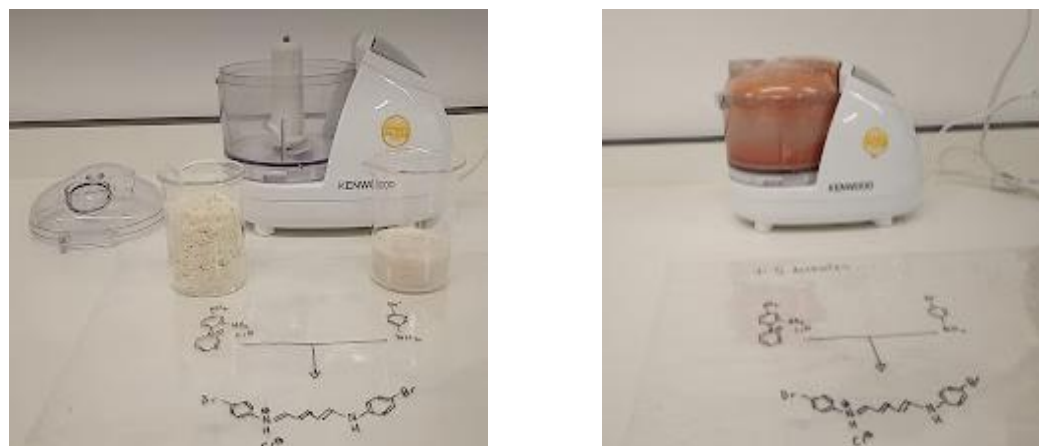


Figure 5-17 Unsuccessful synthesis of **3-8g** by stirring using 1 eq. **1-1** and 2 eq. **3-1g**

We observed a colour change from pale yellow to dull red **Figure 5-16**, but a sample taken directly from the mixture and analysed by ^1H NMR spectroscopy. Spectra **F** in **Figure 5-17** – shows no signals for the product **3-8g** through comparison with the spectra of the starting materials, bromoaniline **3-1g** in spectra **E**, and the mono-Zincke salt **1-1** shown in spectra **F**. With this mixed powder to hand, a new ^1H NMR spectrum of the mixture was taken just prior to extrusion to check for any change that may have occurred after one week on the bench. Spectra (**C**) shows that all the signals have remained unchanged, and no significant chemical shifts were seen. Although the colour had become a deeper rusty red we concluded that as no product **3-8g** could be observed at the sensitivity of the ^1H NMR spectroscopy, and proceeded with the first extrusion experiment. The extrusion took 20 minutes to process 70 g of the **1-1** and **3-1g** mixture, producing a red/brown molten crude. The complete stack of ^1H NMR spectra show the resulting ^1H NMR spectrum of the sample of crude taken directly after extrusion (spectra **A**). Comparison of spectra **A** and **B** (the Bromopyridinium salt **3-2**) shows that our crude mixture contains all the signals for **3-2**, indicating a successful reaction.

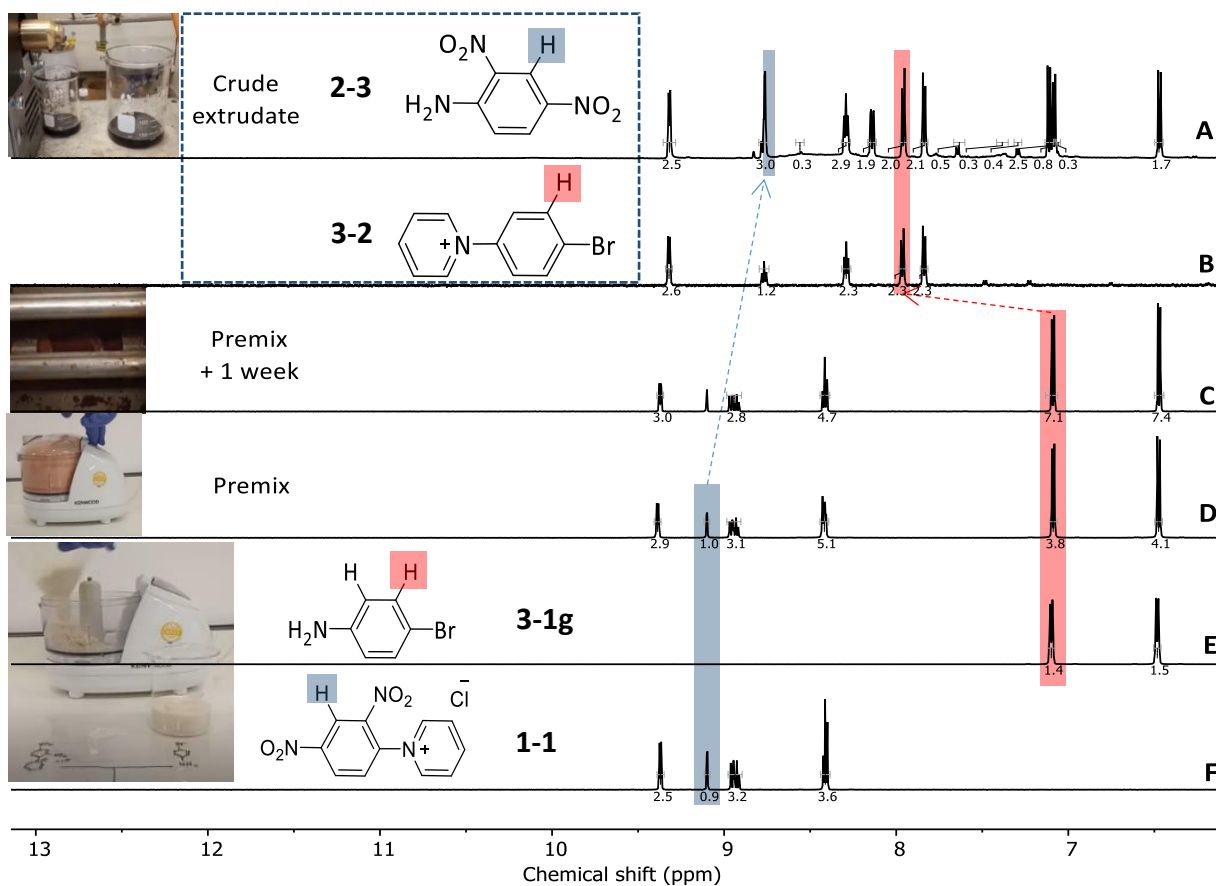
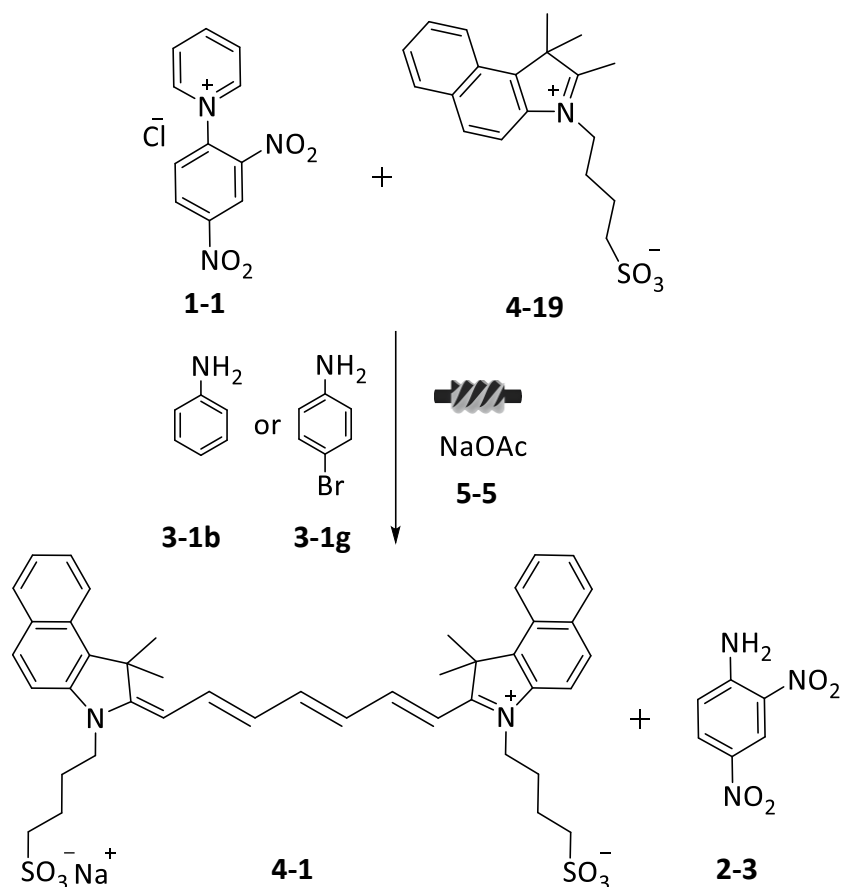


Figure 5-18 Extrusion of bromoaniline **3-1g** with mono-Zincke salt **1-1** where the stack shows ^1H NMR spectra for (A) Crude extruded product (B) bromopyridinium salt **3-2** (C) pre-mix of 'E' used for extrusion experiment one week later (D) bromoaniline **3-1g** premixed with mono-Zincke salt **1-1** in the Kenwood Mini-Chopper (E) bromoaniline **3-1g** (F) mono-Zincke salt **1-1**

The exciting result from this preliminary experiment confirmed that continuous reactive extrusion of mixed starting reagents is possible, and we began work on designing experiments for the extrusion of ICG **4-1**.

5.9 Reactive extrusion of Indocyanine Green **4-1**

Following the success of extruding the two reagents **1-1** and **3-1g** which were blended prior to being added to the hopper of Filafab 350 EX PRO, the same process was used for the extrusion of ICG **4-1**, **Scheme 5-11**. by initially putting all four reagents into a blender.



Scheme 5-11 SSE of Indocyanine Green 4-1

All four reagents were weighed out - mono-Zincke salt **1-1** (20 g, 0.07 M) and indolium salt **4-19** (48 g 0.14 M), sodium acetate **5-5** (28 g, 0.28 M) and, bromoaniline **3-1g** (24 g, 0.14 M) in separate beakers then blended in the Kenwood Mini-chopper **Figure 5-18**.

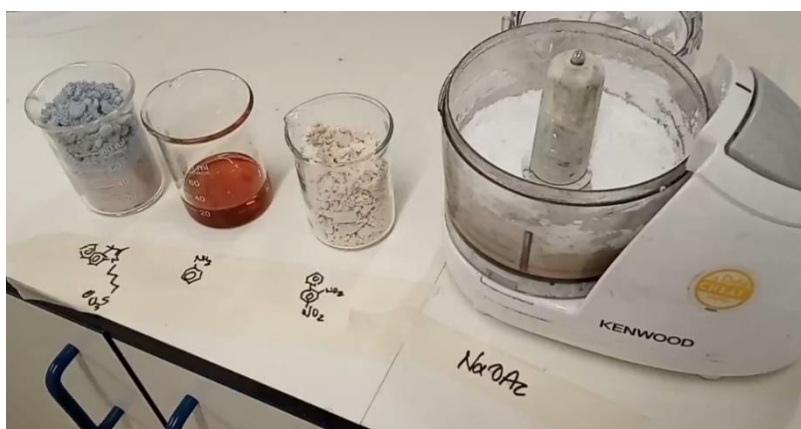


Figure 5-19 Pre-mixing the four reagents for SSE

The pre-mixed reagents were then loaded into the hopper of the extruder which had been pre-heated to 75°C and the screw-motor was switched on. The hopper was filled with all the mixed reagents, and after ~15 minutes, with the motorised screw fully laden with contents from the hopper – the first crude extrudate appeared initially as a deep green/black ‘filament’. Over the course of the 20 minute extrusion, the consistency of the emergent product changed from ‘filament’ to a viscous paste which hardened as it cooled in the collecting beaker.

The unidentified dark substance that was produced in the SSE bore little resemblance to the glossy green product that resulted from ball milling (**Section 5-5**) and so a quick way to visually verify the colour of the SSE product was to sample the extrudate by dissolving it in a little methanol, as seen in **Figure 5-20**. Analysis using ^1H NMR spectroscopy of the first run showed 90% conversion of the starting materials to ICG 4-1.

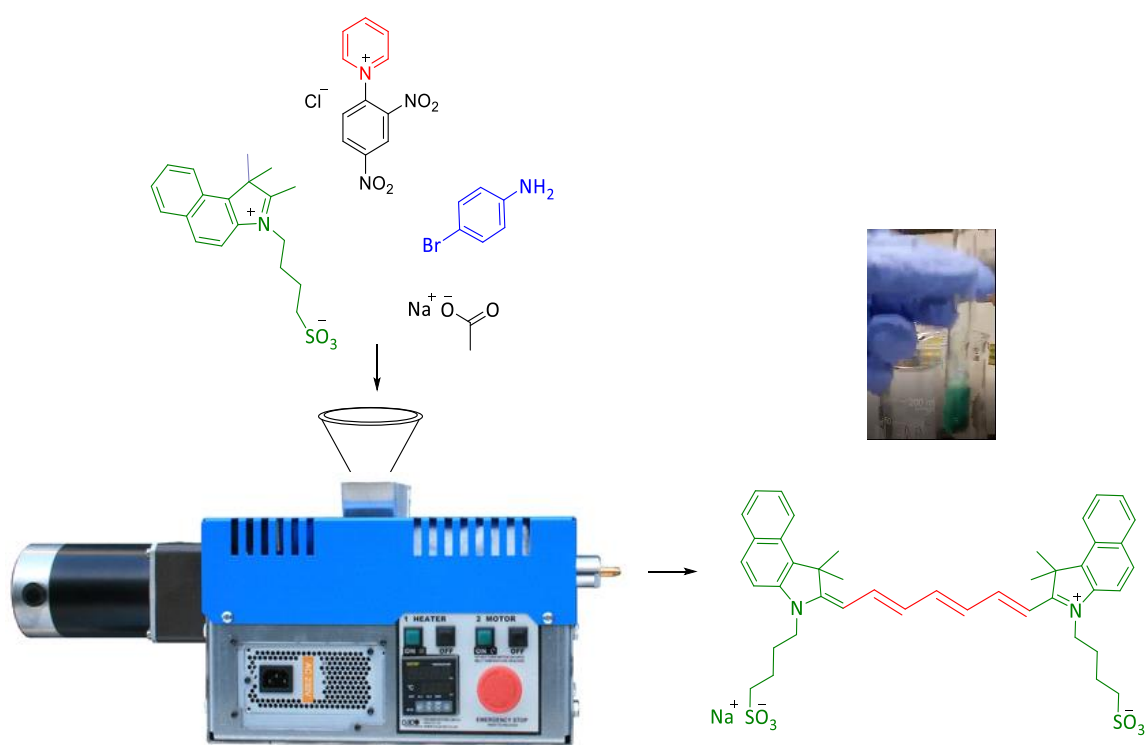


Figure 5-20 The first ICG 4-1 extrudate from the SSE, and dissolving a sample in methanol showing the distinctive green colour of this dye

The extrudate was collected in portions every 5 minutes to check the conversion at different points **Figure 5-21** ^1H NMR spectroscopy was used to analyse the different samples of crude extrudate. The first run showed uniform, *ca.* 90% conversion throughout the extrusion.



Figure 5-21 Quality control: collecting separate fractions for analysis

Adjustments were made with the temperature which ranged from 75-90 °C, although the extruder's temperature sensor gave higher readings than the set temperature, these were noted in the table of results. The run was considered complete when no more extrudate appeared, however, there remained material in the barrel as there was not enough back pressure to push the last of the reaction mixture out.

Over the course of all these extrusions, ^1H NMR spectroscopy of each sample was used to compare the conversion of each run. An example is given in **Figure 5-22** where the signals have all been assigned by colour. For consistency in the conversion calculations, the methylene protons on ICG **4-1** (highlighted in purple) were used in all cases, as they are the only signals to appear between 4-5 ppm and there is no ambiguity as there are no coincidental signals. All the ^1H NMR spectra from these experiments were small variations on this and calculating conversions was a straightforward calculation of the integrated signals for the new product and any starting material that remained.

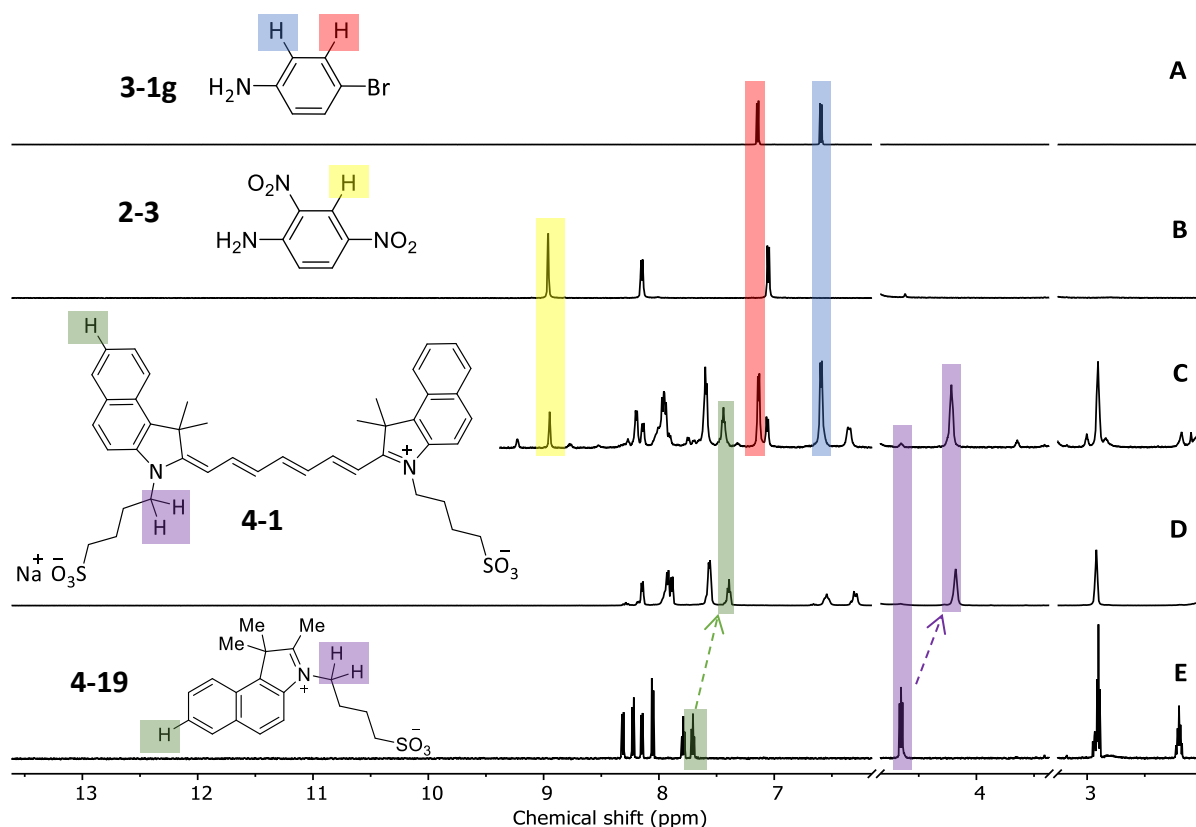


Figure 5-22 A typical stack of ^1H NMR spectra for ICG extrusion experiments to quantify conversion where (A) bromoaniline, **3-1g** (B) the leaving group dinitroaniline **2-3** (C) The crude extrudate (D) isolated ICG **4-1** (E) starting material **4-19**

All yield calculations are therefore based on weighed crude samples that are used before their purification. With the first extrusion completed, further reactions with the reagents in varying amounts were pre-mixed in the blender and a range of temperatures are tabulated in **Table 5-3**. It was of interest to quantify the volume of product synthesised in the extruder and so calculations for the Space Time Yield²³³ (STY) are included where this has been measured. STY is a parameter used in industrial manufacturing contexts and indicates the process intensification and so the higher the value, the greater the profitability of the process. For the Filafab extruder, the reactor volume is taken as the volume of the barrel minus the volume of the screw which is 30 cm^3 .

Entry	Method	Aniline cat.	Cat. (eq.)	NaOAc (eq.)	Conversion by ¹ H NMR	Final Temp. (°C)	Temp. Sensor max. reading (°C)	^a Torque (Nm)	^a RPM	Rate of crude kg/day	^b STY (kg/m ³ day ⁻¹)
1	FF	Bromo	2.0	8.0	90	75	85	45	25	1.07	35700
2	FF	Bromo	1.5	8.0	95	80	91	45	25	2.08	69300
3	FF	Bromo	1.0	4.0	87	90	102	45	25	0.70	23300
4	FF	Aniline	2.0	8.0	94	75	85	45	25	1.68	56000
5	FF	Bromo	1.5	7.6	77	80	93	45	25	3.46	115000
6	FF	Bromo	1.5	7.6	71	85	94	45	25	3.74	125000

FF Filafab

n/c data not collected

^a Values from the Filafab Pro 350 EX Manual

^b Screw volume = 30 mL

Table 5-3 Optimisation of the synthesis of ICG **4-1** by extrusion and Heat and Stir

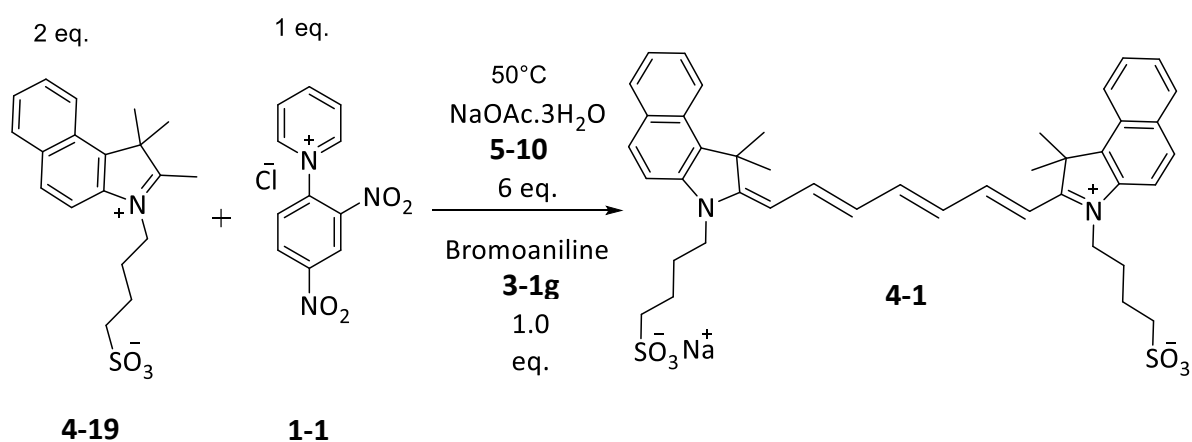
All 6 entries were performed using the extruder, the table shows excellent conversions of **1-1** and **4-19** to ICG **4-1** ranging from 71 - 95%. Entries 1 and 4 in were the first attempts at using the extruder for the scale-up synthesis of ICG. The run-times were exploratory in that a lower starting temperature (60 °C) was used then increased by 5 degree increments every 15 minutes until the product began to extrude. This meant the time to create a sufficiently melted product that could be extruded gave extended timeframes overall for the extrusion to complete. Entry 4 uses liquid aniline as the catalyst because it behaved similarly to bromoaniline in the VBM experiments for conversion to ICG **4-1**. The pre-mixing of liquid aniline with the other three solid reagents produced a dough-like consistency. Consequently, the premix required manually pushing into the hopper to feed it through to the port window and access the rotating screw. This contrasted with the free-flowing powders using solid bromoaniline and slowed the processing of the mixture.

Entries 5 and 6 have greater STYs than the previous entries because the pre-mixed reagents were loaded into a pre-heated extruder at 85°C. All the experiments were timed from the addition of starting material into the hopper, this includes the time needed for the screw to be warmed from RT to the selected temperature. Therefore, the time taken to heat the screw is included and thus gives a lower STY. Entries 5 and 6, used anhydrous sodium acetate, despite having poorer conversions to earlier experiments with 20% less conversion as evidenced by ¹H NMR spectroscopy, they were extruded in shorter time frames as we explored the different starting temperatures of the extruder. The heating element of the

Filafab SSE was very responsive and quick to set, it took seconds rather than minutes to adjust the temperature over a small range 10-20 °C, and the cooling fans controlled the temperature efficiently. The variation in set temperature over the course of all the experiments were in the range 9-13°C showing the reaction's tolerance to temperature fluctuations. A search for the optimum temperature for extrusion of our target compound ICG **4-1**, meant investigating possible candidates within our starting materials that could be utilised. We had already seen that the aniline liquid catalyst, created a dough that was difficult to feed into the extruder. The only other candidate to consider is sodium acetate which is available as a hydrated salt.

5.10 Effect of melting temperature of sodium acetate in the SSE of ICG 4-1

A swift heat and stir experiment of the four reagents would quickly establish the feasibility of a one-pot extrusion synthesis of ICG **4-1** using the hydrated sodium acetate salt.



Scheme 5-12 Heat and stir of ICG **4-1** using sodium acetate trihydrate **5-10**

The reagents were heated and stirred with a magnetic stirrer bar at 50 °C for five minutes, the contents of the flask changed from pale powder mixture into a tacky dark green product. A sample of crude was immediately analysed by ¹H NMR spectroscopy shown in **Figure 5-23**.

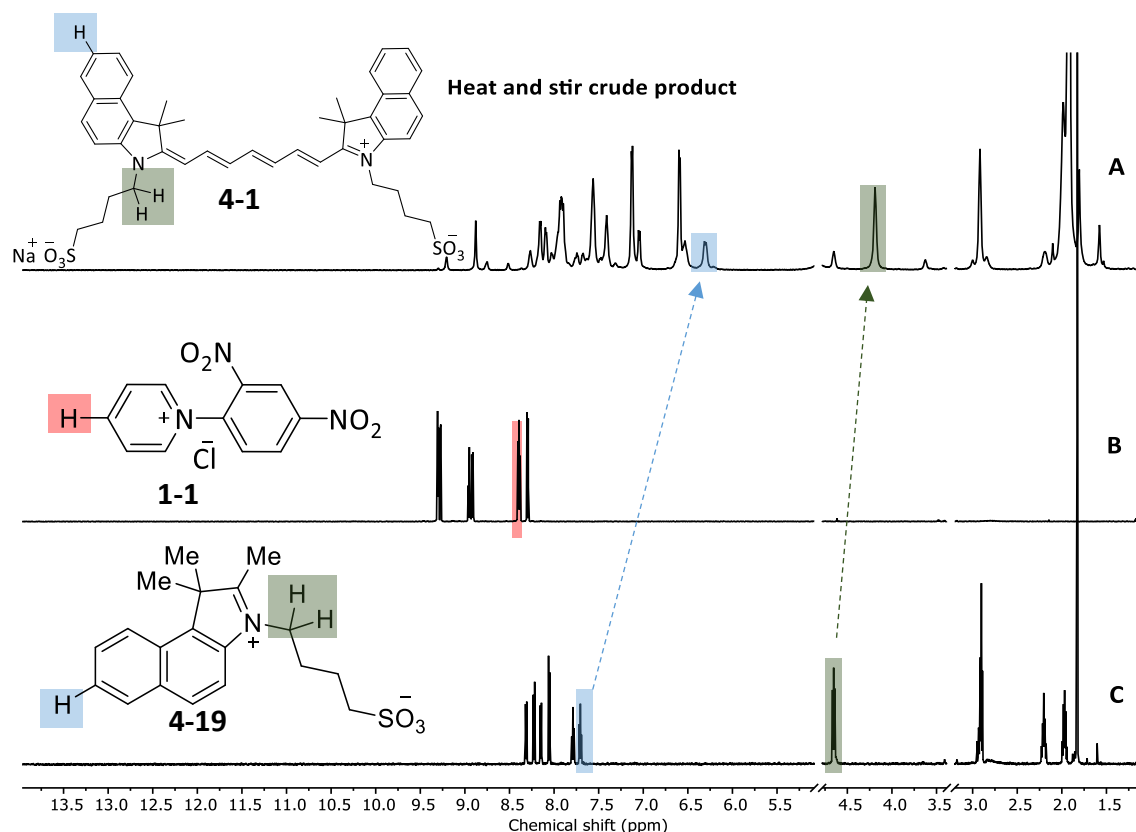


Figure 5-23 Stack of ¹H NMR spectra for starting materials **1-1** (B), **4-19** (C) and the crude product mixture containing target compound ICG **4-1** (A)

Analysis of the spectra in **Figure 5-23** showed no signals from either starting material **1-1** or **4-19** in the crude mixture and the conclusion was >95% conversion (calc. based on the sensitivity of the ¹H NMR spectroscopy) to our target molecule ICG **4-1** using the trihydrate sodium sulfate at 50 °C using heat and stir on a hotplate.

Previously the optimised temperature for extrusion it was noted that the melting point of bromoaniline is 60-64 °C. This was the lowest melting temperature of the four reagents: mono-Zincke salt 191 °C, the indolium salt 264-265 °C and anhydrous sodium acetate **5-5**, 324 °C. It had been possible to extrude the reaction mixture at 85 °C because of the melting temperature of the catalyst; the reaction mixture was sufficiently softened to enable extrusion. Further extrusions using sodium acetate trihydrate **5-10** were conducted (entries 7 and 8) in **Table 5-3**.

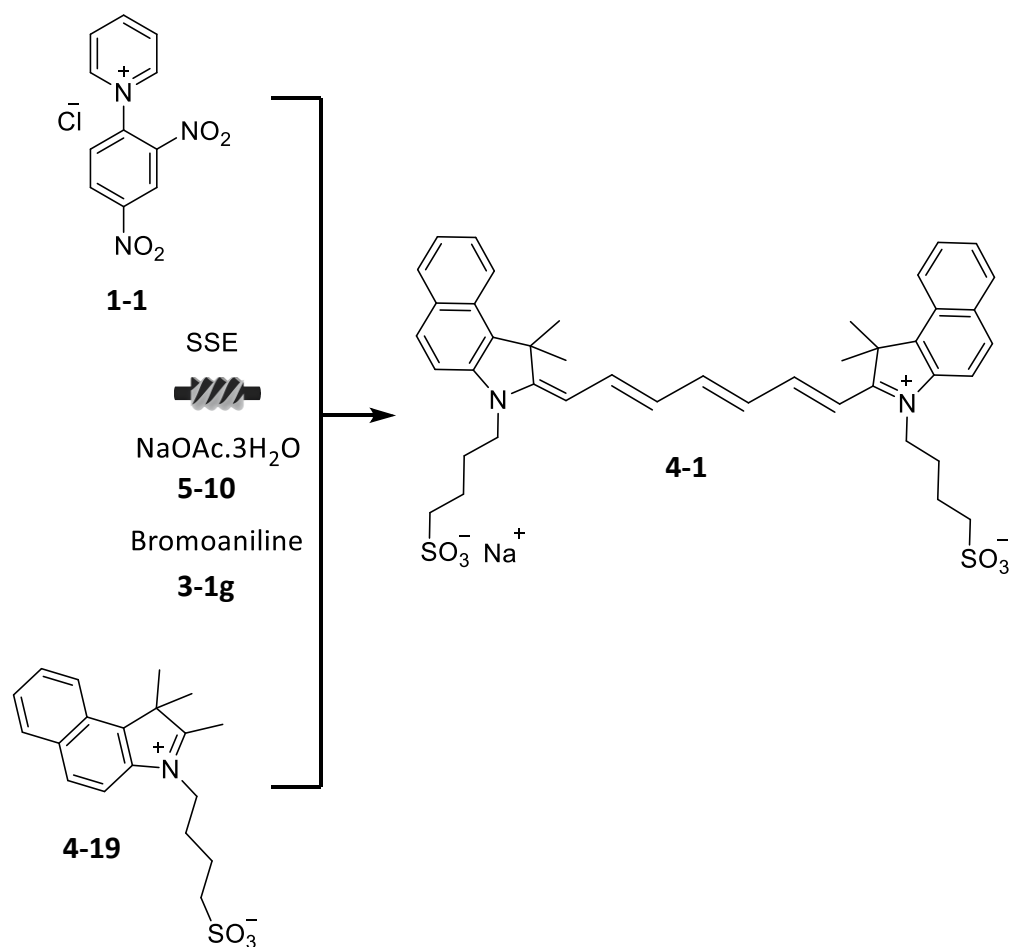


Figure 5-24 Scheme for extrusion of ICG **4-1** using **5-10** sodium acetate trihydrate, conversion by ^1H NMR 74%

When the Heat and Stir experiment using hydrated sodium acetate **5-10** was attempted in the extruder, the crude collected was that of a liquid and was less viscous than previous experiments with anhydrous sodium acetate. Analysis of the crude using ^1H NMR spectroscopy showed comparable conversions (**Table 5-4**) to earlier experiments using anhydrous sodium acetate **5-5**.

Entry	Method	Aniline cat.	Cat. (eq.)	NaOAc.3H ₂ O (eq.)	Conversion by ¹ H NMR (%)	Final Temp. (°C)	Temp. Sensor max. reading (°C)	Torque (Nm)	RPM	Rate of crude kg/day	STY (kg/m ³ day ⁻¹)
7	^c H/S	Bromo	1.5	4	90	85	90	n/a	n/a	n/a	n/a
8	^c H/S	Bromo	1	6	100	50	100	n/a	n/a	n/a	n/a
9	FF	Bromo	1	6	73	50	75	45	25	n/c	n/c
10	FF	Bromo	1	6	74	70	75	45	25	n/c	n/c

FF Filafab

H/S Heat and stir in 100 mL flask

n/a not applicable

n/c data not collected

^a Values from the Filafab Pro 350 EX Manual

^b Screw volume = 30 mL

^c Heat and stir synthesis on a hotplate

Table 5-4 Conversion data, by ¹H NMR spectroscopy, to ICG **4-1**, using sodium acetate trihydrate **5-10**, in heat and stir and extrusion experiments

The experiments using sodium acetate trihydrate **5-10** showed that even at a temperature of 50°C, excellent and complete conversion to ICG **4-1** is possible, the mixed powders are able to be extruded at a lower temperature than when using anhydrous sodium acetate. This is a useful additional finding for any future investigations into extrudable mixtures for one-pot synthesis. It also serves as a practical consideration of melting points of reagents and their solvent-free reactivity which can be easily explored by ‘heat and stir’.

This has also shown that solvent-free single screw extrusion is an effective and efficient means of synthesising small organic molecules and a useful addition to the various types of reaction explored elsewhere.⁹⁸

Isolation of ICG **4-1** from the crude relies on processes and techniques that does requires solvent. Insofar as following guidance from the ACS ‘12 Principles of Green Chemistry’ – our syntheses have kept to the brief, and we look to continue with these aims in the purification of ICG **4-1**.

5.11 Purification of ICG extrudate

The generation of *ca.* 90 g of crude ICG from the first extrusion allowed for an array of purification techniques to be tried. These included recrystallisations, washes and column chromatography. ^1H NMR was used to analyse the efficacy of each system used, a selection of results are shown in **Figure 5-21**. The spectra solvent signals are snipped for clarity.

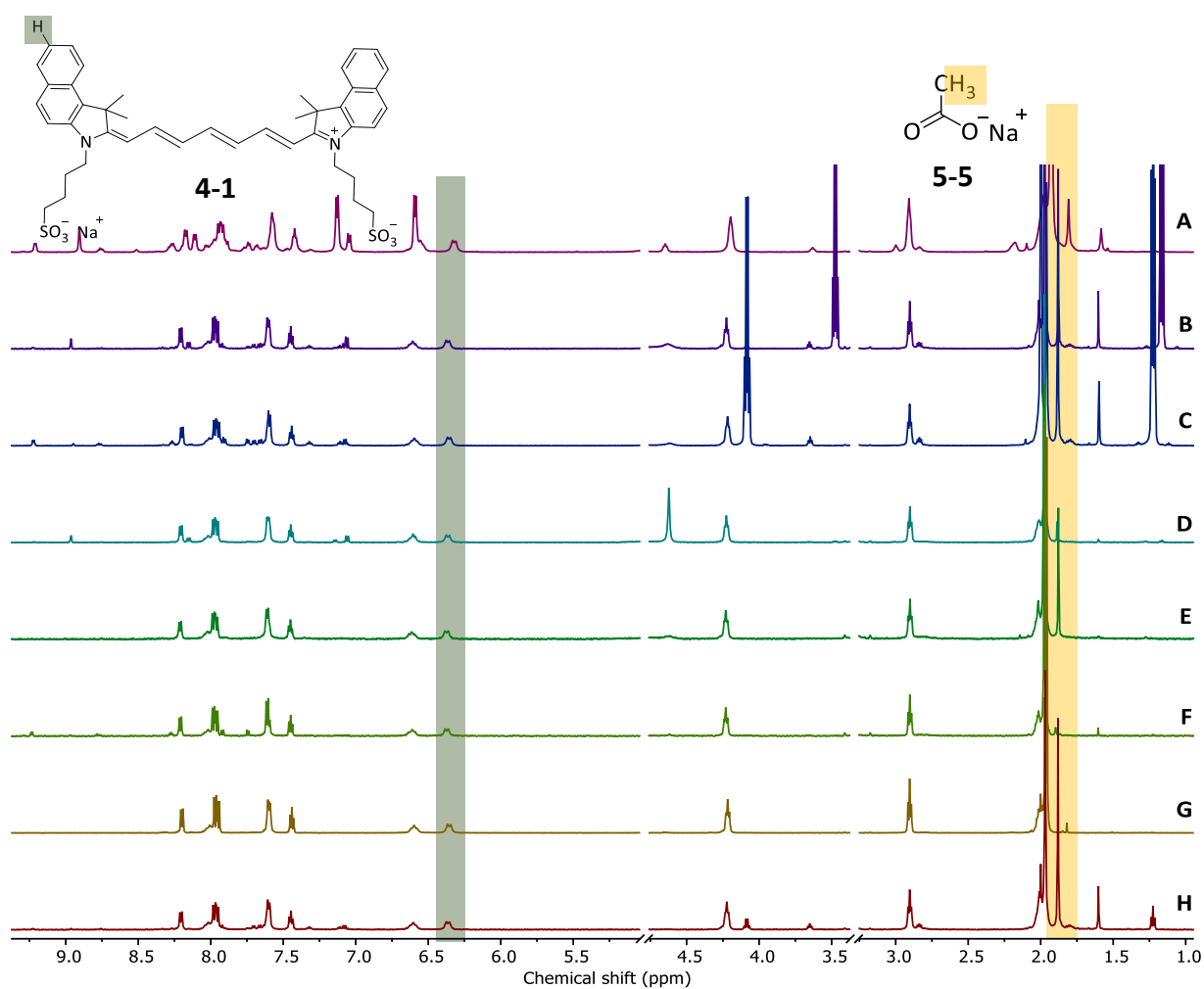


Figure 5-25 ^1H NMR stack (contracted) of purified ICG **4-1** using different techniques with impurities highlighted (A) crude extrudate ICG **4-1** (B) MeOH/Et₂O recrystallisation (C) EtOAc wash (D) H₂O/(CH₃)₂CO recrystallisation (E) MeCN recrystallisation followed by H₂O/(CH₃)₂CO recrystallisation (F) EtOAc/H₂O bisolvent wash – colloidal (G) Column chromatography (H) CH₃Cl/EtOAc bisolvent wash

All have impurities shown in their ^1H NMRs with (B) and (D) not fully dry of diethyl ether and ethyl acetate respectively. The purest sample was by using a EtOAc pre-washed sample

of crude extrudate to remove dinitroaniline, then recrystallised with water/acetone (7.27 g, 83%). A portion 0.62 g of the re-crystallised sample was further treated by column chromatography (**F**), with a methanol/chloroform (2:8) gradient giving ICG **4-1** (174 mg, 38%) This is an improvement upon the Biophore Pharmaceuticals patent²²⁷ where they use the Zincke salt as a starting material, and report 15% linear yield. Just as for many of the other attempted purifications, it retained an impurity but in a small amount, 5% (integrated from ¹H NMR spectra) at 1.82 ppm, can be seen in spectra **G**.

Bi-solvent washing (**E**) resulted in colloidal mixtures and no isolated yield which is the result of the amphiphilic nature of the ICG **4-1** molecule. A recrystallisation from acetonitrile gave a impure result and so was further recrystallised from water with acetone (**D**), with 56% yield but acetate impurities account for 1.5 mol equivalent, compared to ICG **4-1** in the sample. Although yield calculations were performed for all the purifications methods, the presence of impurities in the samples recovered rendered them useful for guidance only and ranged between 5 – 61% with their major impurity, after purification, being sodium acetate at 1.88 ppm and highlighted in yellow in **Figure 5-21**.

Further attempts at purification using the crude extrudates from subsequent experiments produced similarly limited success. ICG's solubility in solvent is the primary reason why finding suitable medium for purification was problematic. An added complication with using water for purification is that the process is time sensitive because ICG **4-1** degrades²³⁴ over 48 h and with increasing temperatures above 45 °C.

5.12 Best purification for ICG **4-1**

The opportunity to try many different purification regimes on crude ICG gave us ample evidence for the most effective and efficient route. Repeating the column chromatography method, using freshly synthesised total crude ICG sample 1.37 g (of which ICG **4-1**, 1.00 mmol) and purified in the flash column using a silica gel cartridge (24 g) with a methanol / chloroform gradient, R_f value 0.3 and t_R 16 minutes yielding the *title compound*, **4-1** (0.50

g 72%). The ^1H NMR spectroscopic analysis shown in **Figure 5-26** was the best spectrum achieved to date.

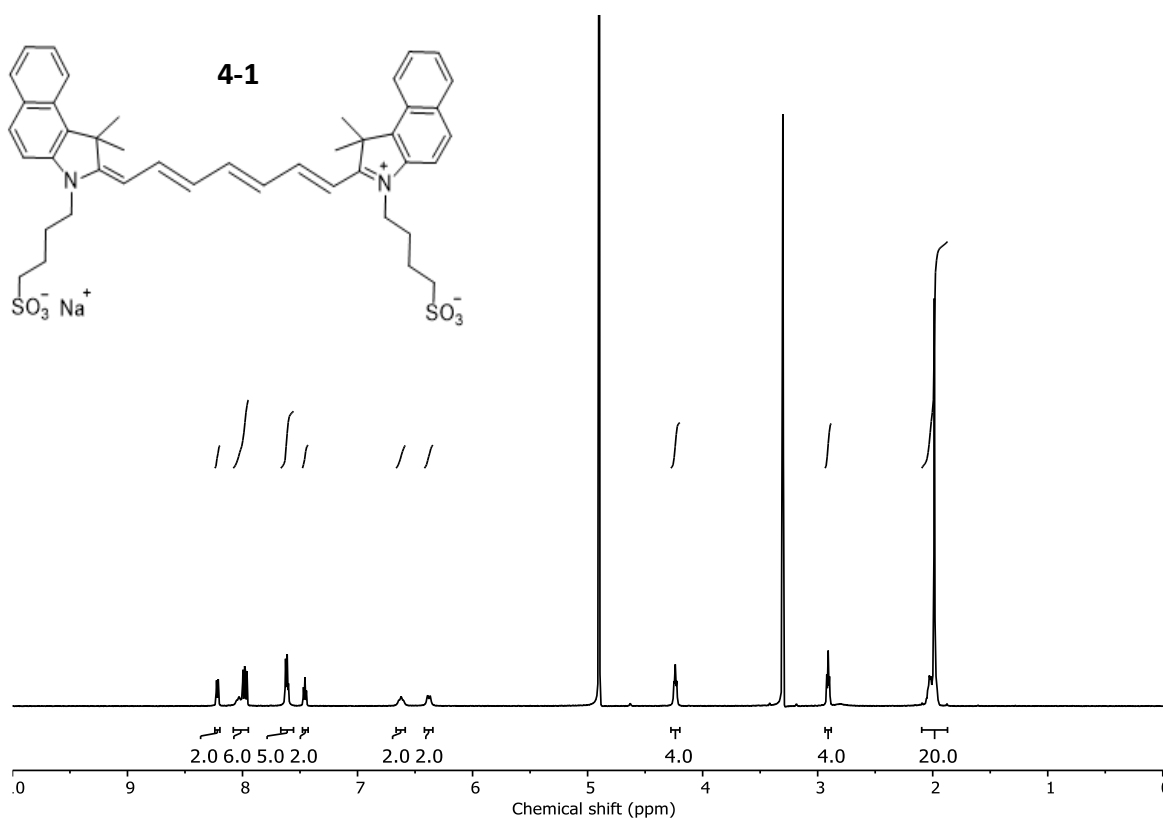
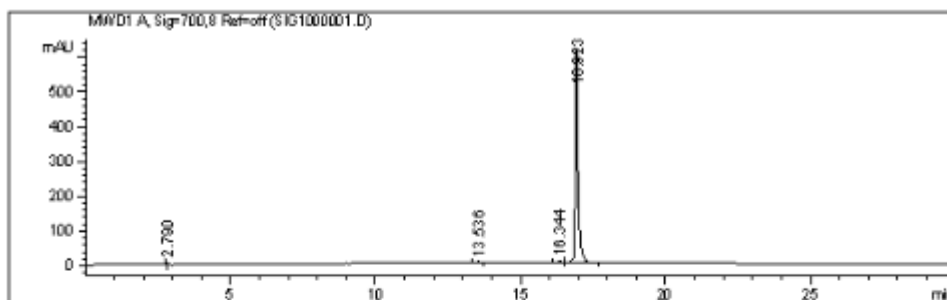


Figure 5-26 ^1H NMR spectrum of ICG **4-1**, 0.5 g (72%) by column chromatography

The search for the best method of purification of ICG **4-1**, using greener solvents gave very mixed results, including multiple attempts following the Dishman patent²²⁶ where they identified recrystallisation via reflux with water and acetone as a purification method.

After purification using column chromatography, a sample sent for purity analysis to the University of Greenwich returned a HPLC result of 97.2%, **Figure 5-27**.



```

=====
                          Area Percent Report
=====

Sorted By      :      Signal
Multiplier     :      1.0000
Dilution       :      1.0000
Use Multiplier & Dilution Factor with ISTDs

Signal 1: HWD1 A, Sig=700,8 Ref=off

Peak RetTime Type  Width   Area    Height   Area
# [min]          [min] [mAU*s] [mAU]    %
-----|-----|-----|-----|-----|
  1  2.790  EV    0.0459  24.81354  8.53176  0.5662
  2  13.536  WV    0.1054  39.94728  5.21099  0.9115
  3  16.344  WV    0.1082  56.93919  7.36726  1.2992
  4  16.923  WV    0.1027 4261.04443 615.96503 97.2232

Totals :                4382.74445  637.07505

```

Figure 5-27 ICG 4-1 obtained using column chromatography, methanol chloroform gradient 2:8, purity 97 % (HPLC UV)

5.13 Reactivity in the SSE

It is of interest to compare our findings with heating and stirring to the process occurring in the extruder. Our examination of heating and stirring had indicated that conversion increased with increasing temperatures for experiments involving anilines **3-1a-p** with the di-Zincke salts **1-2**. Heating and stirring *ca.* 1 g of the reagents for ICG **4-1** for 5 minutes (a) at 85°C with anhydrous sodium acetate gave 90% conversion (**Figure 5-12**) and (b) at 50 °C with sodium acetate trihydrate gave >95% conversion (**Figure 5-23**) as shown by ¹H NMR spectroscopy analysis. ‘Residency time’ or T_R are quoted data in extrusion experiments^{92,98} – a quantity that indicates the minimum amount of time for the process to convert to the product.

With some previously reported reactions in twin screw extruders,^{92,95,235} the equipment used have different components for specific purposes and these are itemised in **Figure 5-**

28. There is an injection port for liquid reagents which is an advantage over the SSE. The kneading and reversing sections will improve homogeneity of the mixture, which is the most important element of conversion to the product.

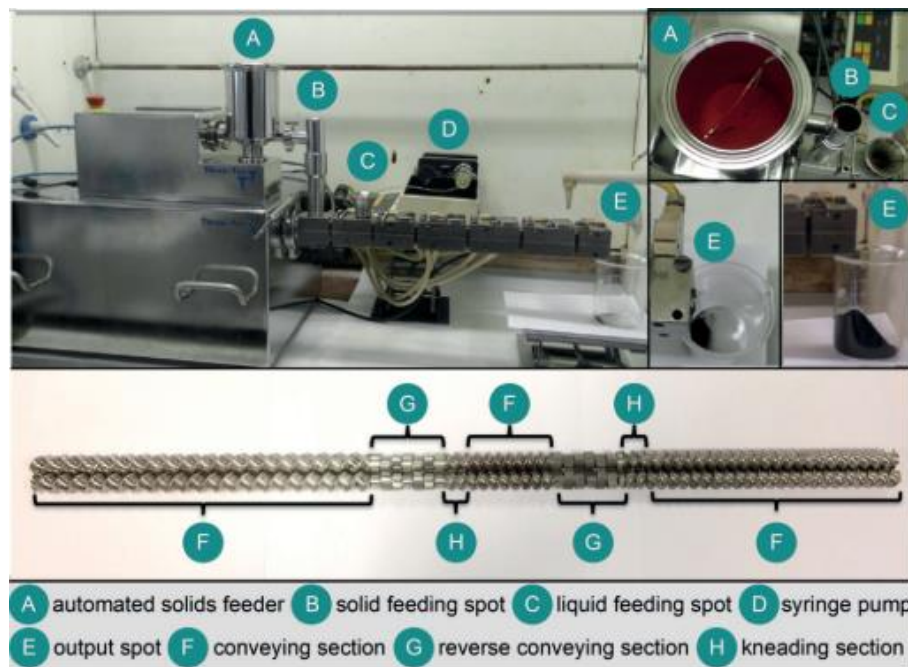


Figure 5-28 A cross-section of the extrusion screws for the manufacture of perylene dyes, picture taken from⁹²

The effect of forces applied during mechanical extrusion could be that two counter-rotating screws are experiencing torque, a rotating force, that is measurable in Nm^{-1} and may have a role in mediating the reaction.

An investigation into whether rotating forces are responsible for the conversion of reagents into products was undertaken with the SSE. The Filafab Pro 350 EX was set with a torque of 45 Nm^{-1} for all the experiments to synthesise ICG **4-1**. If there are the factors affecting/causing the reaction we could investigate it with two sets of NMR experiments using the SSE, (i) The force of pushing the crude through the 1 mm aperture of the die means that the product forms at the point of extrusion. Taking ^1H NMR spectroscopy of samples at different points of the die and nozzle attachment would indicate any differences and (ii) samples taken along the heated screw and barrel to show the effect of 'residency time' T_R .

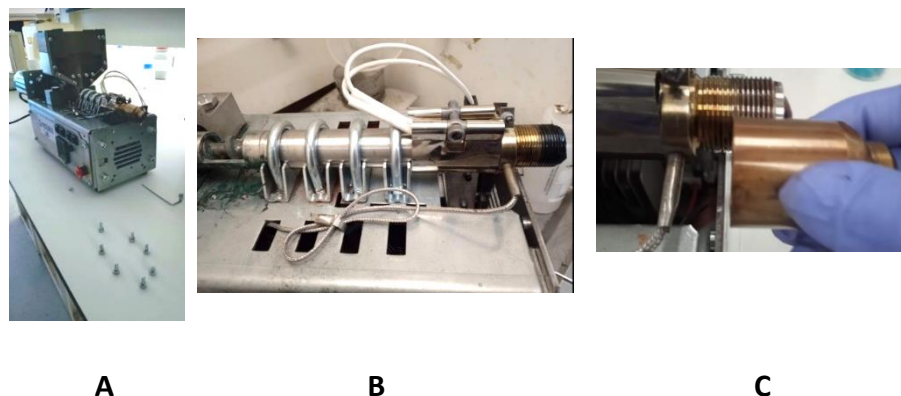


Figure 5-29 The Filafab Pro 350 Ex – (A) outer casing removed (B) The barrel with heating elements (C) The nozzle adapter and die components of the Filafab extruder

The sampling from the (spectra A) die, (spectra B) nozzle and (spectra C) screw end of the extruder was easily achieved. The samples for analysis from the screw itself was necessarily restricted to positions 5, 7 and 9 as marked in **Figure 5-30**.

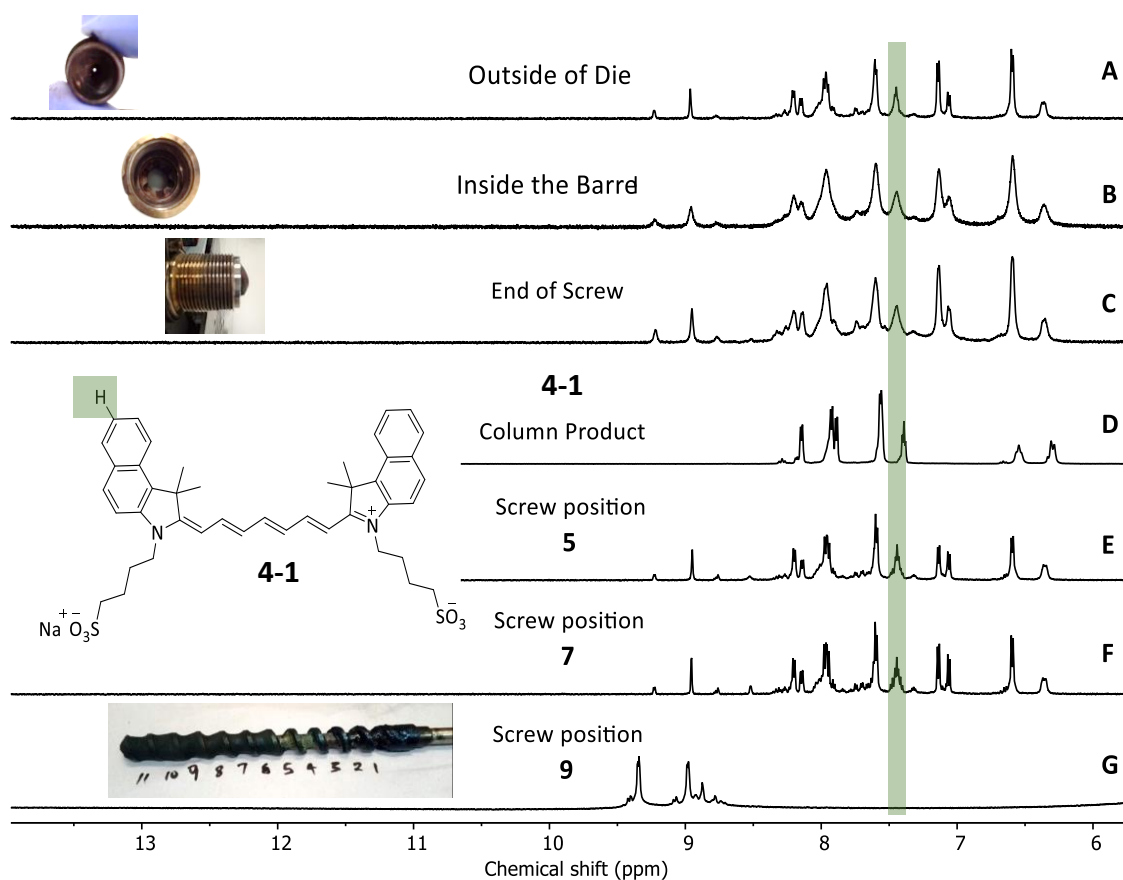


Figure 5-30 ^1H NMR of samples taken from (A) outside the die (B) inside the nozzle (C) End of the screw (D) Column product **4-1** (E), (F) and (G) screw positions marked 5, 7 and 9

The stacked ^1H NMR spectra **A-G** compares the six crude samples taken from the extruder against purified ICG **4-1** (spectrum **D**). Apart from spectrum **G**, it is evident that all the resonances in spectrum **D** that are present in ICG **4-1** are present in spectra **A-F**. The proton highlighted in green is the most unambiguous of the protons identifiable through ^1H NMR spectroscopy, (see **Figure 5-12** for further reference).

The screw removal from the barrel was by application of heat, via a heat-gun, to melt the extrudate solidified within the nozzle so that it was pliable enough to allow turning the thread on the nozzle. The experiment was at the very end of a completed extrusion resulting in no material to sample on positions **1 - 4** on the screw but samples could be obtained from sections **5, 7** and **9**. It is noted that the sample from Position 9 in the screw (Spectra **G**) had been heated to the extent that the crude had disintegrated.

Through these experiments, we can show that the mixture had fully reacted by position 5 which is approximately 10 cm along the 20 cm screw at a rate of 25 rpm as all the peaks are present and correct for our crude ICG product, **Figure 5-30**. As the screw and barrel is maintained at a steady temperature and the hopper sits directly above the barrel, this result indicates that formation of the crude product occurs as soon as the application of conductive heating in the barrel permeates through the premixed powders as they are conveyed by the screw.

This result is consistent with our observations from the heating and stirring experiments, the generality of which could be usefully extended to other reactions and synthetic procedures. A final note that can be made is that a single screw extruder has advantages over its twin-screw counterpart. The SSE of ICG **4-1** shows that a single screw is sufficient for chemical transformation, this is a simpler set-up with fewer mechanical parts, easier to clean and service making preparation for each new experiment relatively easier. Should things go awry during the extrusion process, it is easy to trouble-shoot the problem as there are so few components, the two main ones being the fuses for the heater and the motor. The comparative simplicity and therefore reliability of the equipment makes it arguably more efficient than more complicated set ups, including twin screw instruments for the experiments performed in this work.

5.14 Conclusion for the reactive extrusion of ICG

This work has identified and demonstrated the most efficient, cheap, and solvent-free method to synthesise the NIR imaging dye ICG **4-1** starting with commercially available and cheap starting materials such as pyridine.

Efficiencies for the process when compared with Dishman²²⁶ and Biophore²²⁷ patents, which both use solution methods for synthesis, are found. The new process is a 'one-pot' syntheses using continuous single screw extrusion which is able to produce the crude product from its starting materials at a rate of 2-3 kg per day using a compact desk-top extruder, the Filafab 350 Pro EX. Extensive investigations into the purification of the air and moisture sensitive compound ICG **4-1** were conducted concluding that column chromatography was the most effective and quickest.

We have also identified through testing samples at different points on the extruder that the reaction producing the crude ICG is complete at, or before, the halfway point of the heated, 20 cm long, motorised screw. In addition to discovering that heating and stirring the starting materials for five minutes in a flat bottomed conical flask, we have observed that the application of conductive heat with homogenous mixing of reagents gives conversion to target molecules faster (by a factor of 10-100) than the equivalent which has been dissolved in solvent.

Clearly there is much to gain from applying these findings to other syntheses that are currently inefficient and wasteful of resources. The application of the principle of Heat and Stir may have wide-ranging and unforeseen reaction outcomes, opening up new ways to study solvent-free synthesis. Due to the very simple application of the technique, there is a vast scope to use it wherever possible and appropriate.

Continuing work in imaging NIR dyes could begin with investigating asymmetric cyanine dyes **Figure 5-28**. Aside from ICG **4-1** – heptamethine dyes as a class of imaging dye are generally thought of as non-toxic and exhibit exceptional biocompatibility and sufficiently stable for cellular use. As they can be modified, such carbocyanine dyes could potentially

have extensive applications. Asymmetric heptamethine²³⁶ dyes are of interest as they exhibit less aggregation²³⁷ than NIR dyes such as ICG **4-1** which suffer poorer performance over longer timeframes when used for imaging.

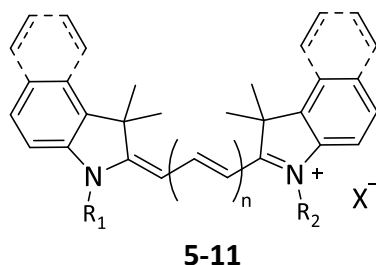


Figure 5-31 General form of an asymmetric heptamethine dye **5-11**

Schemes for their syntheses have included the gluconaldehyde and Fischer bases as discussed in Anderson's *et al.*¹⁶⁵ work. With the use of the ring-opening of the Zincke salt, and solvent free synthesis, there is a possibility of simpler synthetic routes leading to many new analogues with improved properties, with new and useful functionalities.

6. Conclusion

Our investigations into solvent-free synthesis of small molecules began with an overview of emerging mechanochemical methods. This work was developed with the aim of establishing workable, continuous and scalable production methods. The current state-of-the-art in these fields are discussed in the first chapter covering methods used in this thesis, ball-milling, and extrusion.

We have achieved our goal of producing useful molecules in as green a way as practicable through probing the Zincke Reaction mechanism. The reaction was initially investigated as the means to synthesise a series of conjugated oligomeric polymers that have increasing conductivity with increasing chain length. Our investigation in Chapter 2 found that using stoichiometric correct amounts of reagents, when heated and stirred without solvent produced the target molecule ten times more efficiently than published methods.

Employing VBM, we were also able to identify the electronic and steric factors that explained poor conversions by low-yielding anilines, **Figure 6-1**.

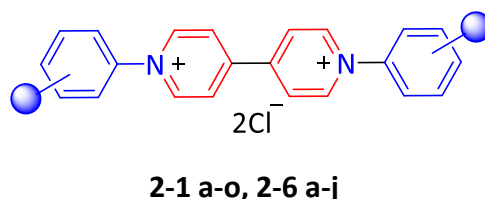


Figure 6-1 Viologens synthesis in VBM **2-1 a-o**, and heat and stir **2-6 a-j** in Chapter 2

The Zincke Reaction mechanism is known to give a thermodynamic product, a vibrant red pentamethine dye (Cy5), as well as a kinetic product which we saw in Chapter 2 in the syntheses of the viologens or bi-pyridinium salts. A set of seven pentamethine dyes were prepared and characterized with their crystal structures investigated for the first time. **Figure**

6-2 is the molecular structure obtained by X-ray Crystallography of the Cyanine 5 crystal, 5-anilino-N-p-aniso-2,4-pentadienyliidinium chloride, **3-8c**.

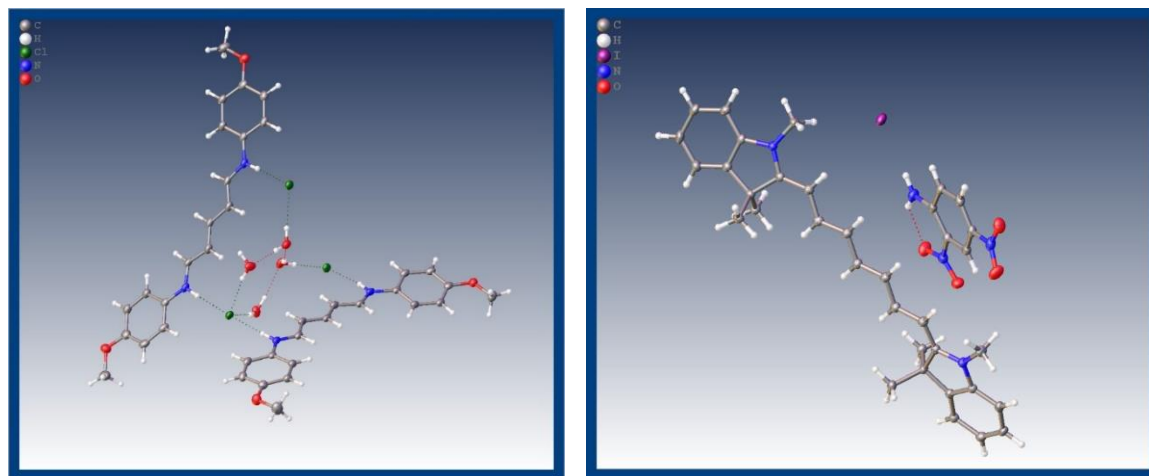
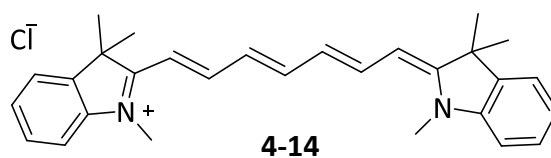


Figure 6-2 (L) 5-anilino-N-p-aniso-2,4-pentadienyliidinium chloride **3-8c** and the (R) dinitroaniline.Cy7 cocrystal **4-14.2-3**

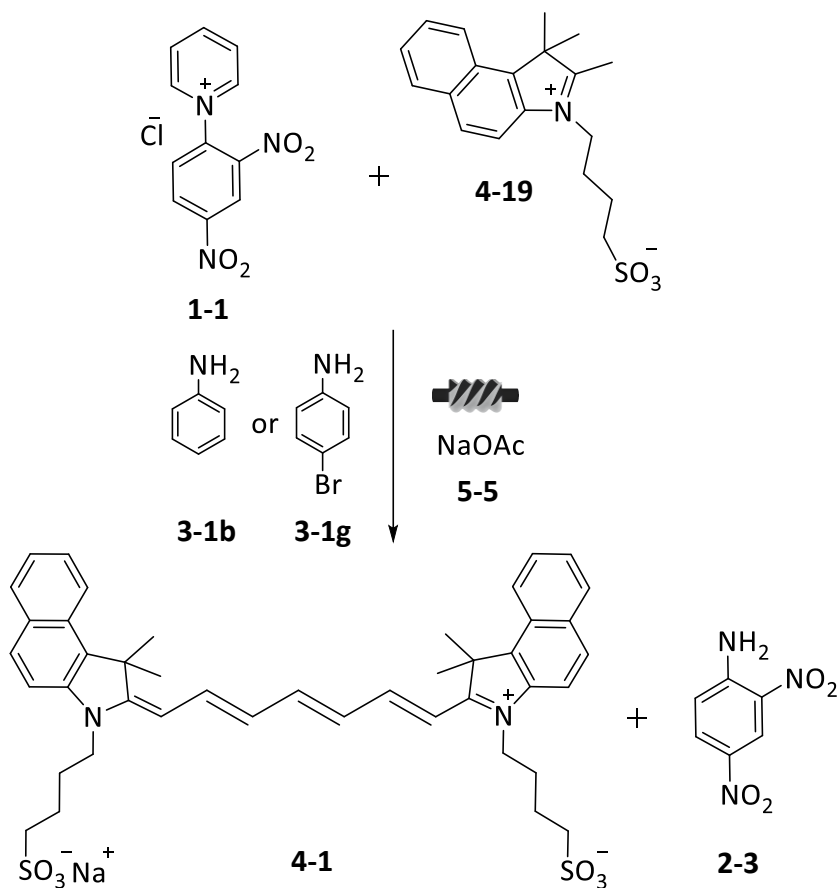
The data from X-ray crystallography of the Cy5s and the Cy7 cocrystal concurs with published literature findings on the charge distribution in polymethine wires Cy3-Cy7 which breaks down for Cy9-Cy11.¹⁶⁵

The Zincke salt was also found to be an excellent precursor to the heptamethine dye (Cy7) **4-14** as seen in the work of Štacková *et al.*¹⁶⁴ The finding in Chapter 4 was the first successful solvent-free synthesis of **4-14** via extrusion using a twin-screw instrument, the Process 11, from ThermoFisher. The result of these explorations gave sufficient evidence that extrusion of a very similar structure, the NIR imaging dye ICG **4-1** was a viable synthesis to pursue.



Chapter 5 discussed the properties and applications of the FDA approved NIR imaging dye ICG **4-1** and that we synthesised it in multi-gram quantities using the Zincke salt and a solvent-free extrusion technique. In the course of preparing the starting materials for ICG **4-1** we also

prepared multi-gram quantities of the Zincke salt **1-1** and the indolium sulfonate salt **4-19** with solvent-free heat and stir with >85% yields under 30 minutes, providing further examples of easily accomplished solvent-free synthesis using conductive heating. Solvent-free synthesis of the key starting materials for ICG **4-1** involved a liquid reagent pyridine (**Section 5.4**) which behaved as the ‘solvent reagent’ in the reaction. The ‘solvent reagent’ was completely consumed upon conductive heating until there remained only the generated solid product in the reaction vessel.



Scheme 6-1 Solvent-free reactive extrusion of the NIR imaging dye indocyanine green **4-1**

The solvent-free reaction investigations were supported by experiments in heating and stirring neat reagents (mostly solids at RT) for the syntheses of viologens and for the optimisation of the ICG **4-1** reaction. By studying the melting points of reagents and their reactivity with increasing temperatures we could optimisation our ICG **4-1** reactions for continuous extrusion.

The culmination of solvent-free syntheses, **Scheme 6-1**, is the high-yielding, efficient, energy-saving and green extrusion of ICG **4-1**.

We embarked on this work with a simple desire to find sustainable and greener methods of organic synthesis. In tandem with this aim, we sought to create new functional materials that could innovate in the fields of organic, electrically conductive technologies. We anticipated that mechanochemistry could be a key solvent-free methodology to new reaction pathways and as yet unexplored chemical phenomena.

The Zincke reaction was first discovered in 1903, its distinctive mechanism explained in 1978 by Van der Plas, and had its incorporation into a scheme for electronically conducting molecular wires by Greenland Group in 2017. The work in this thesis continues in a similar vein by showing that the mono-Zincke salt can be used to form another functional material, Indocyanine Green. This NIR imaging dye can be synthesised with high conversions using solvent-free, continuous, reactive extrusion.

The implications from the findings in this work are that the continued use of non-reactive solvent in chemical syntheses is widespread and possibly unnecessary. New synthetic procedures can be tried very easily by mixing in as small amount as necessary, the starting materials. The homogenised mixture of the reagents can undergo conductive heat (or cooling, depending on the reaction energetics) and with further mixing could, using ^1H NMR spectroscopy, quickly help to identify if the desired result has been achieved. At a stroke, this could minimise the need for solvent in general synthetic procedures. It would be a major undertaking to identify all production processes that would benefit from this change. They were able to if one considers the adaptation from filament light bulbs to LEDs and OLEDs, for example – this switch made enormous savings in energy use.

Indications show that our planet is currently in a perilous condition and that the effects of climate change has caused, and continues to permanently damage, living organisms and

ecosystems. We have also known for some time that global temperature is on the increase which brings on the melting of the polar ice caps at an increased rate.²³⁸ Addressing these threats to our futures takes a combined effort and a common goal. The root to change begins with recognising the problems that we face and offering solutions and using Anastas *et al.*³³ 12 Principles of Green Chemistry has been a guide to responsible chemical practice. Adoption of the suggested re-think of chemical synthetic processes to solvent-free strategies, based on improvements and outcomes in this work, means less energy use and less waste.

More comprehensive work on solvent-free methods to see if they are applicable to a wider range of syntheses would be of benefit to the management of our planet's resources and sustainability.⁴⁷ This could take the form of an assessment of chemical processes used to make commercial products. For ICG 4-1, the reaction could be expressed as shown in **Scheme 6-2**.



Scheme 6-2 Generic SSE of compounds

We already know that extrusion works for a small number of functional materials such as APIs⁹⁶ and in this work. We have also seen reactive extrusion for dyes and pigments, in James's scheme for Perylene Dyes⁹² is simpler still, **Scheme 6-3**. Other small organic molecules⁹⁸ can also be prepared without further purification. Reactive extrusion could be applied to all areas where it is possible to perform the operation in the simplest form.



Scheme 6-3 SSE of new compound

The combined savings in cost and energy for any large-scale manufacturing enterprise makes fiscal and sustainable sense. There are incentives enough for scaling this idea across as many chemical processes as possible.

The best thing of all, investigating whether reactive extrusion is possible for a chemical process requires a simple, solvent-free, heat and stir experiment.

Reader, there is a climate emergency, let us as chemistry practitioners help improve the situation.

7. Experimental

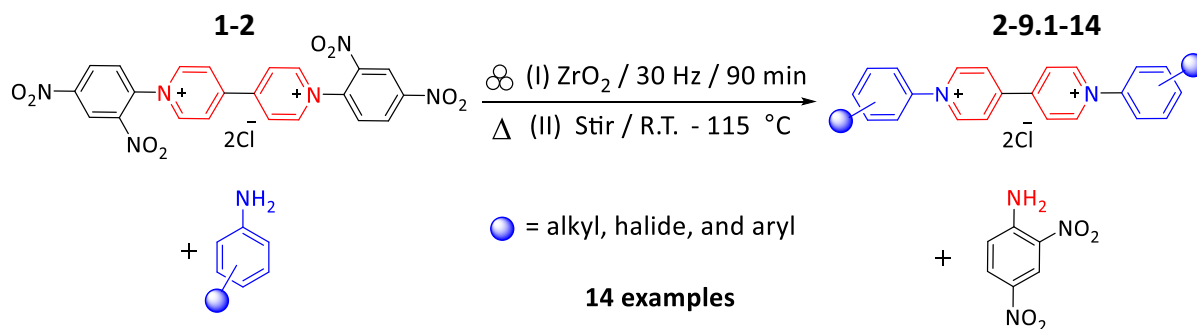
Reagents were purchased from Apollo Scientific, Carbosynth, Merck, Fisher Scientific UK Ltd, Tokyo Chemical Industry UK Ltd or Fluorochem Ltd, and used without further purification. The ball milling reactions were carried out in a Retsch MM400 vibratory ball mill (VBM) operating at 30 Hz and a Retsch PM100 planetary ball mill (PBM). Milling load is defined as the sum of the mass of the reactants per free volume in the jar. Single Screw Extrusion reactions were performed using a FilaFab PRO 350X operating at 25 rpm and variable temperatures. Pre-mixing of reagents was accomplished in a 1 L Kenwood Mini-Chopper.

Unless stated otherwise, purifications were performed via flash column chromatography on silica gel (RediSep® Rf Silica Gel Disposable Flash Columns, 40–60 micron) on Teledyne ISCO CombiFlash Lumen apparatus. Analytical thin layer chromatography (TLC) was performed on silica gel 60 F254 (Merck). IR spectra were recorded over the range of 4000–650 cm^{-1} on a PerkinElmer Spectrum One FT-IR spectrometer fitted with a UATR polarization accessory. UV-Vis sample details: 1 mM stock solution of samples dissolved in methanol and diluted to 0.2 mM for UV-vis measurements. UV-Vis measurements (300-900nm) were recorded at room temperature on a Perkin Elmer Lambda 25 double beam spectrometer. ^1H (600 MHz) and ^{13}C NMR (150 MHz) spectra were recorded on a Varian VNMRS 600 MHz spectrometer, at room temperature, using the residual protic solvent signal in the deuterated solvent for calibration (chloroform- d at δ 7.26 ppm or DMSO- d_6 at δ 2.50 ppm). Chemical shifts are reported in ppm. Spin multiplicities are reported as a singlet (s), doublet (d), triplet (t) or multiplet (m), with coupling constants (J) given to the nearest 0.5 Hz, where applicable. ESI mass spectra were obtained by Dr Alaa Abdul-Sada or by Dr Ramón González-Méndez using a Waters Xevo G2 Q-ToF HRMS (Wilmslow, UK) equipped with analytical flow ESI source. ESI experimental parameters were: capillary voltage 3.0 kV, sampling cone 35 au, extraction cone 4 au, source temperature 120 °C and desolvation gas 450 °C with a desolvation gas flow of 650 L h^{-1} and no cone gas. MS conditions were MS1 in resolution mode between 100-1500 Da. Accurate mass data were obtained using MassLynx software. All accurate mass data were within ± 5 ppm from their theoretical value. ICP-MS analysis for metals was done by Dr Christopher Dadswell using

an Agilent 7500ce ICP-MS instrument with collision cell (He as collision gas) for Fe and standard mode (no collision gas) for Zr and Pd, using ^{72}Ge as internal standard. The following experimental parameters were used: a) plasma: RF power 1500 W, sampling depth 8.5 mm, carrier gas 0.8 L min^{-1} , make-up gas 0.11 L min^{-1} ; b) quadrupole: mass range 1-250 amu, dwell time 100 ms, replicates 3, integration time 0.1 s/point. Calibration solutions were prepared for each element between 0 and 200 ng mL^{-1} using certified reference standards (Fisher Scientific, UK).

High Performance Liquid Chromatography (HPLC) purity data were obtained by Mr Darren Pink of the University Chromatography Service using an Agilent 1290 infinity HPLC equipped with binary pump (G4220A), autosampler (G4226A), and thermostatted column compartment (G1316C); a diode array detector (G4212A) was used to determine purity of all samples in the UV band. Samples in the visible spectrum were run on an Agilent 1260 infinity HPLC equipped with quaternary pump (G1311C), autosampler (G1329A), thermostatted column compartment (G1316C) and multiple wavelength detector (G1365D). Chromatographic separation was achieved using a Hichrom, Kromasil C18, $5\mu\text{m}$ particle size column of $250 \times 4.6 \text{ mm}$ length and i.d. (KR100-5C18-H14708) in a reverse-phase gradient. Additional HPLC analyses were provided by the University of Sheffield and were conducted by Robert Hanson and Mohamed Okhai. Solid State Structure determination: Crystals of compound **3-8a-g** were grown from diethyl ether and IPA using the slow diffusion method at room temperature. Crystals of **4-14.2-3** were precipitated from methanol and diethyl ether at room temperature for 3 weeks. Their X-Ray crystallographic analyses were conducted by Dr Mark Roe. The data were collected either on a Rigaku Gemini Ultra sealed tube source or a Rigaku 007HFM rotating anode source, depending on the inherent diffraction of the crystals. The data was processed with CrysAlisPro and the structures solved, built and refined using ShelxT and ShelxL in the Olex2 suite. Experiments using ThermoFisher Scientific Process 11 Twin Screw Extruder conducted by Dirk Hauch, Germany.

General Scheme for the Synthesis of Viologens



General Protocol (I)

1,1'-Bis(2,4-dinitrophenyl)-4,4'-bipyridinium dichloride (0.50 g, 0.89 mmol) was added to a substituted aniline (2 eq., 1.96 mmol) in a ZrO_2 jar (25 mL) charged with one ZrO_2 balls (12 mm \emptyset) [milling load *ca.* 30 mg.mL⁻¹]. Unless stated otherwise, the mixture was oscillated at 30 Hz in a Retsch MM400 Vibratory Ball Mill for 90 min. The jar was opened, and the crude product was dissolved in methanol (25 mL) and precipitated by the addition of cold (-20°C) EtOAc (100 mL). The solvent was removed *in vacuo* and the product washed with THF (200 mL) then dried overnight in a vacuum oven.

General Protocol (II)

1,1'-Bis(2,4-dinitrophenyl)-4,4'-bipyridinium dichloride (0.50 g, 0.89 mmol) was added to a substituted aniline (2 eq., 1.96 mmol) in a ZrO_2 jar (25 mL) charged with two ZrO_2 balls (15 mm \emptyset) [milling load *ca.* 30 mg.mL⁻¹]. Unless stated otherwise, the mixture was oscillated at 30 Hz in a Retsch MM400 Vibratory Ball Mill for 90 min. The jar was opened, and the crude product was dissolved in methanol (25 mL) and precipitated by the addition of cold (-20°C) EtOAc (100 mL). The solvent was removed *in vacuo* and the product washed with THF (200 mL) then dried overnight in a vacuum oven.

General Protocol (III)

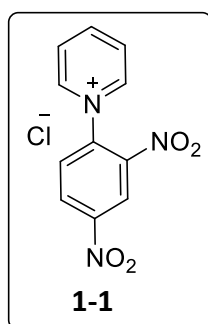
1,1'-Bis(2,4-dinitrophenyl)-4,4'-bipyridinium dichloride (0.50 g, 0.89 mmol) was added to a substituted aniline (2 eq., 1.96 mmol) in a boiling tube in a 12-port carousel reactor fitted with

a water-cooled condensing collar. The reactor was mounted on a variable temperature hotplate and individual stainless-steel spatulas (3 mm) were added to each reaction vessel to stir the mixture. The reagents were stirred initially for 1 hour at room temperature and sampled for ^1H NMR spectroscopic analysis, after which the temperature was increased to 85 $^\circ\text{C}$, manually stirred and sampled again after 1 hour. Finally, the temperature was set to 115 $^\circ\text{C}$, manually stirred for an hour and a final sample was taken. Once ^1H NMR spectroscopic analysis showed >80% conversion, the title compound was isolated by dissolving the crude product mixture in THF (80 mL). The solution was added dropwise to stirred, cold ($-20\text{ }^\circ\text{C}$) ethyl acetate (150 mL) and the precipitated solid was filtered, washed with cold EtOAc and air-dried overnight.

General Protocol (IV)

Mono-Zincke salt with 2 eq. of aniline, 2 x 15 mm in a ZrO_2 jar (25 mL) charged with two ZrO_2 balls (15 mm \varnothing) [milling load *ca.* 30 mg mL^{-1}]. Unless stated otherwise, the mixture was oscillated at 30 Hz in a Retsch MM400 Vibratory Ball Mill for 60 min. The crude product was dissolved in methanol (25 mL), the product was precipitated out of warmed diethyl ether (100 mL). This was filtered and washed with diethyl ether and dried overnight in a vacuum oven.

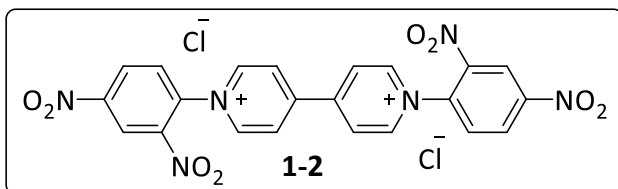
Synthesis of *N*-(2,4-dinitrophenyl) pyridinium chloride 1-1



Pyridine (7.91 g, 0.100 mol) were poured into a 500 mL round-bottomed flask. 2,4-Dinitrochlorobenzene (20.3 g, 0.100 mol) was added and heated for 15 minutes with vigorous stirring. After cooling to room temperature, acetone (50 mL) was added to wash down the sides of the flask. The solid was triturated with 400 mL acetone then filtered *in vacuo* and washed with further acetone through a glass frit. After drying overnight under high vacuum at 65 $^\circ\text{C}$ to give the title compound **1-1** as a pale yellow solid (27.7 g, 97%), mp 192–193 $^\circ\text{C}$, (in agreement with the literature).¹⁷⁵ ^1H NMR (600 MHz, Methanol- d_4) δ 9.32 – 9.28 (m, 2H), 9.27 (d, $J = 2.5$ Hz, 1H), 8.98 – 8.89 (m, 2H), 8.42 – 8.37 (m, 2H), 8.30 (d, $J = 8.5$ Hz, 1H). ^{13}C

NMR (151 MHz, d_6 -DMSO) δ 149.3, 146.6, 143.6, 139.2, 132.5, 131.1, 128.5, 121.8. IR ν_{max}/cm^{-1} 784 (C-H), $\nu = 1542$ (N-O). HRMS [ES⁺] 246.0500, C₁₁H₈N₃O₄ requires 246.0509. EA for C₁₁H₈N₃O₄ calc. C, 46.91; H, 2.86; N, 14.97; found C, 46.96; H, 2.79; N, 14.77.

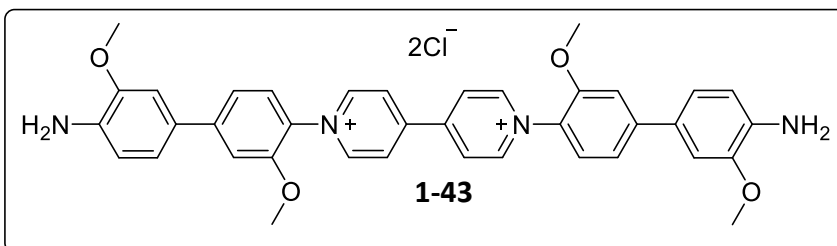
Synthesis of 1,1'-bis(2,4-dinitro)-4,4'-bipyridinium dichloride, 1-2



4,4'-Bipyridine (1.60 g, 10.2 mmol) and 1-chloro-2,4-dinitrobenzene (7.40 g, 36.5 mmol) were dissolved in anhydrous acetonitrile (15 mL) under argon. The

solution was heated to reflux and stirred for 9 days until a large amount of pale-yellow precipitate had formed. Water (5 mL) were added to the flask and warmed until the precipitate dissolved. Ethanol (10 mL) was then added dropwise forming a yellow precipitate. The contents of the flask were filtered and dried *in vacuo* to give the *title compound* **1-2** (5.12 g, 89%) as a pale-yellow powder, mp 244-246 °C, (in agreement with the literature).¹²⁷ ¹H NMR (600 MHz, D₂O) δ 9.32 (d, $J = 6.5$ Hz, 4H), 9.24 (d, $J = 2.0$ Hz, 2H), 8.81 – 8.74 (m, 6H), 8.15 (d, $J = 8.5$ Hz, 2H). ¹³C NMR (151 MHz, CD₃OD) δ 152.2, 147.2, 147.2, 143.1, 138.4, 127.2, 127.2, 121.9, 121.8. IR ν_{max}/cm^{-1} 839 (C-H), 1532 (N-O). HRMS [ES⁺] found 490.0867. C₂₂H₁₄N₆O₈⁺ requires 490.0873, [M-H]¹⁺, HPLC Purity (UV) = 99%, t_R 13.9 min.

Synthesis of 1,1'-bis(4'-amino-3,3'-dimethoxy-[1,1'-biphenyl]-4-yl)-[4,4'-bipyridine]-1,1'-dium chloride, 1-43

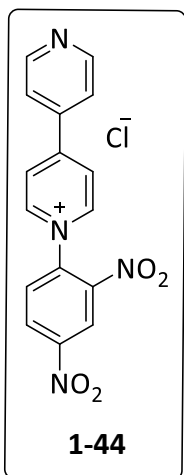


The di-Zincke salt **1-2** (575 mg, 1.00 mmol) was dissolved in 12 mL of methanol/water (1 : 1, v/v) with 3,3'-

dimethoxybenzidine (733 mg, 3.00 mmol). The reaction mixture was heated with stirring to reflux for 3 days, after which the solvent was removed *in vacuo*. The residue was dissolved in

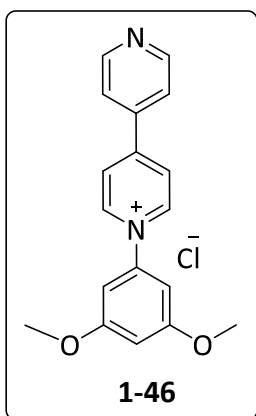
methanol (50 mL) and precipitated into EtOAc (400 mL) with stirring. THF (400 mL) were added and the whole stirred for 48 h then filtered. The crude product was precipitated twice from MeOH/EtOAc (1 : 8, v/v then filtered and dried under high vacuum to afford **1-40** as a dark brown solid (645 mg, 93%), mp 280 °C (dec.) in agreement with the lit.¹²⁶ ¹H NMR (600 MHz, CD₃OD) δ 9.43 (d, *J* = 6.0 Hz, 4H), 8.90 (d, *J* = 6.0 Hz, 4H), 7.83 (d, *J* = 8.0 Hz, 2H), 7.63 (s, 2H), 7.58 (d, *J* = 8.0 Hz, 2H), 7.44 (s, 2H), 7.38 (d, *J* = 7.5 Hz, 2H), 7.25 (d, *J* = 8.0 Hz, 2H), 4.06 (s, 12H). ¹³C NMR (151 MHz, CD₃OD) δ 152.2, 150.9, 150.7, 149.7, 147.5, 146.3, 129.9, 126.7, 126.6, 120.2, 120.0, 119.7, 111.2, 110.1, 55.9, 55.3, 48.1. IR ν_{\max} /cm⁻¹ 3407 (primary amine), 1125 (C-O). HRMS [ES⁺] 306.1342, C₃₈H₃₆N₄O₄²⁺ requires 306.1366, [m/z].

Synthesis of 1-(2,4-Dinitrophenyl)-[4,4'-bipyridin]-1-ium chloride **1-44**



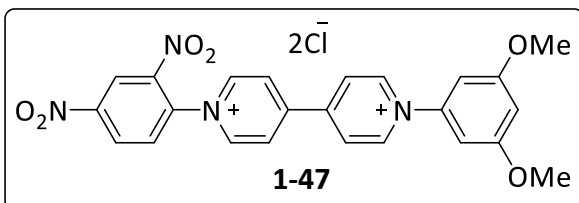
Bipyridine (10.09 g, 64.6 mmol) were heated with 1-chloro-2,4-dinitrobenzene (13.08g, 64.6 mmol) with acetone (6 mL) to 80 °C with stirring. After 15 minutes the crude mixture became too thick for stirring and the vessel was allowed to cool to room temperature. Acetone was added and the reaction mixture was stirred for a further 15 min at 50 °C. After cooling the solid was broken up with a pestle and mortar and triturated overnight in acetone. The product was filtered and washed with further acetone to give the title compound as a brown solid (21.01 g, 90.8%), mp 149 °C, (in agreement with the literature).¹²³ ¹H NMR (600 MHz, CD₃OD) δ 9.44 – 9.41 (m, 2H), 9.30 (d, *J* = 2.5 Hz, 1H), 8.95 (dd, *J* = 8.5, 2.5 Hz, 1H), 8.92 – 8.88 (m, 2H), 8.83 (d, *J* = 7.0 Hz, 2H), 8.34 (dd, *J* = 8.5, 2.0 Hz, 1H), 8.14 – 8.12 (m, 2H). ¹³C NMR (151 MHz, CD₃OD) δ 156.6, 150.6, 149.8, 146.4, 143.2, 141.7, 138.5, 131.4, 129.8, 125.7, 122.4, 121.8. IR ν_{\max} /cm⁻¹ 1222 (C-N), 1533 (N-O). HRMS [ES⁺] 323.0789, C₁₆H₁₁N₄O₄⁺ requires 323.0780 [M]⁺. HPLC Purity (UV) = 99+% *t*_R 9.8 min.

Synthesis of 1-(3,5-bis(methoxyphenyl)-[4,4'-bipyridin]-1-ium dichloride 1-46



1-(2', 4'-Ditrophenyl)-[4,4'-bipyridin]-1-ium chloride (1.92 g, 5.35 mmol) was dissolved in ethanol (6 mL) with 3,5-dimethoxyaniline (0.82 g, 5.35 mmol). The mixture was heated to reflux and stirred vigorously for 2 h. After cooling to room temperature hot methanol was added until the paste was completely dissolved and hot acetonitrile (1:3 v/v) was added. The recrystallised product was collected via filtration and washed with acetonitrile (100 mL) then air dried overnight giving the title compound as a yellow solid (1.08 g, 61%). ^1H NMR (600 MHz, CD_3OD) δ 9.34 (d, $J = 7.0$ Hz, 2H), 8.89 – 8.85 (m, 2H), 8.64 (d, $J = 7.0$ Hz, 2H), 8.08 – 8.04 (m, 2H), 7.03 (d, $J = 2.0$ Hz, 2H), 6.86 (s, 1H), 3.92 (s, 6H). ^{13}C NMR (151 MHz, CD_3OD) δ 161.6, 154.6, 150.4, 145.1, 143.6, 142.1, 125.0, 123.4, 101.4, 55.3, -0.16, mp 217 °C. IR $\nu_{\text{max}}/\text{cm}^{-1}$ 1204 (C-O), 1628 (C=C). HRMS [ES^+] 293.1283, $\text{C}_{18}\text{H}_{17}\text{N}_2\text{O}_2^+$ requires 293.1290, $[\text{M}]^+$. HPLC Purity (UV) = 96% t_{R} 11.5 min.

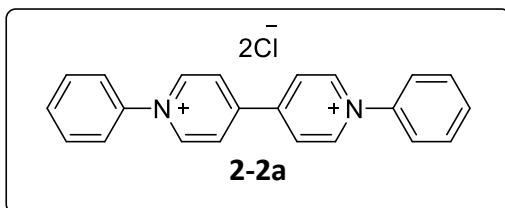
Synthesis of 1-(3,5-bis(methoxyphenyl)-[4,4'-bipyridin]-1-ium dichloride 1-47



1-(3'',5''-Dimethoxyphenyl)-[4,4'-bipyridine]-1-ium chloride (0.94 g, 2.86 mmol) and 1-chloro-2,4-dinitrobenzene (5.07 g, 25.00 mmol) were dissolved in ethanol (8 mL) and heated to reflux with stirring for 3 days. The crude product was dissolved in THF (70 mL) then filtered. The residue was washed with further THF (100 mL) then EtOAc (100 mL). It was dried overnight in an oven at 60 °C to give the title compound as a brown solid **1-47** (5.57 g, 79%), mp 217 °C (dec.). ^1H NMR (600 MHz, CD_3OD) δ 9.64 (d, $J = 6.0$ Hz, 2H), 9.61 – 9.56 (m, 2H), 9.34 (s, 1H), 9.06 (d, $J = 6.0$ Hz, 2H), 8.98 (d, $J = 9.0$ Hz, 1H), 8.94 (d, $J = 6.5$ Hz, 2H), 8.39 (d, $J = 8.5$ Hz, 1H), 7.10 (s, 2H), 6.91 (s, 1H), 3.94 (d, $J = 2.0$ Hz, 6H). ^{13}C NMR (151 MHz, CD_3OD) δ 162.2, 152.6, 150.2, 150.0, 147.1, 145.9, 144.1, 143.1, 138.4, 131.3, 129.9, 127.1, 127.0, 121.8, 103.0,

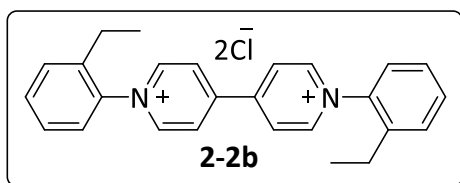
102.7, 55.3. IR ν_{\max} /cm⁻¹ 1163 (C-O), 1537 (N-O). HRMS [ES⁺] 460.1360, C₂₄H₂₀N₄O₆²⁺ requires 460.1383, [M]⁺.

Synthesis of *N,N'*-di(phenyl)-4,4'-bipyridinium dichloride 2-2a



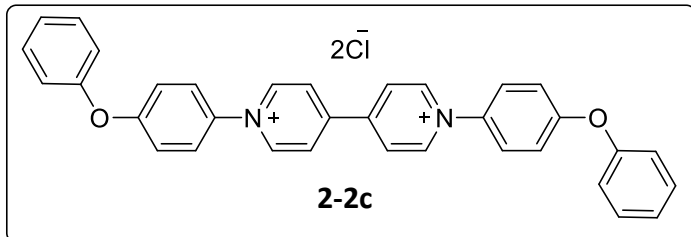
The title compound was synthesized following general protocol (I) using **1-2** (0.50 g, 0.89 mmol) added to aniline (0.18 g, 1.96 mmol) and oscillated for 30 minutes using ZrO₂ balls (1 x 12 mm \emptyset). The reaction mixture was washed with THF (50 mL) and EtOAc (50 mL), filtered then purified by flash chromatography using a reverse phase C18 column (43 g cartridge), to yield **2-2a**, as a pale brown powder, 1,1'-phenyl-(4,4'-bipyridine)-1, 1'-dium dichloride (86 mg, 26%), mp 395 °C (dec). ¹H NMR (600 MHz, D₂O) δ 9.33 – 9.23 (m, 4H), 8.71 – 8.63 (m, 4H), 7.87 – 7.49 (m, 10H). ¹³C NMR (151 MHz, CD₃CN) δ 150.4, 145.7, 142.4, 132.2, 130.7, 127.3, 124.5. IR ν_{\max} /cm⁻¹ 757 (C-H). HRMS [ES⁺] found 309.1390. C₁₈H₁₄N₂⁺ requires 309.1386 (in agreement with the literature),¹²⁷ HPLC Purity (UV) = 95%, t_R 12.6 min.

Synthesis of *N,N'*-di(2-ethylphenyl)-4,4'-bipyridinium dichloride 2-2b



The title compound was synthesized following general protocol (I) using **1-12** (0.50 g, 0.89 mmol) added to 2-ethylaniline (0.25 mg, 1.98 mmol) and oscillated for 60 minutes to give the title compound (0.22 g, 56%) as a brown solid, mp 247 – 248 °C. ¹H NMR (600 MHz, CD₃OD) δ 9.49 – 9.42 (m, 4H), 8.94 – 8.91 (m, 4H), 7.75 (td, J = 7.5, 1.5 Hz, 2H), 7.70 (dd, J = 8.0, 1.5 Hz, 2H), 7.65 (dd, J = 8.0, 1.5 Hz, 2H), 7.59 (td, J = 7.5, 1.5 Hz, 2H), 2.56 (q, J = 7.5 Hz, 4H), 1.22 (t, J = 7.5 Hz, 6H). ¹³C NMR (151 MHz, CD₃OD) δ 151.1, 147.2, 141.5, 138.1, 132.1, 130.2, 127.7, 127.3, 125.6, 22.9, 13.5. IR ν_{\max} /cm⁻¹ 693 (C-H), 1344 (C-N). HRMS [ES⁺] found 365.2013, C₂₆H₂₆N₂⁺ requires 365.2012, HPLC Purity (UV) = 95%, t_R 12.6 min.

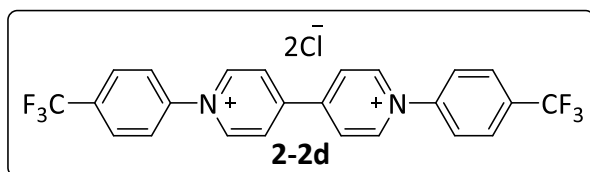
Synthesis of *N,N'*-bis(4-phenoxy)-4,4'-bipyridinium dichloride 2-2c



The title compound was synthesized following general protocol (I) using **1-2** (0.50 g, 0.89 mmol) with 4-phenoxyaniline (363 mg, 1.98 mmol) to give the title compound (0.32 g, 64%

yield) as a metallic yellow-gold powder, mp 326 – 328 °C (dec). ¹H NMR (600 MHz, DMSO-*d*₆) δ 9.72 (d, *J* = 6.5 Hz, 4H), 9.20 – 9.09 (m, 4H), 8.08 – 7.97 (m, 4H), 7.57 – 7.47 (m, 4H), 7.40 – 7.25 (m, 6H), 7.23 – 7.11 (m, 4H). ¹³C NMR (151 MHz, CD₃OD) δ 161.0, 155.3, 150.0, 145.6, 137.0, 130.1, 126.9, 125.9, 124.9, 119.9, 118.7. IR ν_{max} /cm⁻¹ 1233 (C-N), 1583 (arene). HRMS [ES⁺] found 493.1898, C₃₄H₂₆N₂O₂⁺ requires 493.1911, [M-H]¹⁺. HPLC Purity (UV) = 96%, *t*_R 12.9 min.

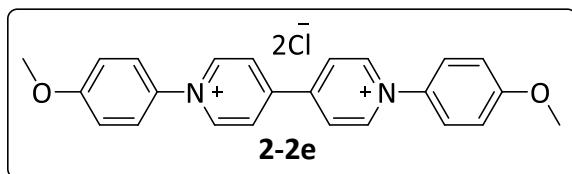
Synthesis of *N,N'*-bis[4-(trifluoromethylphenyl)]-4,4' bipyridinium Dichloride 2-2d



The title compound was synthesized by following general protocol (II) with **1-2** (0.50 g, 0.89 mmol) and 4-trifluoromethyl aniline **2-1d** (0.42 g, 1.96 mmol) to give a yellow-brown

powder (0.13 g, 45%), mp 312-314 °C (dec.), ¹H NMR (600 MHz, D₂O) δ 9.39 – 9.35 (m, 4H), 8.76 – 8.71 (m, 4H), 8.01 (d, *J* = 8.0 Hz, 4H), 7.93 (d, *J* = 8.0 Hz, 4H), ¹³C NMR (151 MHz, D₂O) δ 151.0, 145.6, 144.6, 132.8 (q, ²*J*_{CF} = 30.0 Hz), 127.9 (q, ³*J*_{CF} = 4.5 Hz), 127.2, 125.1, 120.8 (q, ¹*J*_{CF} = 302 Hz). ¹⁹F NMR (376 MHz, DMSO) δ -61.3. IR ν_{max} /cm⁻¹ 1252 (C-N), 824 (alkene). HRMS [ES⁺] 445.1142, C₂₄H₁₆F₆N₂⁺ requires 445.1134, [M-H]¹⁺. HPLC Purity (UV) = 95%, *t*_R 14.6 min.

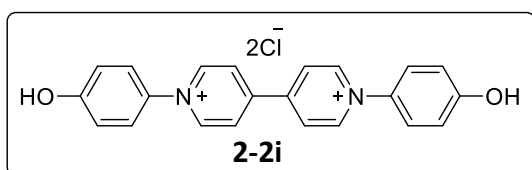
Synthesis of *N,N'*-bis[4-(methoxy)]-4,4' bipyridinium Dichloride 2-2e



The *title compound* was synthesised by following general protocol (I) using **1-2** (0.50 g, 0.89 mmol) and *p*-anisidine **2-1e** (0.24 g, 1.96

mmol) with an oscillation time of 90 minutes. Purification using general protocol (I) gave the title compound, a yellow powder (195 mg, 50%), mp 278.4 – 279.6 °C (dec), ¹H NMR (600 MHz, DMSO-*d*₆) δ 9.64 (s, 4H), 9.06 (s, 4H), 7.95 (d, *J* = 8.0 Hz, 4H), 7.32 (d, *J* = 8.5 Hz, 4H), 3.93 (s, 6H). ¹³C NMR (151 MHz, DMSO-*d*₆) δ 161.4, 148.3, 145.4, 135.1, 126.5, 126.1, 115.2, 55.9. IR ν_{\max} /cm⁻¹ 825 (para-disubstituted benzene), 1494 (C-N), 1592 (C=C). HRMS [ES⁺] 369.1584, C₂₄H₂₂N₂O₂⁺ requires 369.1598, [M-H]¹⁺ in agreement with lit. HPLC Purity (UV) = 97%, *t*_R 18.4 min.

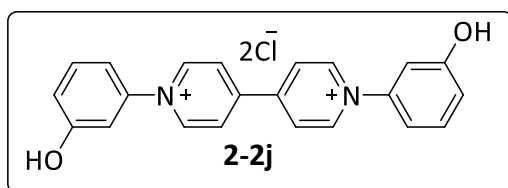
Synthesis of *N,N'*-bis(4-phenol)-[4,4'-bipyridin]-1,1'-dium dichloride 2-2i



The title compound was synthesised by following general protocol (I) using **1-2** (0.700 g, 1.25 mmol) was added to 4-aminophenol **2-1i** (0.273 mg, 2.50 mmol), giving a brown paste which was dissolved

in methanol (60 mL). Precipitation of the solid was by the dropwise addition of the crude methanol solution, into stirred, cold (-20 °C) ethyl acetate (150 mL). ICP-MS analysis established that zirconium residues were present in the sample and quantified as 3% by weight. The zirconium residues were removed by dissolving the sample in methanol, then filtering through 2 cm depth of oven-dried celite. The solvent was removed from the filtrate, *in vacuo*, and the solid was dried overnight in a vacuum oven at 70 °C to give a brown powder (0.413 g, 96%), mp 311 °C (dec) ¹H NMR (600 MHz, DMSO) δ 10.59 (s, 2H), 9.56 (d, *J* = 6.5 Hz, 4H), 8.97 (d, *J* = 6.5 Hz, 4H), 7.76 (d, *J* = 8.5 Hz, 4H), 7.09 (d, *J* = 8.5 Hz, 4H). ¹³C NMR (151 MHz, CD₃OD) δ 150.0, 147.2, 138.4, 131.2, 129.9, 127.2, 121.9. IR ν_{\max} /cm⁻¹ 3023 (O-H), 816 (C-H). HRMS [ES⁺] 341.1290, C₂₂H₁₈N₂O₂⁺ requires 341.1291, [M-H]¹⁺. HPLC Purity (UV) = 85%, *t*_R 12.2 min.

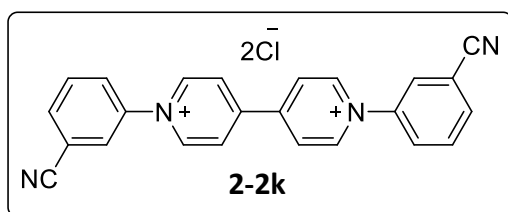
Synthesis of *N,N'*-di[4-(3-phenol)]-[4,4'-bipyridin]-1,1'-dium dichloride 2-2j



The title compound was synthesised by following general protocol (I) using **1-2** (0.50 g, 0.89 mmol) added to 3-aminophenol **2-1j** (0.21 g, 1.98 mmol). The crude product was dissolved in methanol (60

mL), then added, dropwise, into stirred, cold (-20 °C) EtOAc (150 mL). After filtering the solid was washed with further cold EtOAc then dried overnight, *in vacuo*, at 70 °C to give a pale brown powder. A further purification step to remove zirconium residues by dissolving the collected sample in methanol then filtering through 2 cm depth of methanol-washed, oven-dried, celite. The solvent was removed from the filtrate, *in vacuo*, and dried overnight at 70 °C to give the title compound as a pale brown powder (2.68 g, 88%), mp 325 °C (dec) ¹H NMR (600 MHz, DMSO) δ 10.50 (s, 2H), 9.62 (d, *J* = 7.0 Hz, 4H), 8.99 (d, *J* = 6.5 Hz, 4H), 7.55 (d, *J* = 8.0 Hz, 2H), 7.32 (d, *J* = 8.0 Hz, 2H), 7.29 (s, 2H), 7.16 (d, *J* = 8.0 Hz, 2H), ¹³C NMR (151 MHz, CD₃OD) δ 150.0, 147.2, 143.1, 138.4, 131.2, 129.9, 127.2, 121.9, 48.0. IR ν_{\max} /cm⁻¹ 812 (C-H), 3405 (O-H). HRMS [ES⁺] 341.1290, C₂₂H₁₈N₂O₂⁺ requires 341.1291, [M-H]¹⁺. HPLC Purity (UV) = 98%, *t*_R 12.7 min.

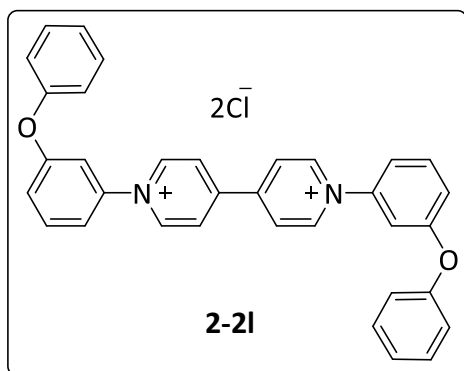
Synthesis of *N,N'*-di[4-(3-benzonitrile)]-[4,4'-bipyridin]-1,1'-dium dichloride 2-2k



1-2 (0.18 g, 3.16 mmol) was slowly added to melted aminobenzonitrile **2-1k** (1.027 g, 8.69 mmol) and stirred on a hotplate with a magnetic stirrer bar until the mixture until the stirrer bar was immobilised.

The crude product was dissolved in methanol then added dropwise to cold (-20 °C) ethyl acetate (150 mL). This was filtered and washed with cold ethyl acetate then air dried overnight to give a beige powder, (0.734 g, 64%), mp 342 °C (dec). ¹H NMR (600 MHz, CD₃OD) δ 9.63 (d, *J* = 6.5 Hz, 2H), 8.99 (d, *J* = 6.5 Hz, 2H), 8.46 – 8.43 (m, 1H), 8.29 (dd, *J* = 8.5, 2.5 Hz, 1H), 8.20 (d, *J* = 8.0 Hz, 1H), 8.00 (t, *J* = 8.0 Hz, 1H). ¹³C NMR (151 MHz, CD₃OD) δ 151.0, 146.1, 142.8, 135.3, 131.6, 129.1, 128.4, 127.2, 116.5, 114.4. IR ν_{\max} /cm⁻¹ 1638 (C=C), 2231 (C≡N). HRMS [ES⁺] 360.1390, C₂₄H₁₆N₄⁺ requires 360.1375, [M-H]¹⁺. HPLC Purity (UV) = 95% *t*_R 9.7 min.

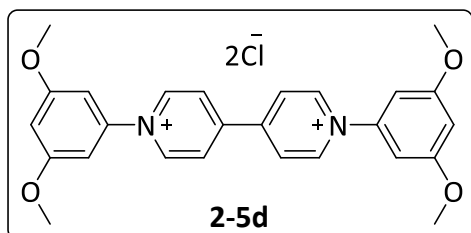
Synthesis of 1,1'-bis[4-(3-phenoxy)]-[4,4'-bipyridin]-1,1'-dium dichloride, 2-2l



The *title compound* was synthesised by following general protocol (I) using **1-2** (0.50 g, 0.89 mmol) added to 3-phenoxyaniline **2-2l** (0.21 g, 1.98 mmol). The crude product was dissolved in methanol (60 mL), then added, dropwise, into stirred, cold (-20 °C) EtOAc (150 mL). After filtering the solid was washed with further cold EtOAc then dried overnight, *in vacuo*, at 70 °C to give a

brown powder. Further purification, to remove zirconium residues, was achieved by dissolving the collected impure sample in methanol, filtering it through a 2 cm depth of methanol-washed, oven-dried, celite. The solvent was removed from the filtrate, *in vacuo*, and dried overnight at 70 °C to give the title compound as a metallic yellow/gold powder (0.220 g, 44% yield), mp 326-328°C (dec). ¹H NMR (600 MHz, CD₃OD) δ 9.53 – 9.52 (m, 4H), 8.86 – 8.84 (m, 4H), 7.74 (t, *J* = 8.0 Hz, 2H), 7.61 – 7.59 (m, 2H), 7.56 (s, 2H), 7.48 – 7.42 (m, 4H), 7.39 – 7.34 (m, 2H), 7.24 (tt, *J* = 7.5, 1.0 Hz, 2H), 7.16 (dt, *J* = 7.5, 1.0 Hz, 4H). ¹³C NMR (151 MHz, CD₃OD) δ 159.3, 155.6, 150.6, 145.8, 143.7, 131.8, 130.1, 127.1, 124.6, 120.8, 118.5, 113.9. IR ν_{\max} /cm⁻¹ 1216 (C-N), 1586 (C=C). HRMS [ES⁺] 493.1911, C₃₄H₂₅N₂O₂⁺ requires 493.1897 [M-H]¹⁺. HPLC Purity (UV) = 95.4% *t*_R 17.2 min.

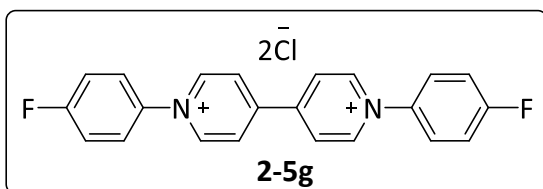
Synthesis of *N,N'*-bis[4-(2,5-dimethoxyphenyl)]-4,4' bipyridinium Dichloride 2-5d



The *title compound* was synthesized by following general protocol (I) using **1-2** (0.50 g, 0.89 mmol) with 3,5-dimethoxyaniline **2-4d** (0.30 g, 1.96 mmol) to give the titled compound as a sand-coloured powder (0.20 g, 87% yield). ¹H NMR (600 MHz, CD₃OD) δ 9.55 (d, *J* = 6.0

Hz, 4H), 8.88 (d, *J* = 6.5 Hz, 4H), 7.09 (s, 4H), 6.90 (s, 2H), 3.94 (s, 12H), mp 332 °C (dec). ¹³C NMR (151 MHz, CD₃OD) δ 162.6, 145.4, 149.7, 135.5, 126.8, 125.5, 115.4, 55.2. IR ν_{\max} /cm⁻¹ 1064 (C-O), 1339 (C-N), 1164. HRMS [ES⁺] found 429.1809, C₂₆H₂₅O₄N₂⁺ requires 429.1802, [M-H]¹⁺ (in agreement with the lit.¹²⁶) HPLC Purity (UV) = 94%, *t*_R 9.8 min.

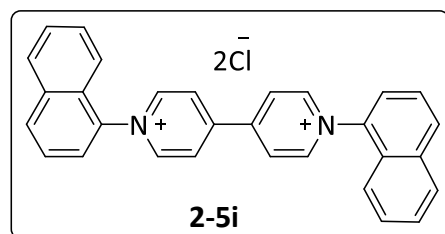
Synthesis of 1,1'-bis(4-fluoro)-[4,4'-bipyridin]-1,1'-dium dichloride **2-5g**



The *title compound* was synthesised by following general protocol (II) using **1-2** (0.50 g, 0.89 mmol) added 4-fluoroaniline **2-4g** (0.36 g, 1.98 mmol).

The crude product was dissolved in warm methanol (10 mL), then precipitated out into EtOAc (30 mL). After filtration it was washed with ethyl acetate (50 mL). The solid was triturated in THF (100 mL) then filtered and air-dried overnight giving a beige powder (0.18 g, 49% yield), mp 331 °C (dec). ¹H NMR (600 MHz, CD₃OD) δ 9.56 (d, *J* = 6.0 Hz, 4H), 8.93 (d, *J* = 6.0 Hz, 4H), 8.01 (dd, *J* = 9.0, 4.5 Hz, 4H), 7.57 (t, *J* = 8.5 Hz, 4H). ¹³C NMR (151 MHz, CD₃OD) δ 163.6 (d, ¹*J*_{CF} = 252 Hz), 150.4, 145.9, 138.8, 127.1, 126.8 (d, ³*J*_{CF} = 11 Hz), 117.2 (d, ²*J*_{CF} = 24 Hz). IR *v*_{max} /cm⁻¹ 812 (C-H), 1241 (C-F). HRMS [ES⁺] 346.1282, C₂₂H₁₆F₂N₂²⁺ requires 346.1270 [M]⁺. HPLC Purity (UV) = 95%, *t*_R 19.0 min.

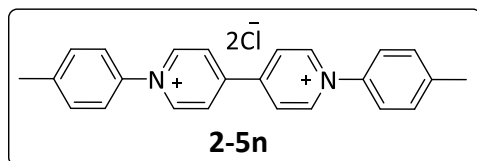
Synthesis of *N,N'*-bis[4-(1-naphthyl)]-4,4' bipyridinium Dichloride **2-5i**



The *title compound* was synthesised by following general protocol (I) using **1-2** (0.50 g, 0.89 mmol) with 1-naphthylamine **2-4i** (0.28 mg, 1.96 mmol) with an oscillation time of 20 min, to give a yellow-brown powder (0.31 g, 75%), mp 247 – 248 °C (dec.), ¹H NMR (600 MHz,

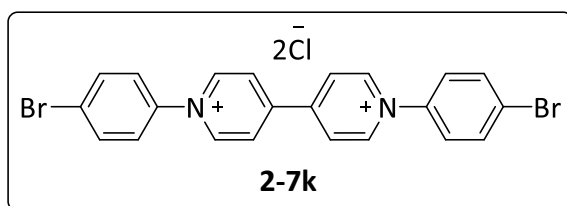
CD₃OD) δ 9.68 – 9.56 (m, 4H), 9.08 – 9.03 (m, 4H), 8.37 (d, *J* = 8.5 Hz, 2H), 8.28 – 8.15 (m, 2H), 8.03 (dd, *J* = 7.5, 1.0 Hz, 2H), 7.84 (dd, *J* = 8.5, 7.5 Hz, 2H), 7.77 (tt, *J* = 7.0, 5.5 Hz, 4H), 7.64 – 7.54 (m, 2H). ¹³C NMR (151 MHz, CD₃OD) δ 159.3, 149.7, 145.5, 143.3, 138.6, 133.4, 133.1, 131.4, 129.8, 129.7, 128.4, 124.4, 121.8. IR *v*_{max} /cm⁻¹ 799 (C=C), 1251 (C-N), 2850 (C-H). HRMS [ES⁺] found 409.1712, C₃₀H₂₂N₂⁺ requires 409.1699, [M-H]¹⁺ (in agreement with the lit.¹²⁷) HPLC Purity (UV) = 99+%, *t*_R 3.4 min.

Synthesis of *N,N'*-bis(4-methylphenyl)-4,4'-bipyridinium Dichloride **2-5n**



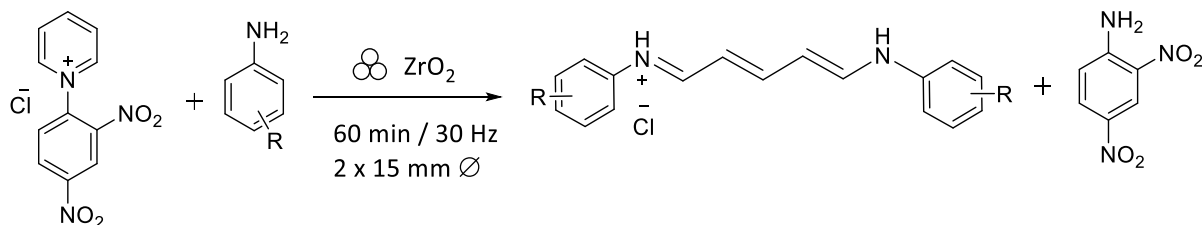
The *title compound* was synthesized by following general protocol (I) using **1-2** was added to *p*-toluidine **2-4n** (236 mg, 2.20 mmol). The title compound was isolated as a pale brown powder by reverse phase C18 (43 g) column chromatography with THF and acetonitrile 70:30 (v/v) $R_f = 0.4$). (82 mg, 20%), mp 291 °C (dec). $^1\text{H NMR}$ (600 MHz, $\text{DMSO-}d_6$) δ 9.66 (d, $J = 6.5$ Hz, 4H), 9.05 (d, $J = 6.5$ Hz, 4H), 7.85 (d, $J = 8.0$ Hz, 4H), 7.58 (d, $J = 8.0$ Hz, 4H), 3.37 (s, 6H). $^{13}\text{C NMR}$ (151 MHz, Acetonitrile- d_3) δ 218.6, 150.0, 145.5, 143.2, 131.1, 124.2, 127.2, 20.3. IR ν_{max} / cm^{-1} 823 (C-H bending). HRMS [ES $^+$] found 337.700, $\text{C}_{24}\text{H}_{21}\text{N}_2^+$ requires 337.1699, [M-H] $^{1+}$.

Synthesis of 1,1'-bis(4-bromo)-[4,4'-bipyridin]-1,1'-dium dichloride **2-7k**

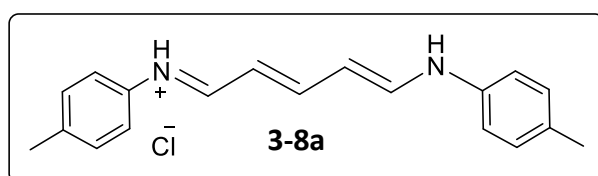


The *title compound* was synthesised using **1-2** 1,1'-bis(2,4-dinitrophenyl)-4,4'-bipyridinium dichloride (0.55 g, 1.96 mmol) was added slowly to melted 4-bromoaniline **2-6k** (1.04 g, 6.07 mmol) and stirred on a hotplate with a magnetic stirrer bar until the mixture was too thick to stir, forming a dark brown paste. The product was dissolved in methanol. The crude solution was added dropwise to cold (-20 °C) EtOAc (150 mL). It was filtered then washed with cold ethyl acetate and air dried overnight giving a yellow-brown powder (0.53 g, 51%), mp 326 °C (dec.). $^1\text{H NMR}$ (600 MHz, CD_3OD) δ 9.57 (d, $J = 6.5$ Hz, 2H), 8.93 (d, $J = 6.5$ Hz, 2H), 7.99 (d, $J = 8.5$ Hz, 2H), 7.88 (d, $J = 8.5$ Hz, 2H). $^{13}\text{C NMR}$ (151 MHz, D_2O) δ 150.6, 145.3, 141.1, 133.6, 127.1, 126.0, 125.7. IR ν_{max} / cm^{-1} 163 (C=C), 522 (C-Br). HRMS [ES $^+$] 233.9830, $\text{C}_{22}\text{H}_{16}\text{Br}_2\text{N}_2^{2+}$ requires 233.9825. HPLC Purity (UV) = 95% t_R 14.3 min.

General procedure for cyanine-5 chloride salts, 3-8a-g



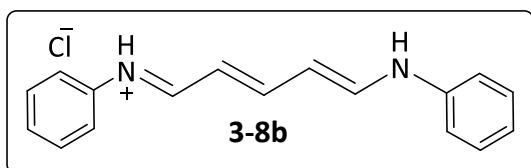
Synthesis of 5-anilino-N-p-tolyl -2,4-pentadienyldeniminium chloride. 3-8a



1-(2,4-Dinitrophenyl)pyridinium chloride (2.26 g, 8.01 mmol) was added to p-toluidine (1.72 g, 16.0 mmol) and oscillated for a total of 60 minutes at 30 Hz in 25 mL

zirconium oxide jars with two, 15 mm diameter zirconium oxide balls. The crude was extracted from the reaction vessels by dissolving in methanol (30-40 mL) and heated until all the solid dissolved. In a separate 500 mL round bottom flask, diethyl ether (300 mL) were warmed to 36 °C with stirring. The crude solution was gradually added to the diethyl ether using a Pasteur pipette, forming a precipitate which was hot filtered through a warm glass frit to give a red powder (2.46 g, 99%), mp 141 °C (in agreement with lit.²³⁹). ¹H NMR (600 MHz, CD₃OD) δ 8.34 (d, *J* = 11.5 Hz, 2H), 7.83 (t, *J* = 12.5 Hz, 1H), 7.25 (d, *J* = 8.0 Hz, 4H), 7.20 (d, *J* = 8.5 Hz, 4H), 6.25 (app t, *J* = 12.0 Hz, 2H), 2.34 (s, 6H, ¹³C NMR (151 MHz, CD₃OD) δ 163.5, 154.8, 136.3, 136.0, 130.1, 116.9, 108.6, 19.5. IR ν_{max} /cm⁻¹ 817 (C-H), 1013 (C-N), HRMS [ES⁺] 277.1705, C₁₉H₂₁N₂ requires 277.1716, HPLC Purity (UV) = 99+%, *t*_R 20.3 min.

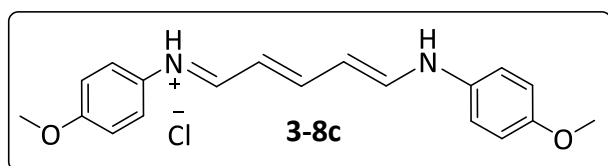
Synthesis of 5-anilino-N-phenyl -2,4-pentadienyldeniminium chloride. 3-8b



1-(2,4-Dinitrophenyl)pyridinium chloride **1-1** (2.26 g, 8.00 mmol) was added to aniline (1.49 g, 16.0 mmol) and oscillated for 60 minutes at 30 Hz in a zirconium oxide jar (25 mL) containing two,

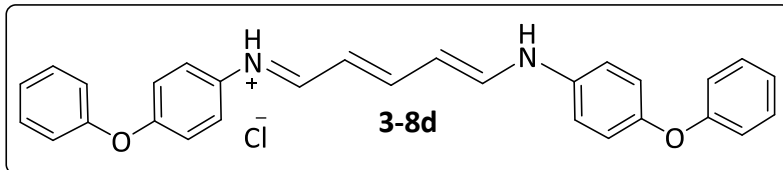
zirconium oxide balls (15 mm dia.). The crude reaction mixture was dissolved in warm, stirred methanol (40 mL). The solution was added dropwise with stirring to warm (36 °C) diethyl ether (300 mL). The precipitated solid was filtered using a warm glass frit to give the title compound (2.46 g, 99%) as a carmine solid, mp 121 °C (lit. 146-147 °C)¹⁴². ¹H NMR (600 MHz, CD₃OD) δ 8.42 (d, *J* = 11.5 Hz, 2H), 7.90 (dd, *J* = 13.0 Hz, 1H), 7.44 (t, *J* = 8.0 Hz, 4H), 7.33 (d, *J* = 8.0 Hz, 4H), 7.25 (t, *J* = 7.5 Hz, 2H), 6.31 (dd, *J* = 12.0 Hz, 2H). ¹H NMR (600 MHz, *d*₆-DMSO) δ 12.04 (s, 2H), 8.59 (d, *J* = 11.5 Hz, 2H), 7.82 (t, *J* = 13.0 Hz, 1H), 7.43 (d, *J* = 4.5 Hz, 8H), 7.21 (q, *J* = 4.5 Hz, 2H), 6.34 (t, *J* = 12.0 Hz, 2H), 2.06 (s, 2H). ¹³C NMR (151 MHz, CD₃OD) δ 162.6, 149.7, 145.4, 126.8, 125.5, 115.4, 55.2. IR ν_{max} /cm⁻¹ 1331 (C-N), 1631 (C=C). HRMS [ES⁺] found 249.1404, C₁₇H₁₇N₂ requires 249.1392. HPLC Purity (UV) = 95%, *t*_R 12.6 min.

Synthesis of 5-anilino-*N*-*p*-aniso-2,4-pentadienylideniminium chloride. 3-8c



1-(2,4-Dinitrophenyl)pyridinium chloride, **1-1** (0.600 g, 2.13 mmol) was added to *p*-anisidine **3-1c** (0.551 g, 4.47 mmol) and mechanically activated for 15 minutes at 30 Hz in 25 mL tungsten carbide jars with two, 15 mm diameter tungsten carbide balls. The crude product was extracted from the reaction vessels by dissolving with methanol (20 mL). Precipitation was carried out by adding the red reaction mix, drop-wise, into stirred, cold (-20°C) ethyl acetate (100mL). The collected solid was then heated, under reflux, in diethyl ether (200 mL), with vigorous stirring for an hour. The purified solid was collected while still warm by filtering through a warm glass frit to yield **3-8c**, a maroon solid (0.663 g, 91%), mp 132.9 °C (lit.²⁴⁰ mp 150-151 °C), ¹H NMR (600 MHz, Methanol-*d*₄) δ 8.25 (d, *J* = 11.5 Hz, 2H), 7.78 (t, *J* = 13.0 Hz, 1H), 7.25 (d, *J* = 8.5 Hz, 4H), 6.98 (d, *J* = 8.5 Hz, 4H), 6.22 (t, *J* = 12.0 Hz, 2H), 3.80 (s, 6H). ¹³C NMR (151 MHz, CD₃OD) δ 54.6, 108.2, 114.8, 118.4, 132.0, 158.1, 154.3, 162.5. IR ν_{max} /cm⁻¹ 1164 (C-O), 2830 (N-H). HRMS [ESI⁺] 309.1594, C₁₉H₂₁N₂O₂⁺ requires 309.1603. HPLC Purity (UV) = 99% *t*_R 18.8 min.

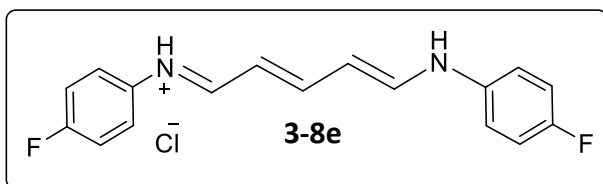
Synthesis of 5-anilino-N-4-phenoxy-2,4-pentadienylideniminium chloride. 3-8d



1-(2,4 Dinitrophenyl)pyridinium chloride, **1-1** (0.60 g, 2.13 mmol) was added to 4-Phenoxyaniline **3-1d** (2.63 g, 14.2 mmol) to give

a maroon powder **3-8d** (3.26 g, 98%), mp 140.5 °C. ¹H NMR (600 MHz, *d*₆-DMSO) δ 12.02 (s, 2H), 8.51 (d, *J* = 12.0 Hz, 2H), 7.75 (app t, *J* = 12.0 Hz, 1H), 7.44 (d, *J* = 8.5 Hz, 4H), 7.41 – 7.37 (m, 4H), 7.13 (t, *J* = 7.5 Hz, 2H), 7.10 – 7.06 (m, 4H), 6.99 (d, *J* = 8.0 Hz, 4H), 6.30 (app t, *J* = 12.0 Hz, 2H), 3.14 (s, 1H). ¹³C NMR (151 MHz, CD₃OD) δ 231.3, 155.0, 130.0, 129.6, 129.6, 128.1, 125.9, 123.5, 119.8, 119.6, 119.6, 118.6, 118.6, 118.3, 108.8. IR *v*_{max} /cm⁻¹ 1149 (C-N), 1239 (C-O). HRMS [ES⁺] 433.1890, C₂₉H₂₅N₂O₂⁺ requires 433.1916, HPLC Purity (UV) = 97%, *t*_R 22.8 min.

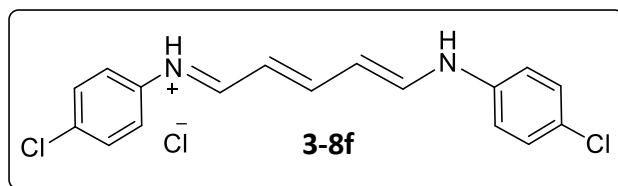
Synthesis of 5-anilino-N-4-fluoro-2,4-pentadienylideniminium chloride. 3-8e



1-(2,4-Dinitrophenyl)pyridinium chloride **1-1** (2.26 g, 8.01 mmol) was added to 4-Fluoroaniline (1.78 g, 16.0 mmol) and oscillated for a total of 60 minutes at 30 Hz

in 25 mL zirconium oxide jars with two, 15 mm diameter zirconium oxide balls. The crude was extracted from the reaction vessels by dissolving in methanol (30-40 mL), heated to and stirred 60 °C to ensure all solids are dissolved. In a separate 250 mL round bottom flask, diethyl ether (300 mL) were warmed to 36 °C with stirring. The crude solution was precipitated gradually into the diethyl ether then hot filtered through a warm glass frit to give a red powder (2.24 g, 87%), mp 124.4 °C (lit.²⁴⁰ 128-129 °C), ¹H NMR (600 MHz, CD₃OD) δ 8.38 (d, *J* = 11.5 Hz, 2H), 7.89 (t, *J* = 13.0 Hz, 1H), 7.36 (dd, *J* = 9.0, 4.5 Hz, 4H), 7.19 (t, *J* = 8.5 Hz, 4H), 6.30 (t, *J* = 12.0 Hz, 2H). ¹³C NMR (151 MHz, CD₃OD) δ 164.4, 161.5, 159.9, 155.7, 135.1, 119.0, 116.3, 108.9. IR *v*_{max} /cm⁻¹ 833 (C=C), 1348 (C-N), (aromatic amine, stretching). HRMS [ES⁺] 285.1190 C₁₇H₁₅F₂N₂, requires 285.1203. HPLC Purity (UV) = 95%, *t*_R 19.0 min.

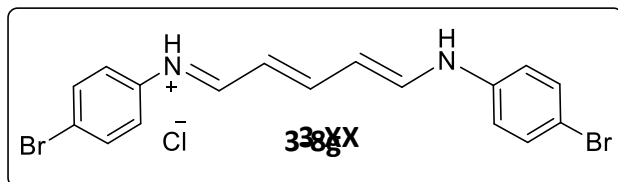
Synthesis of 5-anilino-N-4-chloro-2,4-pentadienylideniminium chloride. 3-8f



1-(2,4-Dinitrophenyl)pyridinium chloride **1-1** (2.72 g, 9.66 mmol) was added to 4-Chloroaniline (2.46 g, 19.3 mmol) and oscillated for a total of 60 minutes at 30 Hz

in 25 mL zirconium oxide jars with two, 15 mm diameter zirconium oxide balls. The crude was extracted from the reaction vessels by dissolving in methanol (30-40 mL). Diethyl ether (150 mL) were added and the mixture was warmed to 45 °C and stirred for an hour. After filtering through a warm frit, the product was recrystallised from toluene (30 mL) and ethanol (5 mL) giving a deep purple crystalline powder (2.11 g, 60%), mp 127.7 °C (Lit.²⁴⁰ 139 °C). ¹H NMR (600 MHz, CD₃OD) δ 8.43 (d, *J* = 11.5 Hz, 2H), 7.91 (t, *J* = 13.0 Hz, 1H), 7.55 – 7.35 (m, 4H), 7.35 – 7.28 (m, 4H), 6.33 (t, *J* = 12.0 Hz, 2H). ¹³C NMR (151 MHz, *d*₆-DMSO) δ 163.7, 156.0, 138.3, 130.5, 130.1, 119.7, 110.3. IR *v*_{max} /cm⁻¹ 832 (C-Cl), 1180 (C-N). HMRS [ES⁺] 404.9592, C₁₇H₁₅Cl₃N₂⁺ requires 404.9602. HPLC Purity (UV) = 99+%, *t*_R 20.0 min.

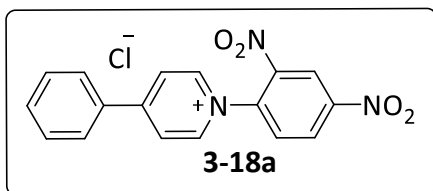
Synthesis of 5-anilino-N-4-bromo-2,4-pentadienylideniminium chloride. 3-8g



1-(2,4-Dinitrophenyl)pyridinium chloride **1-1** (2.72 g, 9.66 mmol) was added to 4-Bromoaniline (2.46 g, 19.3 mmol) were reacted as per general procedure (III). The

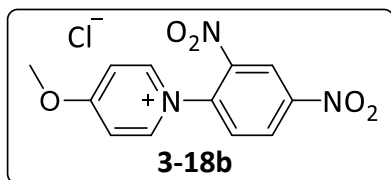
precipitate was recrystallised from toluene (30 mL) and ethanol (5 mL) to give the *title compound* as a deep purple powder (2.60 g, 66%) mp 127.7 °C. ¹H NMR (600 MHz, *d*₆-DMSO) δ 12.08 (s, 2H), 8.60 (d, *J* = 11.5 Hz, 2H), 7.80 (t, *J* = 13.0 Hz, 1H), 7.62 (d, *J* = 8.5 Hz, 4H), 7.38 (d, *J* = 8.5 Hz, 4H), 6.34 (t, *J* = 12.0 Hz, 2H). ¹³C NMR (151 MHz, *d*₆-DMSO) δ 163.8, 156.0, 138.7, 133.0, 120.0, 118.1, 110.5, 56.5, 19.0. IR *v*_{max} /cm⁻¹ 667 (C-Br), 1172 (C-N). HMRS [M-H]⁺ 404.9592, C₁₇H₁₅Br₂N₂ requires 404.9602. HPLC Purity (UV) = 99+%, *t*_R 20.4 min.

Synthesis of 4-phenyl-1-(2,4-dinitrophenyl) pyridinium chloride, 3-18a



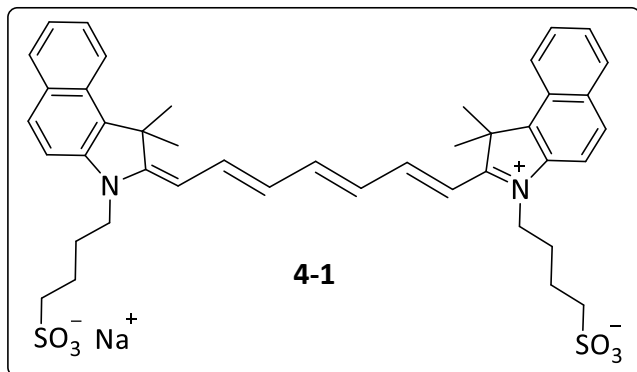
1-chloro-2,4-dinitrobenzene (2.6 g, 13.0 mmol) were added to 4-phenylpyridine (2.01 g, 13 mmol) in acetone (15 mL) and heated to reflux for 24 hours. After cooling to room temperature, the product was filtered and washed with acetone and air-dried to give the *title compound* as a pale brown powder (1.72 g, 37.0% yield), mp 185-186 °C. ¹H NMR (600 MHz, CD₃OD) δ 9.28 (d, *J* = 2.5 Hz, 1H), 9.24 (d, *J* = 6.5 Hz, 2H), 8.93 – 8.90 (m, 1H), 8.71 – 8.68 (m, 2H), 8.33 (d, *J* = 8.5 Hz, 1H), 8.17 (dd, *J* = 7.0, 2.0 Hz, 2H), 7.72 (dt, *J* = 14.5, 7.0 Hz, 3H), in agreement with the lit.¹⁷² ¹³C NMR (151 MHz, *d*₆-DMSO) δ 157.8, 149.5, 146.4, 143.6, 139.0, 133.6, 133.5, 132.5, 130.7, 130.4, 129.2, 124.5, 121.9. IR ν_{max} /cm⁻¹ 1338 (C-N), 1533 (N-O), HRMS [ES⁺] 322.0842, C₁₇H₁₂N₃O₄⁺ requires 322.0828. HPLC Purity (UV) = 99%, *t*_R 16.5 min.

Synthesis of 1-(2,4-dinitrophenyl) pyridinium 4-methoxy chloride, 3-18b



1-chloro-2,4-dinitrobenzene (1.88 g, 9.28 mmol) were added to 4-methoxypyridine (1.00 g, 9.16 mmol) in diethyl ether (15 mL) and heated to reflux for 24 hours. After cooling to room temperature, the product was filtered and washed with diethyl ether through a glass frit then dried in the oven at 60-80 °C to give the *title compound* as a pale yellow solid (2.036 g, 81%), mp 136 - 138 °C, (in agreement with the lit.¹⁷²) ¹H NMR (600 MHz, *d*₆-DMSO) δ 9.13 (d, *J* = 7.0 Hz, 2H), 9.07 (d, *J* = 2.5 Hz, 1H), 8.90 (dd, *J* = 8.5, 2.5 Hz, 1H), 8.33 (d, *J* = 8.5 Hz, 1H), 7.89 (d, *J* = 7.0 Hz, 2H), 4.21 (s, 3H). ¹³C NMR (151 MHz, CD₃OD) δ 173.8, 149.4, 146.7, 143.5, 138.5, 131.5, 129.5, 121.7, 113.1, 58.1. IR ν_{max} /cm⁻¹ 1522 (N-O), 1209 (C-O). HRMS [ES⁺] 276.0633, C₁₂H₁₀N₃O₅⁺ requires 276.0620. HPLC Purity (UV) = 99% *t*_R 13.2 min.

Synthesis of sodium;4-[(2Z)-2-[(2E,4E,6E)-7-[1,1-dimethyl-3-(4-sulfonatobutyl)benzo[e]indol-3-ium-2-yl]hepta-2,4,6-trienylidene]-1,1-dimethylbenzo[e]indol-3-yl]butane-1-sulfonate, ICG, 4-1



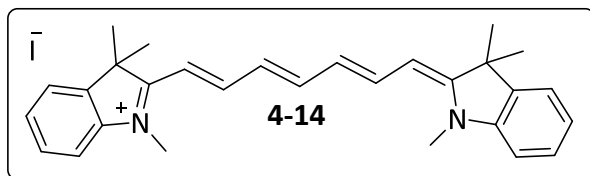
Following general protocol (I) 1-(2,4-Dinitrophenyl) pyridinium chloride (0.20 g, 0.70 mmol) **1-1**, 4-(1,1,2-trimethyl-1H-benzo[e]indolium-3-yl)butane-sulfonate (0.54 g, 1.56 mmol) **4-19**, 4-bromoaniline (0.25 g, 1.96 mmol) **3-8g** and sodium acetate (0.26 g, 3.12 mmol) were oscillated for 120 minutes at 30 Hz in ZrO₂ jars (25 mL) with two ZrO₂ balls (15 mm Ø). The product was dissolved in methanol (30 mL) and diethyl ether (90 mL) were added. It was kept in the freezer (-20 °C) overnight. After filtration through a chilled, glass frit, the collected solid (0.9 g) was added to acetonitrile and heated to reflux (74 °C) for an hour and cooled slowly to room temperature then filtered and washed with acetone. Three further purification attempts were conducted by dissolving in water and recrystallizing from acetone to yield *the title compound* (**4-1**) as a green solid (0.161 g, 29%), mp 235 °C. ¹H NMR (600 MHz, CD₃OD) δ 8.20 (d, *J* = 8.5 Hz, 2H), 8.07 – 7.90 (m, 6H), 7.60 (dd, *J* = 8.5, 6.5 Hz, 4H), 7.44 (t, *J* = 7.5 Hz, 2H), 6.59 (d, *J* = 14.5 Hz, 2H), 6.41 – 6.30 (m, 2H), 4.22 (t, *J* = 7.5 Hz, 4H), 2.90 (t, *J* = 7.0 Hz, 4H), 1.99 (d, *J* = 10.5 Hz, 4H), 1.96 (s, 12H), (in agreement with the lit.²⁰⁰). ¹³C NMR (151 MHz, CD₃OD) δ 179.0, 172.9, 150.7, 139.7, 133.3, 131.9, 130.3, 129.7, 128.1, 127.2, 124.5, 121.9, 110.7, 50.7, 50.4, 43.5, 26.2, 22.8, 22.1. HPLC Purity (UV) = 81%, t_R 20.8 min.

Using General Procedure (II) - 1-(2,4-Dinitrophenyl) pyridinium chloride (0.245 g, 0.9 mmol), 4-(1,1,2-trimethyl-1H-benzo[e]indolium-3-yl)butane-sulfonate **1-1** (0.60 g, 1.7 mmol), 4-bromoaniline **3-8g** (0.232 g, 1.35 mmol) and sodium acetate (0.095 g, 3.60 mmol) were added together in a flat-bottomed conical flask (100 mL) with a 2 cm pivoted magnetic stirrer bar. It was placed on a RT hotplate set to (85 °C) and the stirrer switched on. The pale coloured reagents at RT changed to a deep green mixture within 60 seconds on the hotplate. The stirrer

was immobilised by the reaction mixture at 72 °C and the mixture was manually stirred with a steel spatula. After a further four min on the hotplate, the flask was removed from the heat. The crude product (1.37 g) was purified using silica gel (12 g) column chromatography with MeOH and chloroform gradient (8:2) to give the *title compound 4-1* as a deep green solid (0.50 g, 65%). ¹H NMR (600 MHz, CD₃OD) δ 8.21 (d, *J* = 9.0 Hz, 2H), 7.97 (dd, *J* = 13.1, 8.5 Hz, 6H), 7.61 (dd, *J* = 8.5, 5.5 Hz, 5H), 7.45 (t, *J* = 7.5 Hz, 2H), 6.62 (s, 2H), 6.37 (d, *J* = 13.5 Hz, 2H), 4.23 (t, *J* = 7.5 Hz, 4H), 2.91 (t, *J* = 7.0 Hz, 4H), 2.04 – 1.96 (m, 20H), (in agreement with lit.²⁰³). ¹³C NMR (151 MHz, CD₃OD) δ 172.9, 155.8, 150.7, 139.8, 133.3, 131.9, 130.3, 129.7, 128.1, 127.2, 124.5, 121.9, 110.7, 103.1, 50.7, 50.4, 43.5, 26.2, 22.1, 19.4. HPLC Purity (UV) = 91%, *t*_R 16.8 min.

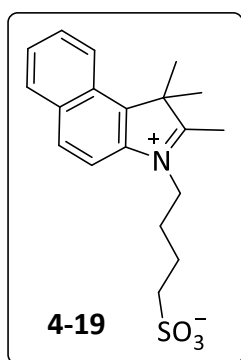
Using Single Screw Extrusion: 1-(2,4-Dinitrophenyl) pyridinium chloride **1-1** (14.3 g, 50.1 mmol), 4-(1,1,2-trimethyl-1H-benzo[e]indolium-3-yl)butane-sulfonate **4-19** (35.0 g, 101 mmol), 4-bromoaniline **3-8g** (13.0 g, 75.2 mmol) and sodium acetate (33.1 g, 404 mmol) were pre-mixed in a Kenwood mini-chopper for one min using 5-second bursts. The SSE extruder, the Filafab 350 PRO EX was preheated to 85°C, with the screw rotation set to 25 rpm. All the contents from the mini-chopper were poured into the extruder's hopper. 90 g of crude were extruded in 19 min. A portion of the crude (0.69 g) was purified using silica gel (24 g) column chromatography with chloroform and MeOH gradient (8:2) to give the *title compound 4-1* as a deep green-black solid (0.50 g, 72%) and linear yield 64% (0.89 x 0.72 x 100). ¹H NMR (600 MHz, CD₃OD) δ 8.14 (d, *J* = 8.0 Hz, 2H), 7.91 (dd, *J* = 21.7, 8.5 Hz, 6H), 7.56 (d, *J* = 7.0 Hz, 5H), 7.40 (q, *J* = 7.6, 7.0 Hz, 2H), 6.55 (s, 2H), 6.30 (d, *J* = 14.0 Hz, 2H), 4.18 (s, 4H), 2.92 (s, 4H), 1.98 (s, 8H), 1.87 (s, 12H), (in agreement with the lit.¹⁹⁷) ¹³C NMR (151 MHz, CD₃OD) δ 173.0, 150.7, 139.8, 133.4, 131.9, 130.3, 129.7, 128.1, 127.2, 125.8, 124.4, 122.6, 121.9, 110.7, 103.2, 50.7, 50.4, 43.5, 26.2, 26.0, 22.1. IR *v*_{max} /cm⁻¹ 781, 836 (C-H), 1338 (C-N). HRMS [ES+] 773.2709, C₄₃H₄₇N₂O₆S₂⁻¹ requires 773.2695. HPLC Purity (UV) = 97%, *t*_R 16.9 min.

Synthesis of 1,1',3,3,3',3'-hexamethyl-2,2'-indotricarbocyanine iodide, HITCI - 1,3,3-Trimethyl-2-((1E,3E,5E)-7-((E)-1,3,3-trimethylindolin-2-ylidene)hepta-1,3,5-trien-1-yl)-3H-indol-1-ium Iodide, 4-14



Following General Procedure (I) 5-anilino-N-bromo-2,4-pentadienylideniminium chloride **3-8g** (0.298 g, 0.734 mmol) and (1,2,3,3-tetramethyl-3H-indolium iodide (0.283 g, 1.624 mmol) were added to sodium acetate (0.132, 1.609 mmol) and oscillated for 135 minutes. The crude product was dissolved in methanol (25 mL). Diethyl ether (70 mL) was added and the solution was placed in the freezer (-20 °C) overnight. After filtration through a chilled glass frit the solid was washed with diethyl ether to give *the title compound 4-14* as bright green fine needles (0.174 g, 44%), mp 212 °C, in agreement with Štacková *et al.*¹⁶⁴, ¹H NMR (600 MHz, CD₃OD) δ 7.92 (t, *J* = 13.0 Hz, 2H), 7.58 (s, 1H), 7.46 (d, *J* = 7.5 Hz, 2H), 7.39 (td, *J* = 7.5, 1.0 Hz, 2H), 7.27 – 7.20 (m, 4H), 6.54 (t, *J* = 12.5 Hz, 2H), 6.25 (d, *J* = 14.0 Hz, 2H), 3.58 (s, 6H), 1.68 (s, 12H). ¹³C NMR (151 MHz, CD₃OD) δ 172.4, 151.5, 143.0, 140.9, 131.3, 128.3, 125.6, 124.5, 121.8, 116.5, 103.4, 48.8, 30.0, 26.5, HRMS [ES⁺] 409.2652, C₂₉H₃₃N₂ requires 409.2644. IR ν_{max} /cm⁻¹ 790 (C-H), 994 (C=C), HPLC Purity (UV) = 99+%, *t_R* 24.1 min.

Synthesis of Trimethyl-1-(4-sulfobutyl)-indolium inner salt 4-19



1,1,2-trimethyl-1H-benzo[e]indole (12.71 g, 60.7 mmol) were poured into a 500 mL round-bottomed flask. 1,4-Butane sultone (8.27 g, 60.7 mmol) was added and heated to reflux for 30 minutes with vigorous stirring until the stirrer bar could no longer move. While warm, DCM (400 mL) was added to creating a slurry and stirred while it cooled for 4 h to RT. After filtration the solid was washed again with DCM (400 mL), with stirring, then filtered and washed with DCM through a glass frit. It was dried overnight under high vacuum at 65 °C to give the title compound **4-19** as a lilac powder (18.4 g, 88%) mp 264 -265 °C (lit.²⁴¹ 263 °C), ¹H NMR (600 MHz, *d*₆-DMSO) δ 8.34 (d, *J* = 8.5 Hz, 1H), 8.25 (d, *J* = 9.0 Hz, 1H), 8.18 (dd, *J* = 8.7, 4.0 Hz, 2H), 7.75 (ddd, *J* = 8.5, 6.5, 1.5 Hz, 1H), 7.70

(ddd, $J = 8.0, 7.0, 1.0$ Hz, 1H), 4.58 (t, $J = 8.0$ Hz, 2H), 2.92 (s, 3H), 2.51 (s, 2H), 2.00 (p, $J = 7.5$ Hz, 2H), 1.76 (q, $J = 7.5$ Hz, 2H), 1.72 (s, 6H). ^{13}C NMR (151 MHz, CD_3OD) δ 197.6 139.9, 138.2, 134.3, 131.9, 131.0, 129.6, 128.5, 124.7, 115.2, 114.8, 56.7, 51.4, 48.8, 27.5, 23.4, 22.8, 22.0, 14.9. IR $\nu_{\text{max}}/\text{cm}^{-1}$ 1031 (S=O), 1190 (C-N), HRMS $[\text{ES}^+]$ 346.1461, $\text{C}_{19}\text{H}_{23}\text{NO}_3\text{S}$ requires 346.1477, HPLC Purity (UV) = 99%, t_{R} 14.2 min.

Bibliography

- 1 A. A. L. Michalchuk, E. V. Boldyreva, A. M. Belenguer, F. Emmerling and V. V. Boldyrev, *Front. Chem.*, 2021, **9**, 1–29.
- 2 N. R. Rightmire and T. P. Hanusa, *Dalt. Trans.*, 2016, **45**, 2352–2362.
- 3 R. R. A. Bolt, J. A. Leitch, A. C. Jones, W. I. Nicholson and D. L. Browne, *Chem. Soc. Rev.*, 2022, **51**, 4243–4260.
- 4 S. Begin-Colin, G. Le Caër, M. Zandona, E. Bouzy and B. Malaman, *J. Alloys Compd.*, 1995, **227**, 157–166.
- 5 R. Thorwirth, A. Stolle and B. Ondruschka, *Green Chem.*, 2010, **12**, 985–99.
- 6 A. Stolle, B. Ondruschka, W. Hopfe and W. Simon, 2011, 7–11.
- 7 C. Suryanarayana, *Prog. Mater. Sci.*, 2001, **46**, 1–184.
- 8 S. L. James, C. J. Adams, C. Bolm, D. Braga, P. Collier, T. Friščic, F. Grepioni, K. D. M. Harris, G. Hyett, W. Jones, A. Krebs, J. Mack, L. Maini, A. G. Orpen, I. P. Parkin, W. C. Shearouse, J. W. Steed and D. C. Waddell, *Chem. Soc. Rev.*, 2012, **41**, 413–447.
- 9 S. M. Hsu, J. Zhang and Z. Yin, *Tribol. Lett.*, 2002, **13**, 131–139.
- 10 I. Hwang, C.-Y. Kang and J.-B. Park, *J. Pharm. Investig.*, 2017, **47**, 123–132.
- 11 S. Li, T. Yu, Y. Tian, C. P. McCoy, D. S. Jones and G. P. Andrews, *Mol. Pharm.*, 2016, **13**, 3054–3068.
- 12 M. Maniruzzaman, *Pharmaceutics*.
- 13 G. Kaupp, *CrystEngComm*, 2009, **11**, 388–403.
- 14 A. Hadjiafxenti, I. E. Gunduz, T. Kyratsi, C. C. Doumanidis and C. Rebholz, *Vacuum*, 2013, **96**, 73–78.
- 15 P. G. B. T.-H. on the P. and C. of R. E. McCormick, Elsevier, 1997, vol. 24, pp. 47–81.
- 16 M. I. Florez-Zamora, C. A. Martínez-Pérez, M. García-Guaderrama, I. Estrada-Guel, F. Espinosa-Magaña and R. Martínez-Sánchez, *Rev. Adv. Mater. Sci.*, 2008, **18**, 301–304.
- 17 E. Bajramović, M. Jurković, D. Gačo, E. Bajramović and E. Bajramović, eds. N. Ademović, E. Mujčić, Z. Akšamija, J. Kevrić, S. Avdaković and I. Volić, Springer International Publishing, Cham, 2022, pp. 337–347.

- 18 G. Ayoub, B. Karadeniz, A. J. Howarth, O. K. Farha, I. Đilović, L. S. Germann, R. E. Dinnebier, K. Užarević and T. Friščić, *Chem. Mater.*, 2019, **31**, 5494–5501.
- 19 L. Takacs, *Acta Phys. Pol. A*, 2014, **126**, 1040–1043.
- 20 J. L. Howard, Q. Cao and D. L. Browne, *Chem. Sci.*, 2018, **9**, 3080–3094.
- 21 Y. Chen, G. Mellot, D. Van Luijk, C. Creton and R. P. Sijbesma, *Chem. Soc. Rev.*, 2021, **50**, 4100–4140.
- 22 T. Friščić, C. Mottillo and H. M. Titi, *Angew. Chemie - Int. Ed.*, 2020, **59**, 1018–1029.
- 23 L. Takacs, *Bull. Hist. Chem.*, 2003, **28**, 26–34.
- 24 B. P. Hutchings, D. E. Crawford, L. Gao, P. Hu and S. L. James, *Angew. Chemie - Int. Ed.*, 2017, **56**, 15252–15256.
- 25 D. C. James, Stuart L., Adams, C. J, Bolm, C., Braga, D., Collier, P., Friščić, T., Grepioni, F., Harris, K. D. M., Hyett, G. Jones, W. C., Krebs. A., Mack, J., Mani, L., Orpem, A. G., Parkin, I. P., Shearouse, W. C., Steed, J. W. Waddell, *Chem. Soc. Rev.*, 2013, **44**, 0–78.
- 26 D. Tan and T. Friščić, *European J. Org. Chem.*, 2018, **2018**, 18–33.
- 27 F. Komatsi, Koichi; Kitigawa, Toshikazu; Mori, Sadayuki; Nishinaga, Tohru; Murata, Yasujiro; Cheng, *Organic Materials Chemistry -High-Pressure Organic Chemistry- Scope of Research Research Activities, 2001*, .
- 28 A. M. Omer, *Renew. Sustain. Energy Rev.*, 2008, **12**, 2265–2300.
- 29 F. C. Menz and H. M. Seip, *Env. Sci Policy*, 2004, **7**, 253–265.
- 30 F. Geiger, J. Bengtsson, F. Berendse, W. W. Weisser, M. Emmerson, M. B. Morales, P. Ceryngier, J. Liira, T. Tschardtke, C. Winqvist, S. Eggers, R. Bommarco, T. Pärt, V. Bretagnolle, M. Plantegenest, L. W. Clement, C. Dennis, C. Palmer, J. J. Onate, I. Guerrero, V. Hawro, T. Aavik, C. Thies, A. Flohre, S. Hanke, C. Fischer, P. W. Goedhart and P. Inchausti, *Basic Appl. Ecol.*, 2010, **11**, 97–105.
- 31 M. Eriksen, L. C. M. Lebreton, H. S. Carson, M. Thiel, C. J. Moore, J. C. Borerro, F. Galgani, P. G. Ryan and J. Reisser, *PLoS One*.
- 32 J. Ding, C. Zheng, L. Wang, C. Lu, B. Zhang, Y. Chen, M. Li, G. Zhai and X. Zhuang, *J. Mater.Chem. A*, 2019, **7**, 23337–23360.
- 33 P. Anastas and N. Eghbali, *Chem. Soc. Rev.*, 2010, **39**, 301–312.

- 34 K. Wright, *Paléorient*, 1991, **17**, 19–45.
- 35 R. Shimelmitz, I. Groman-Yaroslavski, M. Weinstein-Evron and D. Rosenberg, *J. Hum. Evol.*, 2021, **150**, 102909.
- 36 L. Takacs, *J. Met.*, 2000, 12–13.
- 37 D. E. Eichholz, *Theophrastus de Lapidibus*, Oxford University Press, Oxford, 1965.
- 38 K. Tanaka and F. Toda, *Chem. Rev.*, 2000, **100**, 1025–1074.
- 39 W. Zincke, Th.; Heuser, G.; Moller, Zincke salt synthesis, <https://www.reaxys.com/>, (accessed 17 November 2021).
- 40 L. G. Wade and W. J. Simek, *Organic Chemistry*, Pearson, 2016.
- 41 N. Chhabra, M. Aseri and D. Padmanabhan, *Int. J. Appl. Basic Med. Res.*, 2013, **3**, 16.
- 42 G. S. Adams, B. A. Converse, A. H. Hales and L. E. Klotz, *Nature*, 2021, **592**, 258–261.
- 43 O. Edenhofer, R. P. Madruga, Y. Sokona, K. Seyboth, P. Matschoss, S. Kadner, T. Zwickel, P. Eickemeier, G. Hansen, S. Schlömer and C. von Stechow, *Renewable energy sources and climate change mitigation: Special report of the intergovernmental panel on climate change*, 2011.
- 44 F. P. Byrne, S. Jin, G. Paggiola, T. H. M. Petchey, J. H. Clark, T. J. Farmer, A. J. Hunt, C. Robert McElroy and J. Sherwood, *Sustain. Chem. Process.*, 2016, **4**, 1–24.
- 45 L. Soh and M. J. Eckelman, *ACS Sustain. Chem. Eng.*, 2016, **4**, 5821–5837.
- 46 A. Gevorgyan, K. H. Hopmann and A. Bayer, *ChemSusChem*, 2020, **13**, 2080–2088.
- 47 O. Y. R. Yu and B. Zhou (eds.). Masson-Delmotte, V., P. Zhai, A. Pirani, S. L. Connors, C. Péan, S. Berger, N. Caud, Y. Chen, L. Goldfarb, M. I. Gomis, M. Huang, K. Leitzell, E. Lonnoy, J. B. R. Matthews, T. K. Maycock, T. Waterfield, *IPCC, 2021: Climate Change 2021: The Physical Science Basis. Contribution of Working Group I to the Sixth Assessment Report of the Intergovernmental Panel on Climate Change*, 2021.
- 48 Retsch, Retsch, <https://www.retsch.com/products/milling/ball-mills/>, (accessed 27 September 2022).
- 49 C. K. Chua, Z. Sofer, B. Khezri, R. D. Webster and M. Pumera, *Phys. Chem. Chem. Phys.*, 2016, **18**, 17875–17880.
- 50 W. Pickhardt, S. Grätz and L. Borchardt, *Chem. - A Eur. J.*, 2020, **26**, 12903–12911.

- 51 C. G. Vogt, S. Gratz, S. Lukin, I. Halasz, M. Etter, J. D. Evans and L. Borchardt, *Angew. CHEMIE-INTERNATIONAL Ed.*, 2019, **58**, 18942–18947.
- 52 L. Takacs, *Prog. Mater. Sci.*, 2002, **47**, 355–414.
- 53 L. L. Wang, Z. A. Munir and Y. M. Maximov, *J. Materials Sci.*, 1993, **28**, 3693–3708.
- 54 M. Gazvoda, M. Virant, B. Pinter and J. Košmrlj, *Nat. Commun.*, 2018, **9**, 1–9.
- 55 E. Tullberg, D. Peters and T. Frejd, *J. Organomet. Chem.*, 2004, **689**, 3778–3781.
- 56 V. P. Balema, J. W. Wiench, M. Pruski and V. K. Pecharsky, *J. Am. Chem. Soc.*, 2002, **124**, 6244–6245.
- 57 L. A. Panther, D. P. Guest, A. McGown, H. Emerit, R. K. Tareque, A. Jose, C. M. Dadswell, S. J. Coles, G. J. Tizzard, R. González-Méndez, C. A. I. Goodall, M. C. Bagley, J. Spencer and B. W. Greenland, *Chem. – A Eur. J.*, 2022, **28**, e202201444.
- 58 K. Kubota, T. Seo, K. Koide, Y. Hasegawa and H. Ito, *Nat. Commun.*, 2019, **10**, 1–11.
- 59 Q. Cao, J. L. Howard, E. Wheatley and D. L. Browne, *Angew. Chemie*, 2018, **130**, 11509–11513.
- 60 T. K. Achar, A. Bose and P. Mal, *Beilstein J. Org. Chem.*, 2017, **13**, 1907–1931.
- 61 C. Schumacher, J. G. Hernandez and C. Bolm, *Angew. Chem., Int. Ed.*, 2020, **59**, 16357–16360.
- 62 J. A. Leitch and D. L. Browne, *Chem. – A Eur. J.*, 2021, **27**, 9721–9726.
- 63 Y. D. Pang, J. W. Lee, K. Kubota and H. Ito, *Angew. Chem., Int. Ed.*, 2020, **59**, 22570–22576.
- 64 K. Kubota, Y. Pang, A. Miura and H. Ito, *Science (80-.)*, 2019, **366**, 1500–1504.
- 65 I. Lim, A. Vian, H. L. Van De Wouw, R. A. Day, C. Gomez, Y. Liu, A. L. Rheingold, O. Campàs and E. M. Sletten, *J. Am. Chem. Soc.*, 2020, **142**, 16072–16081.
- 66 A. R. Pedrazzo, F. Caldera, M. Zanetti, S. L. Appleton, N. K. Dahkar and F. Trotta, *BEILSTEIN J. Org. Chem.*, 2020, **16**, 1554–1563.
- 67 E. O. Miranda, V. H. R. Silva, M. Lea, E. Cabral-Albuquerque, S. Cunha and R. L. L. Fialho, *J. Clean. Prod.*
- 68 X. H. Ou, S. S. Chen, X. M. Lu and Q. H. Lu, *Compos. Commun.*
- 69 J. W. Lee, J. Park, J. Lee, S. Park, J. G. Kim and B. S. Kim, *ChemSusChem*, 2021, **14**, 3801–

3805.

- 70 S. Park and J. G. Kim, *Beilstein J. Org. Chem.*, 2019, **15**, 963–970.
- 71 Y. Z. Huang, C. Y. Cai, Z. C. Wei, P. Wang, L. X. Deng, Y. Q. Wang and Y. Fu, *J. Mater. Pro. Tech.*, 2021, **292**, 7052.
- 72 S. Darwish, S. Q. Wang, D. M. Croker, G. M. Walker and M. J. Zaworotko, *ACS Sustain. Chem. Eng.*, 2019, **7**, 19505–19512.
- 73 T. Stolar, A. Prasnikař, V. Martinez, B. Karadeniz, A. Bjelic, G. Mali, T. Friscic, B. Likozar and K. Uzarevic, *ACS Appl. Mater. Interfaces*, 2021, **13**, 3070–3077.
- 74 X. C. Li, Z. H. Zhang, W. M. Xiao, S. J. Deng, C. Chen and N. Zhang, *J. Mater. Chem. A*, 2019, **7**, 14504–14509.
- 75 V. Martinez, B. Karadeniz, N. Biliskov, I. Loncari, S. Muratovic, D. Zilic, S. M. Avdoshenko, M. Roslova, A. A. Popov and K. Uzarevic, *Chem. Mater.*, 2020, **32**, 10628–10640.
- 76 S. Grätz and L. Borchardt, *RSC Adv.*, 2016, **6**, 64799–64802.
- 77 S. Haferkamp, A. Paul, A. A. L. Michalchuk and F. Emmerling, *Beilstein J. Org. Chem.*, 2019, **15**, 1141–1148.
- 78 S. Gratz, M. Oltermann, C. G. Vogt and L. Borchardt, *ACS Sustain. Chem. Eng.*, 2020, **8**, 7569–7573.
- 79 N. G. Khaligh, T. Mihankhah and M. R. Johan, *Res. Chem. Intermed.*, 2019, **45**, 3291–3300.
- 80 M. Mokhtar, G. Alzhrani, E. S. Aazam, T. S. Saleh, S. Al-Faifi, S. Panja and D. Maiti, *Chem. Eur. J.*, 2021, **27**, 8875–8885.
- 81 K. Kubota and H. Ito, *Trends Chem.*, 2020, **2**, 1066–1081.
- 82 G. E. M. Schukraft, S. Ayala, B. L. Dick and S. M. Cohen, *Chem. Commun.*, 2017, **53**, 10684–10687.
- 83 M. A. Ghanem, A. Basu, R. Behrou, N. Boechler, A. J. Boydston, S. L. Craig, Y. Lin, B. E. Lynde, A. Nelson, H. Shen and D. W. Storti, *Nat. Rev. Mater.*, 2021, **6**, 84–98.
- 84 A. Krusenbaum, S. Grätz, G. T. Tigineh, L. Borchardt and J. G. Kim, *Chem. Soc. Rev.*, 2022, **51**, 2873–2905.
- 85 H. Kulla, M. Wilke, F. Fischer, M. Röllig, C. Maierhofer and F. Emmerling, *Chem.*

- Commun.*, 2017, **53**, 1664–1667.
- 86 J. G. Schiffmann, F. Emmerling, I. C. B. Martins and L. Van Wüllen, *Solid State Nucl. Magn. Reson.*
- 87 K. Užarević, N. Ferdelji, T. Mrla, P. A. Julien, B. Halasz, T. Friščić and I. Halasz, *Chem. Sci.*, 2018, **9**, 2525–2532.
- 88 M. Carta, S. L. James and F. Delogu, *Molecules*, 2019, **24**, 3600.
- 89 F. Gomollón-Bel, *Chem. Int.*, 2020, **42**, 3–9.
- 90 ThermoFisher Scientific, <https://www.thermofisher.com/order/catalog/product/567-7600>, <https://www.thermofisher.com/order/catalog/product/567-7600>, (accessed 24 August 2022).
- 91 Dynisco, https://www.dynisco.com/userfiles/files/Introduction_To_Extrusion.pdf, https://www.dynisco.com/userfiles/files/Introduction_To_Extrusion.pdf, (accessed 24 August 2022).
- 92 Q. Cao, D. E. Crawford, C. Shi and S. L. James, *Angew. Chem., Int. Ed.*, 2020, **59**, 4478–4483.
- 93 D. E. Crawford, *Beilstein J. Org. Chem.*, 2017, **13**, 65–75.
- 94 Q. Cao, J. L. Howard, D. E. Crawford, S. L. James and D. L. Browne, *Green Chem.*, 2018, **20**, 4443–4447.
- 95 D. Crawford, J. Casaban, R. Haydon, N. Giri, T. McNally and S. L. James, *Chem. Sci.*, 2015, **6**, 1645–1649.
- 96 D. E. Crawford, A. Porcheddu, A. S. McCalmont, F. Delogu, S. L. James and E. Colacino, *ACS Sustain. Chem. Eng.*, 2020, **8**, 12230–12238.
- 97 M. A. E. A. A. Ali El-Remaily, A. M. M. Soliman and O. M. Elhady, *ACS Omega*, 2020, **5**, 6194–6198.
- 98 B. M. Sharma, R. S. Atapalkar and A. A. Kulkarni, *Green Chem.*, 2019, **21**, 5639–5646.
- 99 D. E. Crawford, C. K. G. Miskimmin, A. B. Albadarin, G. Walker and S. L. James, *Green Chem.*, 2017, **19**, 1507–1518.
- 100 K. Prabha, P. Ghosh, A. S. R. M. Joseph, R. Krishnan, S. S. Rana and R. C. Pradhan, *Futur. Foods*, 2021, **3**, 100019.

- 101 B.-J. Gu, R. J. Kowalski and G. Ganjyal, *WSU Peer Rev.*, 2017, 1–8.
- 102 J. M. Bouvier and O. H. Campanella, *Extrusion Processing Technology: Food and Non-Food Biomaterials*, Wiley, 2014.
- 103 D. K. Tan, M. Maniruzzaman and A. Nokhodchi, *Pharmaceutics*.
- 104 C. Tzoganakis, *Adv. Polym. Technol.*, 1989, **9**, 321–330.
- 105 G. Wypych, in *PVC Formulary (Second Edition)*, ed. G. Wypych, ChemTec Publishing, San Diego, Second Edi., 2015, pp. 131–180.
- 106 D. V Rosato, D. V Rosato and M. V Rosato, in *Plastic Product Material and Process Selection Handbook*, eds. D. V Rosato, D. V Rosato and M. V Rosato, Elsevier, Oxford, 2004, pp. 227–281.
- 107 S. Louhenkilpi, in *Treatise on Process Metallurgy*, ed. S. Seetharaman, Elsevier, Boston, 2014, pp. 373–434.
- 108 T. Dorin, A. Vahid and J. Lamb, in *Fundamentals of Aluminium Metallurgy*, ed. R. N. Lumley, Woodhead Publishing, 2018, pp. 387–438.
- 109 R. Kent, in *Energy Management in Plastics Processing (Third Edition)*, ed. R. Kent, Elsevier, Third Edit., 2018, pp. 211–318.
- 110 M. Gajda, K. P. Nartowski, J. Pluta and B. Karolewicz, *Int. J. Pharm.*, 2019, **558**, 426–440.
- 111 M. Dhaval, S. Sharma, K. Dudhat and J. Chavda, *J. Pharm. Innov.*, 2020, **17**, 294–318.
- 112 C. Martin, *AAPS PharmSciTech*, 2016, **17**, 3–19.
- 113 K. Boksa, A. Otte and R. Pinal, *J. Pharm. Sci.*, 2014, **103**, 2904–2910.
- 114 Y. Yeboue, B. Gallard, N. Le Moigne, M. Jean, F. Lamaty, J. Martinez and T. X. Métro, *ACS Sustain. Chem. Eng.*, 2018, **6**, 16001–16004.
- 115 D. E. Crawford, S. L. James and T. McNally, *ACS Sustain. Chem. Eng.*, 2018, **6**, 193–201.
- 116 D. A. Leister, Continuous Manufacturing of Pharmaceuticals : Scale-up of a Hot Melt Extrusion Process, <https://assets.thermofisher.com/TFS-Assets/MSD/Application-Notes/PT0616-continuous-manufacturing-pharma-hme-scale-up.pdf>, (accessed 19 September 2022).
- 117 Lider Makina, No Title, <https://limaextrusion.com/en/projects/profile-extrusion-parallel-twin-screw-extruder>, (accessed 13 September 2022).

- 118 H. Heeger, Alan J. ; MacDiarmid, Alan G. ; Shirakawa, *Nobel Media AB 2019*, 1974, 1–16.
- 119 C. Burroughes, J. H. Cavendish Laboratory, C. Bradley, D. D.C. Cavendish Laboratory, C. Brown, A. R., Cavendish Laboratory, C. Marks, R.N (Cavendish Laboratory, C. Mackay, K (Cavendish Laboratory, C. Friend, R. H. (Cavendish Laboratory, C. Burns, P. L. University Chemistry Laboratory and C. Holmes, A. R (University Chemistry Laboratory, *Nature*, 1990, **347**, 539–541.
- 120 J. B. Ravensbæk and T. M. Swager, *ACS Macro Lett.*, 2014, **3**, 305–309.
- 121 H. G. Gilch and W. L. Wheelwright, *J. Polym. Sci. Part A-1 Polym. Chem.*
- 122 D. Izuhara and T. M. Swager, *JACS Commun.*, 2009, 17724–17725.
- 123 L. Chen, E. Vivier, C. J. Eling, T. S. Babra, J.-S. G. Bouillard, A. M. Adawi, D. M. Benoit, F. Hartl, H. M. Colquhoun, O. A. Efremova and B. W. Greenland, *Synth. Met.*, 2018, **241**, 31–38.
- 124 T. Zincke, G. Heuser and W. Möller, *Justus Liebigs Ann. Chem.*, 1904, **333**, 296–345.
- 125 H. C. Van Der Plas, *Acc. Chem. Res.*, 1978, **11**, 462–468.
- 126 L. Chen, H. Willcock, C. J. Wedge, F. Hartl, H. M. Colquhoun and B. W. Greenland, *Org. Biomol. Chem.*, 2016, **14**, 980–988.
- 127 L. Chen, F. Hartl, H. M. Colquhoun and B. W. Greenland, *Tetrahedron Lett.*, 2017, **58**, 1859–1862.
- 128 F. Miklós, V. Hum and F. Fülöp, *Arkivoc*, 2014, **2014**, 25–37.
- 129 L. Tröbs and F. Emmerling, *Faraday Discuss.*, 2014, **170**, 109–119.
- 130 N. Zeghib, P. Thelliere, M. Rivard and T. Martens, *J. Org. Chem.*, 2016, **81**, 3256–3262.
- 131 E. F. . K. Gerasimova, T. N.; Kolchina, *Bull. Acad. Sci. USSR, Div. Chem. Sci.*, 1987, **36**, 2611.
- 132 K. C. Roberts, C. G. M. de Worms and H. B. Clark, *J. Chem. Soc.*, 1935, 196–200.
- 133 Chemaxon, Chemicalize, <https://chemicalize.com/welcome>, (accessed 15 June 2020).
- 134 X. Ma, W. Yuan, S. E. J. Bell and S. L. James, *Chem. Commun.*, 2014, **50**, 1585–1587.
- 135 Conquer Scientific, <https://conquerscientific.com>, (accessed 6 September 2022).
- 136 S. K. Nimkar, A. H. Anderson, J. M. Rimoldi, M. Stanton, K. P. Castagnoli, S. Mabic, Y. X. Wang and N. Castagnoli, *Chem. Res. Toxicol.*, 1996, **9**, 1013–1022.

- 137 J. M. Vandenbelt, C. Henrich and S. G. Vanden Berg, *J. Anal. Chem.*, 1954, **26**, 726–727.
- 138 A. M. Graña, J. M. Hermida-Ramón and R. A. Mosquera, *Chem. Phys. Lett.*, 2005, **412**, 106–109.
- 139 O. Pytela, M. Otyepka, J. Kulhánek, E. Otyepková and T. Nevěčná, *J. Phys. Chem. A*, 2003, **107**, 11489–11496.
- 140 F. C. Brown, H. C.; McDaniel, D. H.; Hafliger, O.; Braude, E. A., Nachod, Ed., *In Determination of Organic Structures by Physical Methods*, Academic Press: New York, 1955.
- 141 L. Robertson and R. C. Hartley, *Tetrahedron*, 2009, **65**, 5284–5292.
- 142 E. N. Marvell, G. Caple and I. Shahidi, *J. Am. Chem. Soc.*, 1970, **92**, 5641–5645.
- 143 W. Zincke Th. and Wurker, *Liebigs Ann Chem*, 1905, **338**, 107.
- 144 I. Yamaguchi, Y. Gobara and M. Sato, *Org. Lett.*, 2006, **8**, 4279–4281.
- 145 L. Shi, D. Lundberg, D. G. Musaev and F. M. Menger, *Angew. Chemie Int. Ed.*, 2007, **46**, 5889–5891.
- 146 M. Christl, *Angew. Chem., Int. Ed.*, 2007, **46**, 9152–9153.
- 147 C. J. Kassi, D. C. Swenson and F. C. Pigge, *Cryst. Growth Des.*, 2015, **15**, 4571–4580.
- 148 V. M. and V. Š. J. Kaválek, A. Lyčka, *Collect. Czech. Chem. Commun*, 1976, **41**, 67–77.
- 149 A. van Dormael and J. Nys, *Bull. des Sociétés Chim. Belges*, 1952, **58**, 614–621.
- 150 I. Marvell, E. N.; Caple, G.; Shahidi, *Tetrahedron Lett.*, 1967, **8**, 277.
- 151 I. Yamaguchi, Y. Tanaka and A. Wang, *RSC Adv.*, 2018, **8**, 29988–29994.
- 152 A. Amine Khodja, Imene; Boulcina, Raouf; Debache, *Lett. Org. Chem.*, 2015, **12**, 77–84.
- 153 R. N. Adams, 1968, **3618**, 6596–6599.
- 154 I. Parikh, H. Hilpert and K. Hermann, *Helv. Chim. Acta - HELV CHIM ACTA*, 1986, **69**, 1588–1596.
- 155 O. Maury, J. P. Guégan, T. Renouard, A. Hilton, P. Dupau, N. Sandon, L. Toupet and H. Le Bozec, *New J. Chem.*, 2001, **25**, 1553–1566.
- 156 K. T. Cheng, E. Garanger, V. Josserand, Z. Jin, S. Foillard, D. Boturyn, P. M. C. Favrot, P. Dumy and J.-L. Coll, 2004, 2–8.
- 157 B. G. Moreira, Y. You and R. Owczarzy, *Biophys. Chem.*, 2015, **198**, 36–44.

- 158 J. Cao, J. Fan, W. Sun, Z. Yang, C. Hu and X. Peng, *Dye. Pigment.*, 2017, **141**, 379–387.
- 159 C. Gebhardt, M. Lehmann, M. M. Reif, M. Zacharias, G. Gemmecker and T. Cordes, *ChemPhysChem*, 2021, **22**, 1566–1583.
- 160 I. Marvell, Elliot N.; Caple, Gerald; Shahidi, *Nature*, 1959, **183**, 1433.
- 161 S. Sutthiruangwong and G. Mori, *Int. J. Refract. Met. Hard Mater.*, 2003, **21**, 135–145.
- 162 S. E. Steinhardt, J. S. Silverston and C. D. Vanderwal, *J. Am. Chem. Soc.*, 2008, **130**, 7560–7561.
- 163 T. Katoh, K. Ogawa, Y. Inagaki and R. Okazaki, *Bull. Chem. Soc. Jpn.*, 1997, **70**, 1109–1114.
- 164 L. Štacková, P. Štacko and P. Klán, *J. Am. Chem. Soc.*, 2019, **141**, 7155–7162.
- 165 W. Xu, E. Leary, S. Sangtarash, M. Jirasek, M. T. González, K. E. Christensen, L. Abellán Vicente, N. Agraït, S. J. Higgins, R. J. Nichols, C. J. Lambert and H. L. Anderson, *J. Am. Chem. Soc.*, 2021, **143**, 20472–20481.
- 166 X. Guo and A. Facchetti, *Nat. Mater.*, 2020, **19**, 922–928.
- 167 T. M. Swager, *Macromolecules*, 2017, **50**, 4867–4886.
- 168 A. J. Heeger, S. Kivelson, J. R. Schrieffer and W. P. Su, *Rev. Mod. Phys.*, 1988, **60**, 781–850.
- 169 F. H. Allen, O. Kennard, D. G. Watson, L. Brammer, A. G. Orpen and R. Taylor, *J. Chem. Soc. Perkin Trans. 2*, 1987, 1–19.
- 170 W.-C. Cheng and M. J. Kurth, *Org. Prep. Proced. Int.*, 2002, **34**, 585–608.
- 171 and C. D. V. Sarah E. Steinhardt, Joel S. Silverston, 1997, **12**, 1–5.
- 172 R. S. Paton, S. E. Steinhardt, C. D. Vanderwal and K. N. Houk, *J. Am. Chem. Soc.*, 2011, **133**, 3895–3905.
- 173 A. N. Kost, S. P. Gromov and R. S. Sagitullin, *Tetrahedron*, 1981, **37**, 3423–3454.
- 174 J. Becher, *Synthesis (Stuttg.)*, 1980, **1980**, 589–612.
- 175 S. Zhao, X. Xu, L. Zheng and H. Liu, *Ultrason. Sonochem.*, 2010, **17**, 685–689.
- 176 A. Kumari and S. Gupta, *J. Biophotonics*, 2019, **12**, 1–7.
- 177 H. Wan, J. Yue, S. Zhu, T. Uno, X. Zhang, Q. Yang, K. Yu, G. Hong, J. Wang, L. Li, Z. Ma, H. Gao, Y. Zhong, J. Su, A. L. Antaris, Y. Xia, J. Luo, Y. Liang and H. Dai, *Nat. Commun.*, 2018,

- 9, 1171.
- 178 M. Y. Berezin, K. Guo, W. Akers, R. E. Northdurft, J. P. Culver, B. Teng, O. Vasalatiy, K. Barbacow, A. Gandjbakhche, G. L. Griffiths and S. Achilefu, *Biophys. J.*, 2011, **100**, 2063–2072.
- 179 E. A. Owens, M. Henary, G. El Fakhri and H. S. Choi, *Acc. Chem. Res.*, 2016, **49**, 1731–1740.
- 180 M. Henary, S. Paranjpe and E. A. Owens, 2013, *Heterocyclic Comm.* **19**, 1–11.
- 181 J. Atchison, S. Kamila, H. Nesbitt, K. A. Logan, D. M. Nicholas, C. Fowley, J. Davis, B. Callan, A. P. McHale and J. F. Callan, *Chem. Commun.*, 2017, **53**, 2009–2012.
- 182 X. H. Chang, J. Zhang, L. H. Wu, Y. K. Peng, X. Y. Yang, X. L. Li, A. J. Ma, J. C. Ma and G. Q. Chen, *Micromachines*, 2019, **10**, 1–20.
- 183 N. Wolf, L. Kersting, C. Herok, C. Mihm and J. Seibel, *J. Org. Chem.*, 2020, **85**, 9751–9760.
- 184 J. Lavaud, M. Henry, P. Gayet, A. Fertin, J. Vollaire and Y. Usson, *Int J Biol Sci.*, 2020, **16**, 1616–1628.
- 185 R. Thirumalai, R. D. Mukhopadhyay, V. K. Praveen and A. Ajayaghosh, *Sci. Rep.*, 2015, **5**, 1–11.
- 186 C. Joyce, S. M. Fothergill and F. Xie, *Mater. Today Adv.*, 2020, **7**, 100073.
- 187 F. Guo, A. Karl, Q.-F. Xue, K. C. Tam, K. Forberich and C. J. Brabec, *Light Sci. Appl.*, 2017, **6**, e17094.
- 188 E. A. Owens, N. Bruschi, J. G. Tawney and M. Henary, *Dye. Pigment.*, 2015, **113**, 27–37.
- 189 D. Saccone, S. Galliano, N. Barbero, P. Quagliotto, G. Viscardi and C. Barolo, *European J. Org. Chem.*, 2016, **2016**, 2244–2259.
- 190 G. Li, R. Zhu and Y. Yang, *Nat. Photonics*, 2012, **6**, 153–161.
- 191 Edinburgh Instruments Ltd, <https://www.edinst.com/blog/jablonski-diagram/>, (accessed 29 April 2020).
- 192 S. Gunasekaran, D. Hernangómez-Pérez, I. Davydenko, S. Marder, F. Evers and L. Venkataraman, *Nano Lett.*, 2018, **18**, 6387–6391.
- 193 Alfa Chemistry, <https://www.alfa-chemistry.com/product/hitci-cas-19764-96-6-94215.html>, (accessed 15 July 2022).

- 194 M. Bai and S. Achilefu, *Bioorganic Med. Chem. Lett.*, 2011, **21**, 280–284.
- 195 R. Xu, A. Xu, C. Du, Y. Cong and J. Wang, *J. Chem. Thermodyn.*, 2016, **102**, 178–187.
- 196 O. Semenova, D. Kobzev, F. Yazbak, F. Nakonechny, O. Kolosova, A. Tatarets, G. Gellerman and L. Patsenker, *Dye. Pigment.*, 2021, **195**, 109745.
- 197 D. H. Li and B. D. Smith, *Chem. Eur. J.*, 2021, **27**, 14535–14542.
- 198 S. S. Matikonda, G. Hammersley, N. Kumari, L. Grabenhorst, V. Glembockyte, P. Tinnefeld, J. Ivanic, M. Levitus and M. J. Schnermann, *J. Org. Chem.*, 2020, **85**, 5907–5915.
- 199 L. G. S. Heseltine, Donald W; Brooker, *US Pat.*,.
- 200 X. Fang, W. Liu, X. Wu, W. Zhou, J. Chen, X. Liu and Z. Xu, *Results Chem.*, 2021, **3**, 100092.
- 201 M. Bai and S. Achilefu, *Bioorg. Med. Chem. Lett.*, 2011, **21**, 280–284.
- 202 X. G. Yang, Y. H. Mou, Y. J. Wang, J. Wang, Y. Y. Li, R. H. Kong, M. Ding, D. Wang and C. Guo, *Molecules*, 2019, **24**, 1–13.
- 203 F. Rüttger, S. Mindt, C. Golz, M. Alcarazo and M. John, *European J. Org. Chem.*, 2019, **2019**, 4791–4796.
- 204 S. Ghelli and G. Ponterini, *J. Mol. Struct.*, 1995, **355**, 193–200.
- 205 D. Abergel and A. G. Palmer, *ChemPhysChem*, 2004, **5**, 787–793.
- 206 L. Plougastel, M. R. Pattanayak, M. Riomet, S. Bregant, A. Sallustrau, M. Nothisen, A. Wagner, D. Audisio and F. Taran, *Chem. Commun.*, 2019, **55**, 4582–4585.
- 207 L. Štacková, E. Muchová, M. Russo, P. Slavíček, P. Štacko and P. Klán, *J. Org. Chem.*, 2020, **85**, 9776–9790.
- 208 The Express Wire, Digital Journal, <https://www.digitaljournal.com/pr/global-indocyanine-green-market-is-projected-to-grow-at-an-exemplary-growth-rate-of-around-4-85-by-2028-108-report-pages>, (accessed 10 August 2022).
- 209 I. J. Fox and E. H. Wood, *Proc. Staff Meet. Mayo Clin.*, 1960, **35**, 732–744.
- 210 P. Debie and S. Hernot, *Front. Pharmacol.*
- 211 L. van Manen, H. J. M. Handgraaf, M. Diana, J. Dijkstra, T. Ishizawa, A. L. Vahrmeijer and J. S. D. Mieog, *J. Surg. Oncol.*, 2018, **118**, 283–300.
- 212 G. G. Stokes, *Philos. Trans. R. Soc. Lond.*, 1852, **142**, 463–562.

- 213 S. Gioux, H. S. Choi and J. V. Frangioni, *Mol. Imaging*, 2010, **9**, 237–255.
- 214 Dictionary, NCI Drug, <https://www.cancer.gov/publications/dictionaries/cancer-drug/>, (accessed 25 April 2020).
- 215 A. K. Kirchherr, A. Briel and K. Mäder, *Mol. Pharm.*, 2009, **6**, 480–491.
- 216 W. H. Organisation, World Health Organisation, <https://www.who.int/teams/blueprint/covid-19>, (accessed 15 December 2021).
- 217 M. Izzetoglu, S. Bunce, K. Izzetoglu, B. Onaral and A. Pourrezaei, *IEEE Eng. Med. Biol. Mag.*, 2007, **26**, 38–46.
- 218 S. L. P. Luengas, G. H. Marin, K. Aviles, R. C. Acuña, G. Roque, F. R. Nieto, F. Sanchez, A. Tarditi, L. Rivera and E. Mansilla, *Cancer Biother. Radiopharm.*, 2014, **29**, 435–443.
- 219 J. J. Vos, J. K. G. Wietasch, A. R. Absalom, H. G. D. Hendriks and T. W. L. Scheeren, *Anaesthesia*, 2014, **69**, 1364–1376.
- 220 A. De Gasperi, E. Mazza and M. Prospero, *World J. Hepatol.*, 2016, **8**, 355–367.
- 221 L. Lau, C. Christophi, M. Nikfarjam, G. Starkey, M. Goodwin, L. Weinberg, L. Ho and V. Muralidharan, *HPB Surg.*, 2015, **9**.
- 222 C. Schwarz, I. Plass, F. Fitschek, A. Punzengruber, M. Mittlböck, S. Kampf, U. Asenbaum, P. Starlinger, S. Stremitzer, M. Bodingbauer and K. Kaczirek, *Sci. Rep.*, 2019, **9**, 1–7.
- 223 *Natl. Inst. Clin. Excell.*, 2004, 1–13.
- 224 K. Waseda, J. Ako, T. Hasegawa, Y. Shimada, F. Ikeno, T. Ishikawa, Y. Demura, K. Hatada, P. G. Yock, Y. Honda, P. J. Fitzgerald and M. Takahashi, *JACC Cardiovasc. Imaging*, 2009, **2**, 604–612.
- 225 A. Raabe, D. Ph, J. Beck and D. Ph, *Neurosurgery*, 2003, **52**, 17–19.
- 226 WO2017/093889A1, 2017.
- 227 US Pat. US20190337896 A1, 2019, 12.
- 228 Y. Hayashi, *Chem. Sci.*, 2016, **7**, 866–880.
- 229 K. C. Nicolaou, D. J. Edmonds and P. G. Bulger, *Angew. Chem. Int. Ed. Engl.*, 2006, **45**, 7134–7186.
- 230 L. F. Fieser and U. Beifuss, *Angew. Chem., Int. Ed.*, 1993, **32**, 131.
- 231 Chemical Book,

- https://www.chemicalbook.com/ChemicalProductProperty_DE_CB8150691.htm,
(accessed 19 September 2022).
- 232 E. Clifford, Filafab, <https://d3dinnovations.com/filafab/>, (accessed 9 September 2021).
- 233 C. R. McElroy, A. Constantinou, L. C. Jones, L. Summerton and J. H. Clark, *Green Chem.*, 2015, **17**, 3111–3121.
- 234 S. Mindt, I. Karampinis, M. John, M. Neumaier and K. Nowak, *Photochem. Photobiol. Sci.*, 2018, **17**, 1189–1196.
- 235 V. Isoni, K. Mendoza, E. Lim and S. K. Teoh, *Org. Process Res. Dev.*, 2017, **21**, 992–1002.
- 236 A. Levitz, F. Marmarchi and M. Henary, *Photochem. Photobiol. Sci.*, 2018, **17**, 1409–1416.
- 237 M. Henary and A. Levitz, *Dye. Pigment.*, 2013, **99**, 1107–1116.
- 238 IPCC, in *Global Warming of 1.5°C: IPCC Special Report on Impacts of Global Warming of 1.5°C above Pre-industrial Levels in Context of Strengthening Response to Climate Change, Sustainable Development, and Efforts to Eradicate Poverty*, Cambridge University Press, 2022, pp. 1–24.
- 239 W. Zincke, Th.; Heuser, G.; Moller, *Justus Liebigs Ann. der Chemie (in Ger.)*, 1904, **330**, 361–374.
- 240 E. N. Marvell and I. Shahidi, *J. Am. Chem. Soc.*, 1970, **92**, 5646–5649.
- 241 H. Langhals, A. Varja, P. Laubichler, M. Kernt, K. Eibl and C. Haritoglou, *J. Med. Chem.*, 2011, **54**, 3903–3925.
- 242 Retsch, Retsch, <https://www.retsch.com/downloads/operating-instructions/>, (accessed 1 October 2018).

Appendices

Appendix 1: Ball milling

Retsch Ball Mills²⁴² -

Guidelines for sample amount and ball charge

As a rule of thumb, the grinding balls should be approximately 3 x larger than the largest sample particle. In addition to the instrument settings and the ball size, the filling level of the jar is also of crucial importance for a successful grinding process in ball mills.

When grinding bulk materials, the jar should be filled with approx. 1/3 sample and 1/3 ball charge. The remaining third is the free jar volume that is necessary for the free movement of the balls.

If an increase or decrease in sample volume is to be expected during the grinding process, the filling levels may be changed according to the range given in the table below (in case of an expected decrease in sample volume, a further deviation is possible).

For wet grinding with grinding balls < 3 mm the ball charge should make up 60 % of the jar volume, while the sample amount should be 30 %. The density of the grinding ball materials is used to calculate the mass of the required amount of grinding balls.

Planetary Ball Mills

PM 100 / PM 100 CM / PM 200 / PM 400

Volume of the jar	Sample amount	Max. Feed particle size	Dry Grinding Recommended ball charge (Pieces)						Wet Grinding Recommended ball charge (Mass, g)
			∅ 5 mm	∅ 1 0 mm	∅ 1 5 mm	∅ 20 mm	∅ 3 0 mm	∅ 4 0 mm	∅ ≤ 3 mm
12 ml	< 5 ml	<1 mm	50	5	-	-	-	-	Stainless steel: 35 g
25 ml	< 10 ml	<1 mm	100	8	-	-	-	-	Stainless steel: 75 g
50 ml	5-20 ml	<3 mm	200	10	7	3	-	-	Zirconium oxide: 110 g Stainless steel: 145 g Tungsten carbide: 275 g
80 ml	10-35 ml	<4 mm	250	25	10	5	-	-	Stainless steel: 235 g Tungsten carbide: 440 g
125 ml	15-50 ml	<4 mm	500	30	18	7	-	-	Zirconium oxide: 275 g Stainless steel: 365 g Tungsten carbide: 690 g
250 ml	25-120 ml	<6 mm	1200	50	45	15	6	-	Zirconium oxide: 550 g Stainless steel: 730 g Tungsten carbide: 1380 g
500 ml	75-220 ml	<10 mm	2000	100	70	25	8	4	Zirconium oxide: 1100 g Stainless steel: 1450 g

Mixer Mills MM 200 / MM 400 / MM 500 varia / CryoMill

The MM 400 and the CryoMill (at room temperature) are suitable for wet grinding. For optimal wet grinding results, the MM 500 nano or Planetary Ball Mills should be used (optimized jar geometry).

Volume of the grinding jar	Sample amount	Max. Feed particle size	Dry Grinding Recommended ball charge (Pieces)			
			∅ 5 mm	∅ 7 mm	∅ 10 mm	∅ 12 mm
1.5 ml	0.2-0.5 ml	1 mm	1 - 2	-	-	-
5 ml	0.5-2 ml	2 mm	5 - 6	1-2	-	-
10 ml	2-4 ml	4 mm	17 - 20	9 - 12	1 - 2	1 - 2
25 ml	4-10 ml	6 mm	35 - 40	16 - 20	5 - 6	2 - 4
35 ml	6-15 ml	6 mm	55 - 60	25 - 30	6 - 9	4 - 6
50 ml	8-20 ml	8 mm	80 - 90	45 - 50	12 - 14	6 - 8

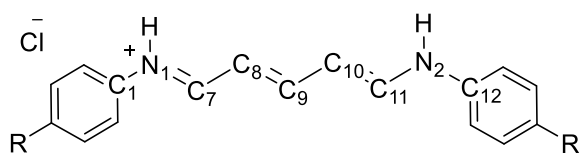
Volume of the grinding jar	Sample amount	Max. Feed particle size	Dry Grinding Recommended ball charge (Pieces)			Wet Grinding Recommended ball charge (Mass, g)
			∅ 15 mm	∅ 20 mm	∅ 25 mm	∅ ≤ 3 mm
1.5 ml	0.2-0.5 ml	1 mm	-	-	-	Stainless steel: 4.5 g
5 ml	0.5-2 ml	2 mm	-	-	-	Stainless steel: 15 g
10 ml	2-4 ml	4 mm	-	-	-	Zirconium oxide: 20 g Stainless steel: 30 g Tungsten carbide: 55 g
25 ml	4-10 ml	6 mm	1 - 2	-	-	Zirconium oxide: 55 g Stainless steel: 75 g Tungsten carbide: 140 g
35 ml	6-15 ml	6 mm	2 - 3	1	-	Zirconium oxide: 75 g Stainless steel: 105 g
50 ml	8-20 ml	8 mm	3 - 4	1	1	Stainless steel: 145 g

The Mixer Mills are also used for cell disruption of biological cells. Specific adapters for 1.5 ml or 2 ml vials are required. The **MM 400** also accepts 5 ml vials, 30 ml wide mouth bottles or 50 ml conical centrifugation tubes. The **MM 500 vario** keeps adapters for 1.5 ml / 2 ml / 5 ml vials. The conical centrifugation tubes are limited suitable for dry grinding. Please contact RETSCH's application team if you wish to homogenize tissues like liver or dried plant materials in conical centrifugation tubes.

Vial	Sample amount	Max. Feed particle size	Dry Grinding Recommended ball charge (Pieces) Stainless steel or zirconium oxide				Cell disruption of biological cells
			∅ 4 mm	∅ 5 mm	∅ 7 mm	∅ 10 mm	Glas beads (0.1-0.25 mm/0.25-0.5 mm/0.75-1 mm/1-1.5 mm) Grinding balls zirconium oxide (< 3 mm)
1.5 ml	0.2-0.5 ml	<1 mm	2-4	-	-	-	~ 0.75 ml
2 ml	0.3-0.75 ml	<2 mm	3-6	2-4	1-2	-	~ 1 ml
5 ml	0.5-2 ml	<2 mm	12	-	-	-	~ 2.5 ml
30 ml*	5-12 ml	<5 mm	40-45	20-22	10-14	6-10	~ 15 ml
50 ml*	8-20 ml	<4 mm	-	-	-	-	~ 25 ml

* Please note for MM 400: The total weight of adapter, bottles, sample and grinding balls should not exceed 650 g per grinding station.

Appendix 2: X-Ray Crystallography Data for Cy5



	3-3 a	3-3 b	3-3 c	3-3 d	3-3 e	3-3 f	3-3 g
N1-C1	1.414 (2)	1.4131 (17)	1.405 (5)	1.410 (4)	1.406 (4)	1.414 (4)	1.417 (11)
N1-C7	1.322(2)	1.3295(17)	1.324(5)	1.337(4)	1.325(4)	1.327(4)	1.319(11)
N2-C12	1.413(2)	1.4062(17)	1.404(5)	1.413(4)	1.406(4)	1.405(4)	1.396(11)
N2-C11	1.330(2)	1.3285(17)	1.327(5)	1.320(4)	1.332(5)	1.318(4)	1.321(11)
C7-C8	1.386(2)	1.3797(19)	1.385(5)	1.380(4)	1.385(5)	1.377(4)	1.319(11)
C8-C9	1.381(2)	1.3860(19)	1.385(5)	1.392(4)	1.376(5)	1.389(4)	1.397(12)